LEVEL *II*

(12)

AD A105668

AN EMPIRICAL METHOD FOR ESTIMATING THE EFFECT OF GROUND PROXIMITY ON THE JET-INDUCED LIFT OF V/STOL AIRCRAFT EMPLOYING RECTANGULAR JETS

by

J. A. Sansone and W. H. Foley

GENERAL DYNAMICS
Fort Worth Division

DTIC
ELECTE
OCT 16 1981
S   D
B

August, 1981

APPROVED FOR PUBLIC RELEASE; DISTRIBUTION UNLIMITED

Prepared For

NAVAL AIR DEVELOPMENT CENTER
WARMINSTER, PENNSYLVANIA 18974
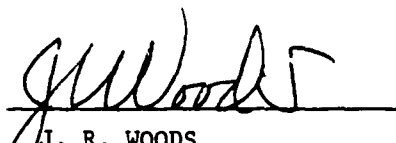
DTIC FILE COPY.

81 10 14

NADC 79298-60

N O T I C E S

REPORT NUMBERING SYSTEM - The numbering of technical project reports issued by the
Naval Air Development Center is arranged for specific identification purposes. Each
number consists of the Center acronym, the calendar year in which the number was
assigned, the sequence number of the report within the specific calendar year, and
the official 2-digit correspondence code of the Command Office or the Functional
Directorate responsible for the report. For example: Report No. NADC-78015-20
indicates the fifteenth Center report for the year 1978, and prepared by the Systems
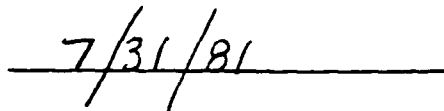Directorate. The numerical codes are as follows:

CODE	OFFICE OR DIRECTORATE
00	Commander, Naval Air Development Center
01	Technical Director, Naval Air Development Center
02	Comptroller
10	Directorate Command Projects
20	Systems Directorate
30	Sensors & Avionics Technology Directorate
40	Communication & Navigation Technology Directorate
50	Software Computer Directorate
60	Aircraft & Crew Systems Technology Directorate
70	Planning Assessment Resources
80	Engineering Support Group

PRODUCT ENDORSEMENT - The discussion or instructions concerning commercial products
herein do not constitute an endorsement by the Government nor do they convey or
imply the license or right to use such products.

APPROVED BY: _____ DATE: ___7/31/81_____

J. R. WOODS
USN   CDR

UNCLASSIFIED

REPORT DOCUMENTATION PAGE		READ INSTRUCTIONS BEFORE COMPLETING FORM
1. REPORT NUMBER NADC-79298-60	2. GOVT ACCESSION NO. AD-A105668	3. RECIPIENT'S CATALOG NUMBER
4. TITLE (and Subtitle) AN EMPIRICAL METHOD FOR ESTIMATING THE EFFECT OF GROUND PROXIMITY ON THE JET-INDUCED LIFT OF V/STOL AIRCRAFT EMPLOYING RECTANGULAR JETS		5. TYPE OF REPORT & PERIOD COVERED Final Technical Report for Period 7/15/80-5/15/81
		6. PERFORMING ORG. REPORT NUMBER
7. AUTHOR(s) J. A. Sansone W. H. Foley		8. CONTRACT OR GRANT NUMBER(s) N62269-80-C-0238
9. PERFORMING ORGANIZATION NAME AND ADDRESS General Dynamics Corp./Fort Worth Div. P. O. Box 748 Fort Worth, Texas 76101 (Mail Zone 2882)		10. PROGRAM ELEMENT. PROJECT, TASK AREA & WORK UNIT NUMBERS Air Task No. A03V-320D/01B/7F41-400-000
11. CONTROLLING OFFICE NAME AND ADDRESS Naval Air Development Center Warminster, PA 18974		12. REPORT DATE August 1981
		13. NUMBER OF PAGES
14. MONITORING AGENCY NAME & ADDRESS(if different from Controlling Office)		15. SECURITY CLASS. (of this report) Unclassified
		15a. DECLASSIFICATION DOWNGRADING SCHEDULE

16. DISTRIBUTION STATEMENT (of this Report)

Unlimited

DISTRIBUTION STATEMENT A

Approved for public release;
Distribution Unlimited

17. DISTRIBUTION STATEMENT (of the abstract entered in Block 20, if different from Report)

Unlimited

DISTRIBUTION STATEMENT A

Approved for public release;
Distribution Unlimited

18. SUPPLEMENTARY NOTES

19. KEY WORDS (Continue on reverse side if necessary and identify by block number)

V/STOL
Ground Effects
Suckdown
Fountain Forces
Rectangular Jets

20. ABSTRACT (Continue on reverse side if necessary and identify by block number)

An empirical method has been developed to predict the propulsive-induced forces on a V/STOL aircraft hovering in proximity of the ground. This method is applicable to configurations employing two, three, or four rectangular exhausts. Planform contour, nozzle pressure ratio, and lift improvement devices are considered. Accuracies on the order of one percent of propulsive thrust are demonstrated.

DD FORM 1473 EDITION OF 1 NOV 65 IS OBSOLETE

UNCLASSIFIED

BLANK PAGE

FOREWORD

This study was conducted under contract to the Naval Air Development Center (Contract N62269-80-C-0238). The Technical Monitor was Mr. Campbell Henderson, Flight Dynamics Branch (6053), Aircraft and Crew Systems Technology Directorate.

Accession For	
NTIS GRA&I	✓
DTIC TAB	☐
Unannounced	☐
Justification	
By	
Distribution/	
Availability Codes	
	Avail and/or
Dist	Special
A	

BLANK PAGE

iv

TABLE OF CONTENTS

TABLE OF CONTENTS (Cont'd)

LIST OF FIGURES

LIST OF FIGURES (Cont'd)

LIST OF FIGURES (Cont'd)

NOMENCLATURE

|	
AR	Nozzle Aspect Ratio
C_S, C_F	Extrapolation Coefficients (Subsection 2.3)
D, d	Nozzle Diameter, Equivalent Nozzle Diameter
d_{wa}	Thrust Weighted Nozzle Diameter (Subsection 3.1.3)
$\bar{D}$	Equivalent Planform Diameter
d_E	Distance Between Nozzles
D_e, d_e	Equivalent Nozzle Diameter (Subsection 3.1.2)
F_j	Nozzle Thrust
h, H	Altitude
h_m	Altitude Where Jets Merge (Figure 2.3-1)
ΔL	Net Lift Loss (or Gain)
ΔL_j	Partial Lift Loss Due to Suckdown (Eqn. 2.0-1)
ΔL_F	Fountain Lift
ΔL_S	Lift Loss Due to Suckdown
ΔL_{S_∞}	Lift Loss Out of Ground Effect
LID	Lift Improvement Device
N	Number of Nozzles
NPR	Nozzle Pressure Ratio
r	Planform Contour Radius
W	Fuselage Width (Figures 2.3-2 and 2.3-4)

Superscripts

II, III, IV	Referring to 2, 3 or 4 Nozzle Planforms

1.0 INTRODUCTION

The flow field in the immediate vicinity of a hovering V/STOL aircraft can be divided into six more or less distinct regions (Figure 1.0-1). Of particular interest here are regions 1, 2, 3, and 5, i.e., those regions wherein the engine exhaust flows combine with induced ambient air flows to produce forces and moments upon the airframe. In the case of aircraft with high engine exhaust velocities combined with appreciable planform areas, such as the AV-8A and the VAK-191B, these forces and moments are almost invariably both large and unfavorable. Consequently, a considerable amount of theoretical and experimental work (e.g., Ref. 1-19) has been devoted to the subject. In 1980 the Naval Air Development Center published the V/STOL Aerodynamic and Stability and Control Manual in order to reduce V/STOL test data and prediction methodologies to a form useful in a preliminary design environment - that is, to develop an engineering tool for doing rapid hand calculations of advanced aircraft performance during the conceptual stage of development. General Dynamics has contributed to the development of these methods through test and analysis work which was conducted both in house and under contracts to ONR (Refs. 7 and 11) and NADC (Ref.16). During this work, noticable differences occurred between the induced lift generated by configurations with rectangular jets when compared with circular jets (Figure 1.0-2). The empirical formulations for hover-induced lift effects for circular jets has now been extended through further testing and analysis to cover configurations employing rectangular jets.

The results of this program are presented in this report, and the methodology itself is contained in Section 3. This was assembled totally independent of the other sections of the report so that it may be removed and used separately from the body of the text. For this reason, the reader may note a certain amount of redundancy between Section 3 and the other sections.
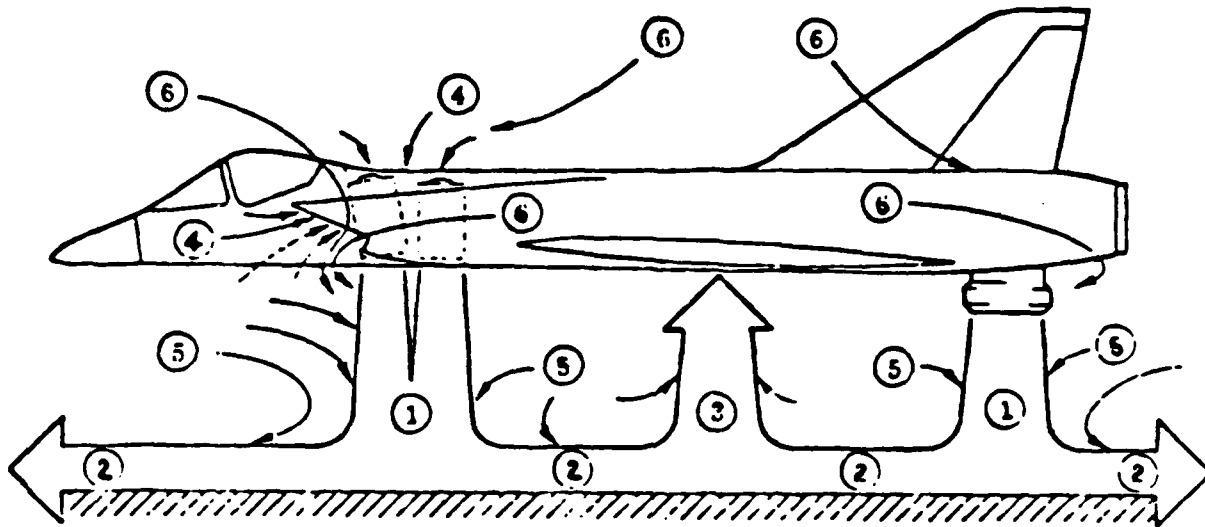
1   EXHAUST FLOW (FREE JET)

2   GROUND JET

3   FOUNTAIN JET

4   ENGINE INLET FLOW

5 & 6   ENTRAINED AMBIENT AIR

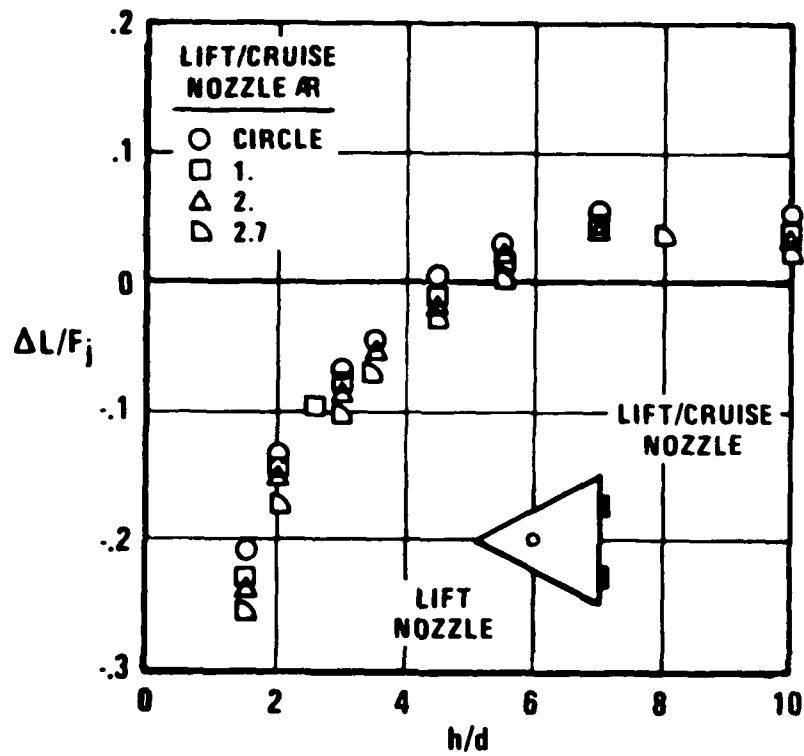Figure 1.0-1   Flow Field Near a Hovering VTOL Aircraft

Figure   1.0-2   Comparison of Induced Lift Between
Rectangular and Circular Jets

2.0 METHODOLOGY DEVELOPMENT

The objective of this program is the development of an empirical method for esti-
mating the effect of ground proximity on the jet-induced lift of V/STOL aircraft employ-
ing rectangular jets. Similar to the work conducted by General Dynamics on circular jets,
a guideline was established, namely, that the resulting empiricisms were to be developed
in an efficient form from the user standpoint. An example of the spirit with which this
guideline was observed can be seen by considering that the method of Karemaa et al,
(Refs. 7 and 8), the point of departure for this work, was modified from

$$\frac{\Delta L}{F_j} = \frac{1}{F_j} \left\{ \Delta L_j + \Delta L_{fc} + \Delta L_{fi} \right\} \tag{2.0-1}$$

to

$$\frac{\Delta L}{F_j} = \frac{1}{F_j} \left\{ \Delta L_S + \Delta L_F \right\} \tag{2.0-2}$$

The terms ΔL_{fc} and ΔL_{fi}, in the Karemaa formulation, represent the incremental lift
due to fountain buoyancy and the change to suckdown due to interference with the en-
trainment process by the fountain, respectively. In the Karemaa work, where the object
was to develop an understanding of the physical processes involved in the flow field, it
was most appropriate to distinguish between the two. Here, however, it was found that
empirically the two could be combined so that only ΔL_F, the net fountain contribution,
appears explicitly. Next, in the Karemaa formulation, ΔL_j represents the suckdown on
those areas of the planform adjacent to each individual exhaust nozzle. Experimentally,
ΔL_j was determined by measuring this force on the adjacent area with the nonadjacent
planform areas physically present but non-metric. A predictive technique for ΔL_j would
require the structuring of the induced flow fields because the locations of the nonadjacent
areas change the flow field itself. Thus, suckdown, ΔL_S, which can be predicted empir-
ically, is the summation of the suckdown produced by each jet upon the entire planform
area.

In all instances, justification for the empiricisms was made, ultimately, a posteriori,
i.e., do they work to an acceptable degree of accuracy over a full range of likely configu-
rations. As will be seen in Appendix B, the complete methodology was tested against a
number of configurations, which were not from the same data base from which the empir-
icisms were developed; the predictions obtained matched the test data within about 1% of
the total lift, which is considered adequate for the applications envisaged for this method-
ology.

2.1 SUCKDOWN

2.1.1 Free-Air Suckdown

The portion of induced lift that accompanies any hovering V/STOL configuration - regardless of altitude, is the free-air suckdown. From Wyatt's (Ref. 4) results, an expression for this force takes the form,

$$\frac{\Delta L_{s\infty}}{F_j} = .0667 \ (d/\bar{D} - .420) \tag{2.1-1}$$

where $d/\bar{D} \leq .420$.

This expression has proven to be accurate at predicting the free-air suckdown associated with configurations employing circular jets (Ref. 16), but fails to correlate the data taken from models tested with rectangular jets (Figure 2.1-1). There appears to be a dependence on AR for the rectangular jet cases which can be related by the expression,

$$\left[\frac{\Delta L_{s\infty}}{F_j}\right]_i = - .004 \left((d/\bar{D})_i + .450 \ (1.28)^{(\bar{D}/d)_i} \right) \left(1 + \frac{AR_i - 1}{20} \right) \left(1 + \frac{AR_i - 1}{(\bar{D}/d)_i} \right) \tag{2.1-2}$$

as shown in Figure 2.1-1.

2.1.2 Altitude Dependent Suckdown

The altitude dependent suckdown associated with planforms employing rectangular nozzles was initially assumed to be similar to that produced by circular jets. The work of Foley and Sansone (Ref. 16) has shown that there is a fine structure to suckdown that is a function of the area ratio $\bar{D}/d$. This structure consists of curves of the same family for planforms employing circular jets, which, in empirical, algebraic form, are described by the relation

$$\frac{\Delta L_s - \Delta L_{s\infty}}{F_j} = -(.00125 \ \bar{D}/d + .0185) \cdot \left[h/(\bar{D}-d) \right]^{-1.59} \tag{2.1-3}$$

Using this equation, an attempt was made to correlate the data reduced from planforms employing rectangular nozzles, Figures A-6 through A-18, Appendix A. The effect of rectangular nozzles appears to be a strong factor on the suckdown, such that Equation 2.1-3 is not within the accuracy desired (Figure 2.1-2). The structure of the suckdown that eminates from planforms with rectangular nozzles of like AR demonstrates a family of curves very similar to those produced from planforms employing circular nozzles (Figure 2.1-3), however, there is little effect of nozzle AR ratio on suckdown for planforms of equal size. This can be seen in Figure 2.1-4. The altitude dependent portion of suckdown can thus be described as

$$\frac{\Delta L_s - \Delta L_{s\infty}}{F_j} = (.00075 \ \bar{D}/d - .022) \left[\frac{h}{\bar{D}-d} \right]^{-(1.5 + .07 \ \bar{D}/d)} \tag{2.1-4}$$
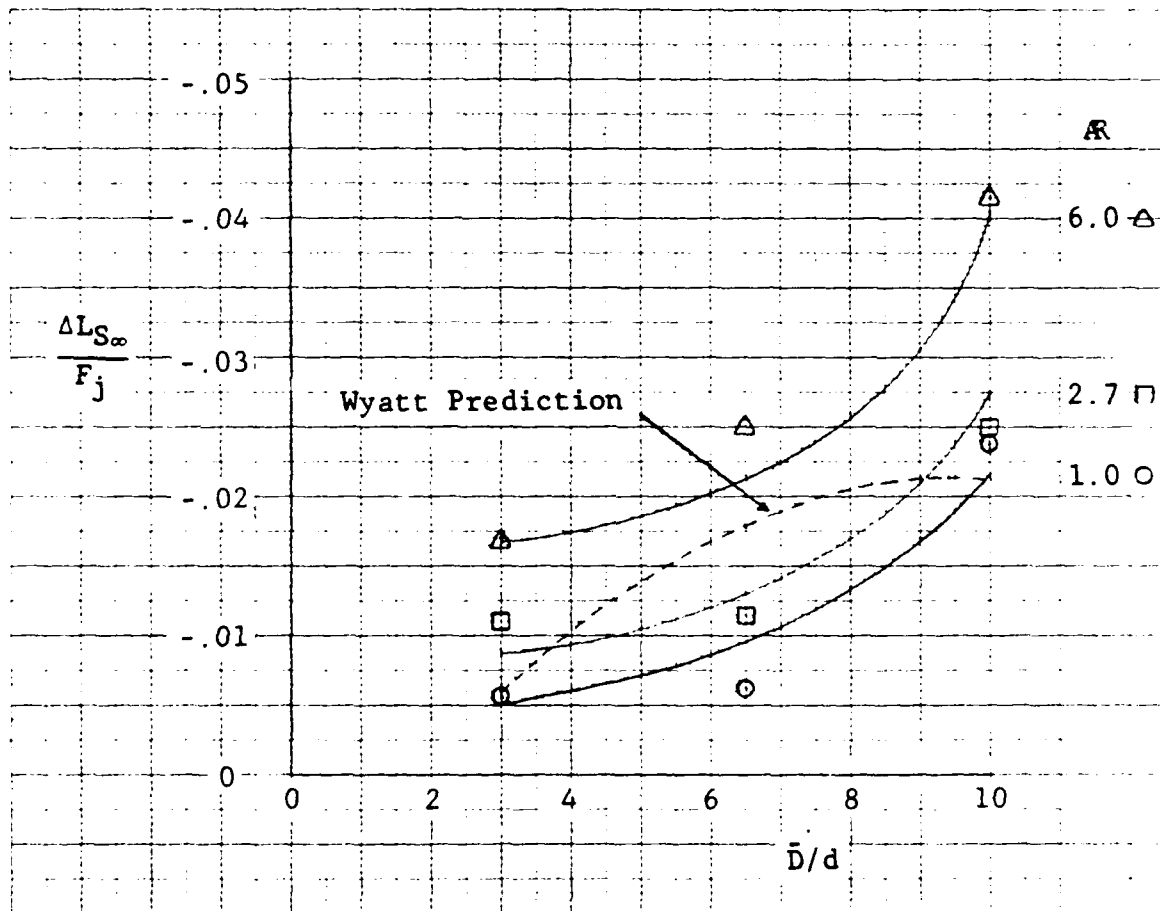
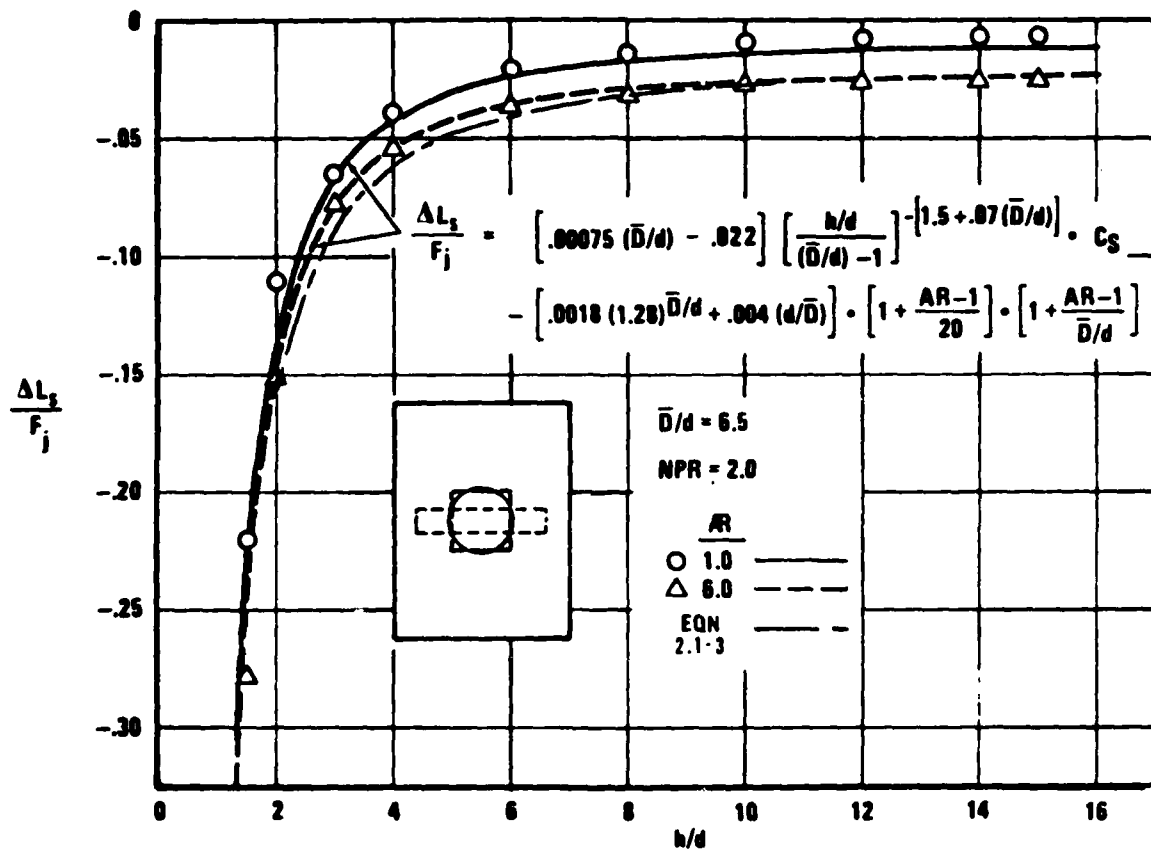Figure 2.1-1 Free-Air Suckdown with Rectangular Jets

Figure 2.1-2 Suckdown of a Rectangular Jet –
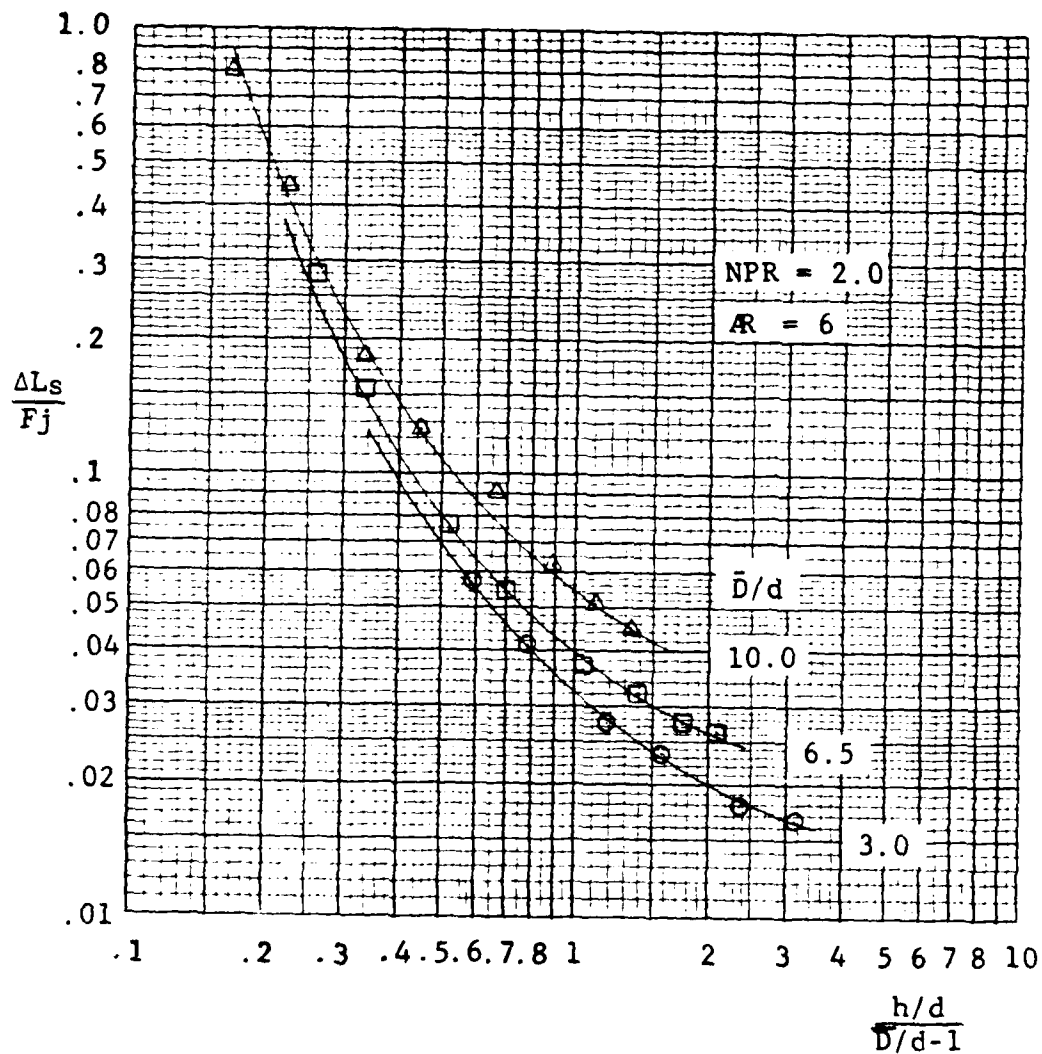Correlation of Test-to-Theory

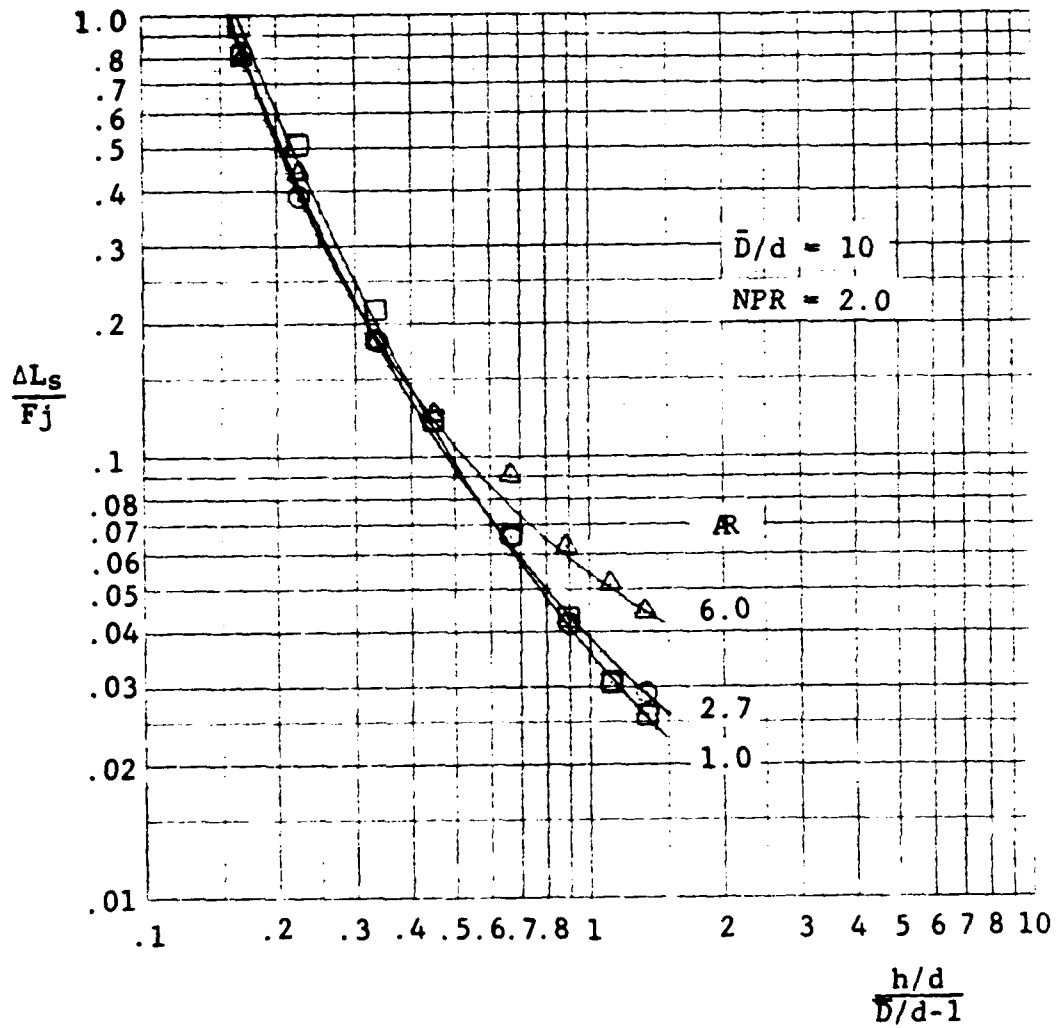Figure 2.1-3 Effect of $\bar{D}/d$ on Rectangular Nozzle Suckdown

Figure 2.1-4 Suckdown with Rectangular Jets of Varied Æ

and is depicted in Figure 2.1-2.

The total suckdown for a configuration can then be determined by adding the free-air suckdown to the altitude dependent suckdown at each height of computation.

$$\frac{\Delta L_S}{F_j} = \frac{\Delta L_S - \Delta L_{S\infty}}{F_j} + \frac{\Delta L_{S\infty}}{F_j} \tag{2.1-5}$$

By definition, the suckdown for a configuration with more than one nozzle is obtained by calculating the individual suckdown for each nozzle and then summing and weight averaging by thrusts, that is

$$\frac{\Delta L_S}{F_j} = \sum_{i=1}^{N} \left(\frac{\Delta L_S}{F_j}\right)_i (F_j)_i \bigg/ \sum_{i=1}^{N} (F_j)_i \tag{2.1-6}$$

2.2 NET FOUNTAIN BUOYANCY

The development of the empirical terms to predict fountain buoyancy required a large data base. In order to gather a sufficient spectrum of test data, it was determined that the selected configurations should resemble a range of planform sizes and shapes employing rectangular nozzles varying in number, AR, NPR and nozzle location. To cover these needs, the configurations shown in Figure 2.2-1 were picked as reasonable test vehicles for parametric variations of the above variables. Appendix A defines these model configurations used during the test phase of the program and also presents the test data acquired. This data formed the basis to develop the fountain effects of typical V/STOL aircraft.

Since each test configuration was designed with a specific class of V/STOL aircraft in mind, it becomes necessary to be conscious of the configuration dependency that accompanies the various sets of fountain lift data. The prediction techniques used to study a particular aircraft should include the selection of the most appropriate set of data from this section based on configuration similarity.

The experimental method of Ref. 11 was used to take force measurements of $\Delta L/F_j$ upon the planforms. For each configuration $\Delta L_f/F_j$ was obtained by subtracting the calculated suckdown from the $\Delta L/F_j$ obtained from the balance data, i.e.,

$$\Delta L_F/F_j = \Delta L/F_j - \Delta L_S/F_j \tag{2.2-1}$$

Since the parameter $\Delta L_F/F_j$ includes interference effects as well as fountain forces, it is noted that negative $\Delta L_F/F_j$ exist for some configurations at certain altitudes. These negative forces may also become more positive as altitude increases because of a reduction in the interference effects.

To determine the effect of fuselage contour and lift improvement devices (LIDs), all configurations were tested with and without LIDs, and with fully contoured fuselage sections. The fuselage contour was varied on Configurations 2B, 3B and 4B.
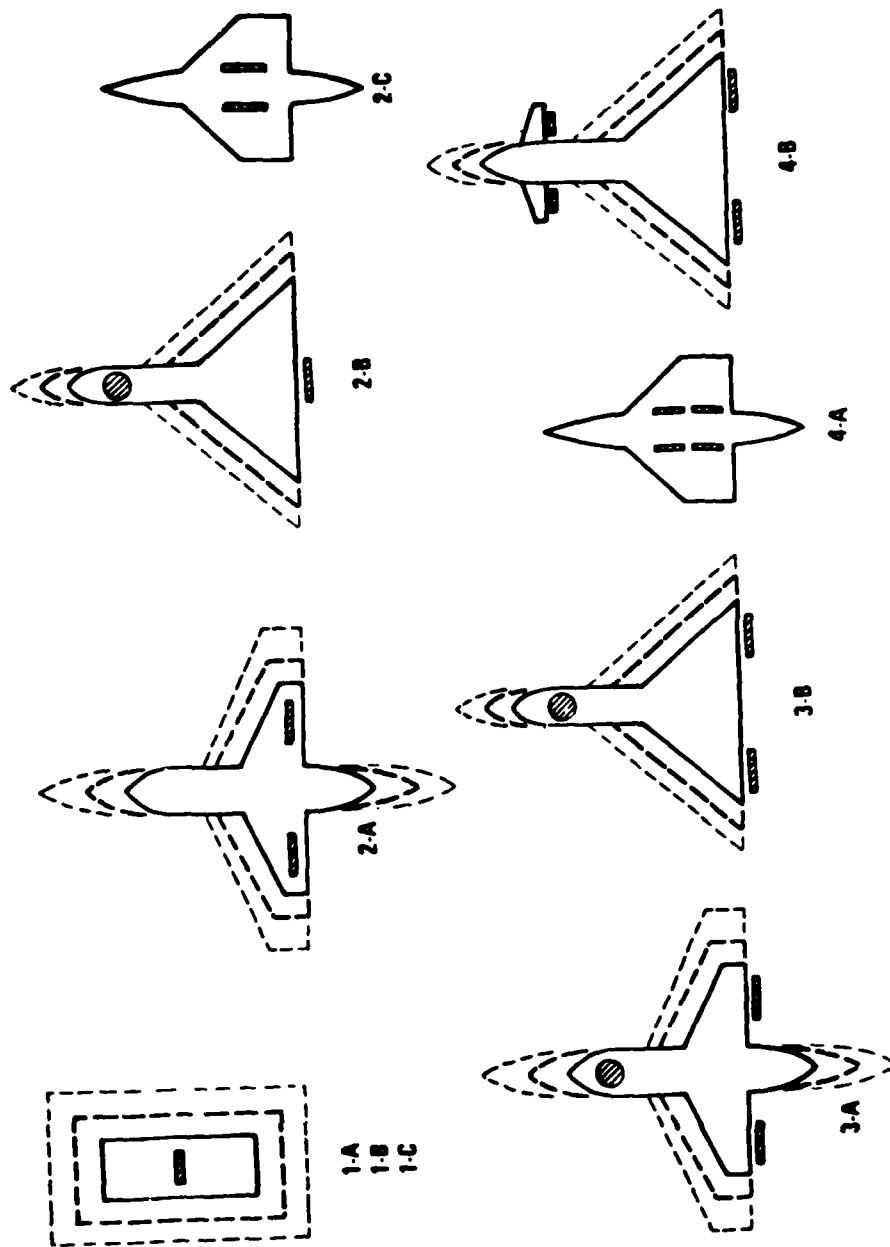
Figure 2.2-1 Rectangular Jet Test Configurations

The effect of a V/STOL aircraft hovering in a crosswind environment was also investigated. Configurations 2B, 3B and 4B were tested with a 25 knot direct crosswind. The influence of the crosswind produced a negligible effect on induced lift since the velocity of the jets dominated any effect produced by the crosswind.

2.2.1 Two-Jet Fountain Lift

Fountain lift data for configurations 2-A, 2-B and 2-C have been developed according to the procedure noted in Section 2.2. The data for Configurations 2-A and 2-B are presented in Figures 2.2-2 through 2.2-6 as $\Delta L_f/F_j$ versus $(\bar{D}/d)wa$, where $(\bar{D}/d)wa$ is the correlating parameter used to relate planform size to nozzle size. (Section 3.1.3 details this parameter). Each graph represents the fountain lift force developed over a range of planform sizes and covering various planform altitudes above the ground. These plots have been produced for a particular nozzle AR and configuration type. This requires the user of this data to extract the fountain forces at the value of $(\bar{D}/d)_{wa}$ desired for the ARs tested. To determine the fountain forces at the proper nozzle AR it then becomes necessary to cross-plot $\Delta L_F/F_j$ versus AR at the desired value of $(\bar{D}/d)_{wa}$. Configuration 2A was tested at AR = 1, 2.7 and 6 over a wide range of $(\bar{D}/d)_{wa}$, whereas Configuration 2-B was tested at AR = 1 and 2.7, the likely range for this type configuration.

Configuration 2-C is a specialized planform shape representing an ejector system. This model was tested at AR = 6 and $(\bar{D}/d)_{wa}$ = 3, therefore, the fountain lift data is presented on Figure 2.2-7 as $\Delta L_F/F_j$ versus h/d_{wa} for the single AR and planform size.

2.2.2 Three-Jet Fountains

The fountain lift data for Configurations 3-A and 3-B is presented on Figures 2.2-8 through 2.2-12 in the manner described in Section 2.2.1. Configuration 3-A, being a variant of 2-A, was tested at AR = 1, 2.7 and 6 while Configuration 3-B, which was a variant of 2-B, was tested at AR = 1 and 2.7.

2.2.3 Four-Jet Fountains

The fountain lift data for Configuration 4-B is shown on Figures 2.2-13 through 2.2-15. The data was developed at AR = 1, 2.7 and 6, consistent with Section 2.2.1.

Configuration 4-A is a modification of 2-C with four nozzles (AR = 2.7) replacing the two existing nozzles (AR = 6.0). The same planform size was tested at identical NPR and altitudes. The fountain data demonstrated that the close proximity of the nozzles caused this model to perform identical to Configuration 2-C, however, effects of AR can be deduced from Configuration 4-A. The jet merging of the fore and aft nozzles was completed before an altitude of h/d_{wa} = 1.5 was reached. Therefore, the fountain lift data for Configuration 2-C also applies to Configuration 4-A.

Figure 2.2-2 Fountain Lift - Configuration 2-A, $\mathbb{R} = 1.0$

Figure 2.2-3 Fountain Lift - Configuration 2-A, $\mathcal{R} = 2.7$

Figure 2.2-4 Fountain Lift - Configuration 2-A, $\mathcal{R} = 6.0$

Figure 2.2-5 Fountain Lift - Configuration 2-B, $A\!R$ = 1.0

Figure 2.2-6 Fountain Lift - Configuration 2-B, $A\!R$ = 2.7

Figure 2.2-7   Fountain Lift - Configuration 2-C

Figure 2.2-8   Fountain Lift - Configuration 3-A, $R = 1.0$

Figure 2.2-9 Fountain Lift - Configuration 3-A, $R = 2.7$

Figure 2.2-10 Fountain Lift - Configuration 3-A, $A\!R$ = 6.0

Figure 2.2-11 Fountain Lift - Configuration 3-B, $\mathbb{R} = 1.0$

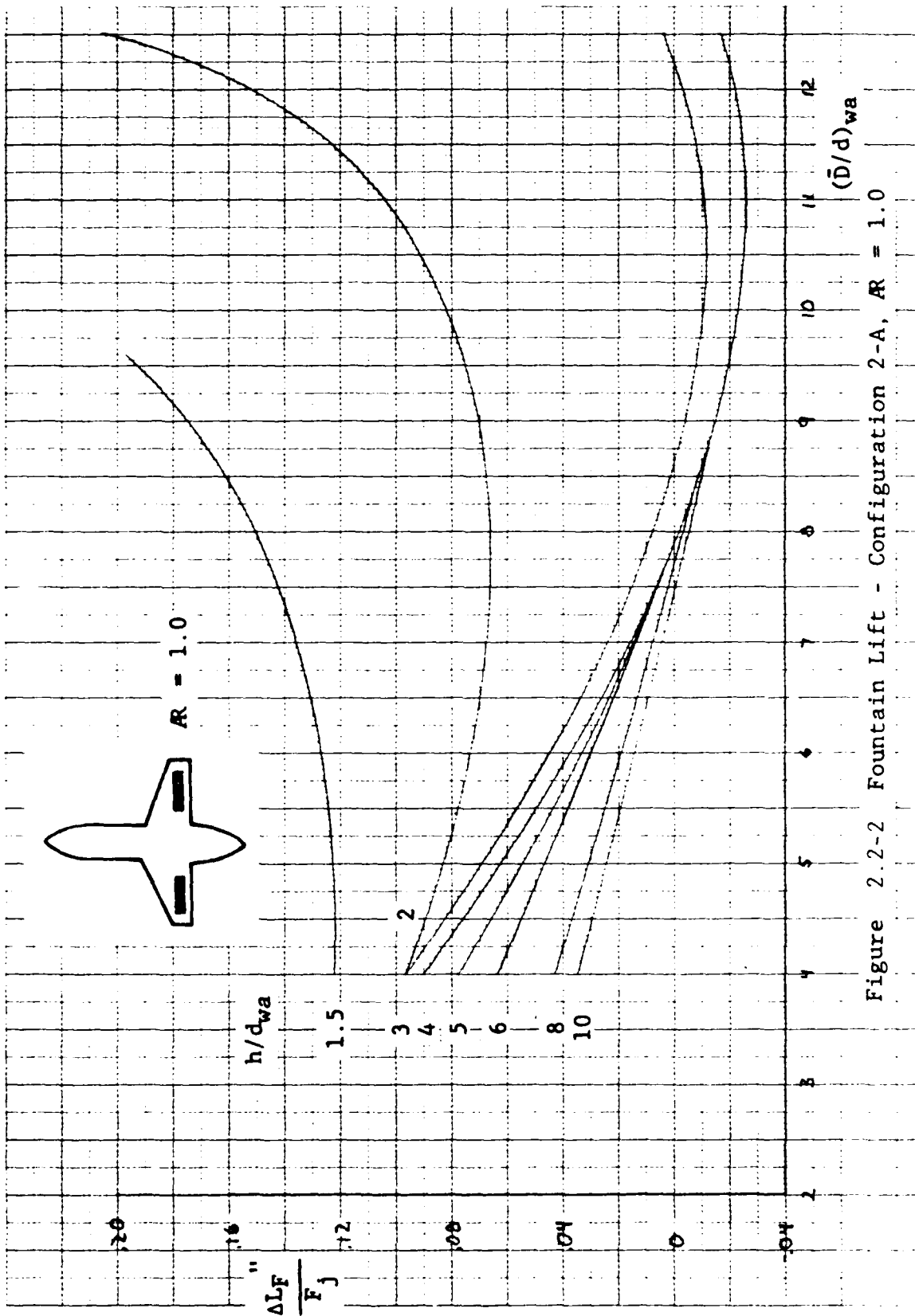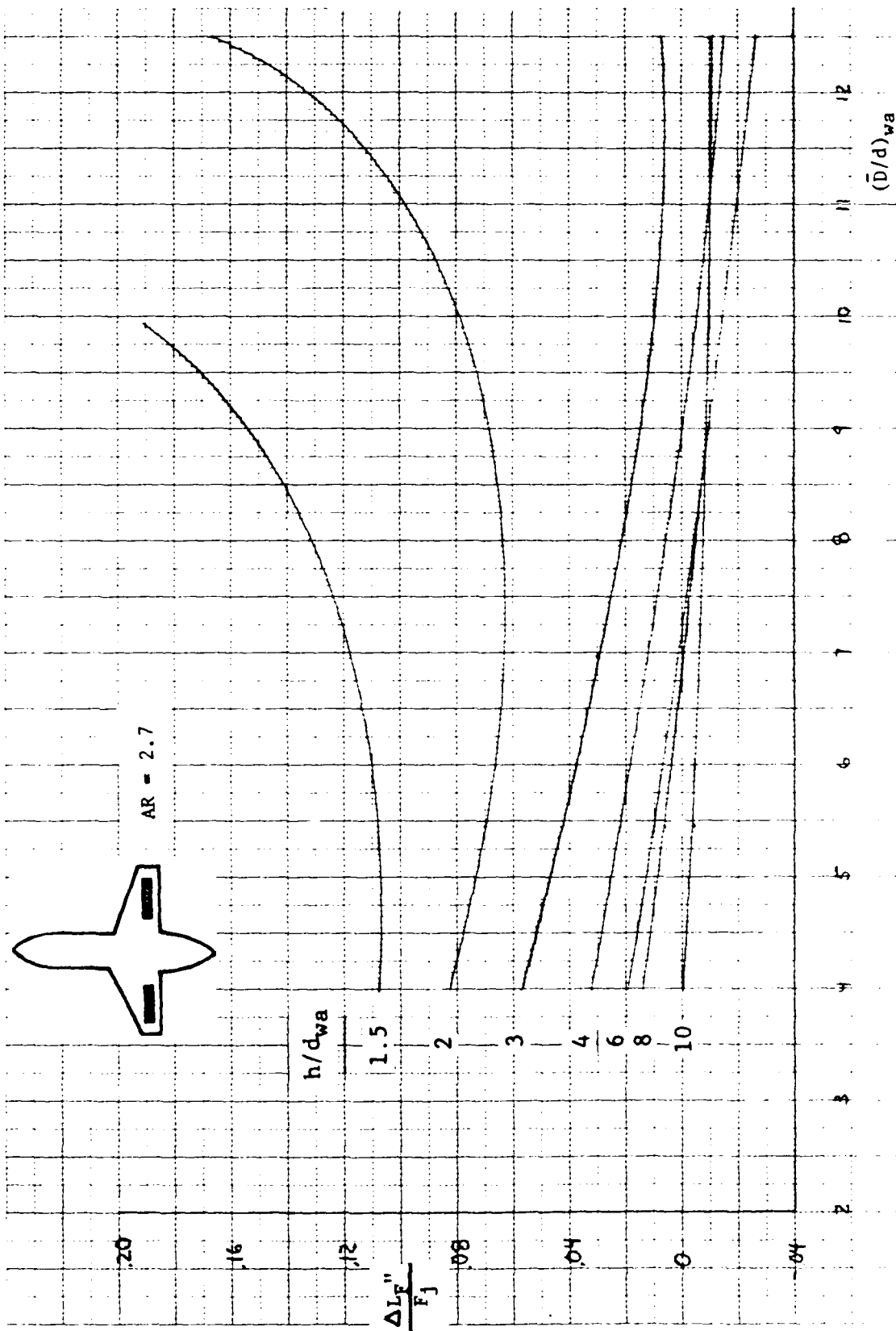Figure 2.2-12 Fountain Lift - Configuration 3-B, $\mathcal{R}$ = 2.7
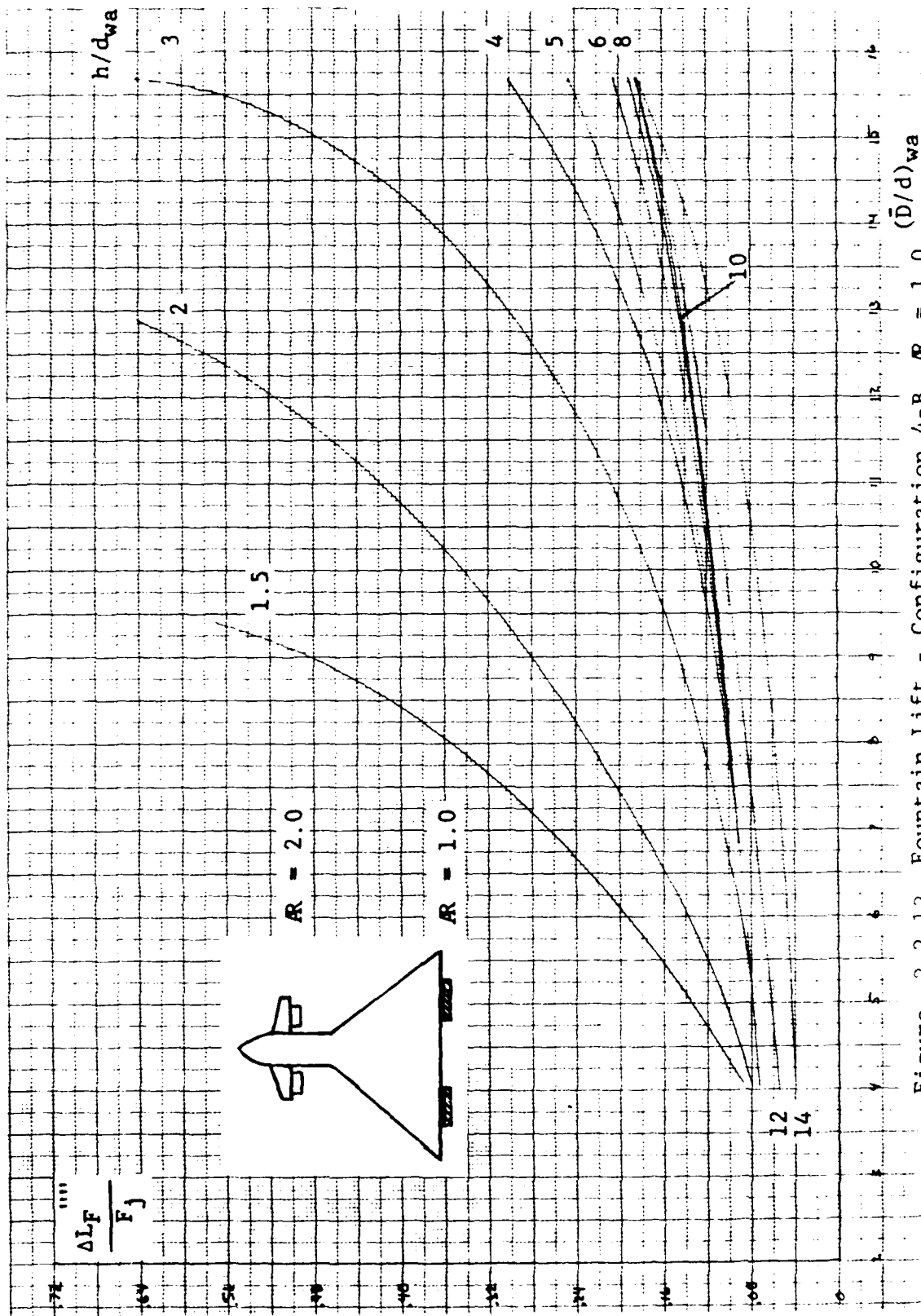
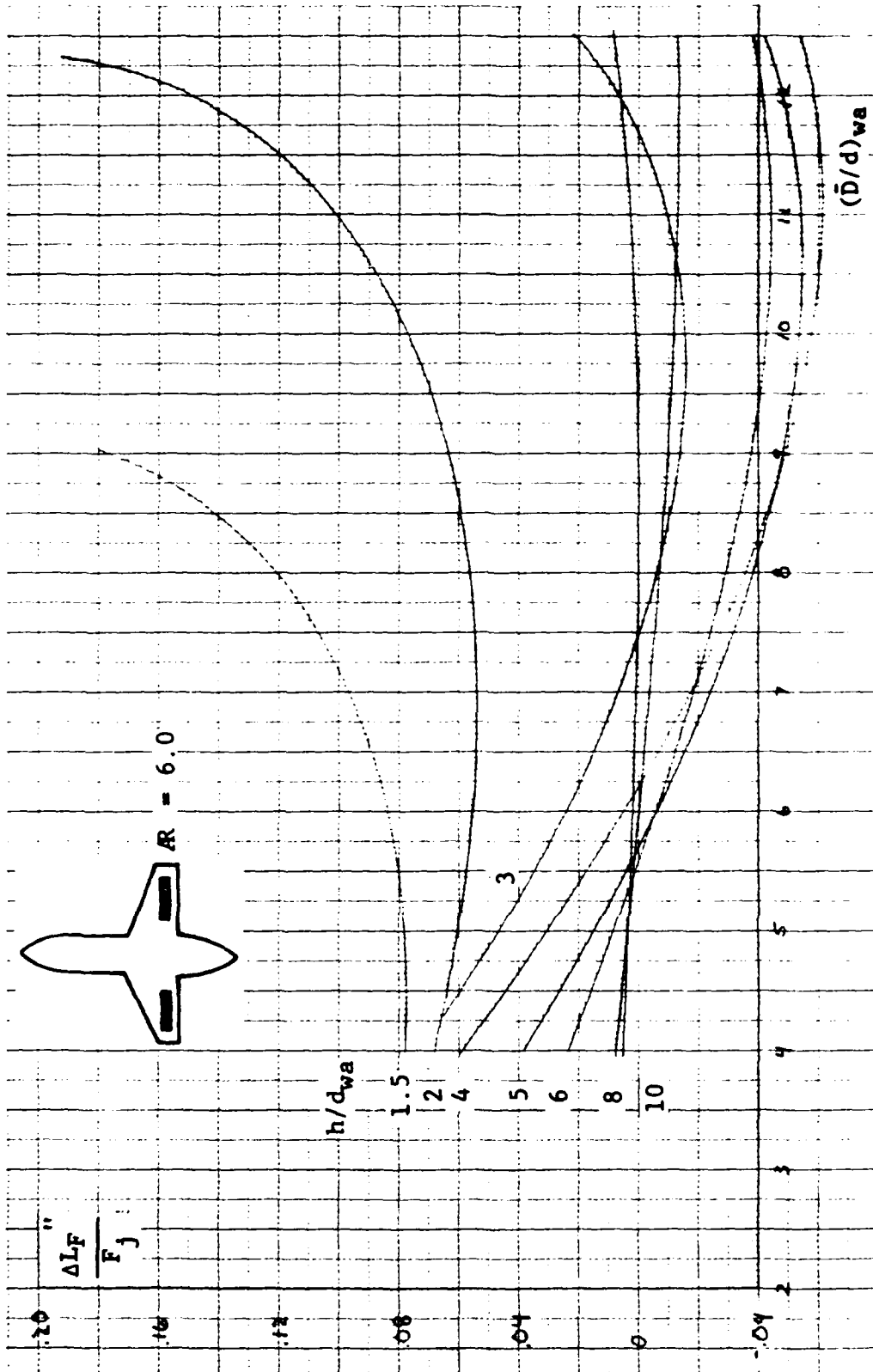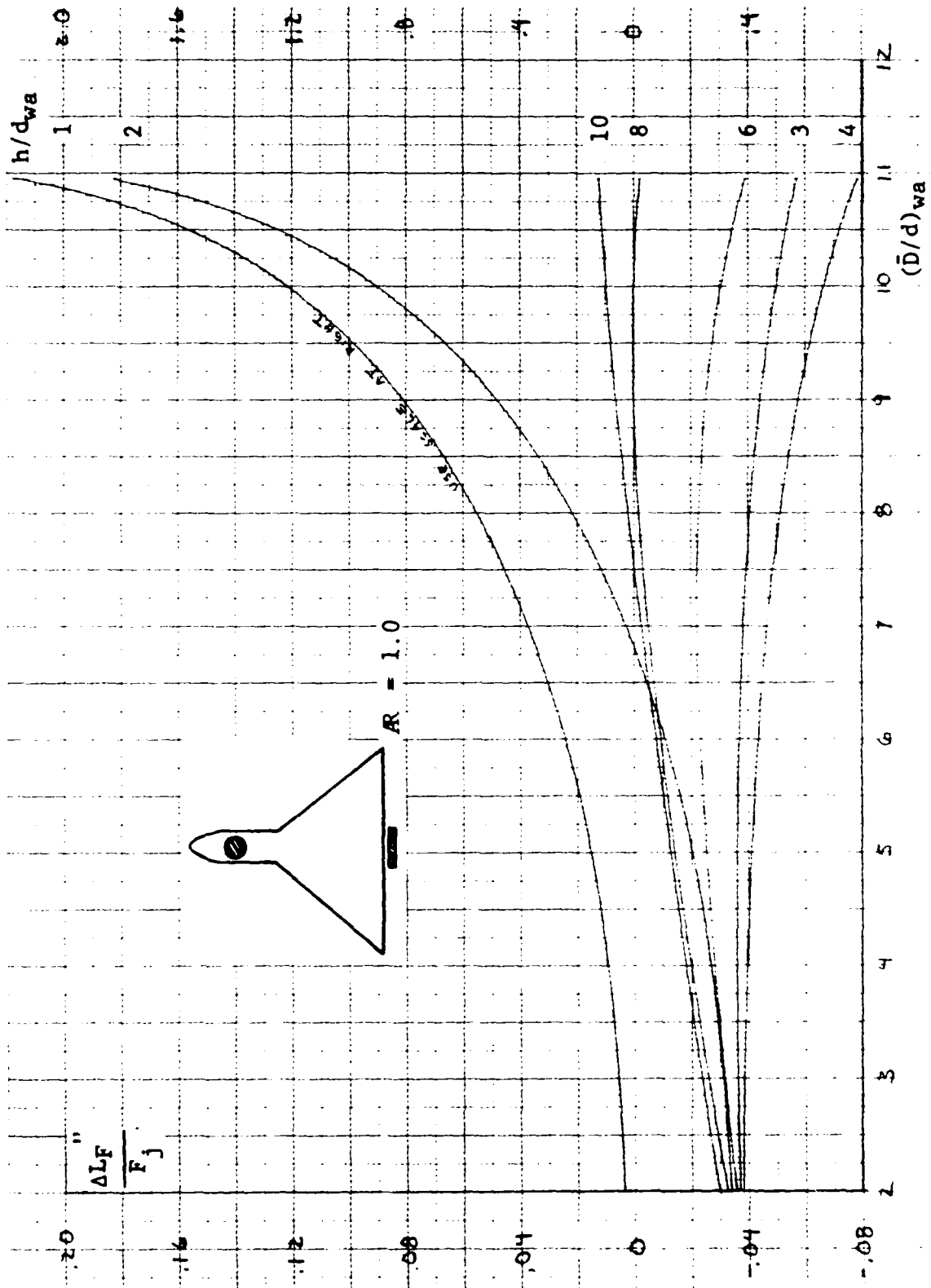Figure 2.2-13 Fountain Lift - Configuration 4-B, $AR = 1.0$
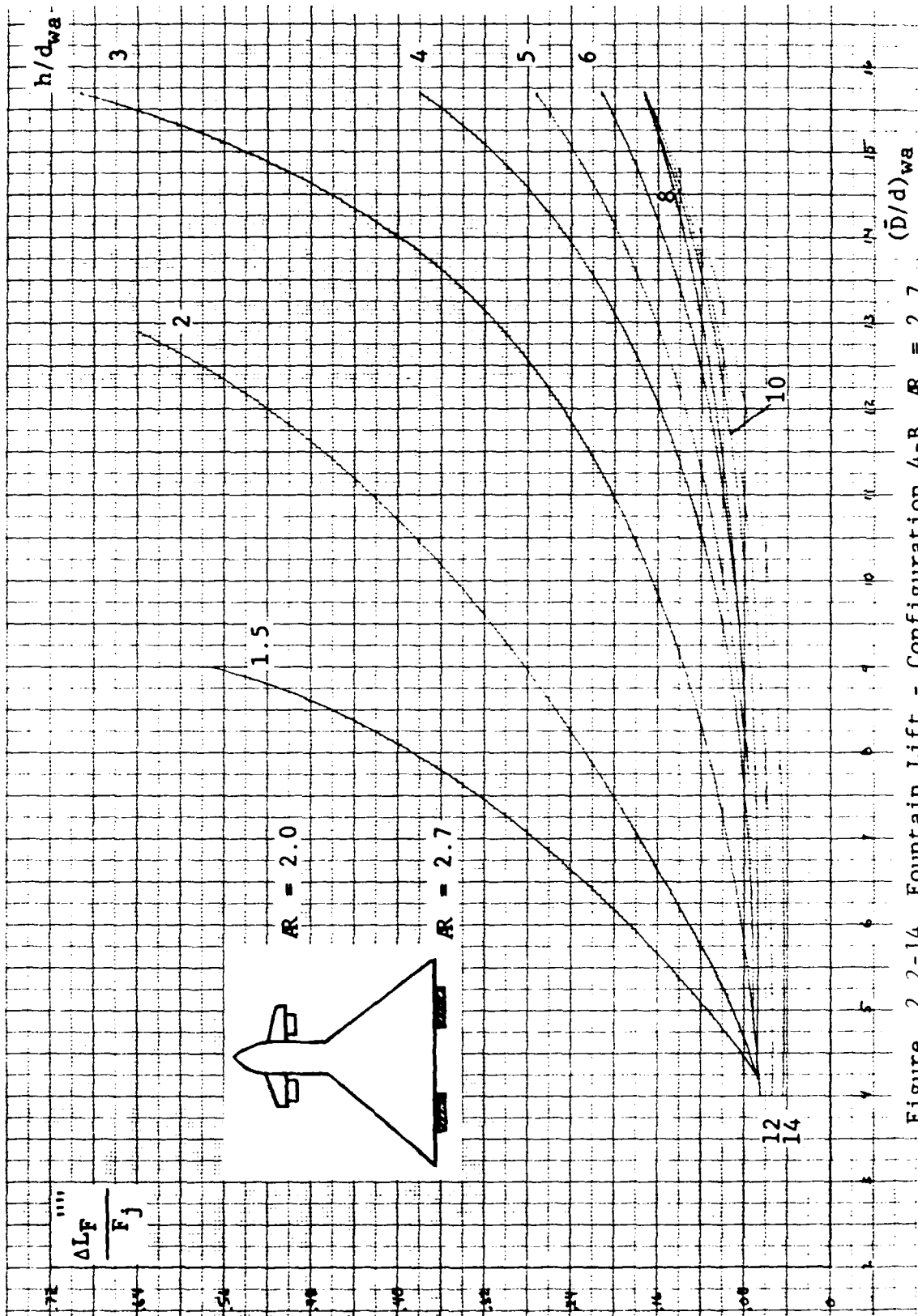
Figure 2.2-14 Fountain Lift - Configuration 4-B, $\mathbb{R} = 2.7$
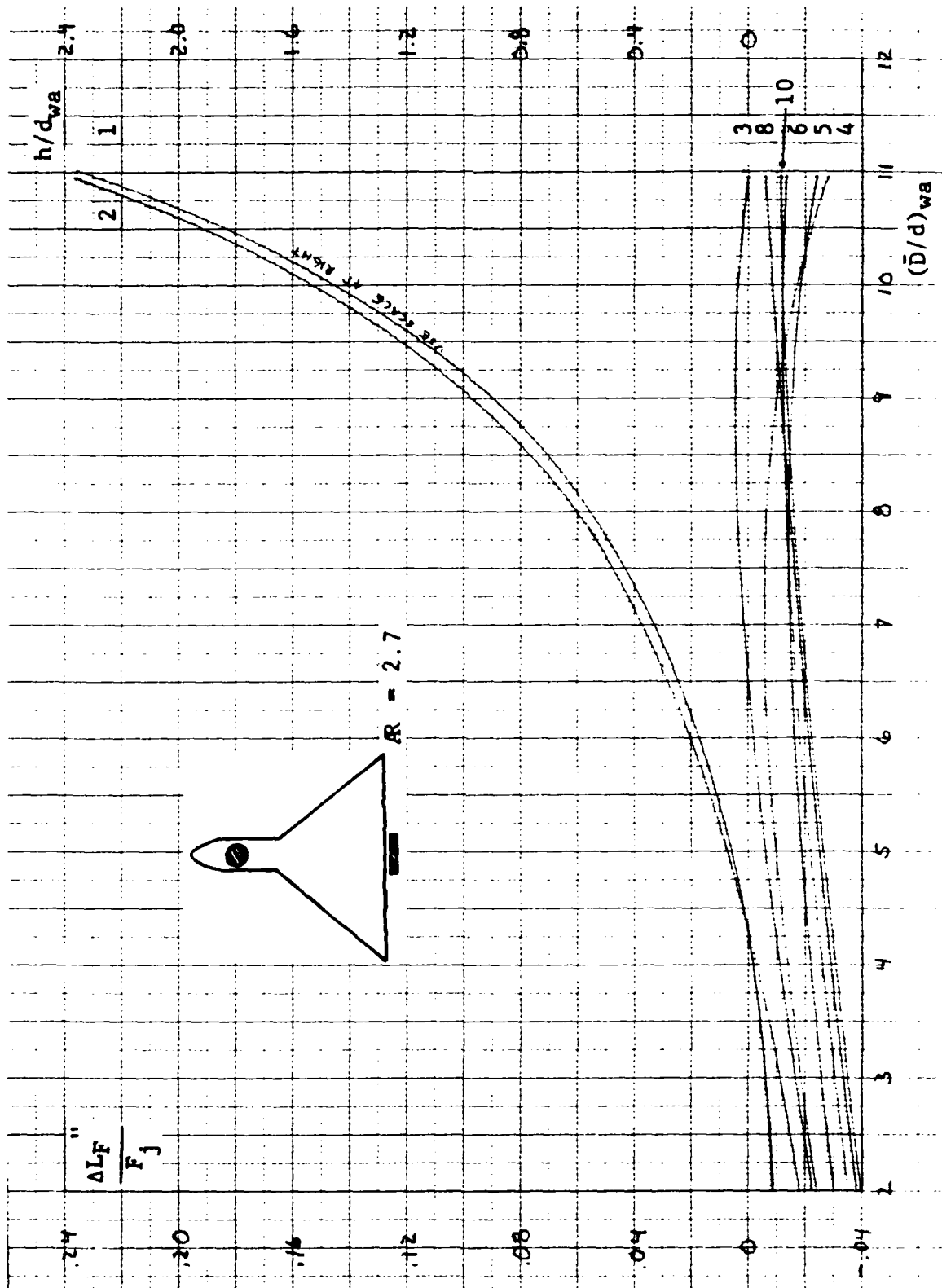
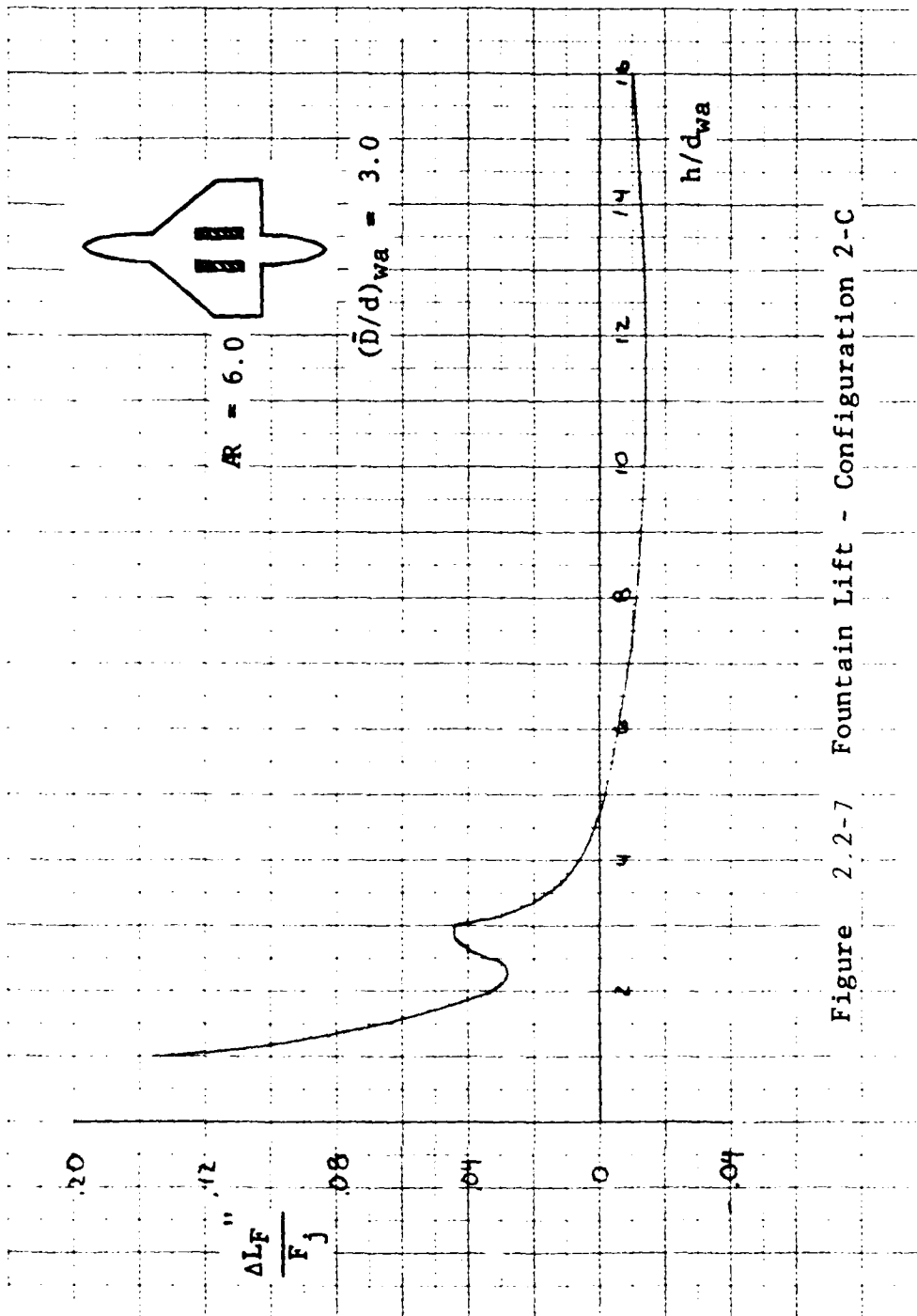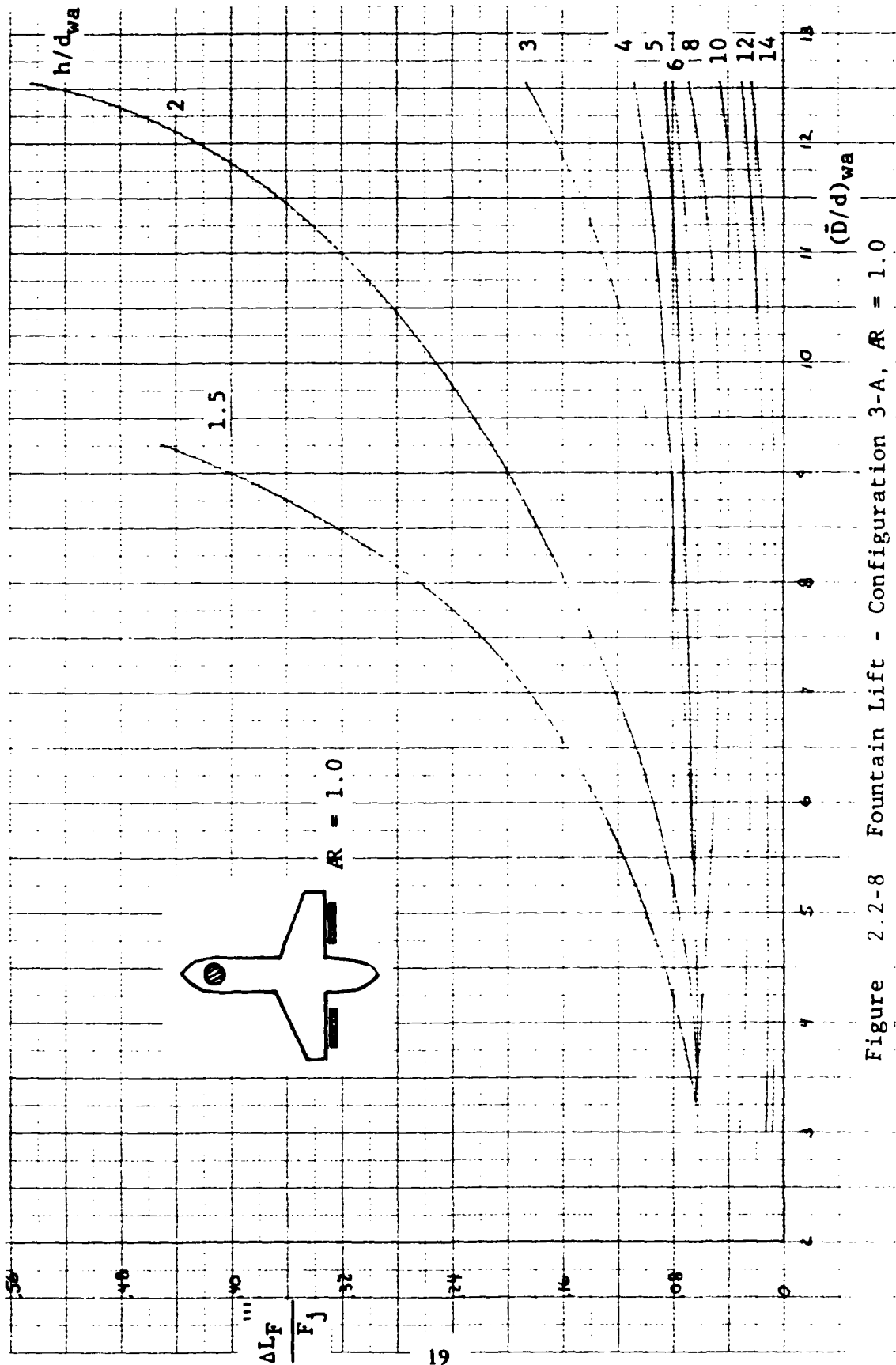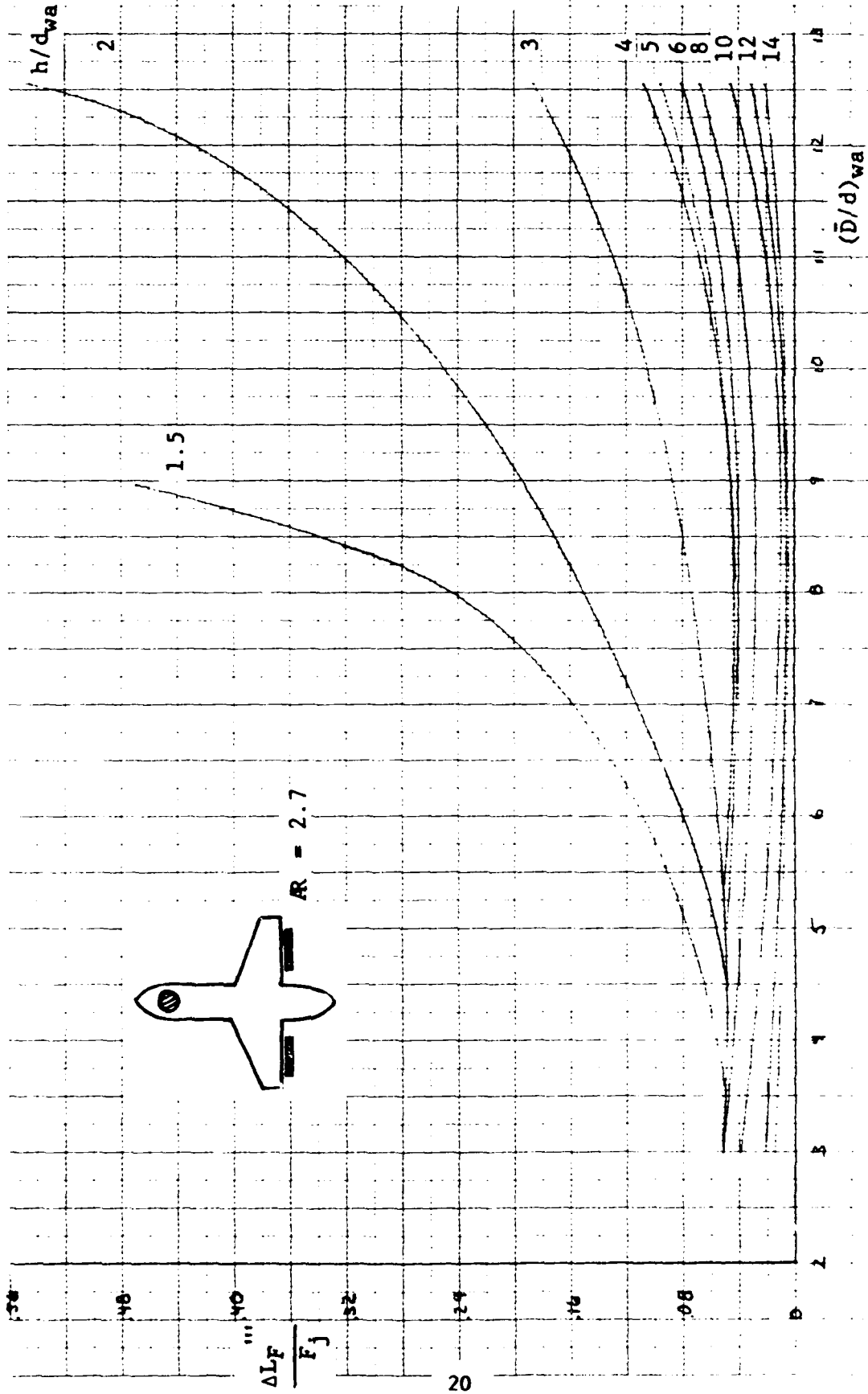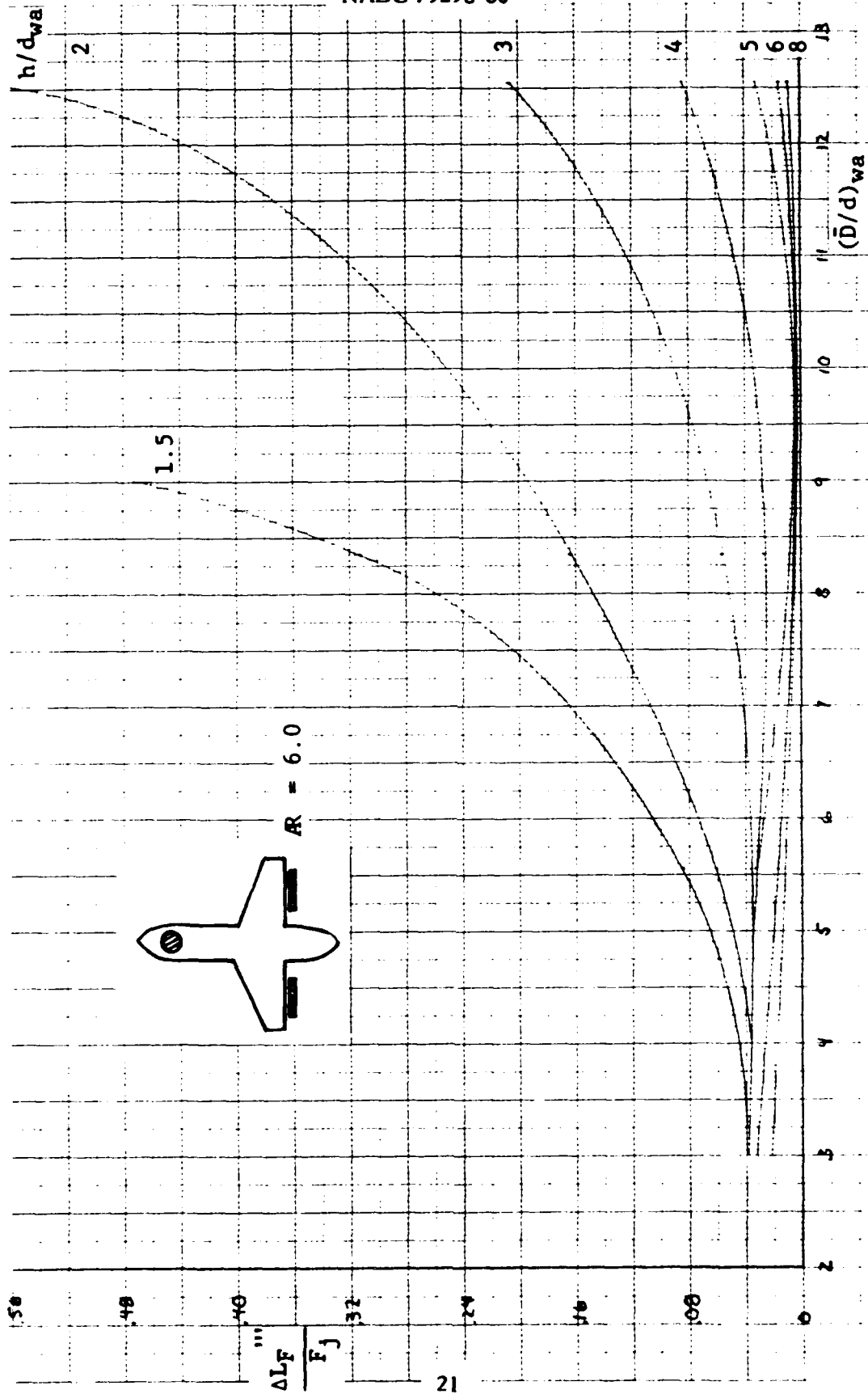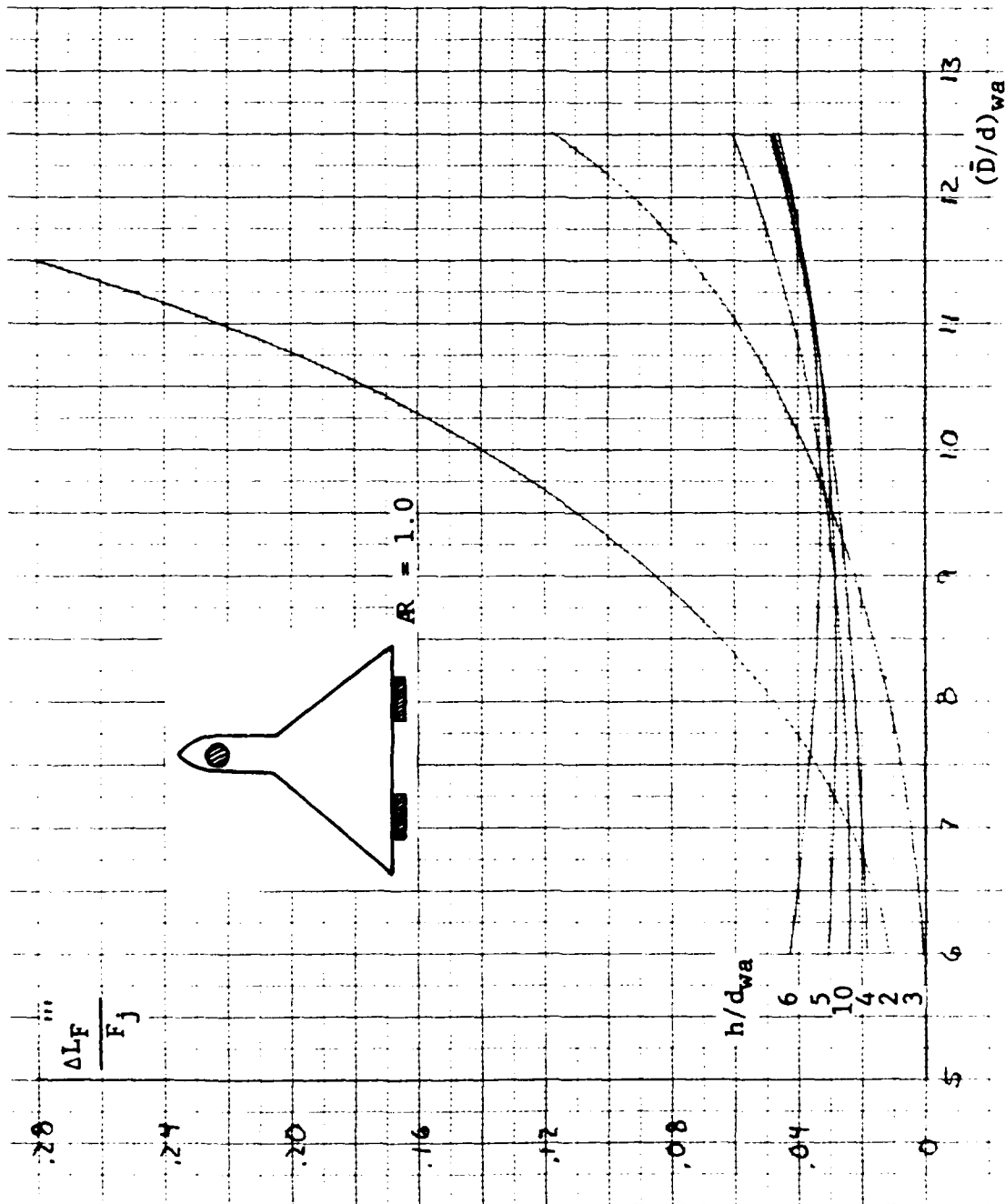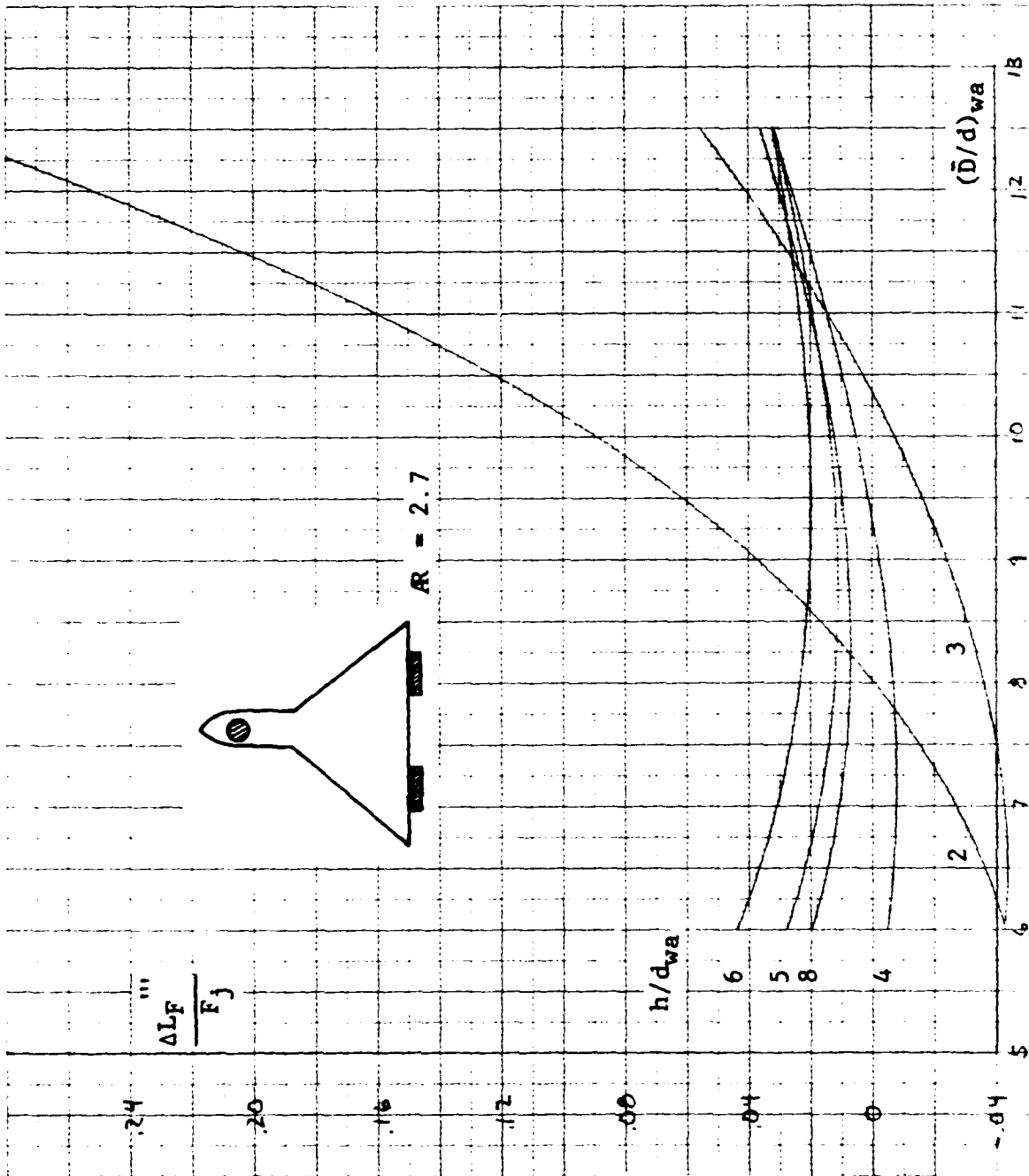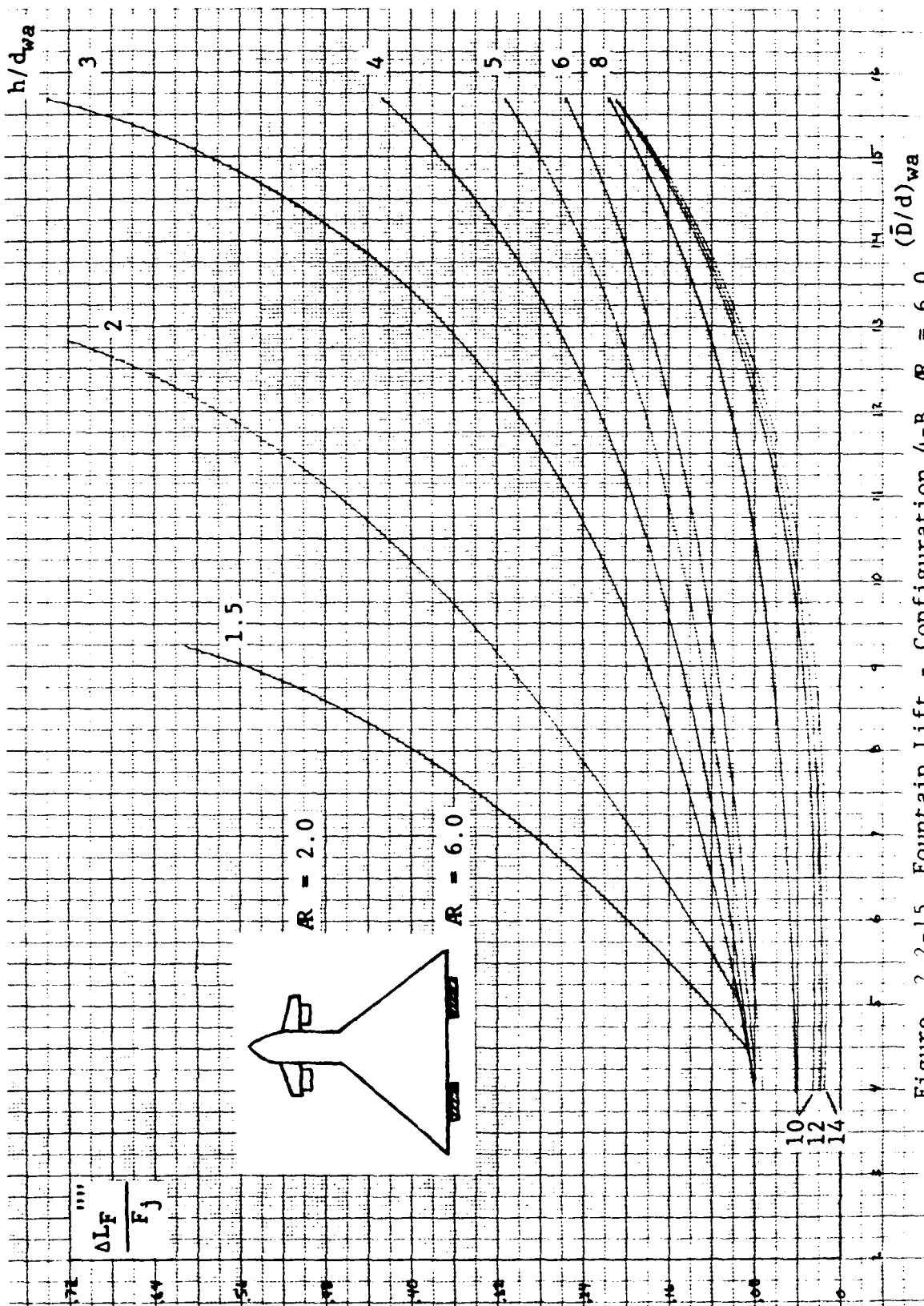Figure 2.2-15 Fountain Lift - Configuration 4-B, $AR = 6.0$

26

2.3 EXTRAPOLATION COEFFICIENTS

Equation 2.0-2 is useful only for calculating ground-induced forces on flat-plate models at low altitudes with nozzle exhaust NPR = 2.0. In order to extend the application of the methodology, a number of extrapolation coefficients were developed in Ref. 16 to account for planform contour, NPR, etc. Equation 2.0-2 now takes the form

$$\frac{\Delta L}{F_j} = \frac{1}{F_j} \left[c_S \Delta L_S + c_F \Delta L_F \right] \tag{2.3-1}$$

The values of the extrapolation coefficients, C_S and C_F, used for computation of the suckdown and fountain forces associated with rectangular jets were found to be identical to those defined in Ref. 16. The testing conducted employing rectangular nozzles was used to confirm those results and as one might expect, the effects of NPR, jet merging, planform contour or LIDs does not vary once the basic fountain strength is set.

2.3.1 Suckdown Extrapolation Coefficient C_S

Work on the effect of turbulence on suckdown (Ref. 11) has shown (1) the possibility of a large-scale effect and (2) a pronounced effect of NPR on suckdown. Therefore, let

$$C_S = C_{S1} \cdot C_{S2} \tag{2.3-2}$$

where C_{S1} is the extrapolation coefficient to account for the difference between model scale and full scale and C_{S2} for variations in NPR from 2.0.

Presently, General Dynamics is undergoing testing and analysis to quantify C_{S1} satisfactorily. It is being retained in the meanwhile as

$$C_{S1} = 1.0 \tag{2.3-3}$$

The coefficient, C_{S2}, as developed in Ref. 12 and confirmed in these tests is given by

$$C_{S2} = \begin{array}{l} 1.173 - .2495 \ \ln \ (NPR) \ \text{if NPR} \leq 2 \\ 1.061 - .0889 \ \ln \ (NPR) \ \text{if NPR} \geq 2 \end{array} \tag{2.3-4}$$

2.3.2 Fountain Extrapolation Coefficient C_F

The fountain coefficient is a little more complex than the suckdown coefficient in that, not only are there terms to reflect scale and NPR, but also terms to account for the effect of jet merging before impact with the ground plane, planform contour, and LIDs. Therefore,

$$C_F = C_{F1} \cdot C_{F2} \cdots C_{F5} \tag{2.3-5}$$

where

C_{F1} is the effect of scale (interim value = 1.0)

C_{F2} is the effect of NPR

27

C_{F3} is the effect of jet merging

C_{F4} is the effect of planform contour

C_{F5} is the effect of LIDs.

For precisely the same reason that $C_{S1} = 1.0$, also $C_{F1} = 1.0$; it is reserved for use when the effect of scale becomes better known.

The effect of NPR on fountain lift as developed in Ref. 11 and confirmed during this test program is given by

$$C_{F2} \begin{array}{l} = .736 \ \ln \text{NPR} + .481 \ \text{if NPR} \leq 2 \\ = .035 \ \ln \text{NPR} + .930 \ \text{if NPR} \geq 2 \end{array} \qquad (2.3\text{-}6)$$

In the case where NPR varies from nozzle to nozzle, the C_{F2}'s are thrust averaged and

$$C_{F2} = \sum_{i=1}^{N} (C_{F2} \ F_j)_i \Big/ \sum_{i=1}^{N} (F_j)_i \qquad (2.3\text{-}7)$$

For any aircraft configuration with more than one nozzle, as altitude increases jets begin to merge so that the character of the fountains change. As an example, a three-jet configuration, as it gains altitude, will reach a point where two jets begin to merge (provided, of course, the nozzles are not equidistant apart). When this occurs, the character of the fountain will begin to change from that of a three-jet to that of a two-jet. At still higher altitude, when the two have completely merged, the fountain will become entirely a two-jet fountain. For many aircraft, such mergings can begin quite close to the ground. Previous work, Ref. 16, has shown that jet merging is a function of nozzle spacing, d_E. Figure 2.3-1 defines this effect on fountain lift.

The cross-sectional shape or contour of a planform has a very strong influence on the amount of available fountain lift that is actually recovered by the planform. In the case where the edges of the planform are rounded, the fountain, after impingement, will then tend to flow, Coanda-style, around the planform (Figure 2.3-2). The negative pressures, which are induced upon the planform and attend this turning, lower the lift. Herein, C_{F4} is shown on Figure 2.3-3. Interestingly, C_{F4}, for two-jet fountains, is not a function of altitude but is very strongly dependent on contour. C_{F4} for three- and four-jet fountains is shown in Figure 2.3-4. Here, C_{F4} is a function of altitude but is not as sensitive to the contour as is the two-jet case. Undoubtedly, the difference is due to the different fountain structure.

All of the configurations were tested with and without LIDs. Figures A-2 through A-5 describe the LIDs tested. By reversing the direction of the fountain flow (Figure 2.3-5), a LID is able to amplify the fountain lift. The effect of a complete longitudinal and transverse LID system (i.e., the LIDs form a closed box) is to nearly double the fountain lift; whereas, if the LIDs are left open on two ends, the lift increases by about 50%. Ref. 16 indicated some other characteristics of LIDs.

1. Except at very low altitudes, the depth of the LIDs is not particularly important.

28

$$h_m = \frac{d_E}{2 \tan 20} = 1.374 \ d_E$$

$(h-h_m) \ / \ d_E$
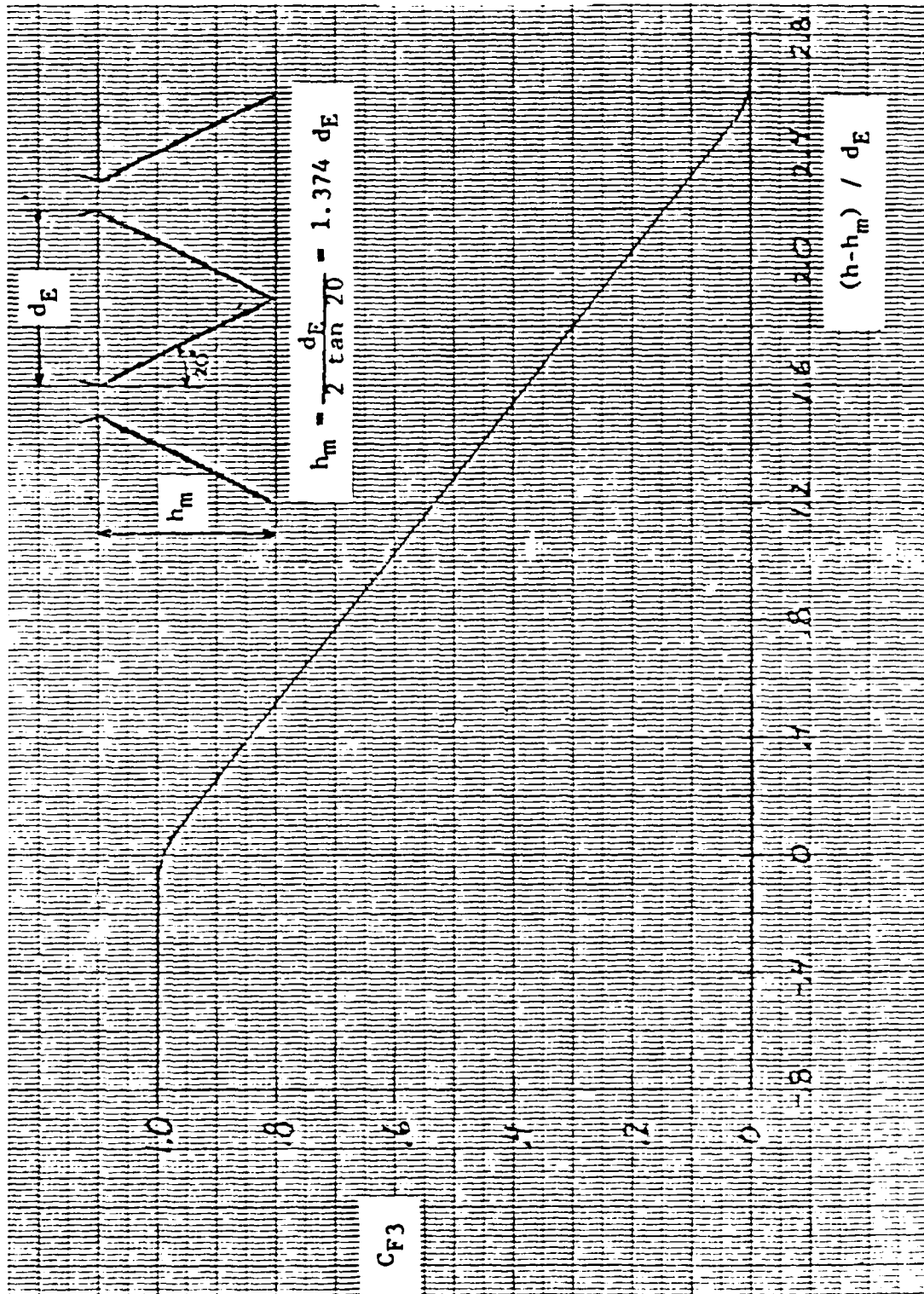
Figure 2.3-1 Effect of Jet Merging, On Fountain Lift
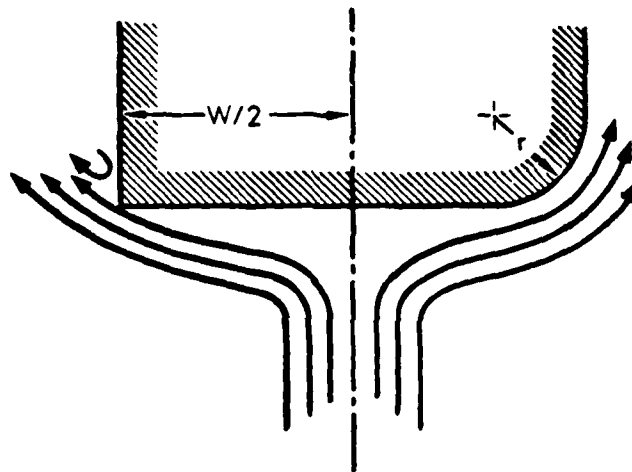
Figure 2.3-2   Fountain/Semi-Rounded Fuselages
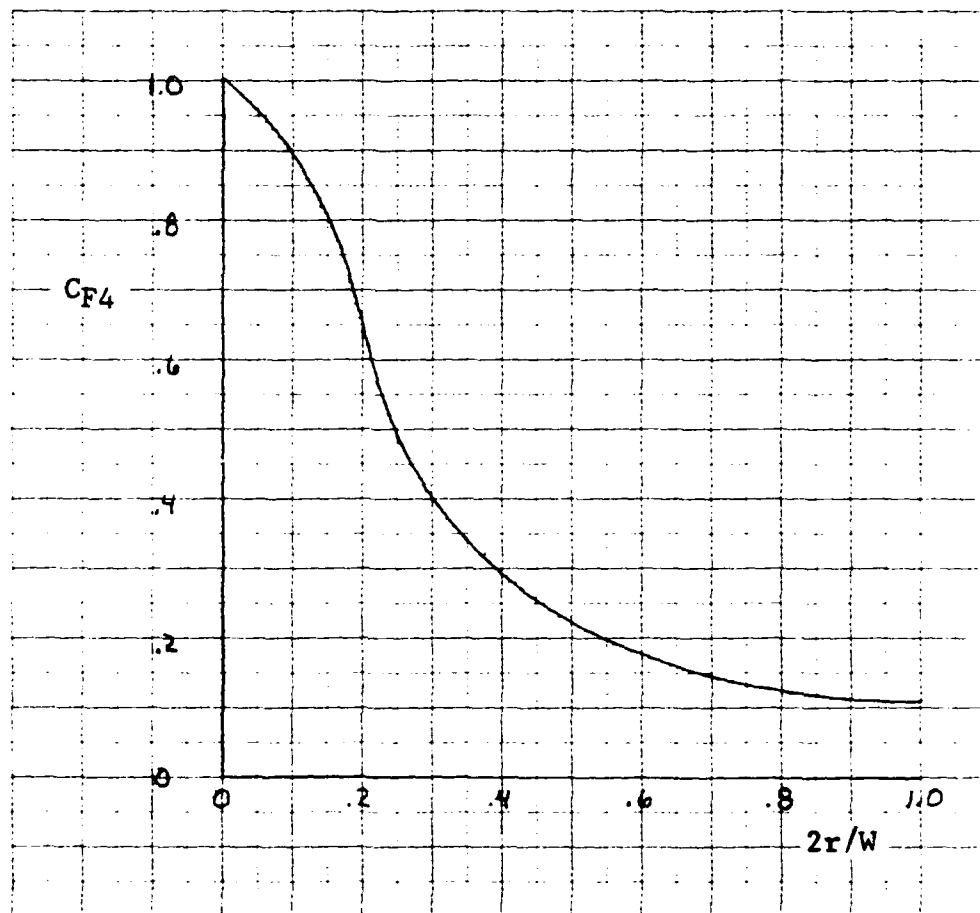
Figure 2.3-3 Effect of Planform Contour - 2 Nozzle Case
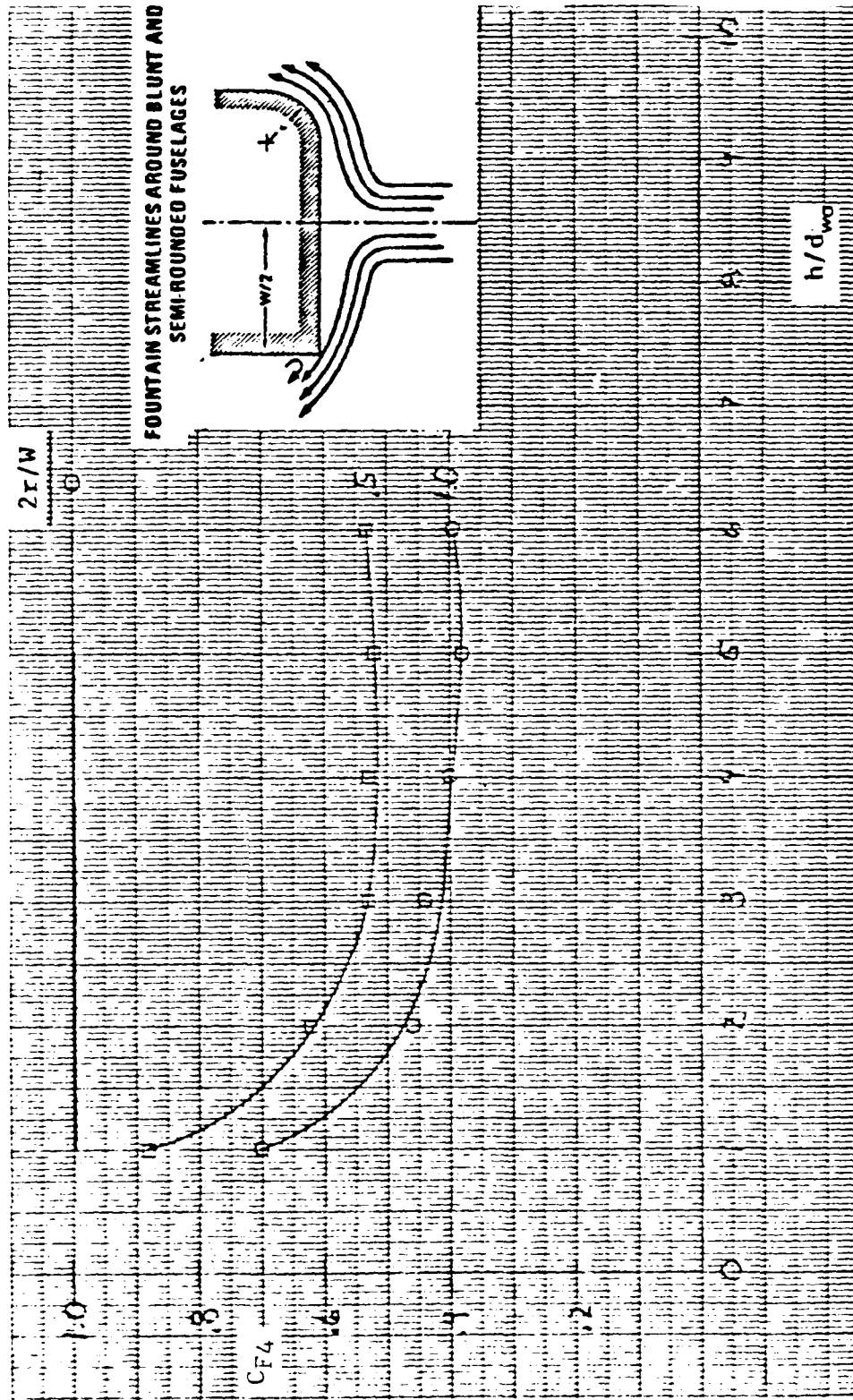
Figure 2.3-4 Effect of Planform Contour - 3 and 4 Nozzle Case
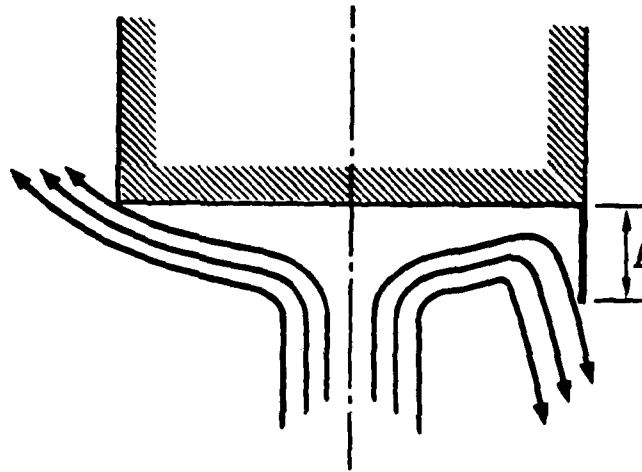
Figure 2.3-5   Fountain Streamlines Around A Blunt Fuselage and A LID

2. LIDs should always be placed interior to the nozzles; exterior LIDs interfere with the entrainment of ambient air at low altitudes to such an extent that suckdown is amplified over and above the beneficial effect of fountain lift enhancement.

3. In the instance where LIDs do not capture the entire fountain, that portion of the fountain whose lift is enhanced can be determined from geometrical considerations (Subsection 3.1).

In general, the size, shape, and extent of a LID system will be restricted by other considerations in aircraft design. Therefore, the values of C_{F5}, presented in Subsection 3.1, should be regarded as probably optimistic indicators of what can be achieved in practice.

3.0 METHODOLOGY APPLICATION PROCEDURE

Procedures and definitions for application of the method to rectangular jet aircraft are presented in this section. The various correlations derived from empirical methods are intended to cover the hover flight conditions of current V/STOL aircraft employing rectangular jets. The methodology has been developed as a prediction technique in the preliminary design environment and is considered accurate to $\pm 1\%$ of the total lift. The effect of various rectangular nozzle and planform configurations, up to four nozzles are considered.

3.1 PROCEDURE

3.1.1 Total Induced Lift, $\Delta L/F_j$

The induced lift during hover can be separated into two parts, as shown in Equation (3.1-1).

$$\Delta L/F_j = \Delta L_s/F_j + \Delta L_F/F_j \qquad (3.1-1)$$

The first, $\Delta L_s/F_j$, is the suckdown generated by the ambient air that is accelerated toward the aircraft because of entrainment by the exhaust flows, creating a low pressure field under the aircraft and, consequently, a downward force on the planform. The second effect, $\Delta L_F/F_j$, is the buoyant force derived from the impact (if any) of the fountain jet formed by a multiple-nozzle configuration upon the planform.

3.1.2 Tabulation

The various components of induced lift are tabulated in Figure 3.1-1. The three main blocks of the table are

I.   Suckdown
II. Fountain Lift
III. Induced Lift

The general arrangement of the table should follow a vertical setup for computing each column as a function of planform height above the ground. This may be done in various ways. As depicted in the example table, a common reference height is listed in nozzle diameters. Because many configurations have multiple nozzles (that are not always equal in equivalent diameter), the approach used here is to normalize altitude by equivalent single nozzle diameter, D_e. However, there are two additional normalizing diameters that are used in the methodology, namely, the individual equivalent nozzle diameter, d, (used in suckdown calculations) and the thrust weighted diameter, d_{wa}, Subsection 3.1.3, (used in fountain lift calculations). It is necessary to use extreme care in setting up a tabulation sheet to reflect the equivalencies between the various altitude normalizations.

A listing of the necessary variables of the problem should be placed on the table for quick reference. The authors have listed those items of primary need on the example table, though more could be added depending on the specific configuration under study.

$\frac{h}{d}$	$\frac{h}{D_e}$	$\frac{\Delta L_S - \Delta L_{S_0}}{F_j}$	$\frac{\Delta L_{S_0}}{F_j}$	$\frac{\Delta L_S}{F_j}$	C_{F_2}	$\frac{h-h_m}{d_E}$	C''_{F_3}	C_{F_4}	$\frac{\Delta L''_F}{F_j}$	$\frac{\Delta L_F}{F_j}$	$\frac{\Delta L}{F_j}$
		$\bar{D}$ (in)									
		d (in)									
		$\bar{D}/d$									
		C_{S_a}									
		d_E									
		$2r/W$									
1.41	1										
2.12	1.5										
2.83	2										
4.24	3										
5.66	4										
7.07	5										
8.49	6										
9.90	7										

SUCKDOWN + FOUNTAIN LIFT = INDUCED LIFT

Figure 3.1-1   Calculation of Induced Lift

The first block is rather straightforward and similar in most configurations. The suckdown will be calculated individually for each nozzle along with the free-air suckdown, $\Delta L_{s\infty}/F_j$. Block II sets up the method for calculating fountain lift. Block II will be the most difficult to set up since a four-jet configuration can produce the fountain characteristics of a three-jet or two-jet configuration when the planform reaches a height of jet-merging for nozzles that are in close proximity. Therefore, Block II will normally be set up for more than one fountain computation. Block II also accounts for the differences in induced lift from the two-dimensional, clean planform. Here, the effects of planform contour and LIDs are incorporated into the basic fountain effects.

The introduction of a high-wing aircraft or other non-coplanar configuration presents additional difficulties in the computation of induced lift on a hovering V/STOL aircraft. Figure 3.1-2, depicts such a planform at two altitudes above the ground - one measured to wing height (h_w) and a different height to fuselage base (h_f). The method of computation for both nozzle suckdown ($\Delta L_s/F_j$) and fountain lift ($\Delta L_F/F_j$) is affected by this type of configuration. This causes the problem tabulation to be expanded to a two-phase setup, whereby, the calculations for fuselage suckdown and fountain lift use h_f whereas the wing planform uses h_w for its computations of suckdown and fountain lift. These values of suckdown and fountain lift can then be summed; due care must be exercised in the summations to reference the induced forces at the correct planform altitude being used in the tabulation.

3.1.3 Suckdown

The equations, parameters, and methods for computing nozzle suckdown are described below:

Equations

$$\left[\frac{\Delta L_s - \Delta L_{s\infty}}{F_j}\right]_i = \left[A\left(\frac{\bar{D}_i}{d_i}\right) + B\right] C_{s_i}\left[\frac{h}{\bar{D}_i - d_i}\right]^C \tag{3.1-2}$$

where

A = .00075
B = -.022
C = $-(1.5 + .07\,(\bar{D}/d))$

and

i = nozzle of interest.

$$\left[\frac{\Delta L_{s\infty}}{F_j}\right]_i = -.004\left((d/\bar{D})_i + .450\,(1.28)^{(\bar{D}/d)_i}\right)\left(1 + \frac{AR_i - 1}{20}\right)\left(1 + \frac{AR_i - 1}{(\bar{D}/d)_i}\right) \tag{3.1-3}$$

Parameters

d_i equivalent nozzle diameter of ith nozzle

37
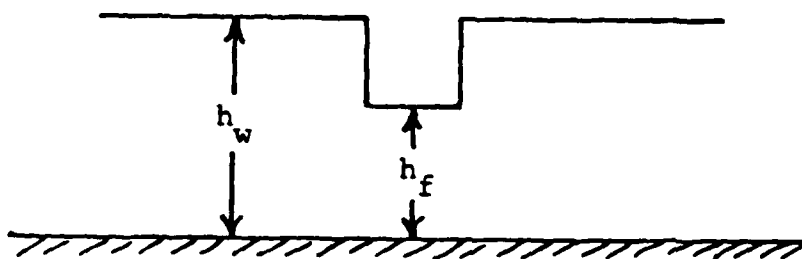
Figure 3.1-2   Non-Coplanar Planform

d_{wa} average nozzle diameter of n nozzles,

$$= \left[\sum_{i=1}^{n} d_i^2 \right]^{\frac{1}{2}}$$

D_e equivalent single nozzle diameter, =

$$= \left[\sum_{i=1}^{n} d_i (F_j)_i \right] / \left[\sum_{i=1}^{n} (F_j)_i \right]$$

$\bar{D}_i$ effective mean diameter,

where

$$= \left[\frac{2}{\pi} \sum_{k=1}^{m} \frac{s_k}{r_k} \right] - d_i - \frac{\pi}{4} \sum_{i=2}^{n} \frac{d_i^2}{r_i}$$

1. The incremental area and its associated radius from the nozzle are s_k and r_k, respectively (see Figure 3.1-3).

2. The individual nozzle diameter (second term) need only be subtracted if d_i falls on the planform.

3. Subsequent effective nozzle diameters (third term) need only be subtracted if they fall on the planform.

4. The entire planform is covered by m elements.

$\bar{D}_{wa}$ thrust weighted average of effective mean diameters,

$$= \left[\sum_{i=1}^{n} \bar{D}_i (F_j)_i \right] / \left[\sum_{i=1}^{n} (F_j)_i \right]$$

Suckdown Extrapolation Coefficient

$$c_S = c_{S1} \cdot c_{S2} \qquad (3.1-4)$$

where

C_{S1} = 1.0, reserved for scale effects

C_{S2} = effect of nozzle pressure ratio

= 1.173 - 0.2495 ln(NPR), NPR $\leq$ 2.0 (3.1-5a)

= 1.061 - .0889 ln(NPR), NPR $\geq$ 2.0 (3.1-5b)

(C_{S2} can be obtained graphically from Figure 3.1-4)

The suckdown associated with each nozzle of the aircraft is calculated from Equation 3.1-2 and then listed in Block I of the tabulation. Because of its AR dependence the
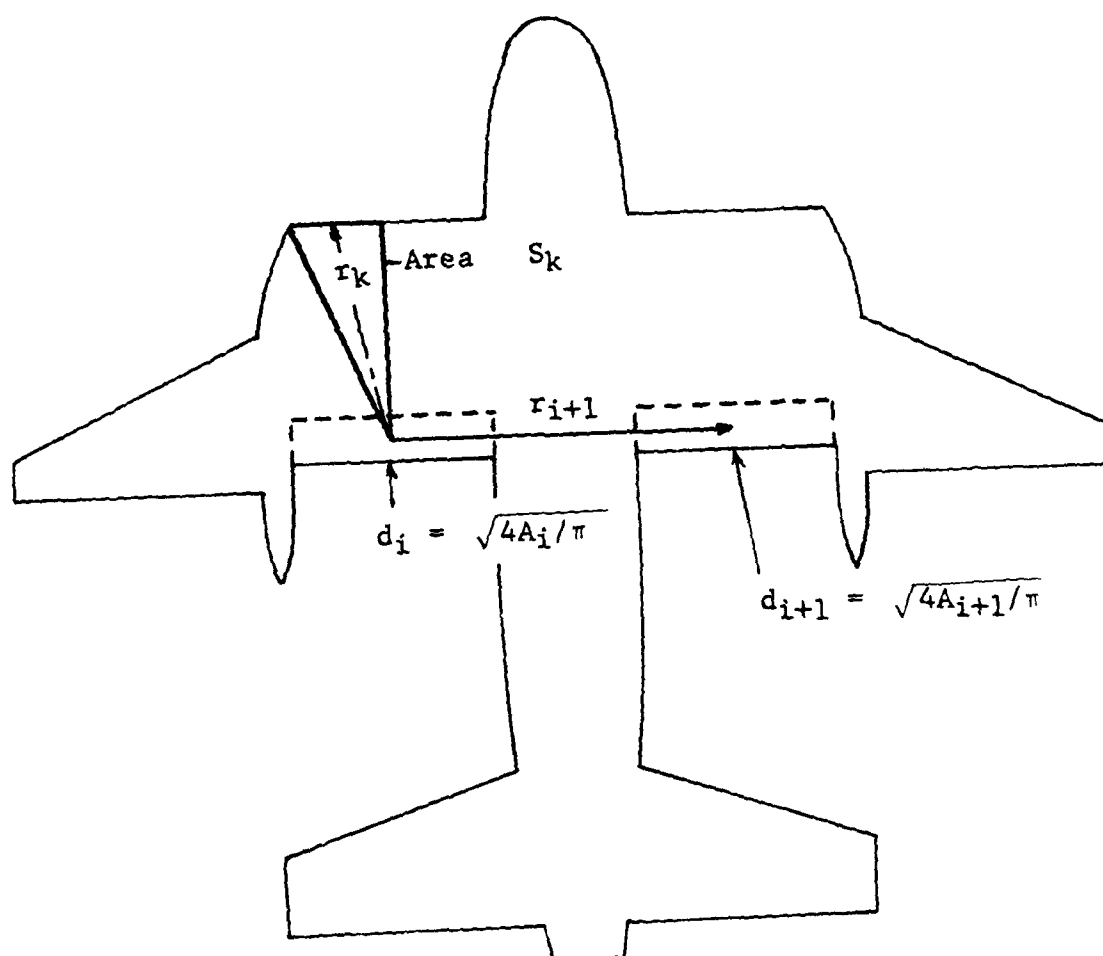
Figure 3.1-3 Calculation of $\tilde{D}_i$
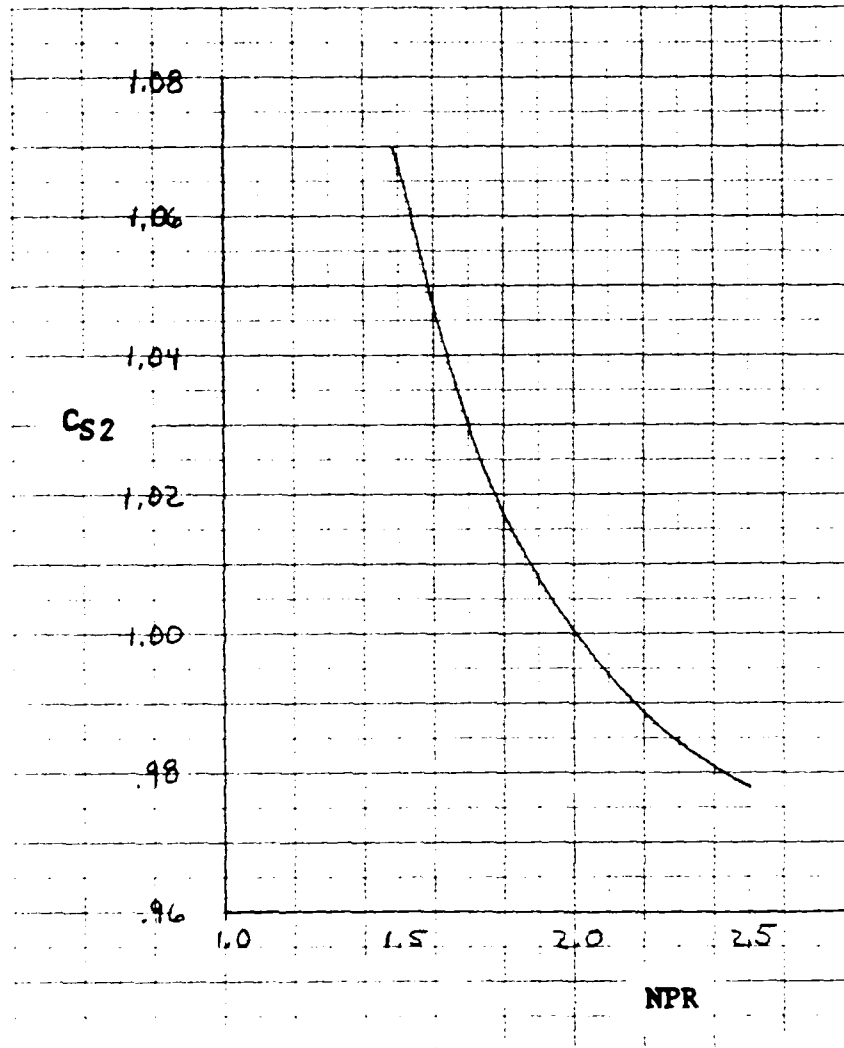
Figure 3.1-4 NPR Extrapolation Coefficient

free-air suckdown of the aircraft must be calculated from Equation 3.1-3 for each individual nozzle using $\bar{D}_j/d_j$ and AR_j. The total suckdown of the aircraft is then the sum of the thrust-weighted average of individual nozzle suckdown and free-air suckdown, i.e.,

$$\Delta L_s/F_j = \left[(\Delta L_s - \Delta L_{s\infty})/F_j\right]_{wa} + \left[\Delta L_{s\infty}/F_j\right]_{wa} \qquad (3.1-6)$$

For the calculation of suckdown on a non-coplanar planform it is necessary to find $(\Delta L_s/F_j)_{wing}$ using $\bar{D}_{wing}$ and h_w where $\bar{D}_w$ is determined for the exposed wing area only. Likewise, the value of $(\Delta L_s/F_j)_{fuselage}$ is determined by use of $\bar{D}_{fuselage}$ and h_f. So that,

$$\Delta L_s/F_j = (\Delta L_s/F_j)_{wing} + (\Delta L_s/F_j)_{fuselage} \qquad (3.1-7)$$

at each planform reference altitude of interest.

3.1.4 Fountain Effects

The equations, parameters, and methods for computing fountain lift are described below:

Equations

$$\Delta L_F/F_j = (\Delta L_F^{II}/F_j) \cdot C_F^{II} + (\Delta L_F^{III}/F_j) \cdot C_F^{III}$$
$$+ (\Delta L_F^{IV}/F_j) \cdot C_F^{IV} \qquad (3.1-8)$$

where ^{II} designates two-jet, ^{III} designates three-jet, and so on.

Parameters

$\bar{D}$ effective mean diameter of the planform

d_E distance between nozzles (near edge to near edge)

h_m height of jet merging, $= 1.374\, d_E$

Fountain Extrapolation Coefficients

$$C_F = C_{F1} \cdot C_{F2} \cdot C_{F3} \cdot C_{F4} \cdot C_{F5} \qquad (3.1-9)$$

where

$C_{F1} = 1.0$, reserved for scale effects

C_{F2} effect of nozzle pressure ratio,

$$= 0.736 \; \ln(NPR) + 0.481, \quad NPR \leq 2.0 \qquad (3.1-10a)$$

$$= 0.035 \; \ln(NPR) + 0.930, \quad NPR \geq 2.0 \qquad (3.1-10b)$$

(C_{F2} can be obtained graphically from Figure 3.1-5)

C_{F3} effect of jet merging, obtained empirically from Figure 3.1-6

C_{F4} effect of planform contour, obtained empirically from

Figure 3.1-7 (three or more jets)
Figure 3.1-8 (two-jet fountain)

C_{F5} effect of Lift Improvement Devices (LIDs),

= 1.0, without LIDs
= 1.5, longitudinal LIDs
= 2.0, longitudinal and transverse LIDs.

A non-coplanar planform will require additional calculation to accurately represent the fountain lift if the fountain impacts both non-coplanar portions of the planform. The fountain effects on the wing, $(\Delta L_F/F_j)_{wing}$, must be computed with $\bar{D}_{wing}$ and h_w as was performed in the suckdown calculations for non-coplanar planforms. Also, $(\Delta L_F/F_j)_{fuselage}$ will depend upon $\bar{D}_{fuselage}$ and h_f.

3.1.4.1 Multi-Nozzle Fountain

The buoyant force produced by the fountain jet of a multi-nozzle configuration has been quantified by empirical means. Figures 2.2-2 through 2.2-15 provide the basic data of fountain lift for two-, three-, and four-nozzle configurations. As previously stated it is sometimes necessary to determine fountain lift for more than one type of fountain due to jet merging with any given configuration. The altitude (h) used for fountain buoyancy calculations is the distance from the ground to the lowest point on the planform that the fountain impacts. The fountain strength is a function of the effective mean diameter over the average nozzle diameter ($\bar{D}_{wa}/d_{wa}$). By indexing the appropriate figure with the value of $\bar{D}_{wa}/d_{wa}$ from Subsection 3.1.3, $\Delta L_F/F_j$ can be extracted at various planform heights (h/d_{wa}). It is essential that the proper figure be used to determine $\Delta L_F/F_j$. Care must be exercised to distinguish the test configuration that most closely resembles the aircraft model under study.

$$\text{NPR} \leq 2 \qquad C_{F2} = 0.736 \ln(\text{NPR}) + 0.481$$

$$\text{NPR} \geq 2 \qquad C_{F2} = 0.035 \ln(\text{NPR}) + 0.930$$
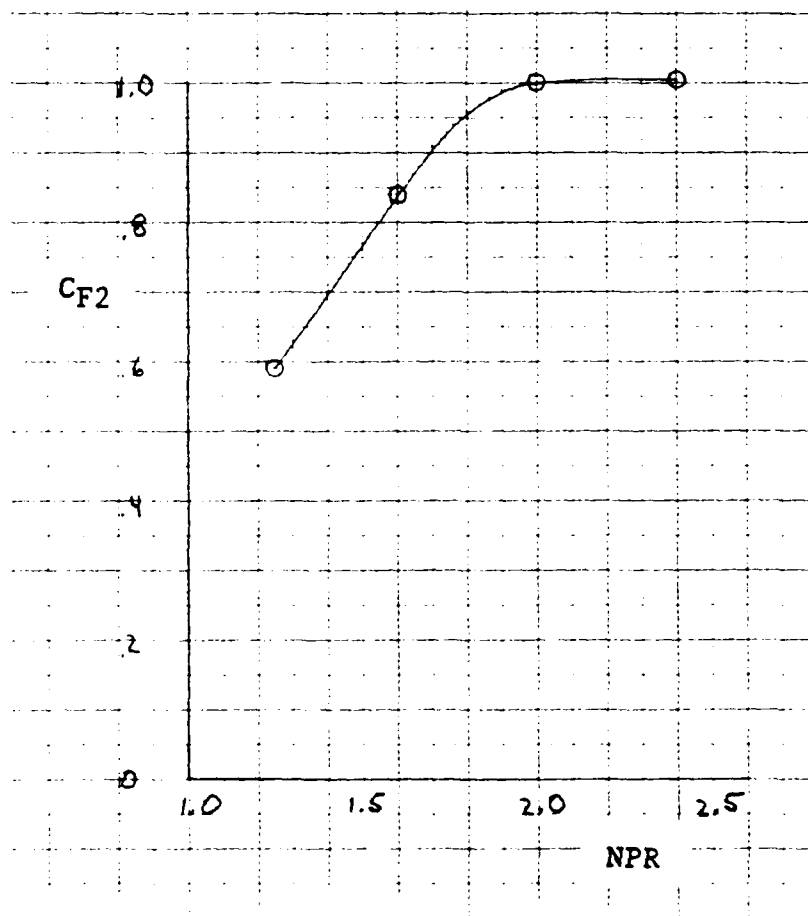

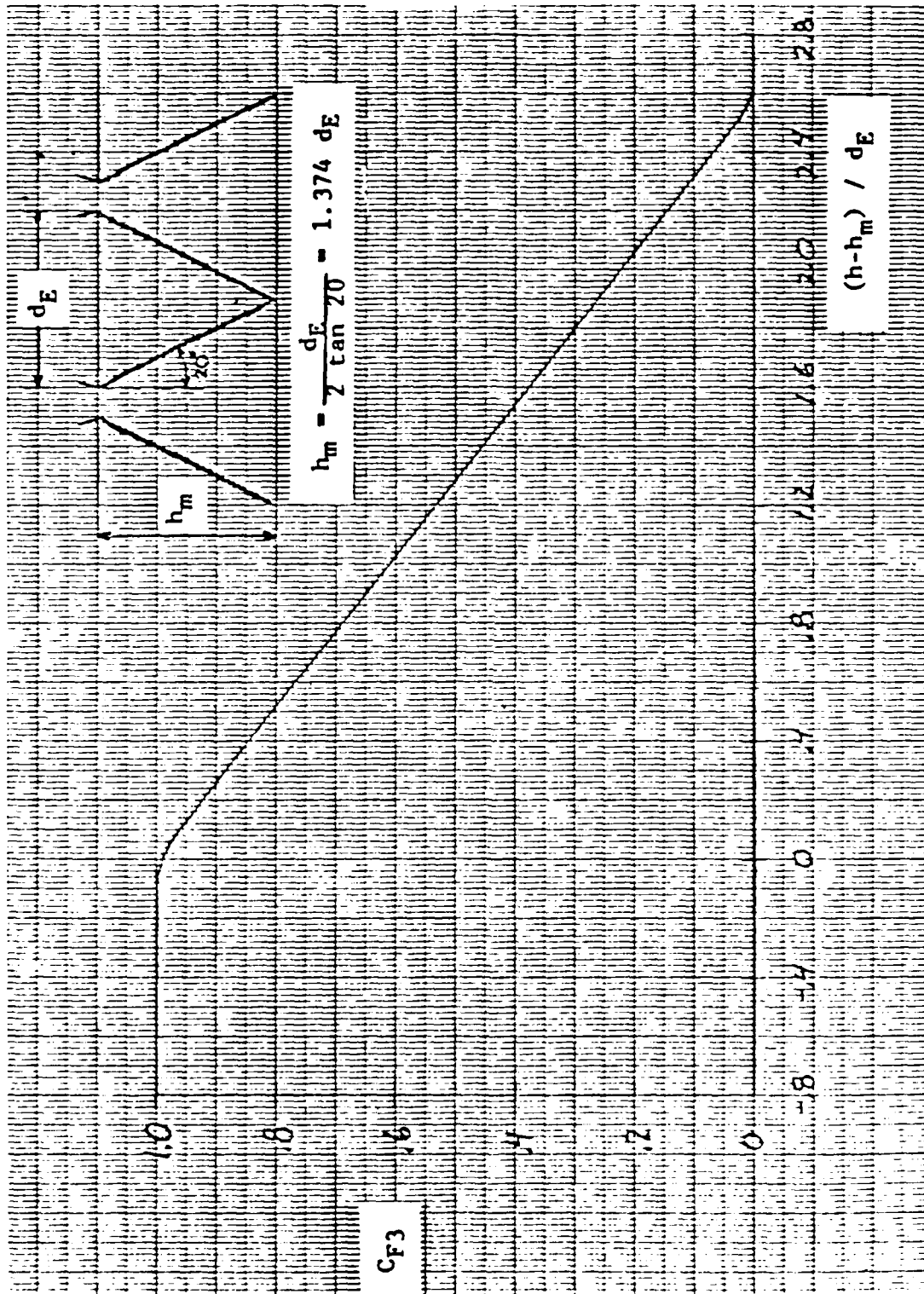Figure 3.1-5
NPR Extrapolation Coefficient

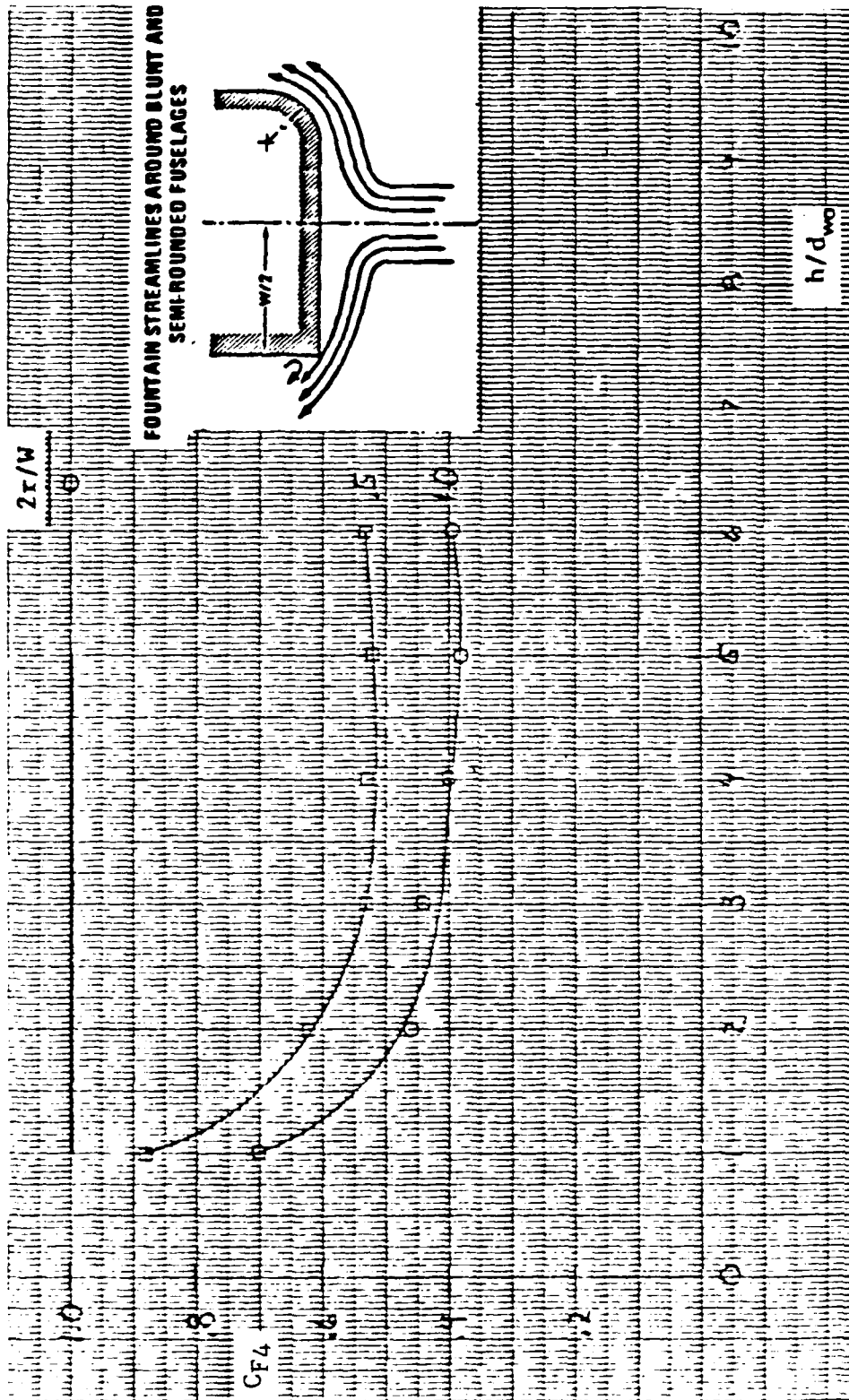Figure 3.1-6 Effect of Jet Merging On Fountain Lift

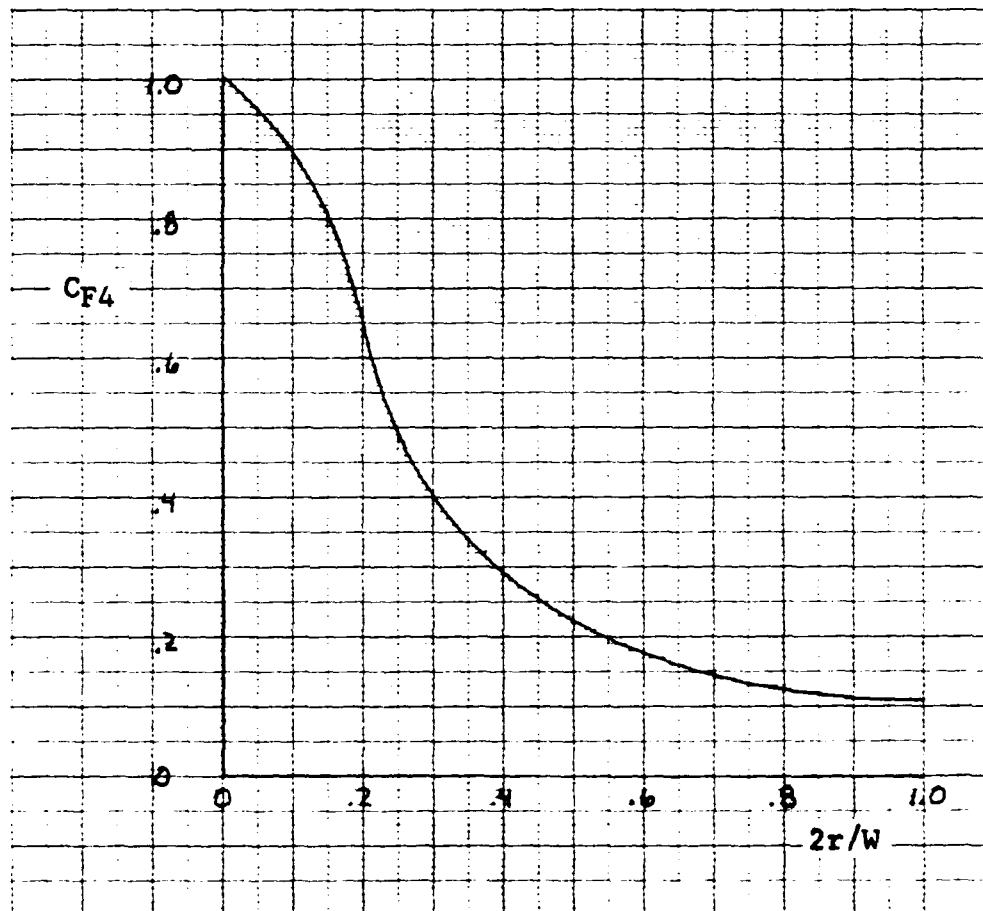Figure 3.1-7 Effect of Planform Contour - 3 and 4 Nozzle Case

Figure 3.1-8   Effect of Planform Contour - 2 Nozzle Case

3.1.4.2   Fountain Extrapolation Coefficients

The coefficients for fountain extrapolation must be considered to fully represent the true fountain lift of the configuration under study.

The correction for nozzle pressure ratio, C_{F2}, must be determined for each nozzle and then weight averaged by thrust to give a composite C_{F2}.

$$C_{F2} = \left[\sum_{i=1}^{n} (C_{F2})_i (F_j)_i \right] / \left[\sum_{i=1}^{n} (F_j)_i \right] \tag{3.1-11}$$

The values of C_{F2} for each nozzle can be determined through Figure 3.1-5 or Equation 3.1-10.

When the altitude of a hovering aircraft increases, the jet dispersion will cause merging of individual jets with other jets and hence, a change in the fountain character. To account for this fountain characteristic, it is necessary to include in Equation 3.1-8 the fountain merging coefficient C_{F3}, for each fountain type.

C_{F3} is determined for all fountain types and at each planform altitude from Figure 3.1-6 by indexing the parameter $(\frac{h}{d_E} - 1.374)$, where d_E is the distance between merging nozzles. At any particular planform height, a multiplicity of fountain types could occur where a four-nozzle fountain, by merging, becomes a three-jet fountain. At the altitude that jet merging commences, the merging coefficient of the four-nozzle fountain, C_{F3}^{IV}, will have a value less than unity and, as altitude increases, decrease to zero. In this regime, the next merging coefficient, C_{F3}^{III}, will have a value

$$C_{F3}^{III} = 1 - C_{F3}^{IV} \tag{3.1-12a}$$

at each particular altitude of interest. Similarly, C_{F3}^{III} will become a driving function for C_{F3}^{II} when an altitude is reached to cause the three-jet case to merge into two jets, i.e.,

$$C_{F3}^{II} = 1 - C_{F3}^{III} \tag{3.1-12b}$$

at these particular planform altitudes. Finally, a point will be reached when the aircraft planform exceeds the height of total jet merging and fountain breakdown, where it can be seen that the summation of jet merging coefficients will be less than unity because the only merging coefficient remaining is C_{F3}^{II} and its value will be less than one. A tabular example is shown in Figure 3.1-9.

The fountain lift of a two-dimensional planform can now be determined using the basic fountain lift, C_{F_2} and C_{F_3}, such that

$$(\Delta L/F_j)_{2-D} = (\Delta L_F/F_j)_{2-D} + \Delta L_S/F_j \tag{3.1-13}$$

It is necessary to correct the two-dimensional fountain lift for effects of planform contour and LIDs by using C_{F4} and C_{F5}. The effect of planform contour is determined by the use of Figures 3.1-7 and 3.1-8. Both figures use the contour parameter 2r/W as the

h/d_{wa}	C_{F3}^{IV}	C_{F3}^{III}	C_{F3}^{II}	ΣC_{F3}	NOTE
1	1	0	0	1	
2	1	0	0	1	
3	.7	.3	0	1	1
4	.4	.6	0	1	
5	0	1	0	1	2
6	0	.5	.5	1	3
7	0	0	1	1	4
8	0	0	1	1	
9	0	0	.3	.3	5
10	0	0	0	0	6

NOTES:

1. Two of the four jets begin to merge, starting a three-jet fountain.

2. Merging of two jets complete; fountain is a three-jet fountain.

3. Two remaining jets begin to merge, starting a two-jet fountain.

4. Completion of merging of two jets; fountain is now a two-jet fountain.

5. Merging of all the jets begins, reducing fountain lift.

6. Merging complete; fountain lift eliminated.

Figure 3.1-9   Example of Jet Merging Process

index of the fountain lift effect on a rounded surface, C_{F4}. Figure 3.1-7 covers the planform roundness coefficient, C_{F4}, of a three- or four-jet fountain; whereas, Figure 3.1-8 must be used to determine C_{F4} for the case of a two-jet fountain. The roundness extrapolation coefficient must be determined uniquely at each planform altitude and then used to correct the two-dimensional fountain strength to a three-dimensional effect. That is, the fountain character (two-jet, three-jet ...) must be known to determine whether Figure 3.1-7 or 3.1-8 will be used for C_{F4} at each height of computation. The fountain lift of a three-dimensional planform then becomes

$$(\Delta L_F/F_j)_{3-D} = C_{F4} \ (\Delta L_F/F_j)_{2-D} \tag{3.1-14}$$

When LIDs are used, $C_{F4} = 1.0$ except for the special case given by Equation 3.1-17. The presence of LIDs will increase fountain buoyance and must be considered through the fountain extrapolation coefficient, C_{F5}. For the general case of fully enclosed longitudinal and transverse LIDs (Figure 3.1-10a and b), the value of C_{F5} is 2.0, as opposed to the configuration without LIDs where $C_{F5} = 1.0$. A configuration with only longitudinal LIDs (Figure 3.1-10c) uses $C_{F5} = 1.5$. The maximum benefit obtained from the LIDs mentioned above will occur only when the LID captures the entire fountain that impinges on the planform. Loss in the theoretical lift improvement of a LID occurs when the device does not fully span the planform width as depicted in Figure 3.1-10a and b. Figure 3.1-10a shows a two-jet fountain which has a LID that only subtends an angle θ_L on the fuselage. The fountain extrapolation coefficient must be decreased in this case by

$$C_{F5} = 1 + (C_{F5}-1) \ \frac{\sin \theta_L}{\sin \theta_2} \tag{3.1-15}$$

For a three- or four-jet fountain (Figure 3.1-10b), a decreased LID size leads to the relationship:

$$C_{F5} = 1 + (C_{F5}-1) \ \frac{\ell_2}{\ell_1} \tag{3.1-16}$$

where (ℓ_2/ℓ_1) is the ratio of LID width to fuselage width.

An additional fountain lift factor must be considered when using LIDs. The loss of lift due to planform contour (C_{F4}) does not occur in the area covered by the LID. Therefore, if the LIDs do not subtend the entire planform, the new coefficient for planform roundness becomes

$$C_{F4} = C_{F4} + (1-C_{F4}) \ \frac{\ell_2}{\ell_1} \tag{3.1-17}$$

3.1.5 Induced Lift

Once the values of the fountain extrapolation coefficients have been determined, it is possible to calculate the fountain buoyance of a two-dimensional planform by use of Equation 3.1-13. The two-dimensional fountain lift is then summed with the planform suckdown in order to compute the induced lift of the configuration

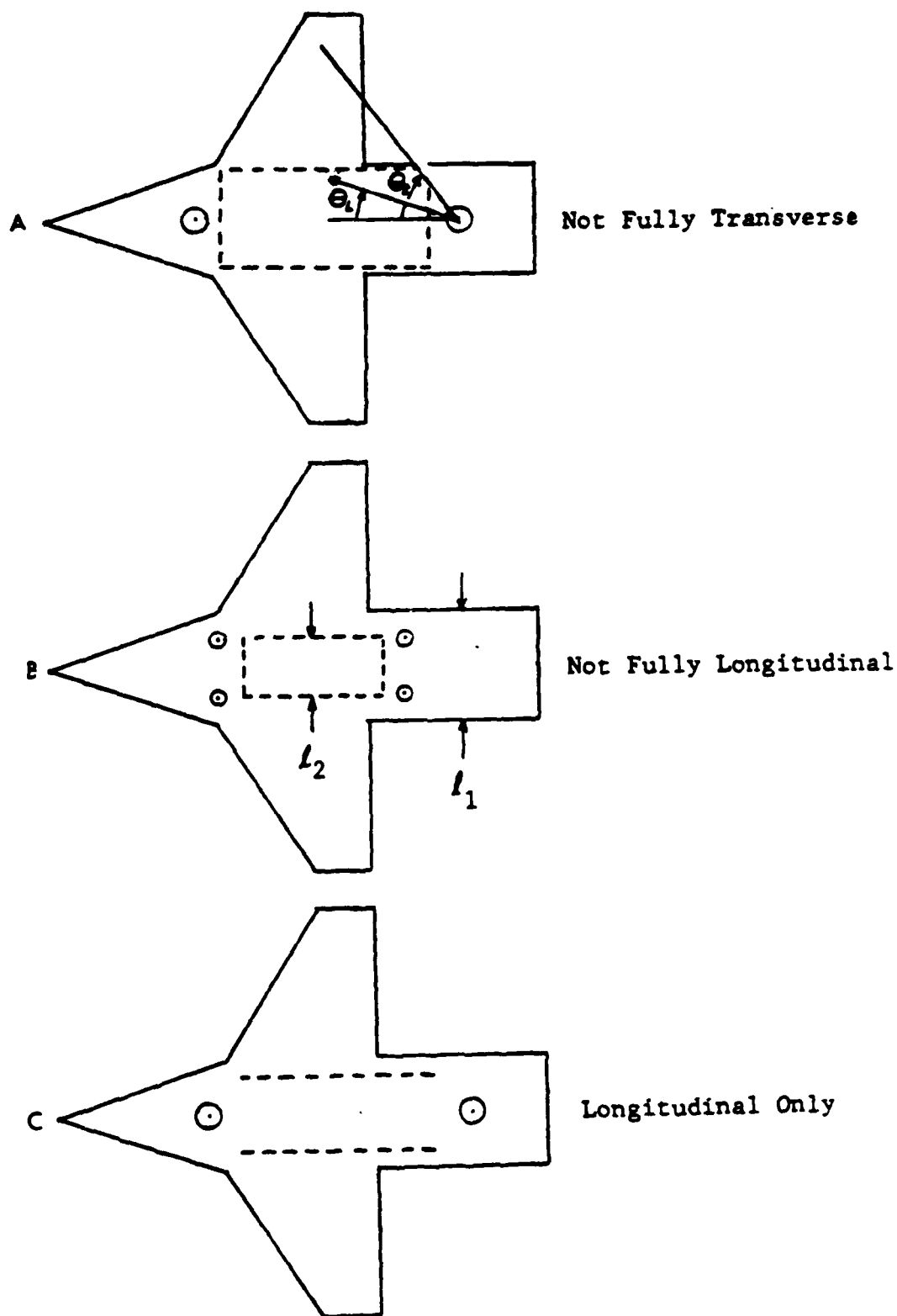$$(\Delta L/F_j)_{LID} = C_{F4} \cdot C_{F5} \cdot (\Delta L_F/F_j)_{2-D} + \Delta L_s/F_j \tag{3.1-18}$$

Not Fully Transverse

Not Fully Longitudinal

Longitudinal Only

Figure 3.1-10 C_{F5} - LIDs, Special Situations

51

The induced lift of planforms with contoured fuselage sections is computed in the same manner using the appropriate fountain lift.

$$(\Delta L/F_j)_{3-D} = (\Delta L_F/F_j)_{3-D} + \Delta L_S/F_j \qquad (3.1\text{-}19)$$

The final step in the determination of total induced lift for a particular configuration is to account for LIDs by use of C_{F_5}.

$$(\Delta L/F_j) = C_{F5} \, (\Delta L_F/F_j)_{3-D} + \Delta L_S/F_j \qquad (3.1\text{-}20)$$

3.2 SAMPLE CALCULATION

3.2.1 Suckdown

The most difficult step toward the computation of suckdown is the calculation of $\bar{D}$ for each nozzle, because it must be performed graphically, as per Section 3.1.3. The effective mean diameter also influences the determination of fountain strength which expands the importance of $\bar{D}$. General Dynamics' Configuration A-311 is analyzed in this section with the following value of $\bar{D}$ graphically determined:

$$\bar{D}_1 = \bar{D}_2 = 6.78 \text{ in}$$

Since this configuration possesses two symmetric rectangular nozzles the weighted average of $\bar{D}$ becomes

$$\bar{D}_{wa} = \frac{(4.84) \, F_{j1} + (4.84) \, F_{j2}}{F_{j1} + F_{j2}} = 6.78 \text{ in}$$

and

$$d_1 = d_2 = d_{wa} = 1.4 \text{ in}$$

$$D_e = 1.98 \text{ in}$$

$$AR_1 = AR_2 = 1.5$$

$$(C_{S2})_1 = (C_{S2})_2 = 1.173 - 0.2495 \ln (1.5) = 1.0718$$

Suckdown forces for this configuration can now be calculated for each jet

$$\frac{\Delta L_S - \Delta L_{S\infty}}{F_j} = (.00075 \; \bar{D}/d - .022) \left[\frac{h}{\bar{D}-d}\right]^{-(1.5 + .07 \; \bar{D}/d)} \cdot C_{S2}$$

$$= -.0184 \left[\frac{h/d}{3.84}\right]^{-1.84} \cdot (1.0718)$$

at each altitude of interest.

As a convention, the computation of $\Delta L/F_j$ will be presented as a function of h/De even though this particular configuration is not as complicated as some aircraft designs that possess multiple nozzles of varying dimensions and thrust. Block I of the tabulation sheet on Figure 3.2-1 lists the values of the computed suckdown forces as a function of h/De. It is important to note that the altitude used in the computation has been re-referenced to h/d, to be compatible with $\bar{D}/d$ in the above equation for single nozzle suckdown.

Because Configuration A-311 has two nozzles of equal thrust one finds

$$\left(\frac{\Delta L_s - \Delta L_{s\infty}}{F_j}\right)_{wa} = \left(\frac{\Delta L_s - \Delta L_{s\infty}}{F_j}\right)_{1,2} = -.1236$$

at h/De = 1.

It is now possible to compute the free-air suckdown of the configuration using $\bar{D}wa/dwa$ and Equation 3.1-3.

$$\left[\frac{\Delta L_{S\infty}}{F_j}\right]_{wa} = -.004 \left(\frac{1}{4.84} + .45 \; (1.28)^{4.84}\right) \left(1 + \frac{5.38-1}{20}\right) \left(1 + \frac{5.38-1}{4.84}\right) = -.0157$$

Then,

$$\frac{\Delta L_s}{F_j} = \left(\frac{\Delta L_s - \Delta L_{s\infty}}{F_j}\right)_{wa} + \left(\frac{\Delta L_{s\infty}}{F_j}\right)_{wa}$$

$$= -.1236 - .0157 = -.1393$$

at h/D$_e$ = 1.

Parameters: $\bar{D}(in)$ 6.78, $d(in)$ 1.4, $\bar{D}/d$ 4.84, C_{S_2} 1.0718, C_{F_2} .779, d_e 2.30, 0.24, $D_e = 1.98$in, NPR = 1.5, AR = 5.38

$\frac{h}{d}$	$\frac{h}{D_e}$	$\frac{\Delta L_s - \Delta L_{sm}}{F_j}$	$\frac{\Delta L_{sm}}{F_j}$	$\frac{\Delta L_s}{F_j}$	$\frac{h-h_m}{d_e}$	C''_{F_3}	C_{F_4}	$\frac{\Delta L''_E}{F_{j_1}}$	$\frac{\Delta L_f}{F_j}$	$\frac{\Delta L}{F_j}$
1.41	1	-.1236	-.0157	-.1393	-.51	1.0	.52	.1500	.0608	-.0785
2.12	1.5	-.0586		-.0743	-.08	1.0		.0610	.0247	-.0496
2.83	2	-.0345		-.0502	.35	.865		.0470	.0165	-.0337
4.24	3	-.0164		-.0321	1.21	.525		.0265	.0056	-.0265
5.66	4	-.0097		-.0254	2.07	.190		.0135	.0010	-.0244
7.07	5	-.0064		-.0221	2.93	0		0	0	-.0221
8.49	6	-.0046		-.0203	--	0		0	0	-.0203
9.90	7	-.0035		-.0192	--	0		0	0	-.0192

SUCKDOWN +   FOUNTAIN LIFT =   INDUCED LIFT

Figure 3.2-1   Calculation of Induced Lift Configuration A-311

3.2.2 Fountain Lift

This two-jet configuration will produce a fountain that dissipates at some altitude due to jet-merging. During the course of the jet-merging the character of the fountain will change. This causes a degree of complexity in the computation of the fountain force but not nearly so much as the case of a four-jet model that transitions from the four-jet *fountain to a three-jet, two-jet and so on.* A more in-depth example of multiple nozzle jet-merging can be seen in Ref. 16.

3.2.2.1   Two-Jet Fountain

The fountain lift that should be expected by Configuration A-311 can be predicted by utilizing the fountain lift presented on Figures 2.2-2 through 2.2-4. It is necessary to acquire the data from these three figures in order to crossplot the fountain force versus AR and thus obtain $\Delta L_F/F_j$ for AR = 5.38 at each altitude desired. By indexing Figures 2.2-2 through 2.2-4 with $\bar{D}_{wa}/d_{wa}$ = 4.84 it was possible to create Figure 3.2-2 which in turn allows for $\Delta L_F/F_j$ to be plotted versus altitude on Figure 3.2-3. Note that Figure 3.2-2 is shown as a function of h/d_{wa} and that this data was transferred to Figure 3.2-3 as a function of h/D_e and then listed in Block II of Figure 3.2-1.

3.2.2.2   Fountain Extrapolation Coefficient C_{F2}

The extrapolation coefficient for NPR, C_{F2}, must be included in the fountain lift computation to obtain proper correlation of results since the subsonic V/STOL has an NPR other than the baseline 2.0. With both nozzles having NPR = 1.5, we have from Subsection 3.1.4

$$C_{F2} = 0.736 \ln(1.5) + 0.481 = 0.779$$

C_{F2} can now be listed in Block II, Figure 3.2-1.

3.2.2.3   Fountain Extrapolation Coefficient C_{F3}

The values of $\Delta L_F/F_j$ listed on Figure 3.2-1 constitute the main character of the fountain lift for Configuration A-311. It is necessary to determine the extent of jet-merging that will occur with this two-jet configuration. The fountain extrapolation coefficient for jet-merging, C_{F3}, must be determined as a function of planform height. Figure 3.1-6 bis is an empirical formulation of the jet-merging coefficient, C_{F3}. The two-jet fountain of the subsonic V/STOL begins to merge at a height

$$h_m = 1.374 \ d_E = 1.374 \ (2.3) = 3.16 \ \text{in} = 1.6 \ h/D_e$$

which causes C_{F3} = 1.0 at h/D_e = 1 and 1.5. At h/D_e = 2.0 we have
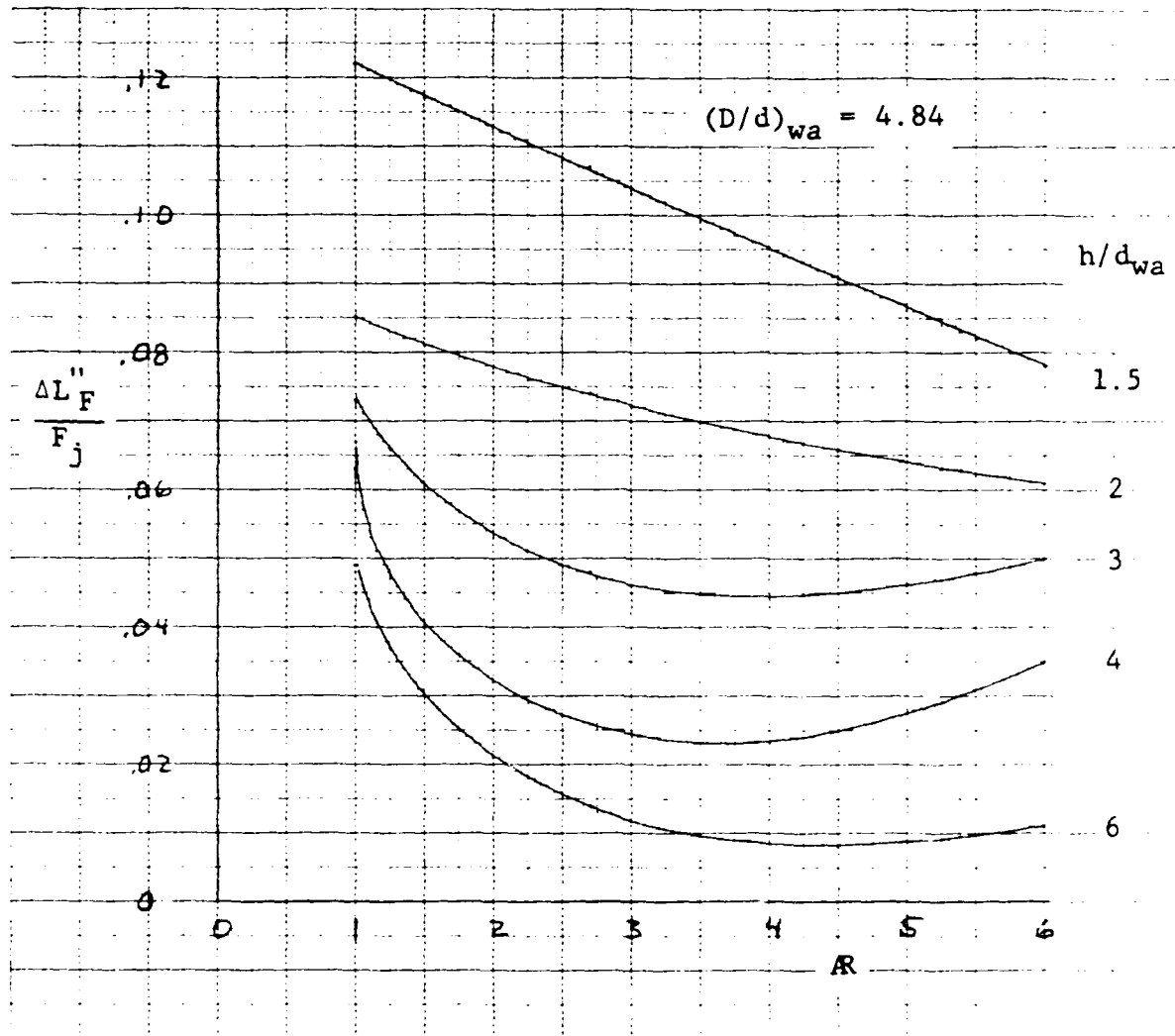
$$(h - h_m) \ / \ d_E = (2(1.98) - 3.16) \ / \ 2.3 = 0.35$$

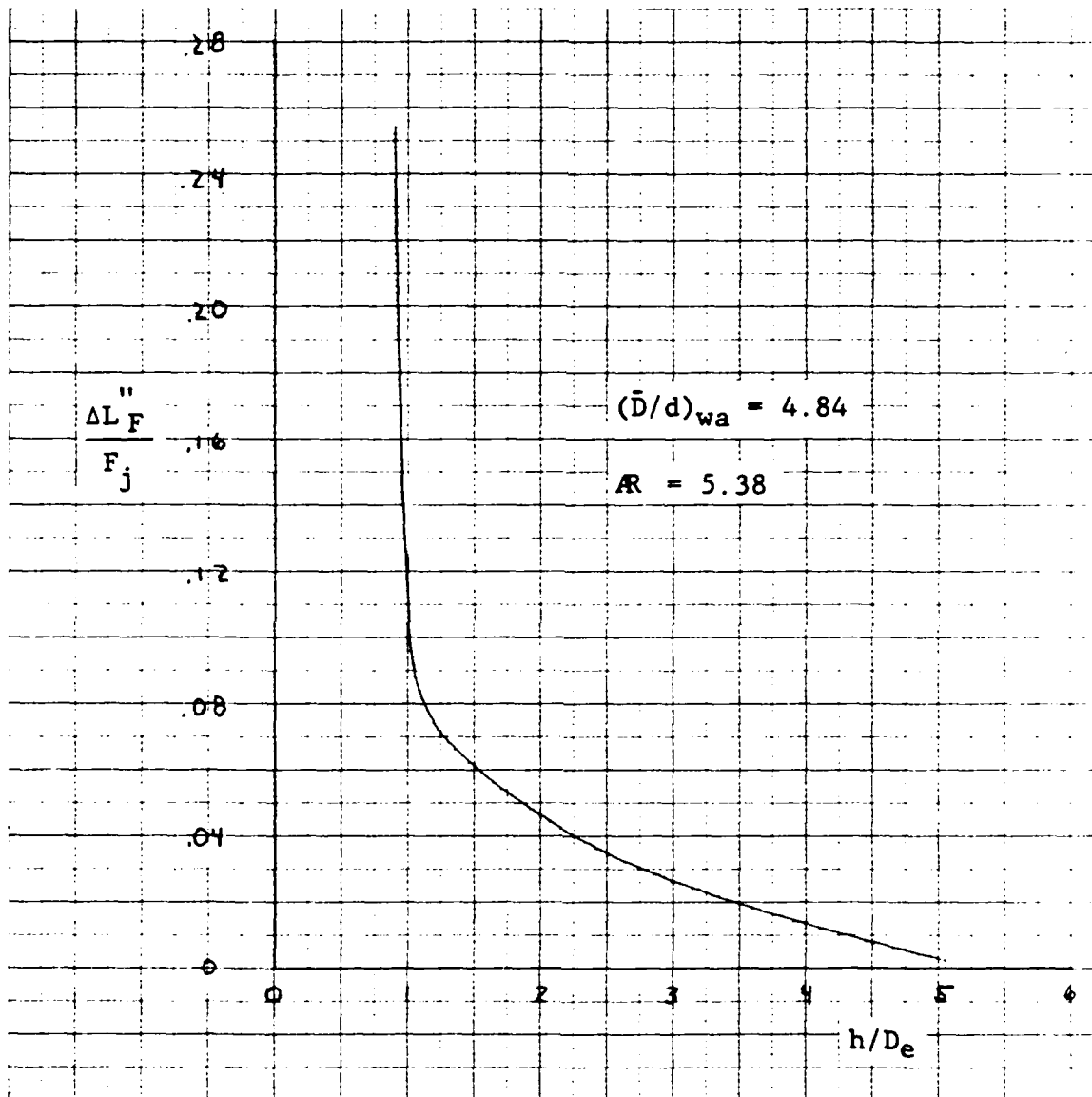Figure 3.2-2 Fountain Lift vs. Æ, Configuration 2-A

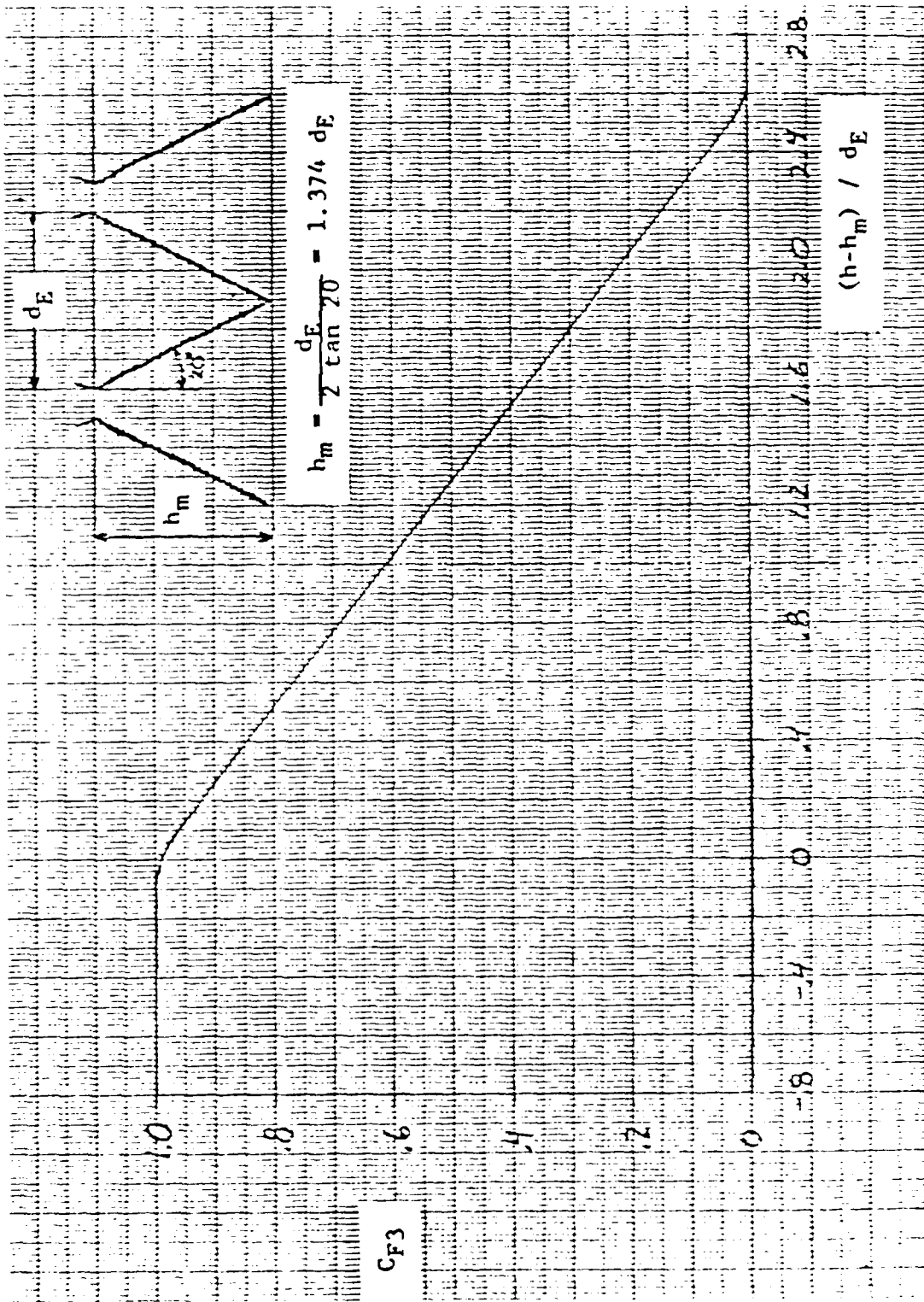Figure 3.2-3 Fountain Lift vs. Altitude, Configuration 2-A

$$h_m = \frac{d_E}{2 \tan 20} = 1.374 \ d_E$$

$(h-h_m) \ / \ d_E$

C_{F3}

Figure 3.1-6 bis. Effect of Jet Merging, On Fountain Lift

and, the fountain extrapolation coefficient for jet-merging can be found in Figure 3.1-6 bis.

$$C_{F3} = .865$$

Further values of C_{F3} are shown in Block II of the tabulation sheet

3.2.2.4 Fountain Extrapolation Coefficient C_{F4}

To incorporate the effect of planform contour into the fountain lift predictions of Configuration A-311 it is necessary to compute the planform contour parameter $2r/W$. As depicted in Figure 3.1-8 bis, the radius of curvature, r, and fuselage width, W, must be measured. For this configuration

$$2r/W = 0.24$$

is used to index Figure 3.1-8 bis to determine the two-jet fountain extrapolation coefficient for planform contour.

$$C_{F4} = 0.52$$

The value of C_{F4} is listed in Block II of Figure 3.2-1 for all h/D_e.

The total fountain lift can now be computed for this configuration. At $h/D_e = 2$ we have

$$\Delta L_F/F_j = C_{F2} \cdot C_{F3} \cdot C_{F4} \cdot \Delta L_F''/F_j$$

$$= .779 \, (.865) \, .52 \, (.0470)$$

$$= .0165$$

3.2.2.5 Fountain Extrapolation Coefficient C_{F5}

The effect of placing a LID on the planform underside causes a change in the planform roundness as described in Subsection 3.1.5.2. The width of the LID and fuselage are

$$\ell_2 = W_{LID} = 3.28 \text{ in}$$

$$\ell_1 = W_{fuselage} = 14.0 \text{ in}$$

Thus, the new value of C_{F4} becomes

$$(C_{F4})_{LID} = .52 + (1 - .52) \, \frac{3.28}{14.0}$$

$$= .632$$

This new value of C_{F4} is posted on Block II of Figure 3.2-4, which has been set up to include the effects of LIDs on Configuration A-311.
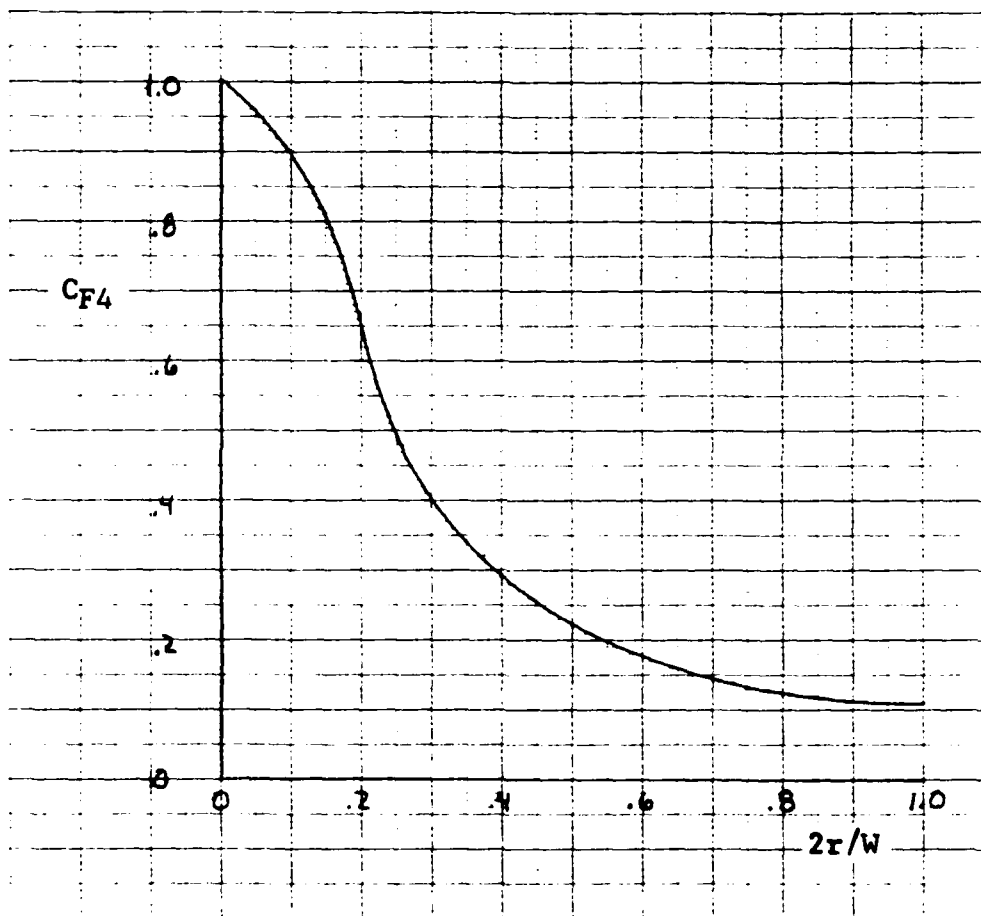
Figure 3.1-8 bis   Effect of Planform Contour - 2 Nozzle Case

$\frac{h}{d}$	$\frac{h}{D_e}$	$\frac{\Delta L_s}{F_j}$	C_{F_2}	C''_{F_3}	C_{F_4}	C_{F_5}	$\frac{\Delta L''_f}{F_j}$	$\frac{\Delta L_f}{F_j}$	$\frac{\Delta L}{F_j}$
		$\bar{D}$ (in) 6.78							
		d (in) 1.4							
		$\bar{D}/d$ 4.84							
		C_{s_z} 1.0718							
1.41	1	-.1393	.779	1.0	.632	1.1408	.1500	.1040	-.0353
2.12	1.5	-.0743		1.0			.0610	.0423	-.0320
2.83	2	-.0502		.865			.0470	.0282	-.0210
4.24	3	-.0321		.525			.0265	.0096	-.0115
5.66	4	-.0254		.190			.0135	.0018	-.0236
7.07	5	-.0221		0			0	0	-.0221
8.49	6	-.0203		0			0	0	-.0203
9.90	7	-.0192		0			0	0	-.0192

D_e = 1.98 in
NPR = 1.5
AR = 5.38

SUCKDOWN + FOUNTAIN LIFT = INDUCED LIFT

Figure 3.2-4 Calculation of Induced Lift Configuration A-311 with LID

61

This A-311 aircraft uses a three-sided LID for fountain lift enhancement. The value of C_{F5} must first be set at a theoretical value of 1.75 for a three-sided LID. Because the LID is not as wide as the full fuselage, the extrapolation coefficient for this LID must be modified as shown in Subsection 3.1.5.2.

$$C_{F5} = 1 + (1.75-1) \left[\frac{\sin 30.5 \text{ degrees}}{\sin 69 \text{ degrees}} \right] = 1.408$$

These values for C_{F5} are shown on Block II of Figure and have been used in conjunction with C_{F4} to correct the fountain strength to account for the LID effect on induced lift. The new fountain lift for this configuration at $h/D_e = 2$ is

$$(\Delta L_F/F_j)_{LID} = C_{F2} \cdot C_{F3} \cdot (C_{F4})_{LID} \cdot C_{F5} \cdot \Delta L_F''/F_j$$

$$= .779 \ (.865) \ .632 \ (1.408) \ .0470$$

$$= .0282$$

3.2.3 Total Induced Lift

3.2.3.1 Induced Lift for Configuration A-311

From the computation of suckdown and fountain forces in the preceding sections the induced lift can be determined from Equation 3.1-14 using the data on Blocks I and II of Figure 3.2-1.

$$\Delta L/F_j = \Delta L_S/F_j + \Delta L_F/F_j$$

$$= -.0502 + .0165$$

$$= -.0337$$

at $h/D_e = 2$.

The values of $\Delta L/F_j$ have been listed on Block III of Figure 3.2-1. The comparison plot of predicted induced lift and actual test data for Configuration A-311 is shown in Figure 3.2-5.

3.2.3.2 Induced Lift for Configuration A-311 with LID

The predicted induced lift for this configuration employing a three-sided lift improvement device is determined using the suckdown and fountain forces found in Blocks I and II on Figure 3.2-4 and Equation 3.1-18. At $h/D_e = 2$

$$\Delta L/F_j = -.0502 + .0282$$

$$= -.0220$$

The induced lift has been calculated at all levels of h/D_e and tabulated on Figure 3.2-4. Figure 3.2-6 compares the prediction and test data for the induced lift of Configuration A-311 with a three-sided LID.
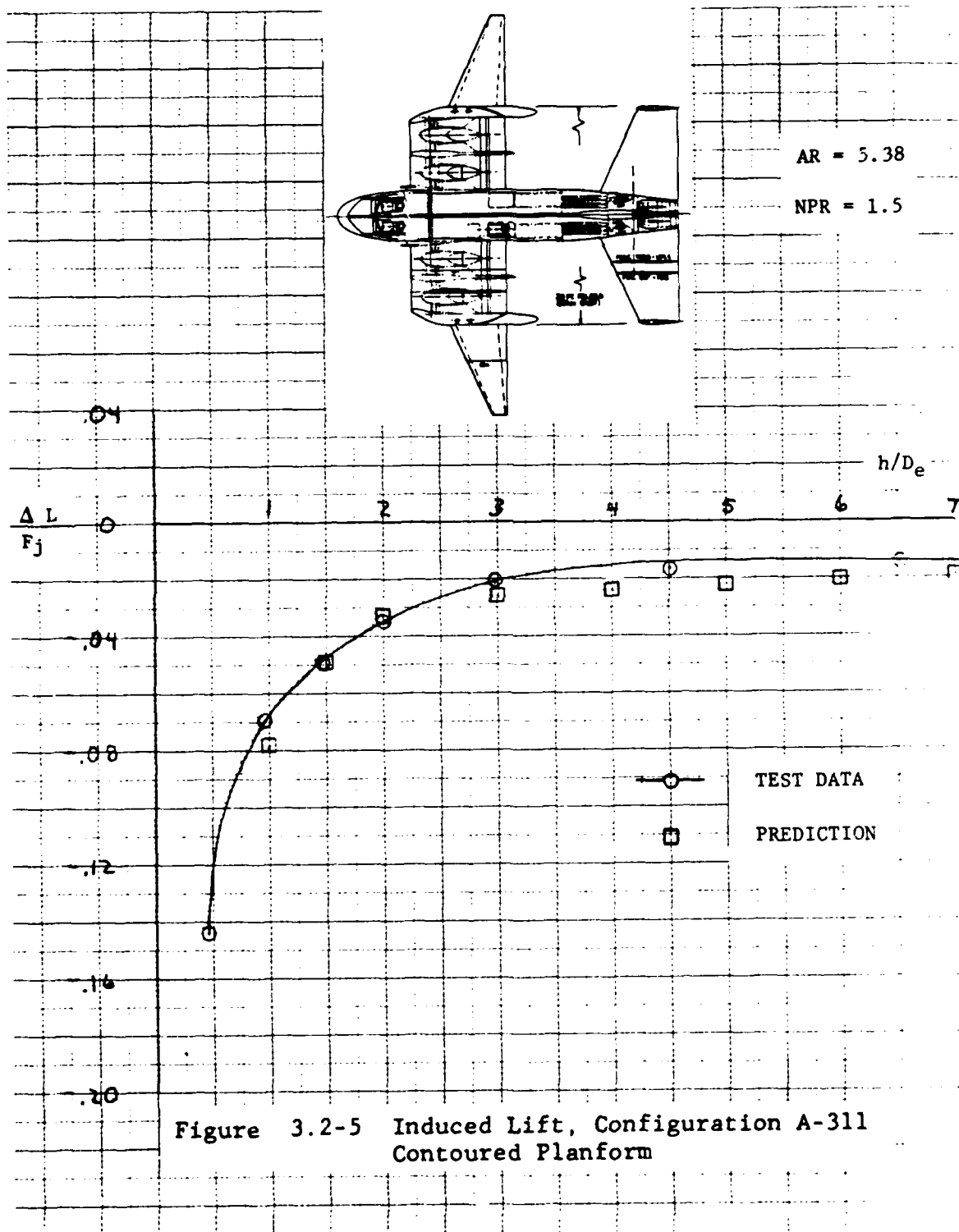
AR = 5.38

NPR = 1.5

h/D_e

$\frac{\Delta L}{F_j}$

TEST DATA

PREDICTION

Figure 3.2-5 Induced Lift, Configuration A-311
Contoured Planform
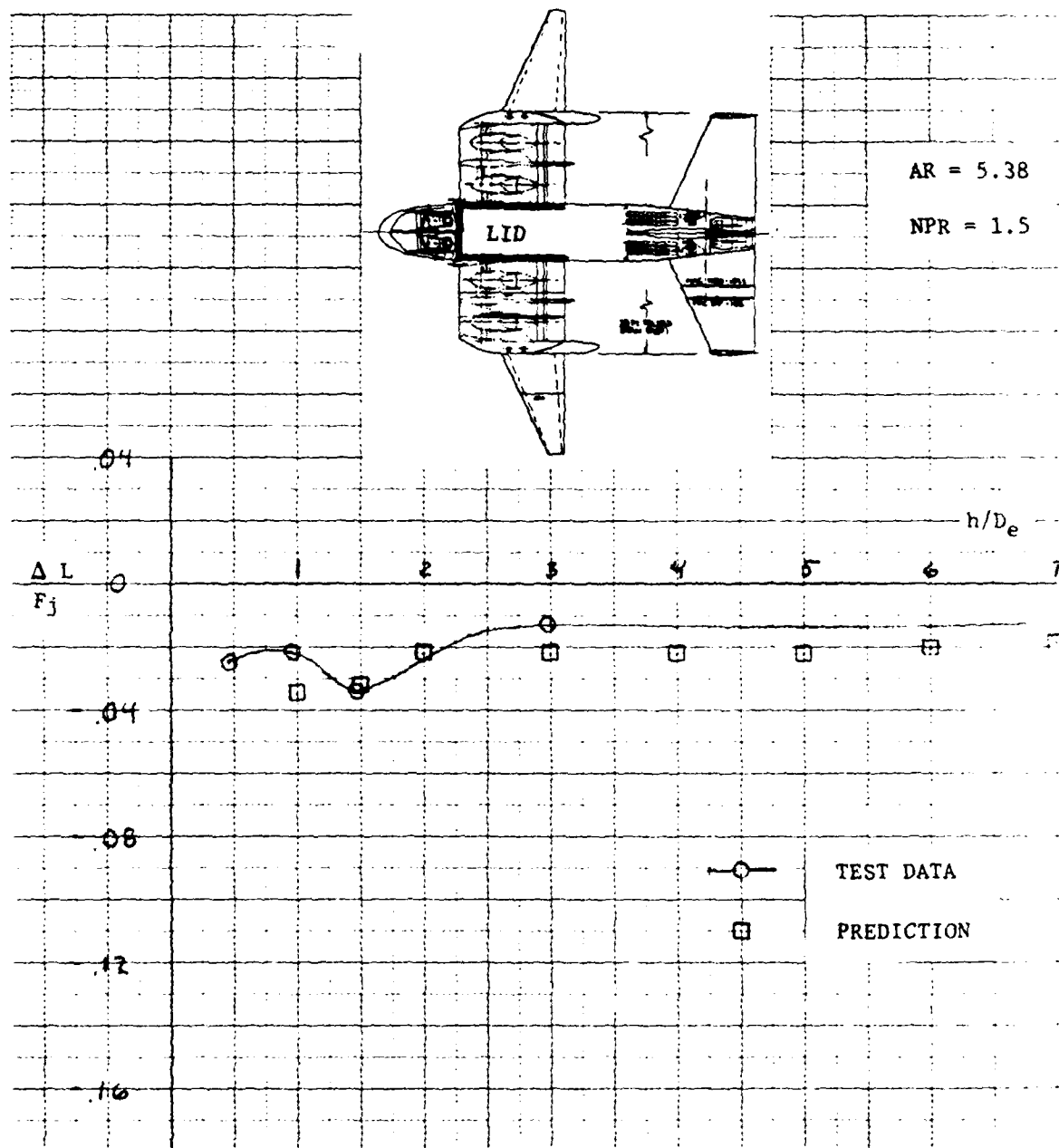
AR = 5.38

NPR = 1.5

Figure 3.2-6 Induced Lift, Configuration A-311
Contoured Planform, 3-Sided LID

4.0 CONCLUSIONS

The work performed under this contract developed a methodology for prediction of jet induced lift for V/STOL aircraft employing rectangular jets. The correlations of Appendix B show a general agreement between methodology predictions and actual test data of $\pm.01$ $\Delta L/F_j$. Analysis was also conducted to describe the effect of a 25 knot crosswind on induced lift. Figure 4.0-1 shows that the velocity of the jets far exceed that of the crosswind which virtually nullifies the effect of the crosswind on induced lift, however, further work could be performed to describe the effect of the crosswind on induced moments. It was found that the AR orientation of nozzles has a negligible effect on $\Delta L_s/F_j$ but that $\Delta L_F/F_j$ has a strong configuration dependence.
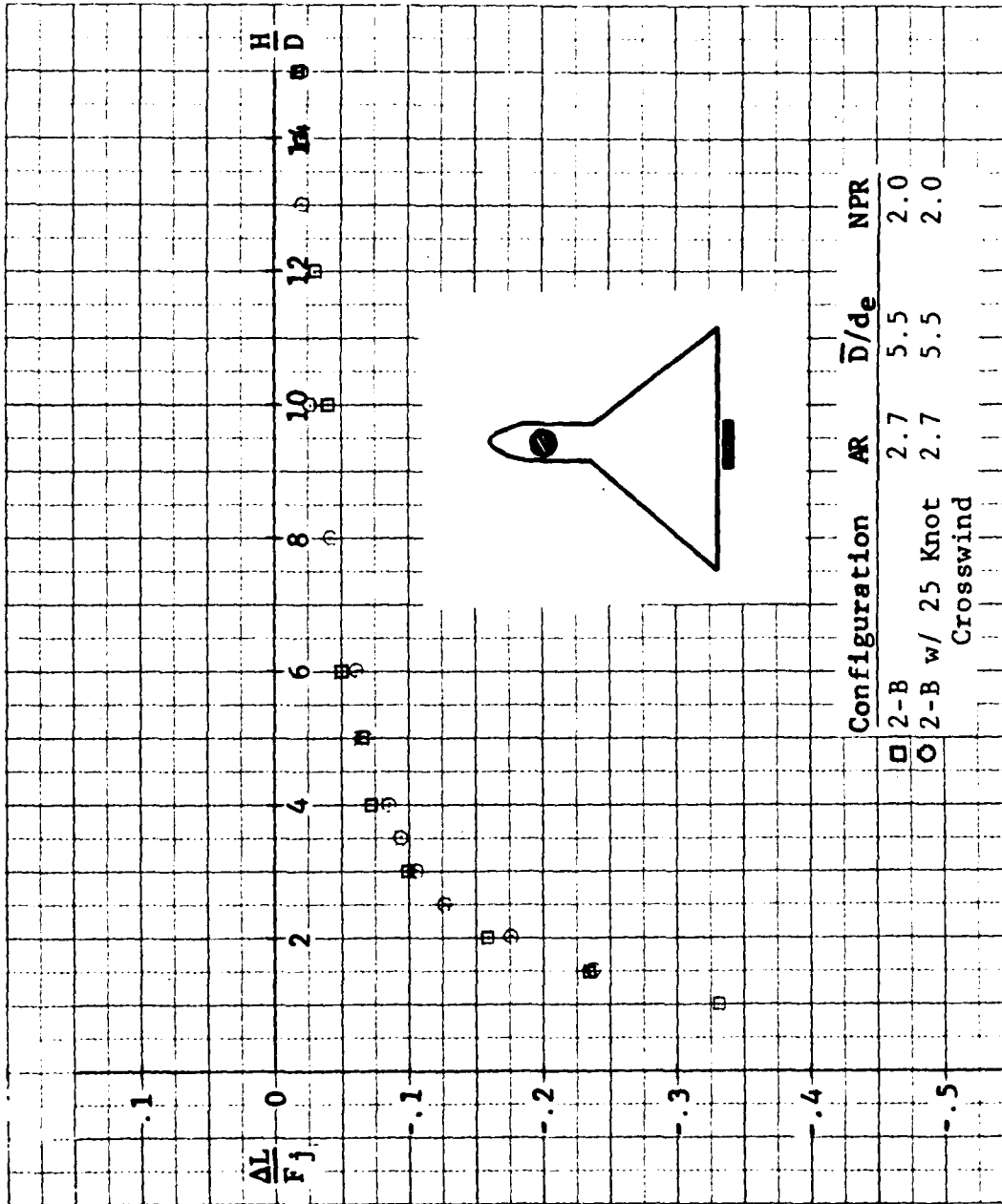
Figure 4.0-1 Induced Lift vs. Altitude
Effect of 25 Knot Crosswind

REFERENCES

1. Spreeman, K. P. and Sherman, I. R., Effects of Ground Proximity on the Thrust of a Simple Downward Directed Jet Beneath a Flat Surface, NACA TN 4407, 1958.

2. Davenport, E. E. and Spreeman, K. P., Thrust Characteristics of Multiple Lifting Jets in Ground Proximity, NASA TN D-513, 1960.

3. Vogler, R. D., Ground Effects on Single and Multiple Jet VTOL Models at Transition Speeds Over Stationary and Moving Ground Planes, NASA TN D-3213, 1966.

4. Wyatt, L. A., Static Tests of Ground Effect on Planforms Fitted with a Centrally Located Round Lifting Jet, Ministry of Aviation C. P. 749, 1962.

5. Kotansky, D. R., Durando, N. A., and Bristow, D. R., Jet-Induced Forces and Moments In and Out of Ground Effect, Report No. NADC 77229, 30 June 1977.

6. Siclari, M. J., Barche, J., and Migdal, D., V/STOL Aircraft Prediction Technique Development for Jet-Induced Lift in Hover, Grumman Aerospace Corp. PDR 623-18, April, 1975.

7. Karemaa, A., Smith, C. W., Weber, H. A., and Garner, J. E., The Aerodynamic and Thermodynamic Characteristics of Fountains and Some Far-Field Temperature Distributions, Office of Naval Research Report ONR-CR212-237-1F, July, 1978.

8. Smith, C. W. and Karemaa, A., Induced Effects of Multiple-Jet Fountains on Flat-Plate Surfaces, AIAA Paper No. 78-1516, August, 1978.

9. Kuhn, R., An Engineering Method for Estimating the Induced Lift on V/STOL Aircraft Hovering In and Out of Ground Effect, NADC-80246-60, January, 1981.

10. Siclari, J. J., Hill, W. G., and Jenkins, R. C., Investigation of Stagnation Line and Upwash Formation, AIAA Paper No. 78-1516, August, 1978.

11. Lummus, J. R., The Criticality of Engine Exhaust Simulations on VSTOL Model-Measured Ground Effects, Office of Naval Research Report No. ONR-CR212-255-1F, August 1979.

12. Foley, W. H., Methodology for Prediction of V/STOL Propulsion Induced Forces in Ground Effect, AIAA Paper 79-1281.

13. Kamman, J. H. and Hall, C. L., Lift System Induced Aerodynamics of V/STOL Aircraft in a Moving Deck Environment, Report No. NADC-77-107-30, September, 1978.

14. Wohllebe, E. A. and Migdal, D., Some Basic Test Results of V/STOL Jet-Induced Lift Effect in Hover, AIAA Paper No. 79-0339, January, 1979.

15. Gentry, G. L. and Margason, R. J., Jet-Induced Lift Losses on VTOL Configurations Hovering In and Out of Ground Effect, NASA TN D-3166, 1966.

16. Foley, W. H. and Sansone, J. A., V/STOL Propulsion-Induced Aerodynamics Hover Calculation Method, General Dynamics, NADC-78242-60, February 1980.

17. Foley, W. H., Test Results of Ground-Induced Forces and Moments on Hovering VSTOL Aircraft, General Dynamics Fort Worth Report No. ERR-FW-1921, December, 1978.

18. Cea, R. A. and Krepski, R. E., Experimental Evaluations of Aero/Propulsion Effects for Lift Plus Lift/Cruise V/STOL Aircraft, Grumman Aerospace Corporation, Workshop Proceedings on Prediction Methods for Jet V/STOL Propulsion Aerodynamics, Arlington, VA, July 1975.

19. Spong, E. D., Kamman, J. H., Flood, J. D., V/STOL Jet Induced Interactions, McDonnell Aircraft Company, Workshop Proceedings on V/STOL Aircraft Aerodynamics, Monterey, CA, May 1979.

APPENDIX A

MODEL CONFIGURATIONS

and

FORCE DATA

(INDUCED LIFT vs ALTITUDE)

The model configurations used during the test phase of this program are detailed on Figures A-1 through A-5.

Two-nozzle configurations incorporating rectangular nozzles are of three types: (a) Configuration 2-A, employing jets through or under the wing (so that the static thrust center and the a.c. are close together), (b) Configuration 2-B, Lift-Lift/Cruise, and (c) Configuration 2-C, with jets longitudinally along each of the fuselage. Configuration 2-A could be used for either a transport or a fighter aircraft and could be powered by either lift/cruise engines, fans, or ejectors. Thus, it was tested over the full range of AR and $\bar{D}/D_e$. Configuration 2-B corresponds to a typical single cruise-engine fighter; appropriate ARs for this engine are 1 and 2.7. However, the lift engine exhaust is circular; there is a weight penalty involved but no performance benefit obtained from transitioning to rectangular. The appropriate $\bar{D}/D_e$'s would be 6.5 through 10. Configuration 2-C, on the other hand, is likely only in an ejector version. It was tested at AR = 6, $\bar{D}/D_e$ = 3.

Three-nozzle Configurations incorporating rectangular nozzles tend all to be lift-lift/cruise aircraft. Configuration 3-A has a circular exhaust for a lift engine, fan, or puffer pipe. This configuration was tested at AR = 1, 2.7 and 6. The range of $\bar{D}/D_e$ was from 3 through 10. The planforms fabricated for Configuration 2-A were modified for this test. Configuration 3-B is typical of a lift-twin lift/cruise aircraft. Again, the forward nozzle is circular as is appropriate for either a lift engine or a RALS nozzle. This type configuration is appropriate for a fighter aircraft so that AR = 1.0 and 2.7, $\bar{D}/D_e$ = 6.5 through 10 were tested. The planform from Configuration 2-B was modified for this configuration.

Four-nozzle Configurations incorporating rectangular nozzles also tend to fall into two types. The first, Configuration 4-A, is simply a varient of Configuration 2-C wherein each ejector is replaced by two, smaller AR ejectors. This has the advantage of permitting an integral pitch control/lift system. Configuration 2-C was modified and tested with the AR = 2.7 nozzles and $\bar{D}/D_e$ = 3. The other four nozzle possibility, Configuration 4-B, is somewhat similar to the XFV-12A arrangement. Configuration 2-B was modified to provide this arrangement and was tested with AR = 2.0 forward and 1, 2.7 and 6 aft. $\bar{D}/D_e$ ranged from 3 through 10.

A complete set of force balance data obtained during this program is contained on Figures A-6 through A-63 and listed on Table A-1. The data is presented as Induced Lift versus Altitude. The height of the test model is measured from the ground board to the underside of the flat plate planform. In the cases of LIDs or contoured fuselage, the height is measured to the underside of the wings. Altitude has been nondimensionalized by $\bar{D}$, the thrust-weighted average of the equivalent diameters of all jets of a configura-

69

tion. Each configuration was tested with all of its jets having the same equivalent nozzle diameter and the same thrust regardless of AR. Thus,

$$D = \frac{d_1 F_{j1} + d_2 F_{j2} + d_3 F_{j3} + d_4 F_{j4}}{F_{j_T}} = d_{1,2,3,4}$$

The models tested were selected as plausible design configurations for aircraft with rectangular nozzles. These configurations were tested with LIDs and contoured fuselage sections that covered the full fuselage width. Each configuration was varied in planform size to account for a range of $\bar{D}/D_e$. During this variation the nozzle locations remained fixed.

Testing was also accomplished in a cross-wind environment. During these runs, a shroud was used to restrict the crosswind from flowing on top of the model and interfering with the balance.
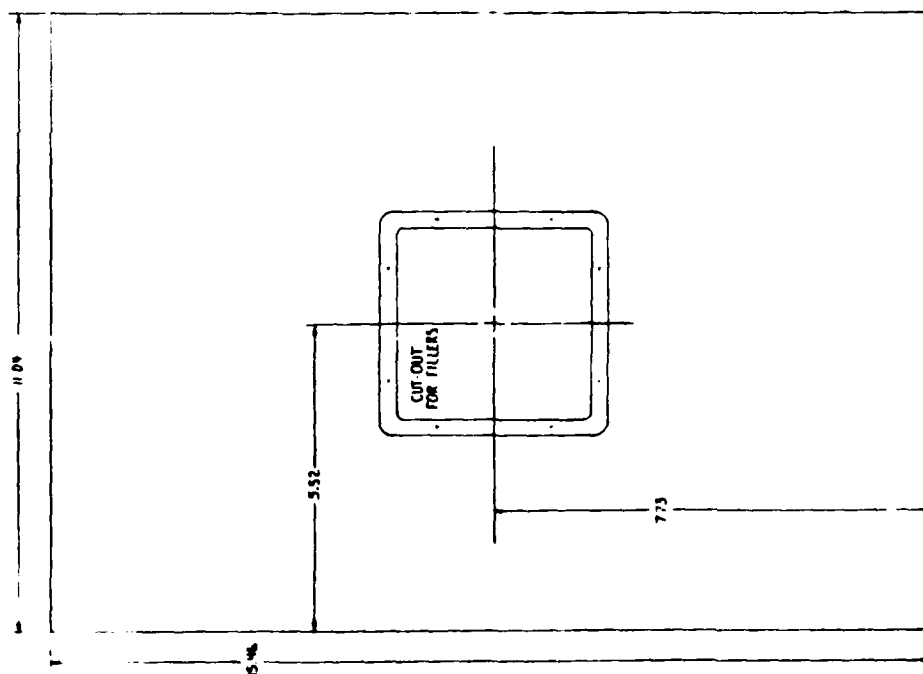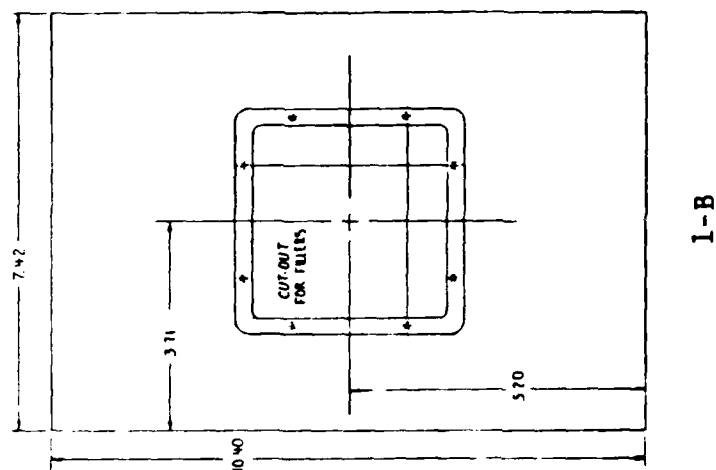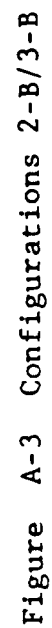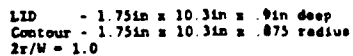
Figure A-1   Configurations 1-A, B, C

71

Figure A-2 Configurations 2-A/3-A

LID - 3.0in x 13.5in x 2.0in deep
Contour - 3.0in x 13.5in x 1.5in radius
2r/W = 1.0, 0.5

Figure A-3   Configurations 2-B/3-B

Figure A-4 Configurations 2-C/4-A

Figure   A-5   Configuration 4-B

FIG. NO.	CONFIGURATION	R 1.0	R 2.7	R 6.0	NPR* 1.3	NPR* 2.0	NPR* 2.5	D̄/de	LID	CONTOUR** 1.0	CONTOUR** 0.5	CROSS WIND
A-6	1-A	X			X	X	X	3.0				
7			X		X	X	X	3.0				
8			X	X	X	X	X	3.0				
9				X	X	X	X	3.0				
10				X	X	X	X	3.0				
11	1-B	X			X	X	X	6.5				
12			X		X	X	X	6.5				
13			X	X	X	X	X	6.5				
14				X	X	X	X	6.5				
15	1-C	X			X	X	X	10.0				
16			X		X	X	X	10.0				
17			X		X	X	X	10.0				
18			X	X	X	X	X	10.0				
19	2-A	X			X	X	X	3.9				
20			X		X	X	X	3.9				
21				X	X	X		3.9				
22		X		X		X	X	6.2	X	X	X	
23		X		X		X	X	6.2	X	X	X	
24				X		X	X	6.2	X	X		
25		X				X	X	8.8				
26				X		X	X	8.8				
27						X	X	8.8				
28		X			X	X		5.5	X	X	X	
29	2-B	X			X	X		5.5	X	X	X	
30				X	X	X		7.7				
31		X			X	X	X	7.7				
32				X	X	X	X	2.9				
33	2-C			X	X	X		2.9				
34				X	X	X		2.9	X	X		
35				X	X	X		2.9				
36	3-A	X			X	X		3.2				
37			X		X	X		3.2				
38				X	X	X		3.2				

*Nominal Value   **2r/W

Table A-1   Summary of Test Configurations and Conditions

FIG. NO.	CONFIGURATION	AR 1.0	AR 2.7	AR 6.0	NPR* 1.3	NPR* 2.0	NPR* 2.5	D̄/de	LID	CONTOUR** 1.0	CONTOUR** 0.5	CROSS WIND
A-39	3-A	X				X		4.8	X	X		
40			X			X		4.8	X	X	X	
41				X		X		4.8	X	X		
42		X				X		7.3				
43			X			X	X	7.3				
44				X		X	X	7.3				
45	3-B	X				X		4.7	X	X		
46			X			X		4.7	X	X	.	
47		X				X		6.8				
48			X			X	X	6.8				
49			X		X	X		3.1				
50	4-A		X		X	X		3.1	X	X		
51				X	X	X		3.1				
52		X			X	X		2.6				
53			X		X	X	X	2.6				
54				X	X	X	X	2.6				
55	4-B	X				X		3.9	X	X	X	
56			X			X		3.9	X	X	X	
57				X		X		3.9	X	X		
58		X				X	X	7.8				
59			X			X	X	7.8				
60				X		X		7.8				
61	2-B		X			X		5.5				X
62	3-B		X			X		4.7				X
63	4-B		X			X		3.9				X

*Nominal Value

**2r/W

Table A-1 (Cont'd.) Summary of Test Configurations and Conditions

$\frac{\Delta L}{Fj}$

.1

0

-.1

-.2

-.3

-.4

-.5

-.6

-.7

-.8

-.9

-1.0

$\frac{H}{D}$

2　4　6　8　10　12　14

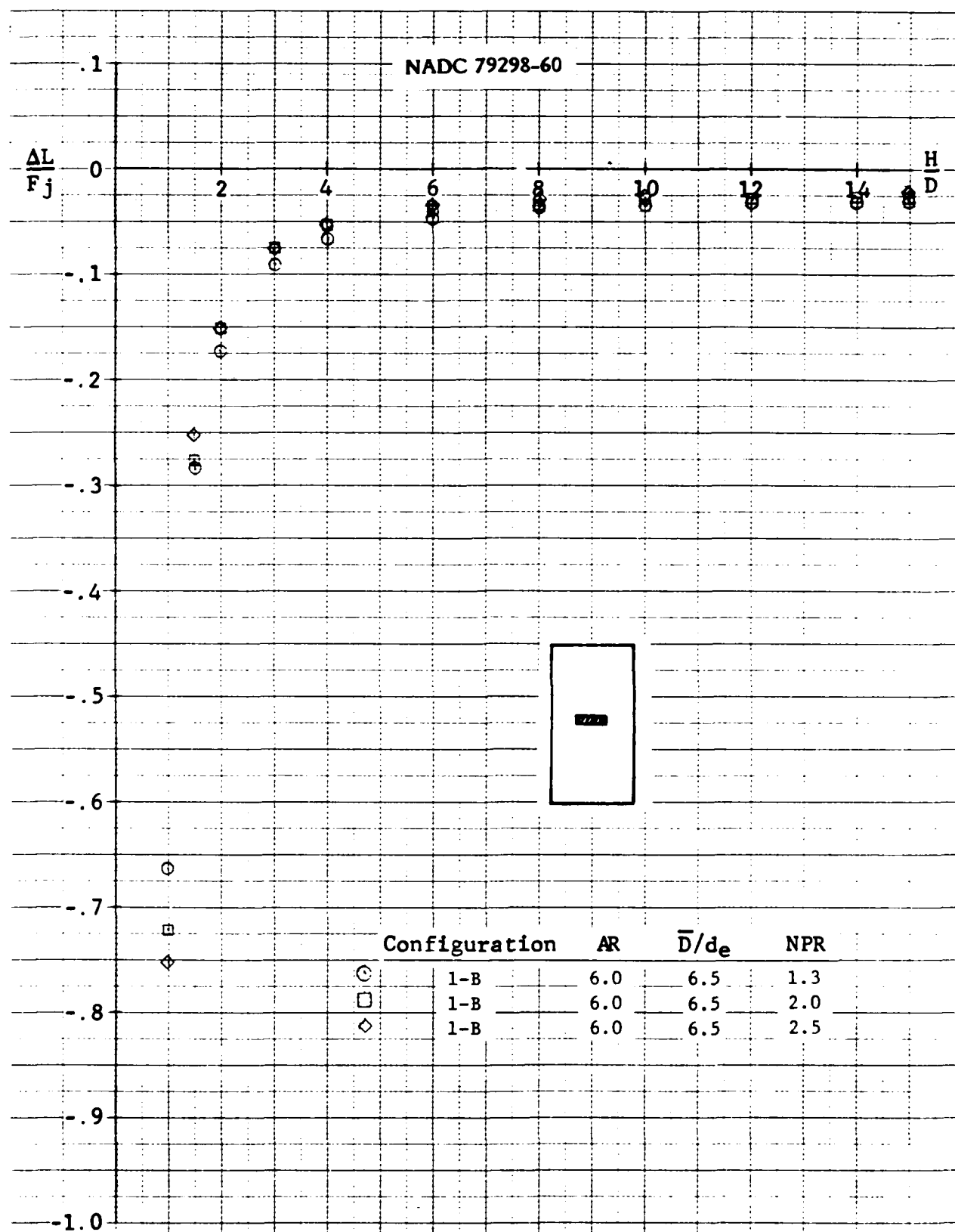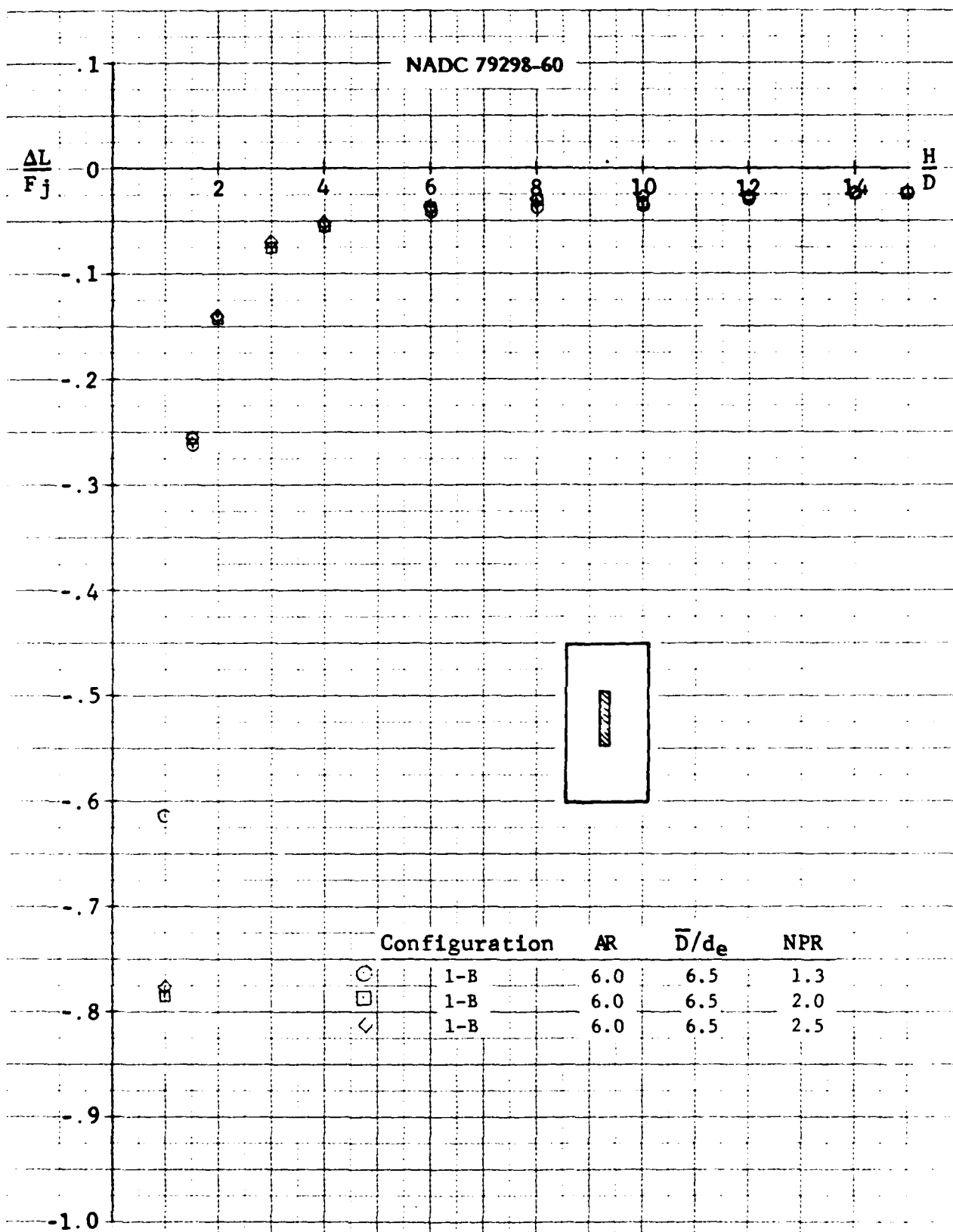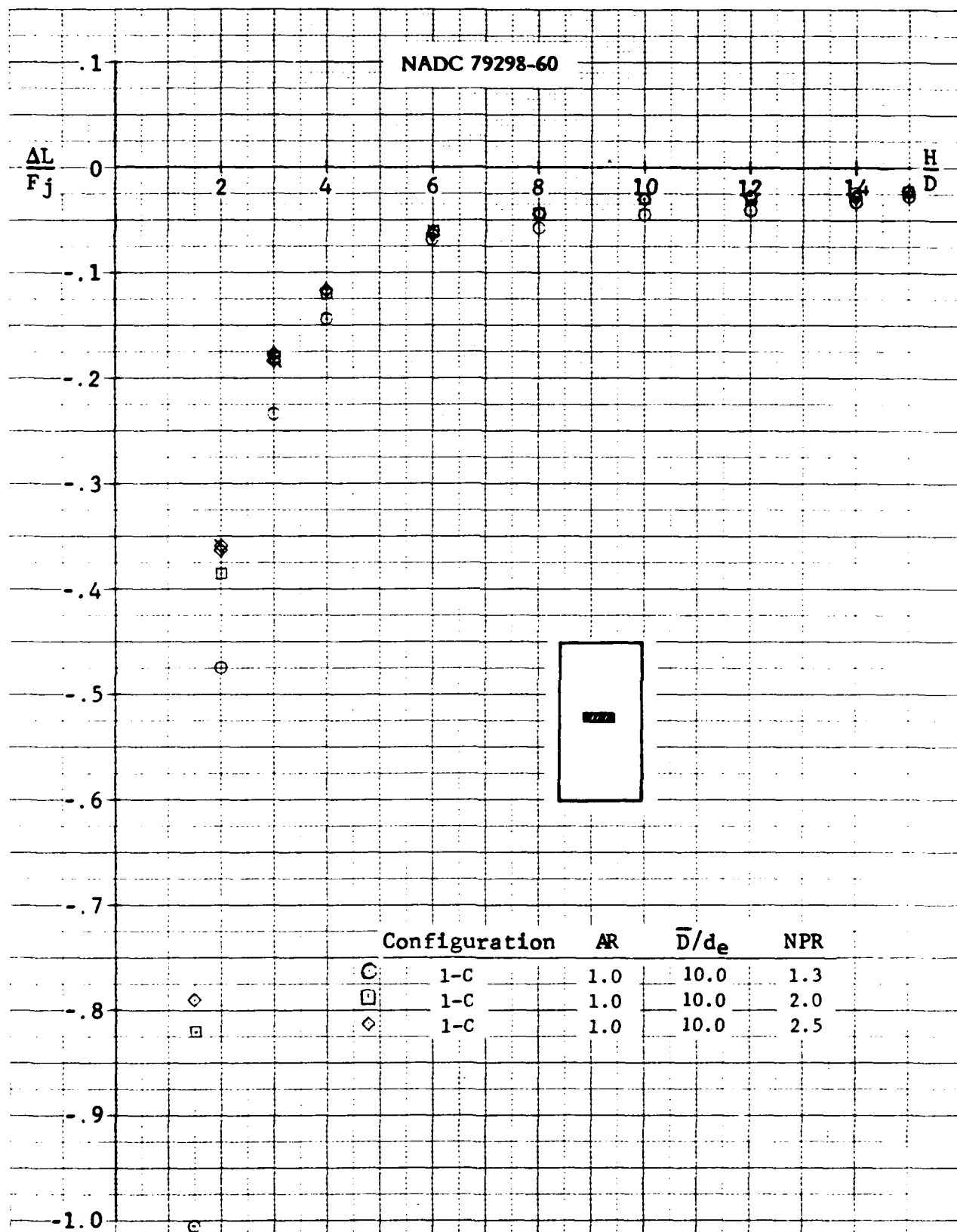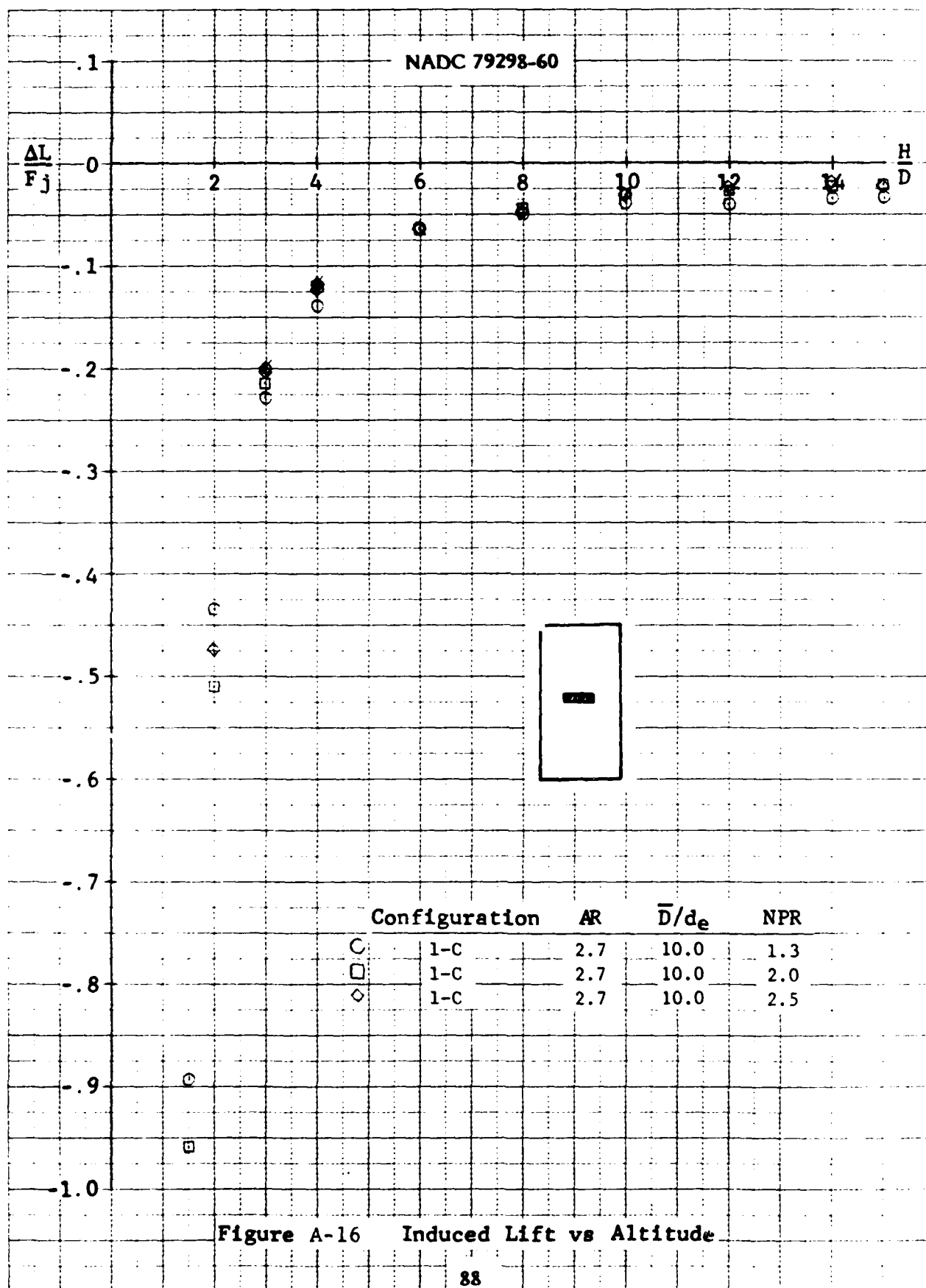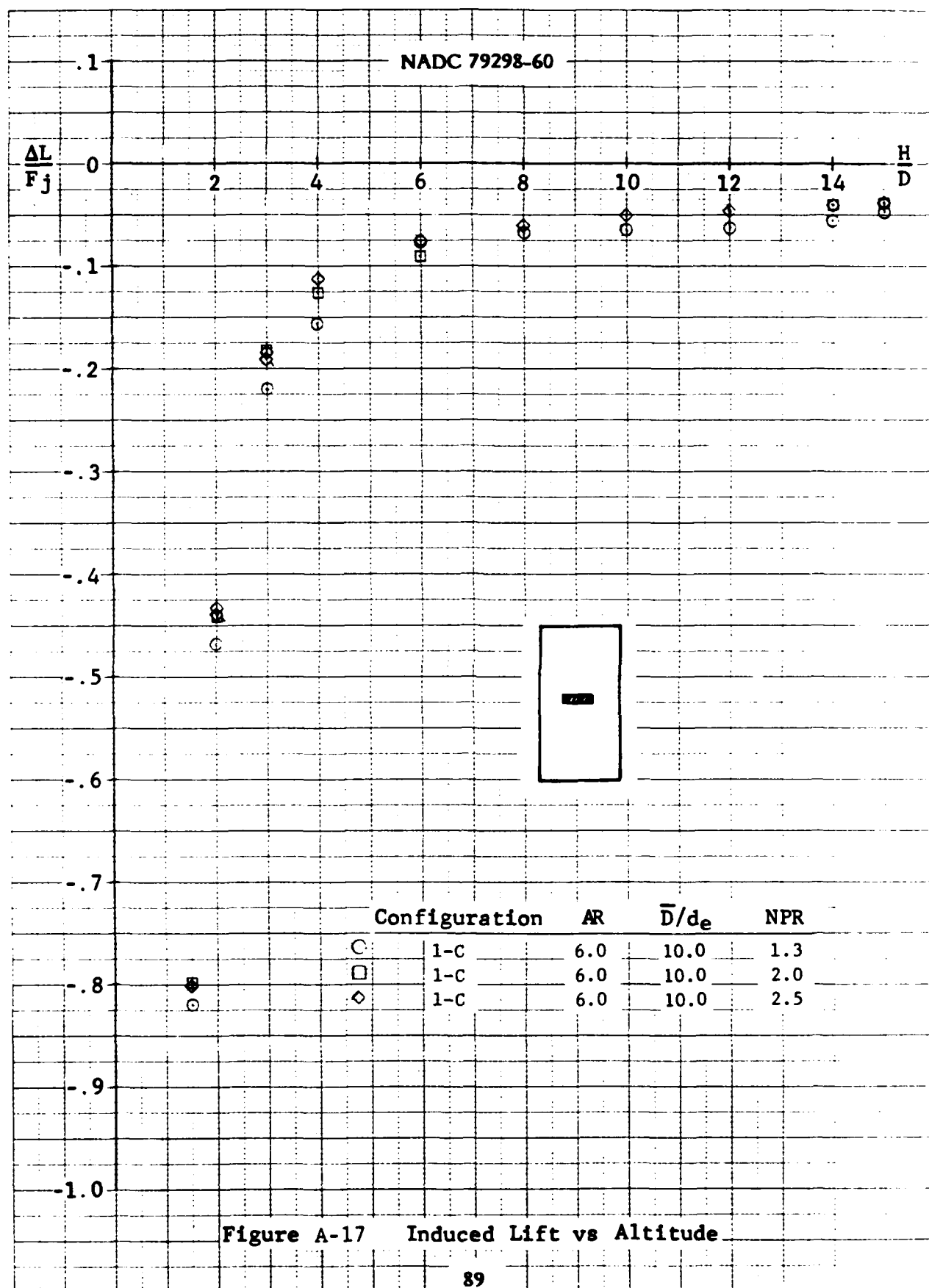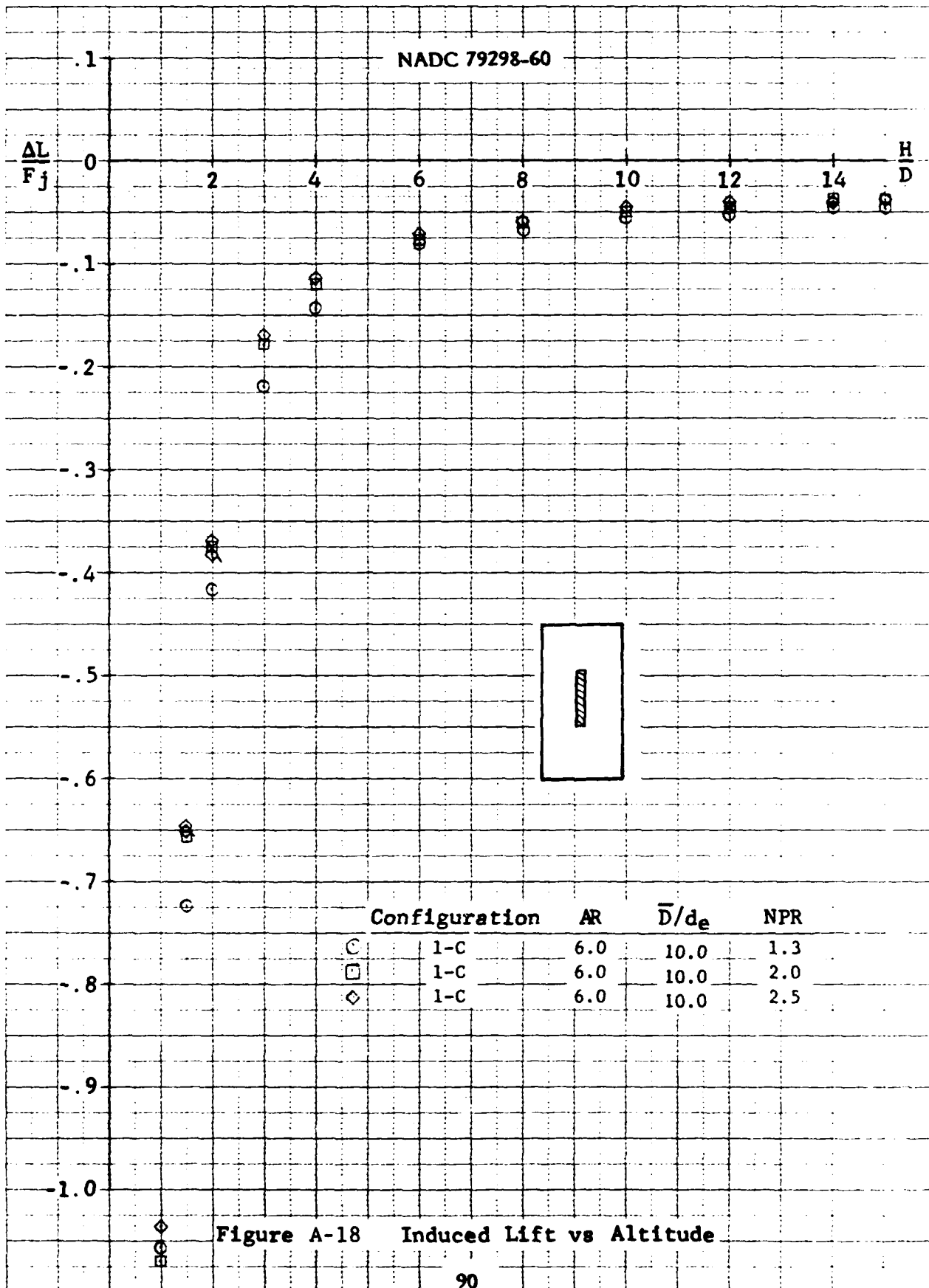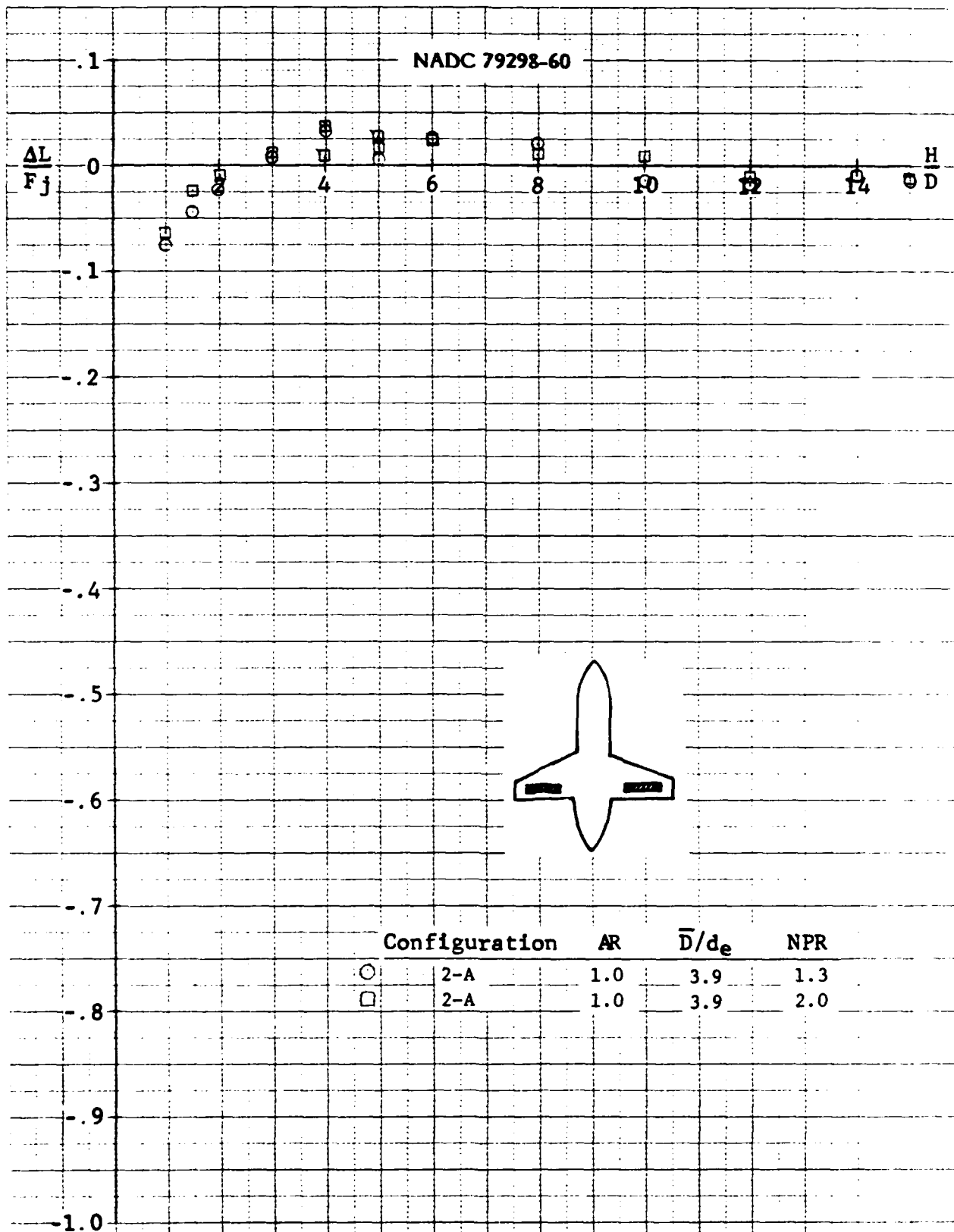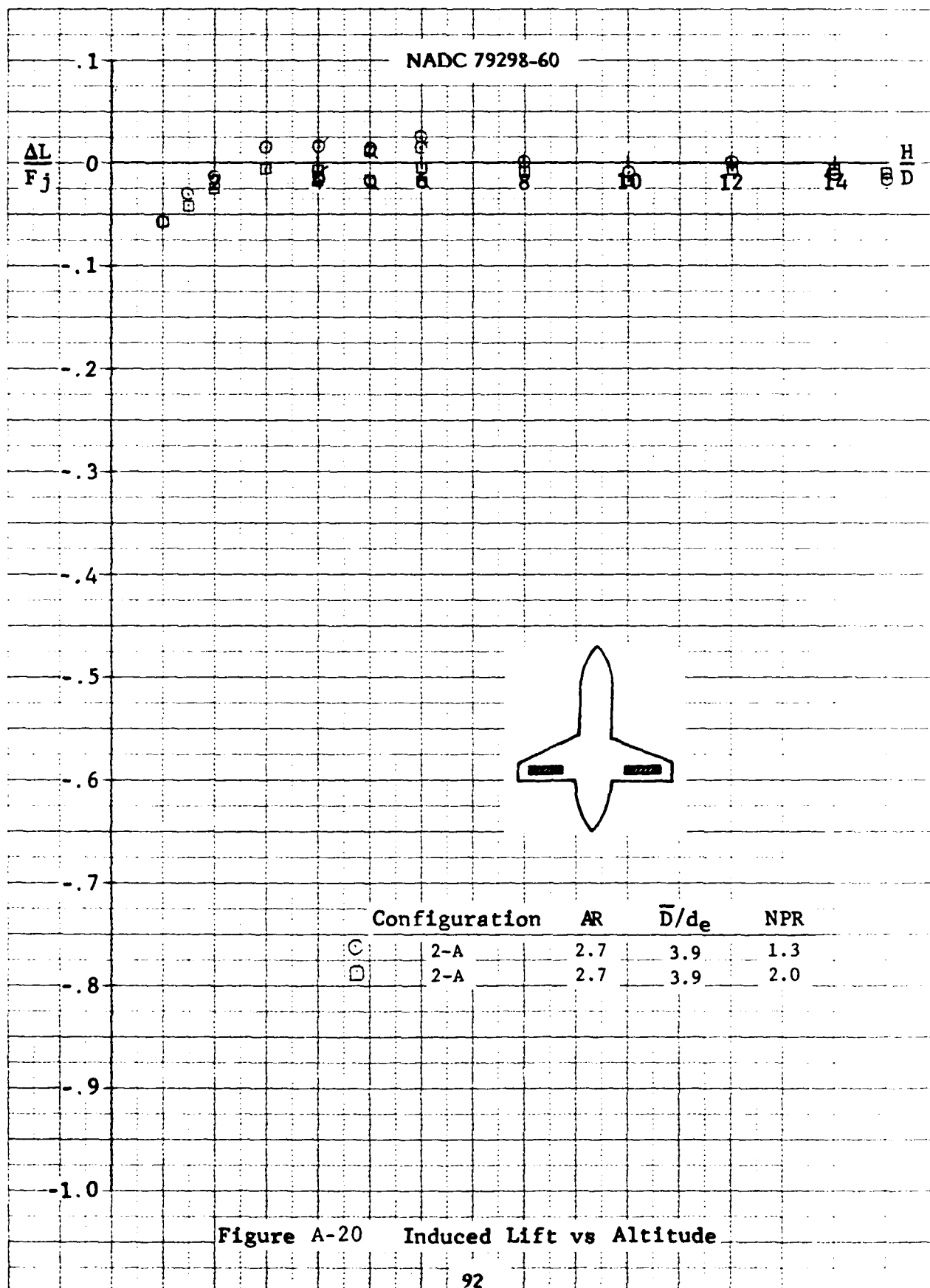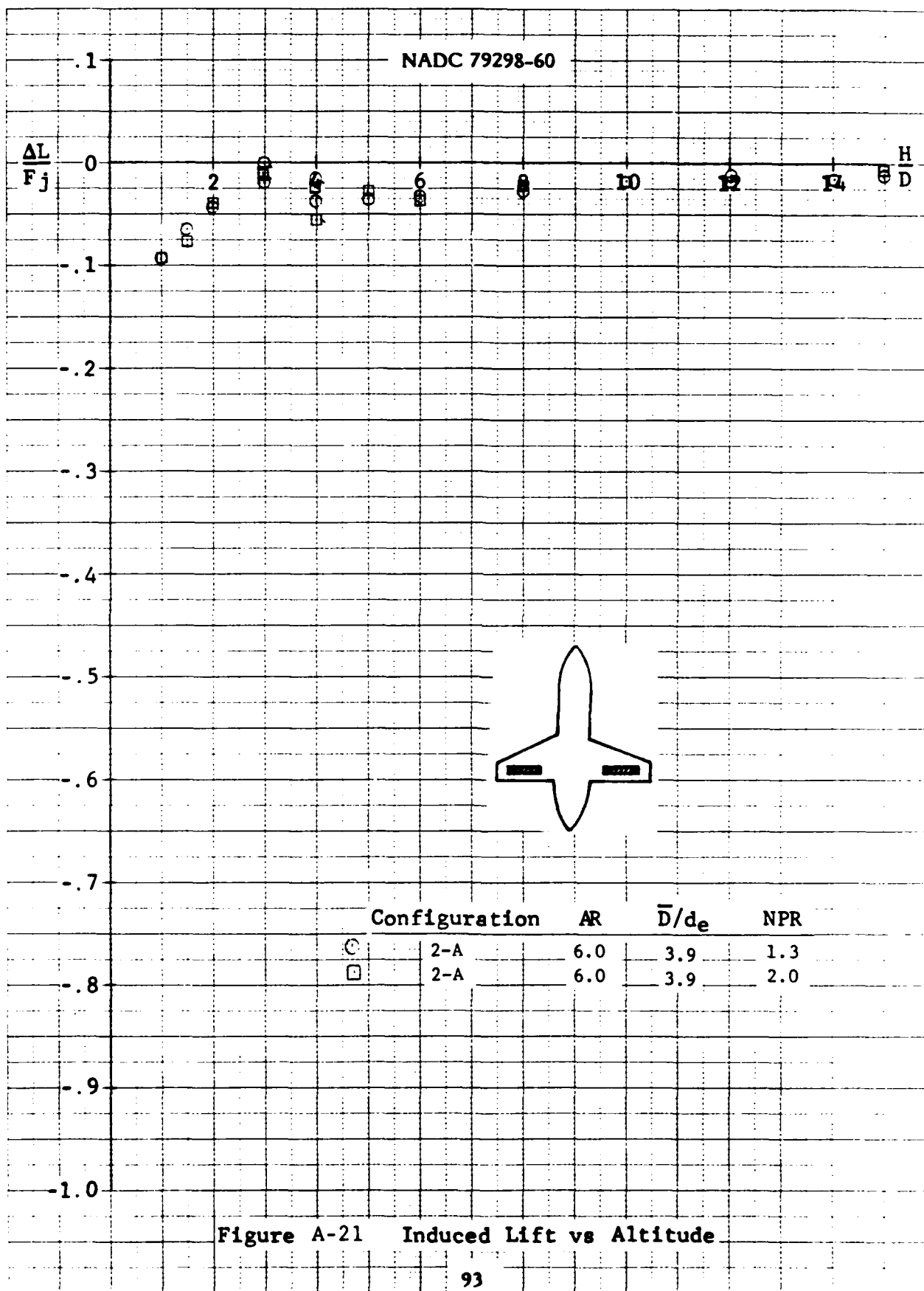|	Configuration	AR	$\overline{D}/d_e$	NPR
☾	1-A	1.0	3.0	1.3
▢	1-A	1.0	3.0	2.0
◇	1-A	1.0	3.0	2.5
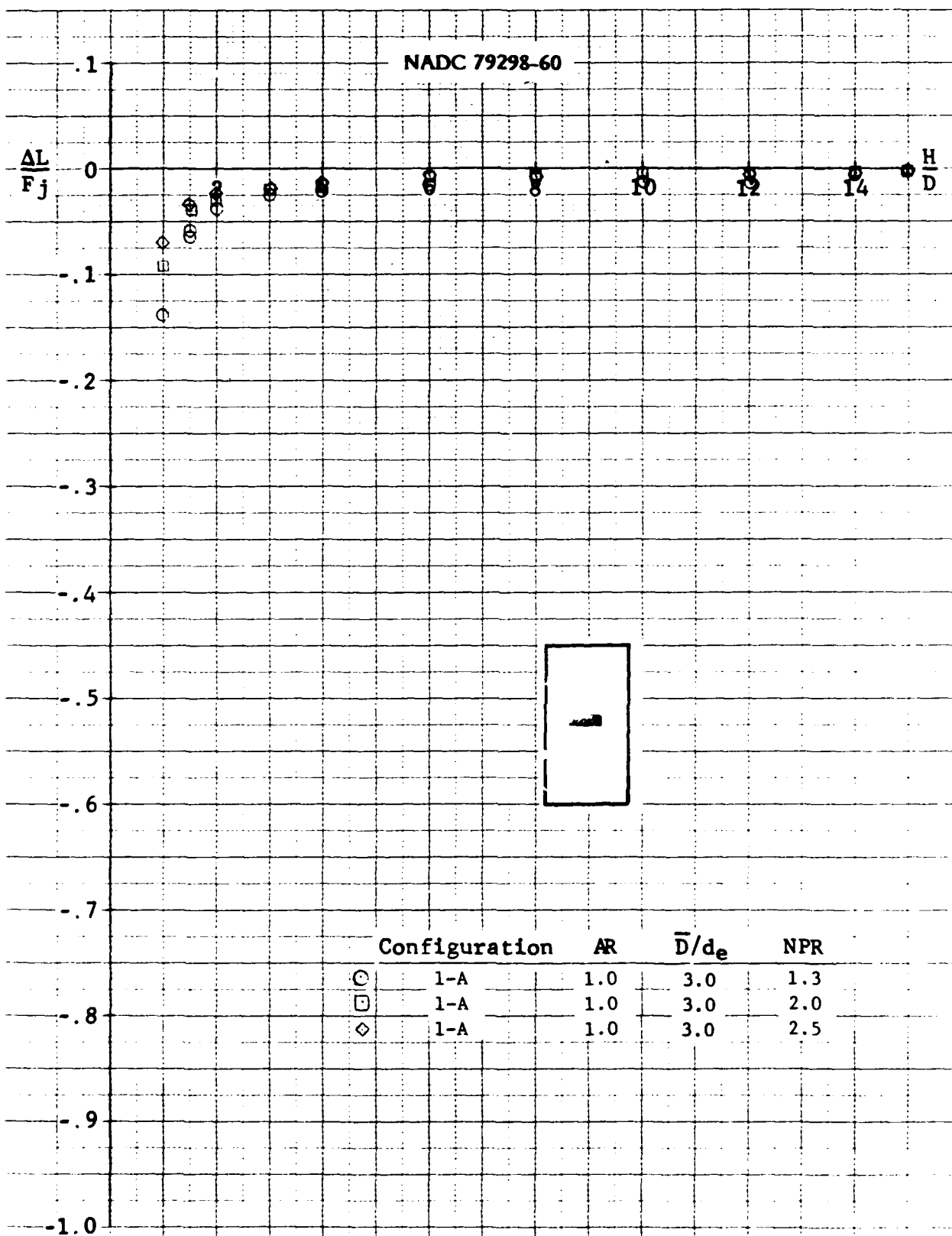
Figure A-6　　Induced Lift vs Altitude
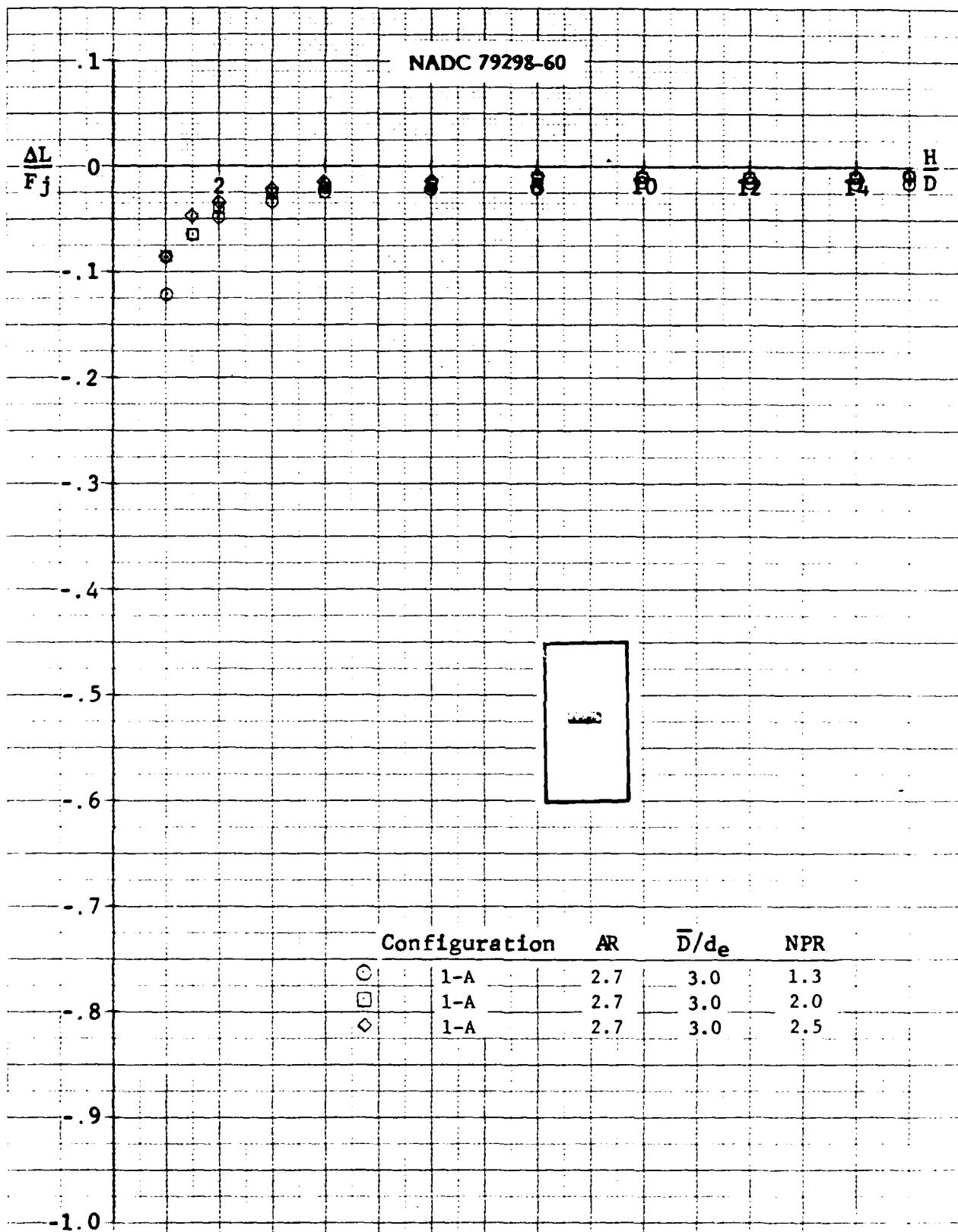
Figure A-7   Induced Lift vs Altitude

NADC 79298-60

$\frac{\Delta L}{F_j}$

.1

0 ⎯ $\frac{H}{D}$

-.1

-.2

-.3

-.4

-.5

-.6

-.7

-.8

-.9

-1.0

2

Configuration	AR	$\overline{D}/d_e$	NPR
○ 1-A	2.7	3.0	1.3
☐ 1-A	2.7	3.0	2.0
◇ 1-A	2.7	3.0	2.5
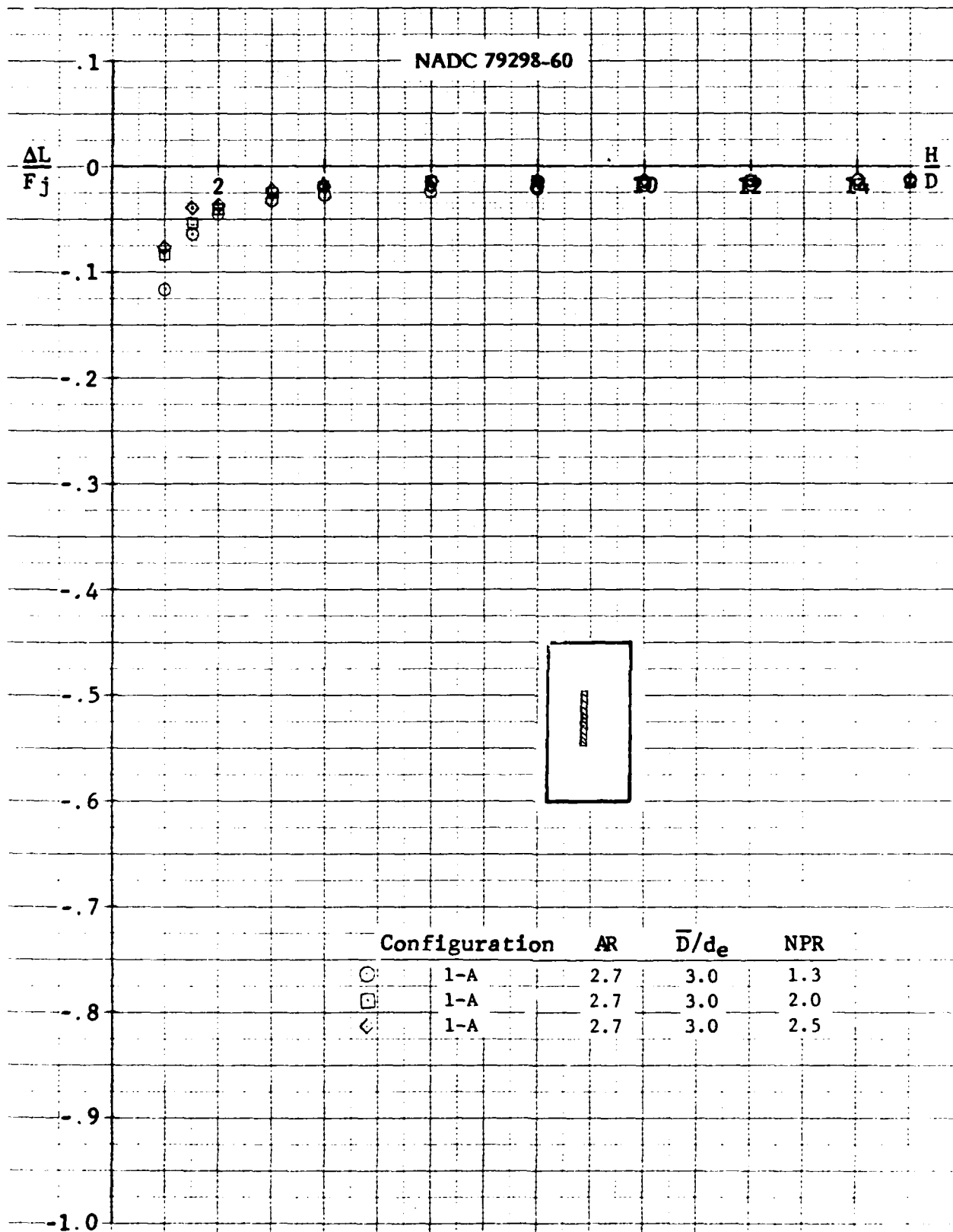
Figure A-8   Induced Lift vs Altitude

80

Configuration	AR	$\overline{D}/d_e$	NPR
◎ 1-A	6.0	3.0	1.3
⬚ 1-A	6.0	3.0	2.0
◇ 1-A	6.0	3.0	2.5
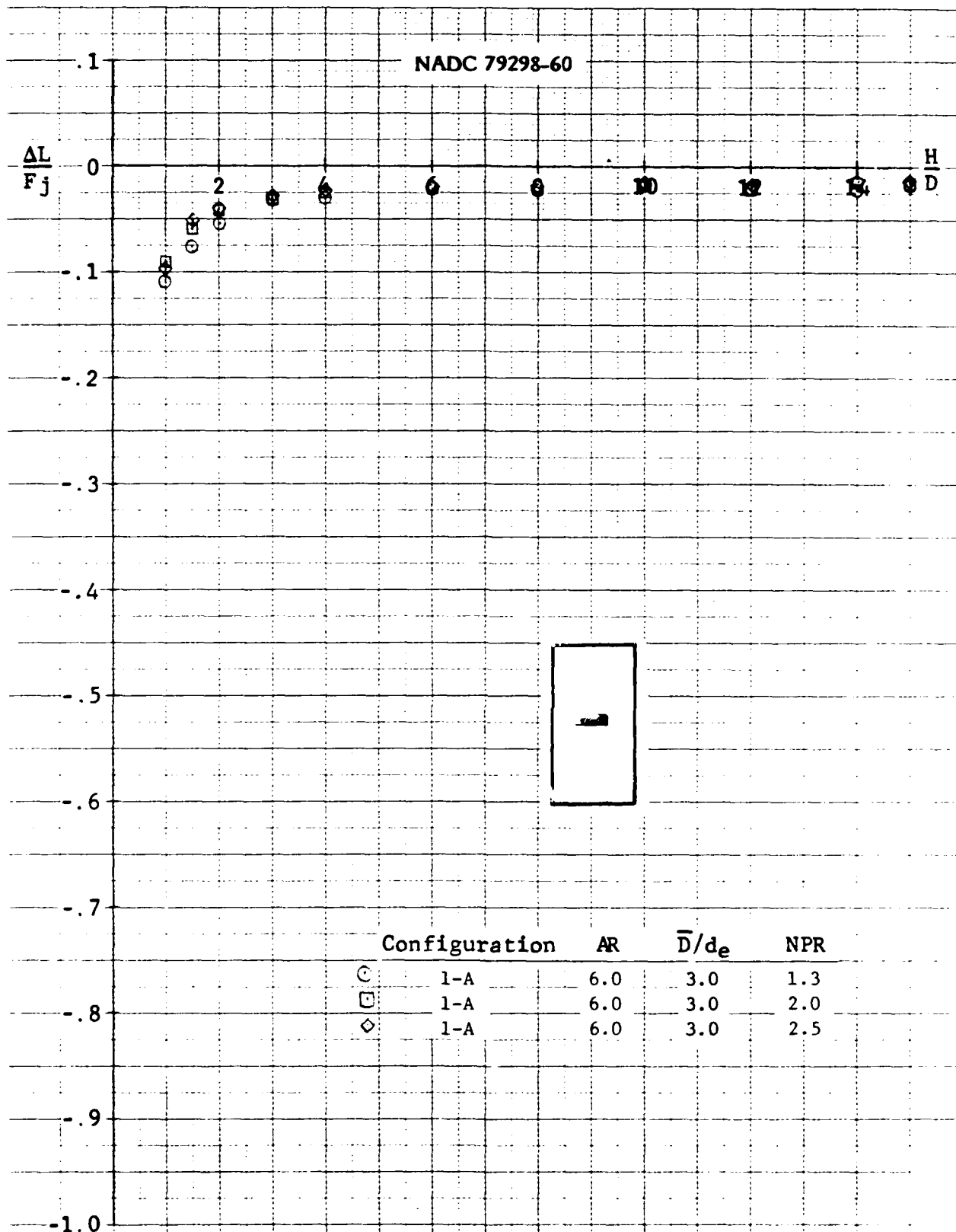
Figure A-9   Induced Lift vs Altitude

$\dfrac{\Delta L}{F_j}$

$\dfrac{H}{D}$

Configuration	AR	$\overline{D}/d_e$	NPR
◯	1-A	6.0	3.0	1.3
◻	1-A	6.0	3.0	2.0
◇	1-A	6.0	3.0	2.5
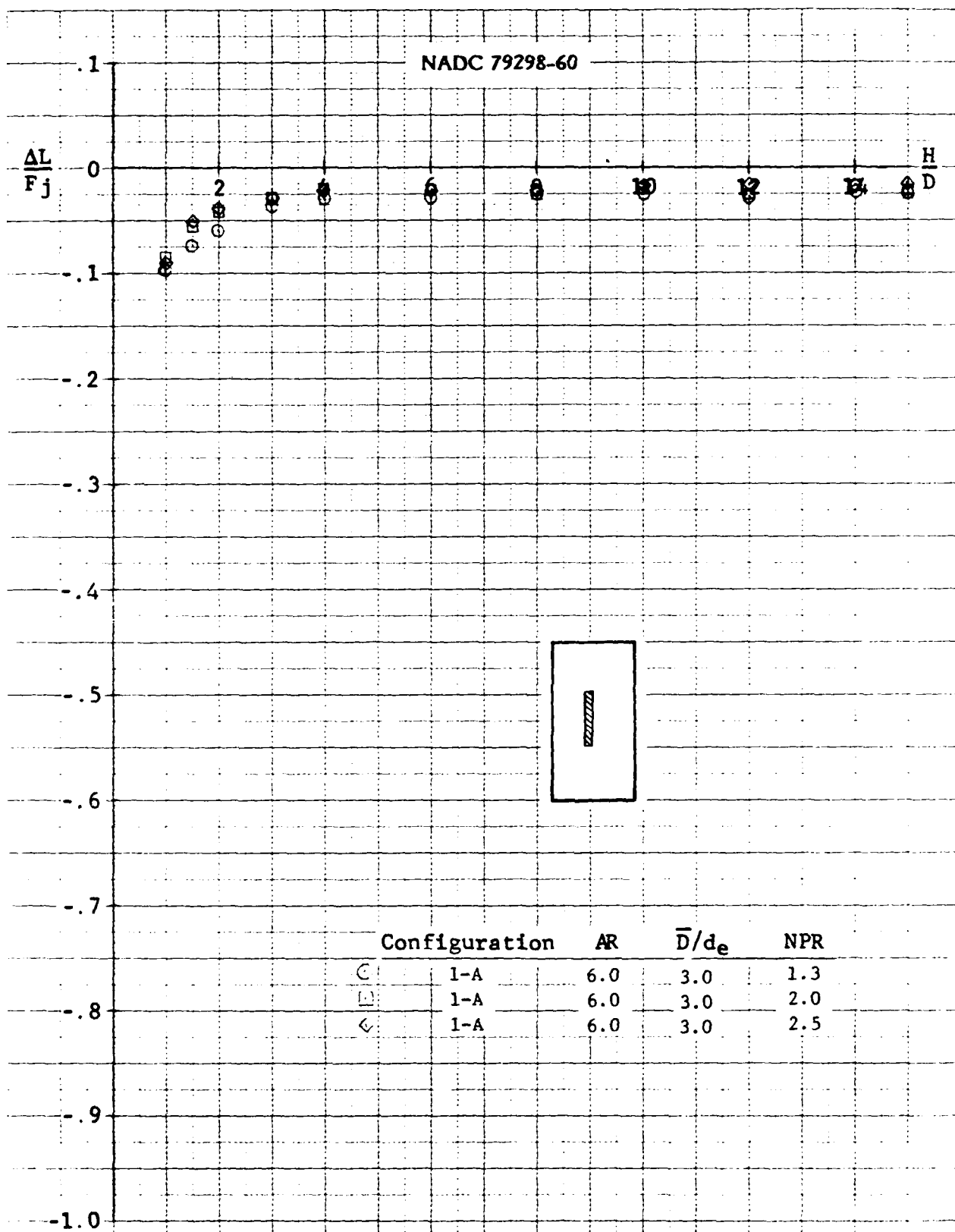
Figure A-10 Induced Lift vs Altitude

$\frac{\Delta L}{F_j}$

.1

0

$-.1$

$-.2$

$-.3$

$-.4$

$-.5$

$-.6$

$-.7$

$-.8$

$-.9$

-1.0

2 4 6 8 10 12 14 $\frac{H}{D}$

Configuration	AR	$\overline{D}/d_e$	NPR
C 1-B	1.0	6.5	1.3
□ 1-B	1.0	6.5	2.0
◇ 1-B	1.0	6.5	2.5
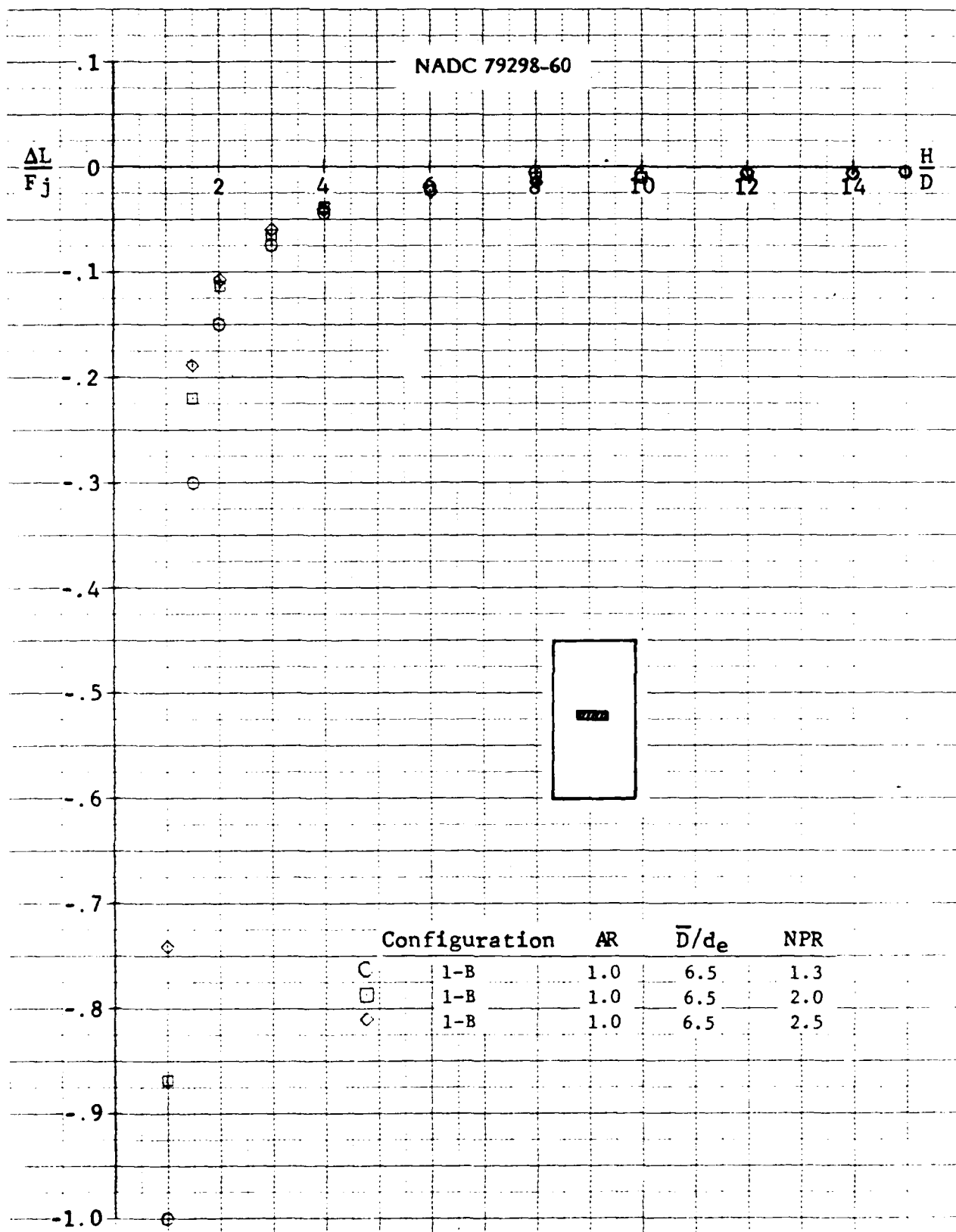
Figure A-11   Induced Lift vs Altitude
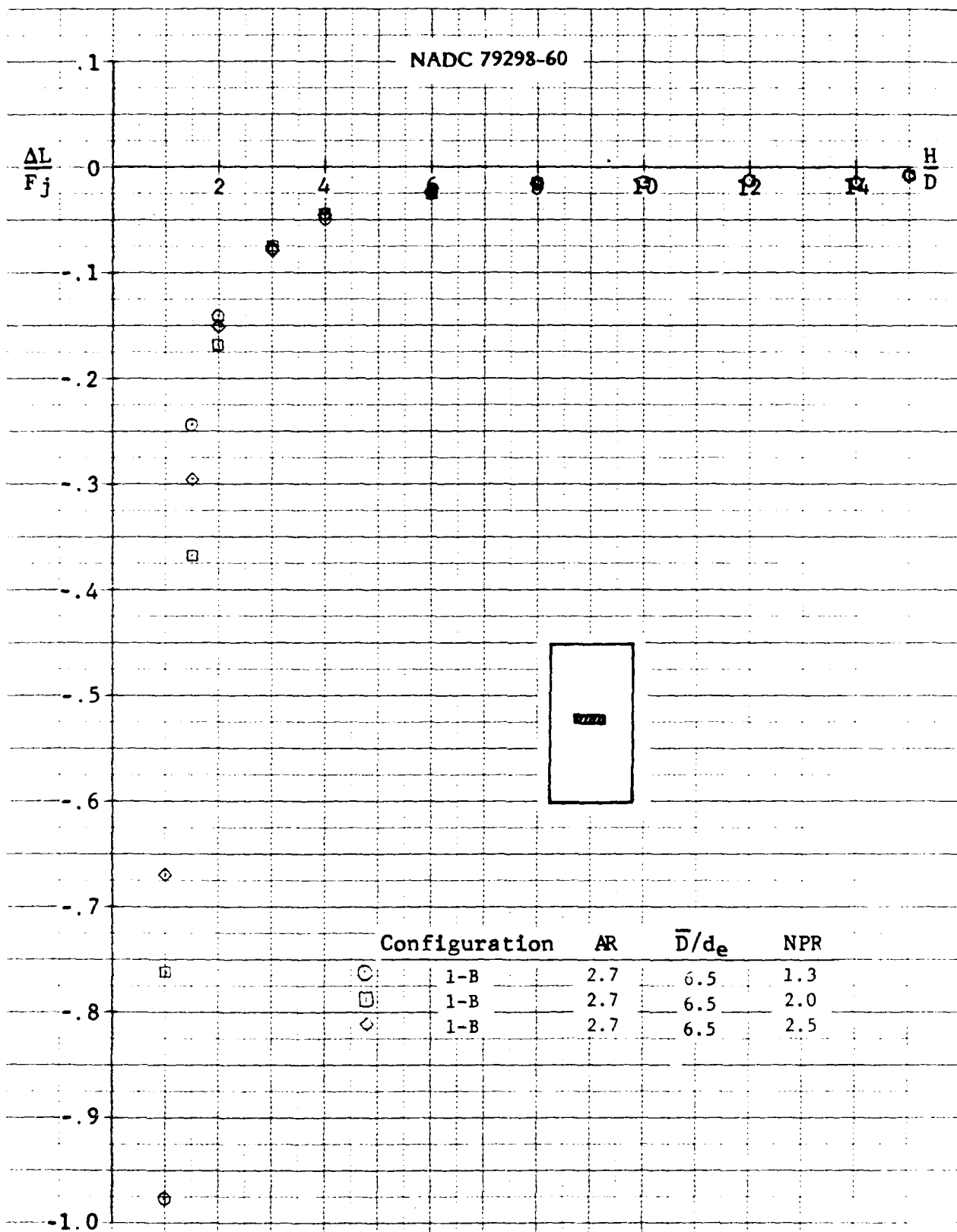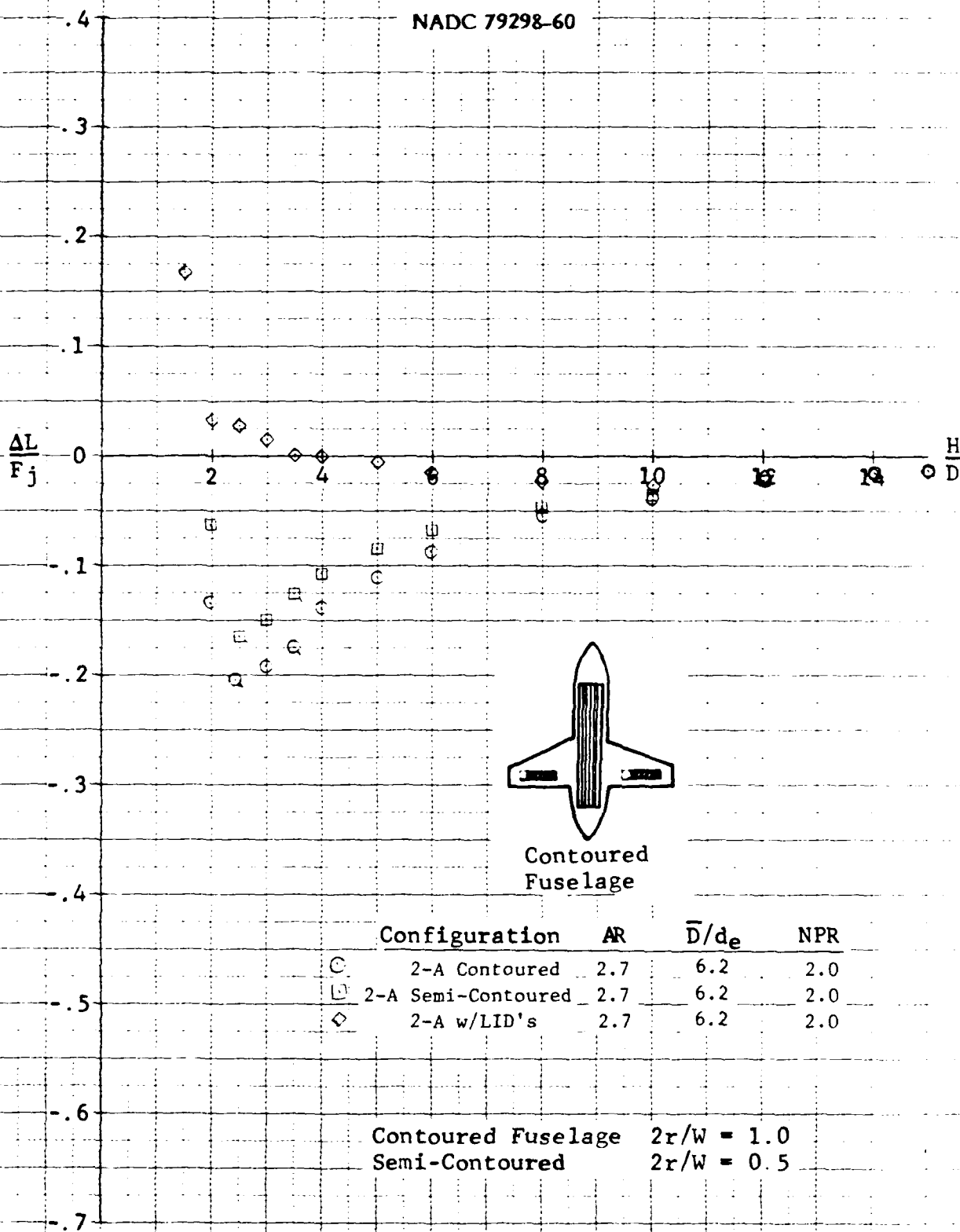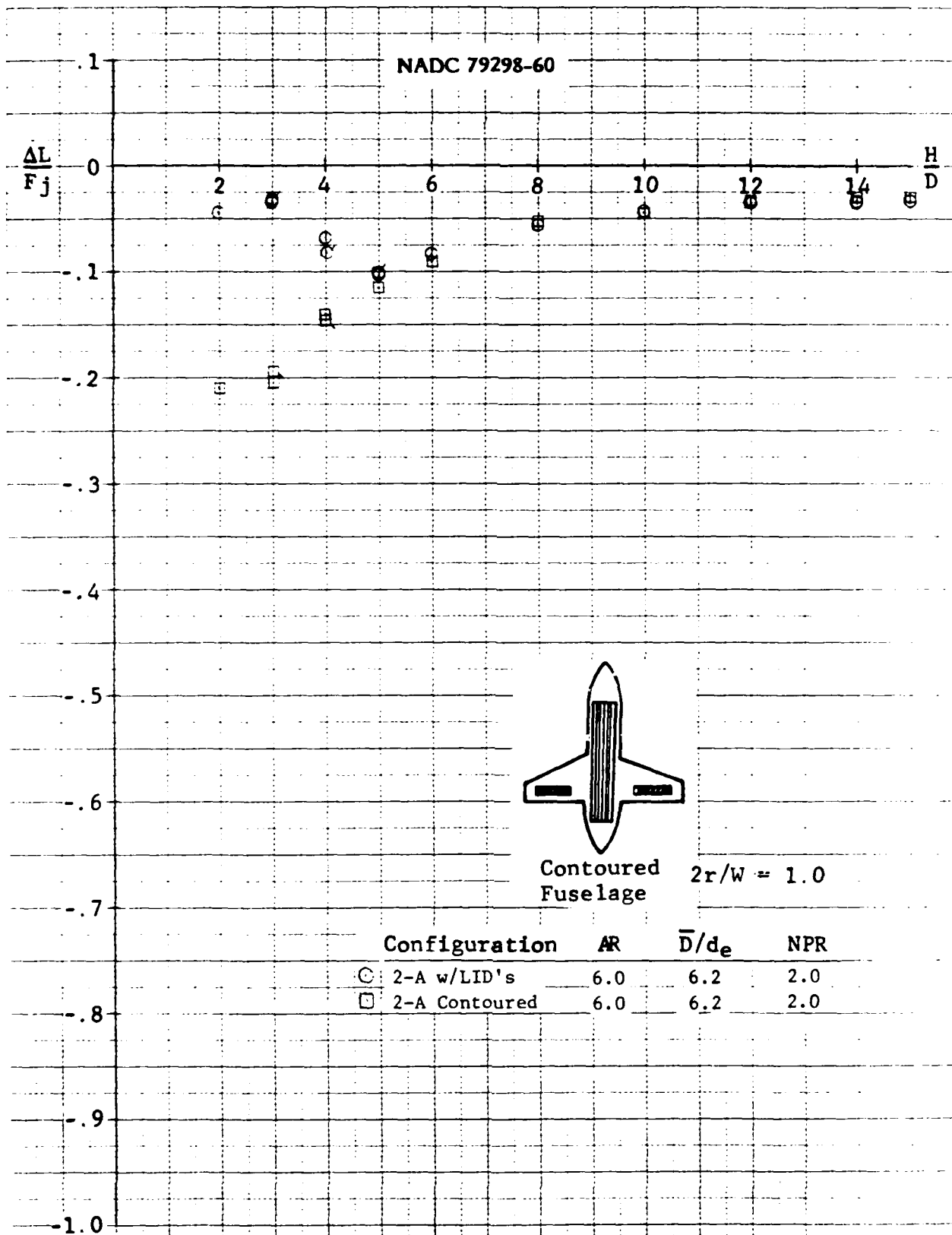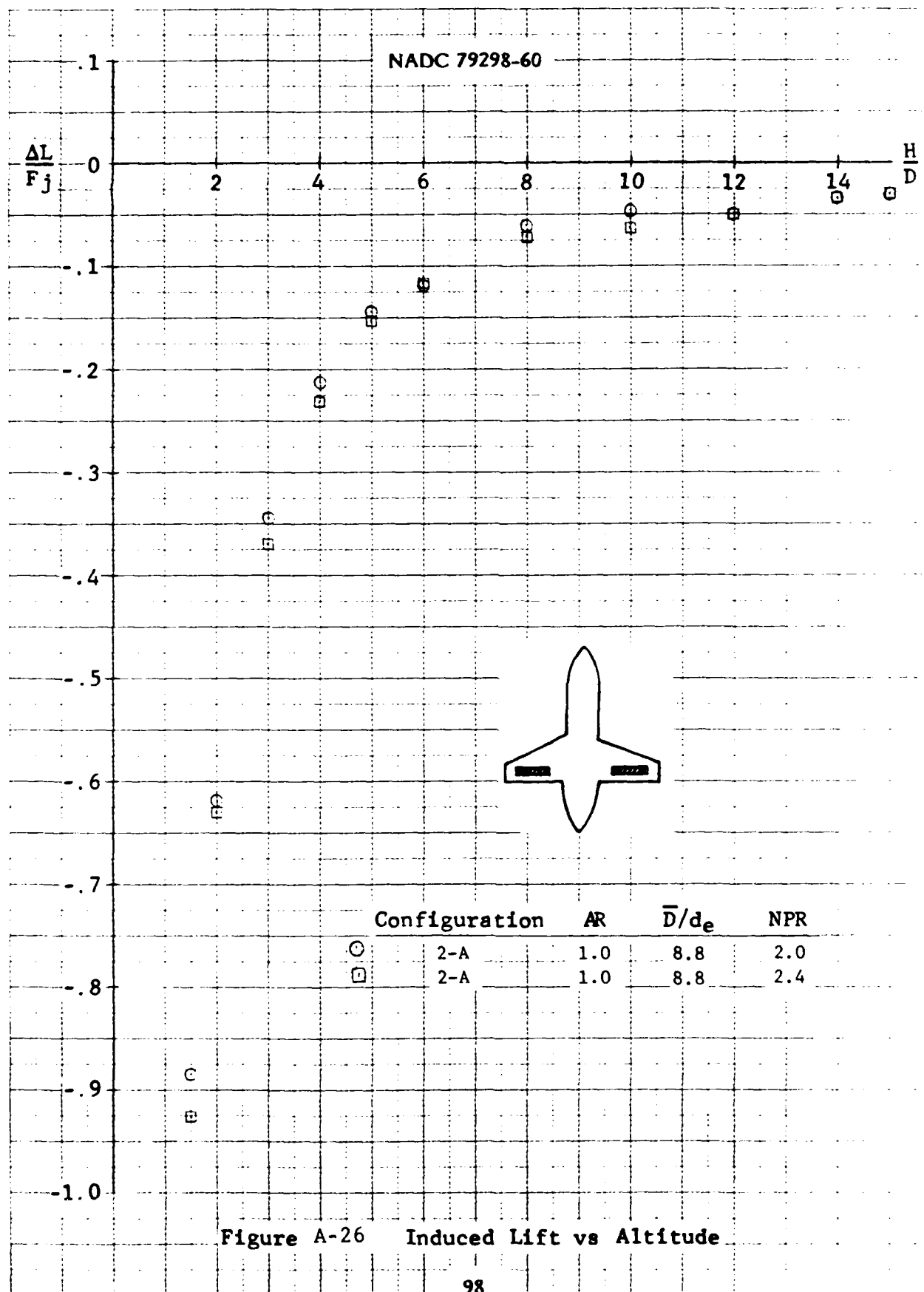
Figure A-12   Induced Lift vs Altitude

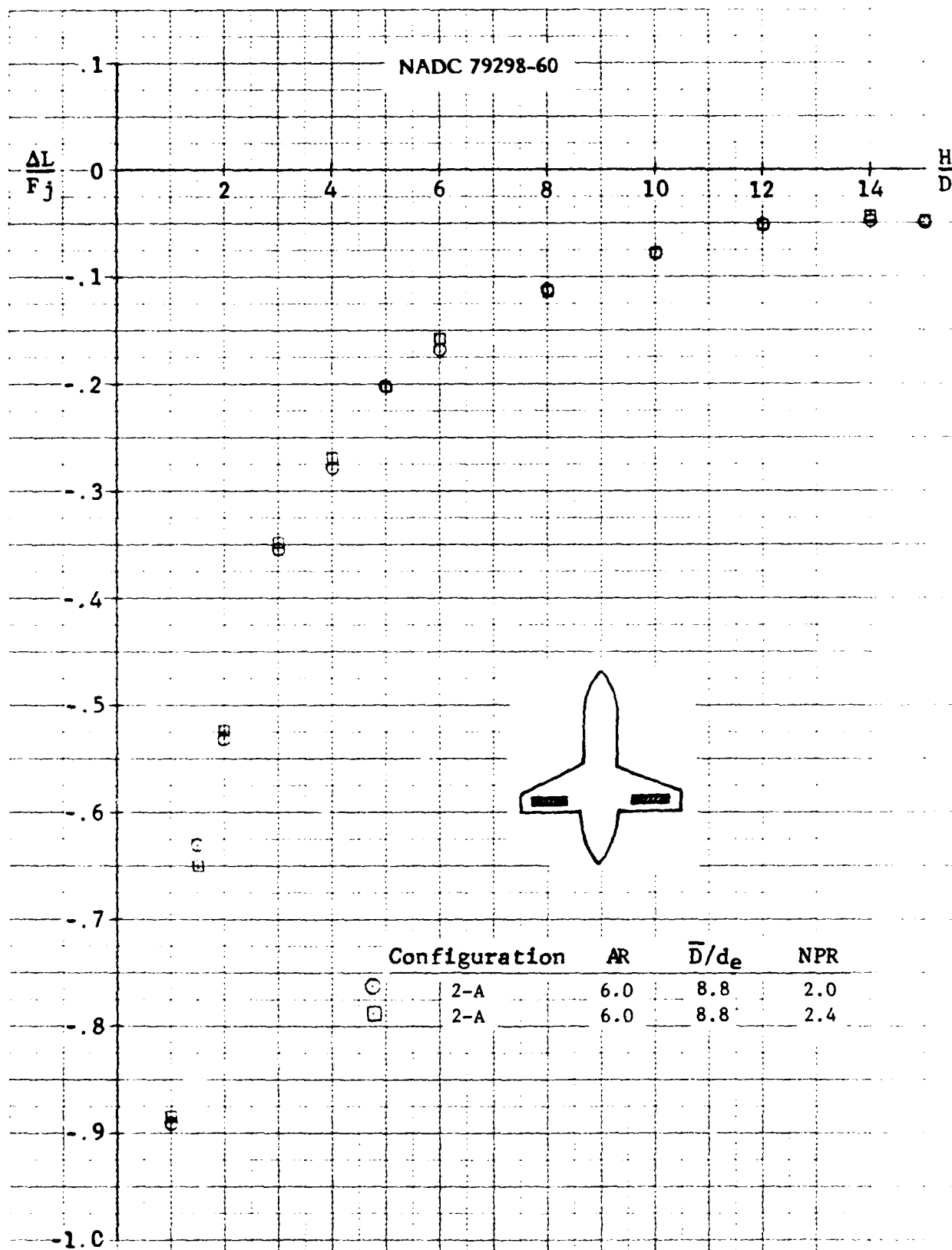| Configuration	AR	$\overline{D}/d_e$	NPR
1-B	2.7	6.5	1.3
1-B	2.7	6.5	2.0
1-B	2.7	6.5	2.5

84

END
DATE
FILMED
11-81
DTIC

Figure A-13   Induced Lift vs Altitude

85

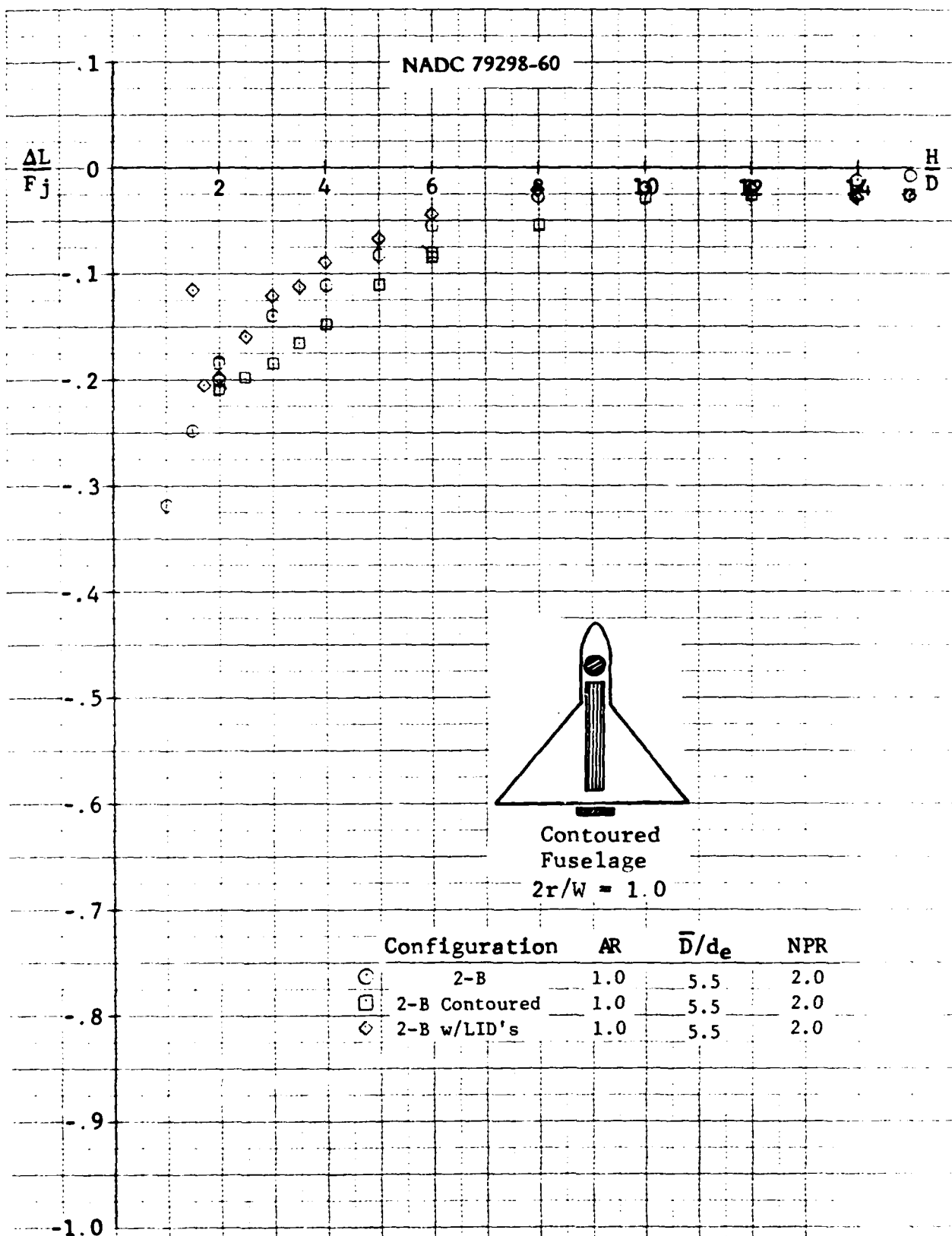| Configuration	AR	$\overline{D}/d_e$	NPR
◯	1-B	6.0	6.5	1.3
◻	1-B	6.0	6.5	2.0
◇	1-B	6.0	6.5	2.5

Figure A-14 Induced Lift vs Altitude

86

Figure A-15   Induced Lift vs Altitude

NADC 79298-60

$\frac{\Delta L}{F_j}$

.1

0

-.1

-.2

-.3

-.4

-.5

-.6

-.7

-.8

-.9

-1.0

2   4   6   8   10   12   14 $\frac{H}{D}$

Configuration		AR	$\overline{D}/d_e$	NPR
◯	1-C	2.7	10.0	1.3
□	1-C	2.7	10.0	2.0
◇	1-C	2.7	10.0	2.5

Figure A-16   Induced Lift vs Altitude

88

$\dfrac{\Delta L}{F_j}$

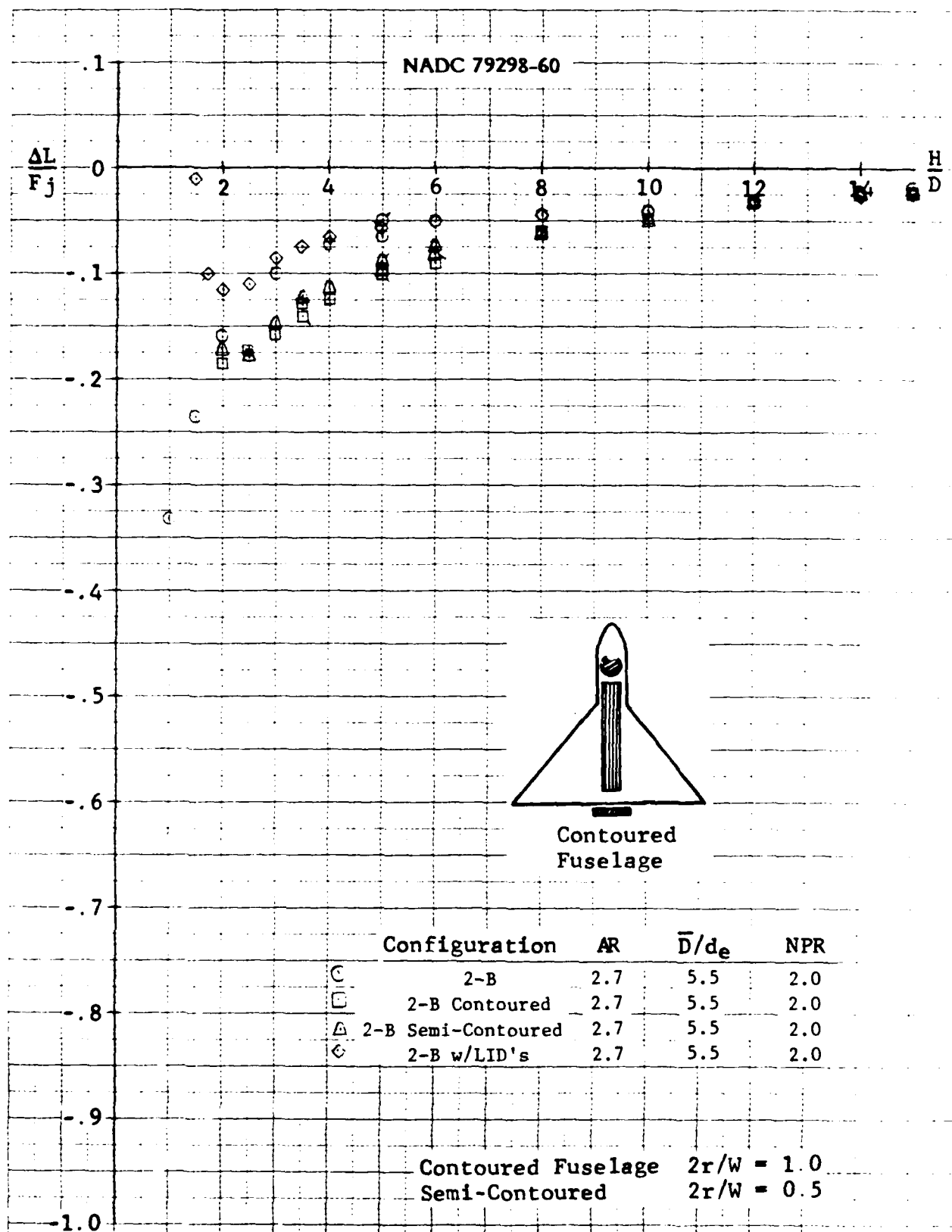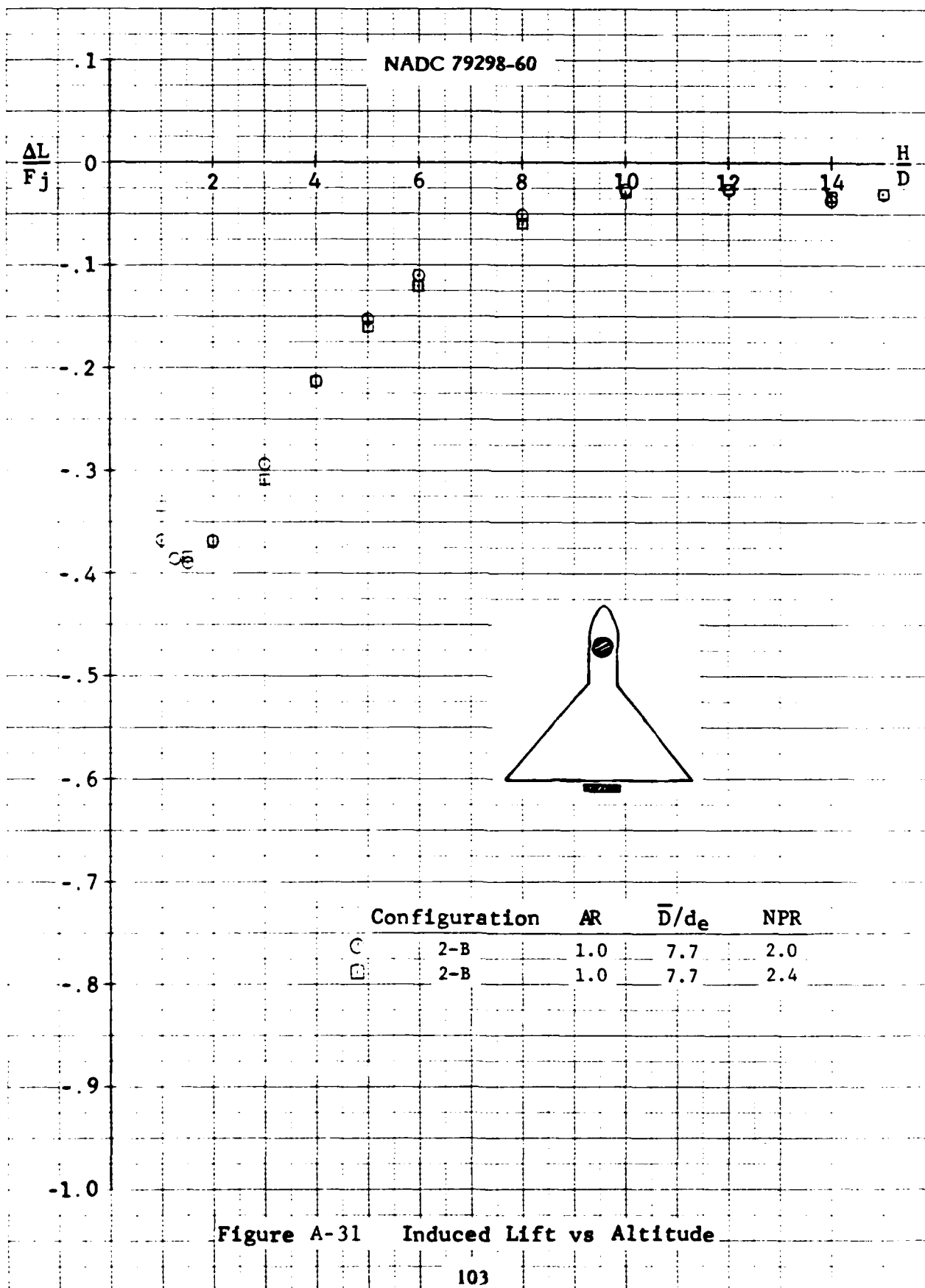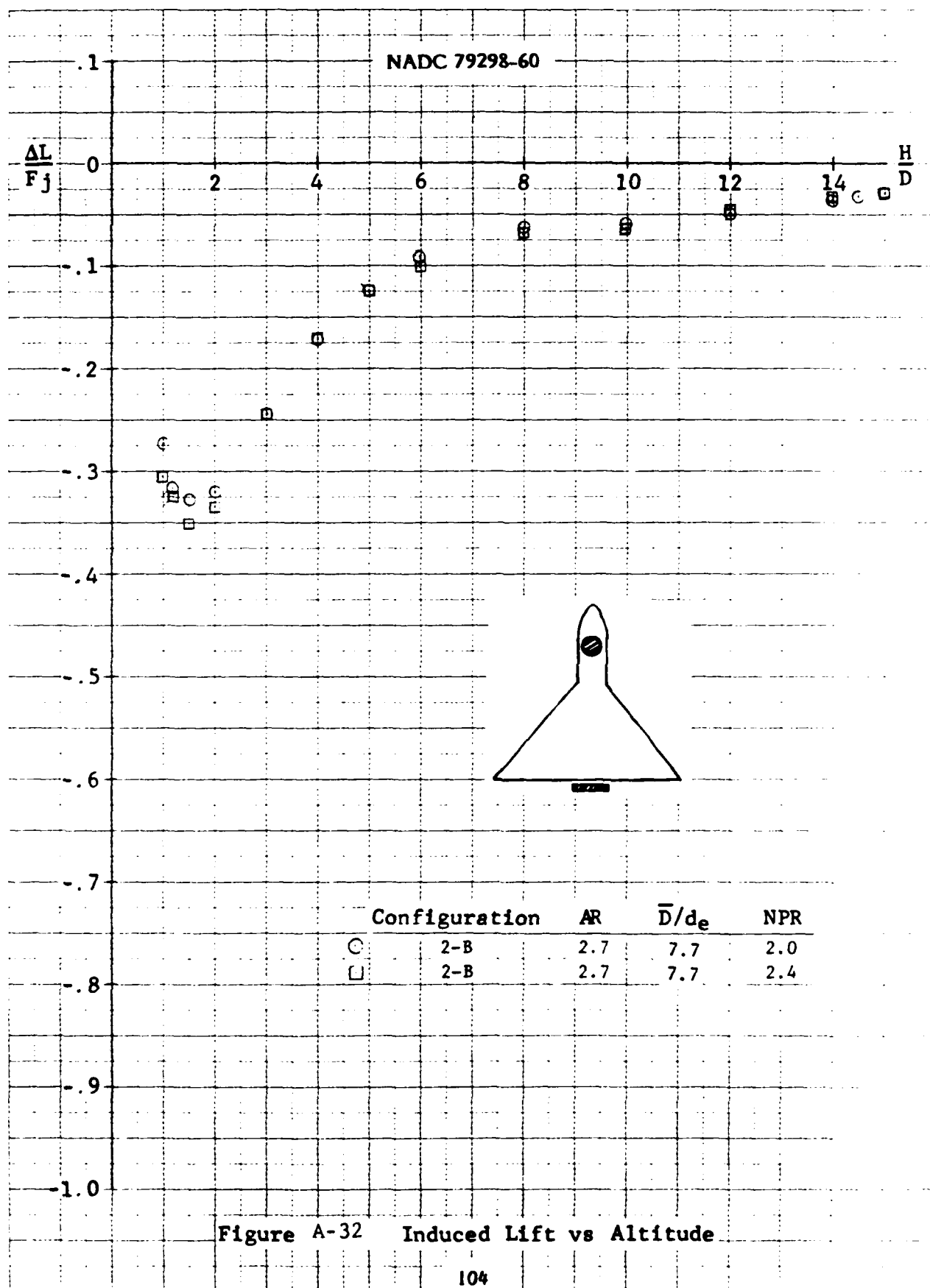|	Configuration	AR	$\overline{D}/d_e$	NPR
⟲	1-C	6.0	10.0	1.3
□	1-C	6.0	10.0	2.0
◇	1-C	6.0	10.0	2.5

Figure A-17   Induced Lift vs Altitude
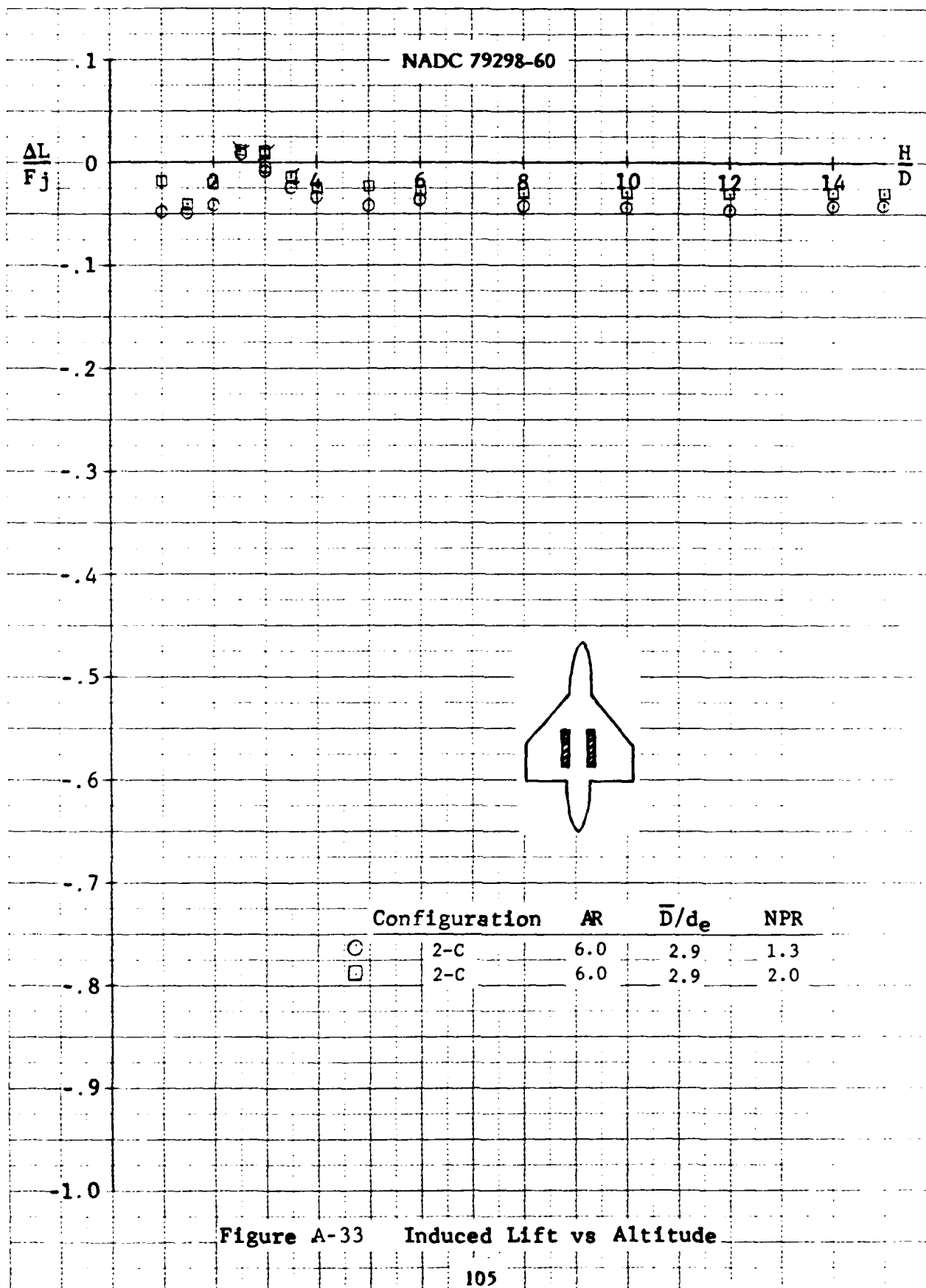
Figure A-18   Induced Lift vs Altitude

Configuration	AR	$\overline{D}/d_e$	NPR
Ꮯ	1-C	6.0	10.0	1.3
⊡	1-C	6.0	10.0	2.0
◇	1-C	6.0	10.0	2.5

NADC 79298-60

$\frac{\Delta L}{F_j}$

.1

0

−.1

−.2

−.3

−.4

−.5

−.6

−.7

−.8

−.9

−1.0

4 6 8 10 12 14 $\frac{H}{D}$

Configuration		AR	$\overline{D}/d_e$	NPR
○	2–A	1.0	3.9	1.3
□	2–A	1.0	3.9	2.0

Figure A-19   Induced Lift vs Altitude

Figure A-20   Induced Lift vs Altitude
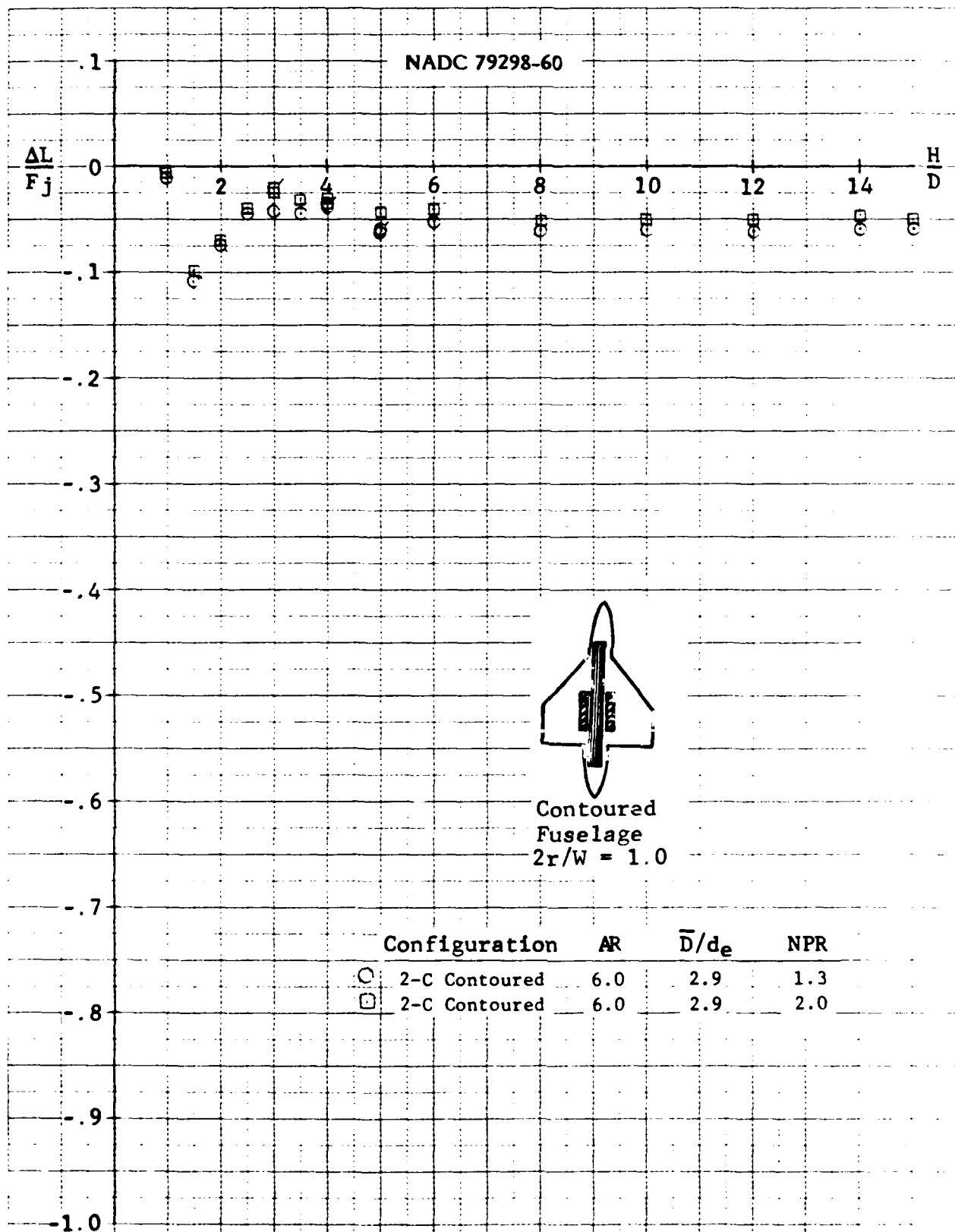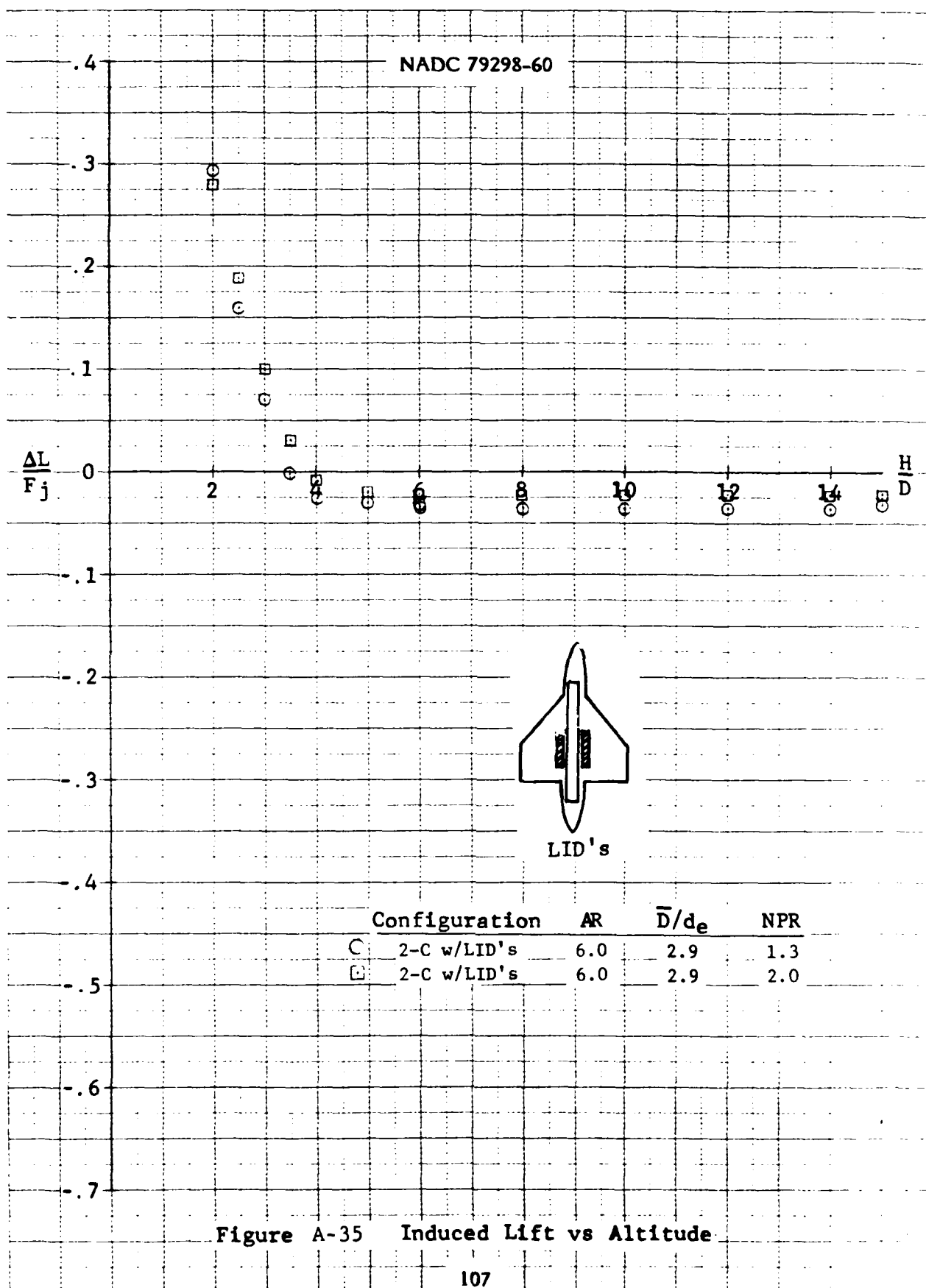
Configuration	AR	$\overline{D}/d_e$	NPR
C	2-A	2.7	3.9	1.3
D	2-A	2.7	3.9	2.0

Figure A-21   Induced Lift vs Altitude
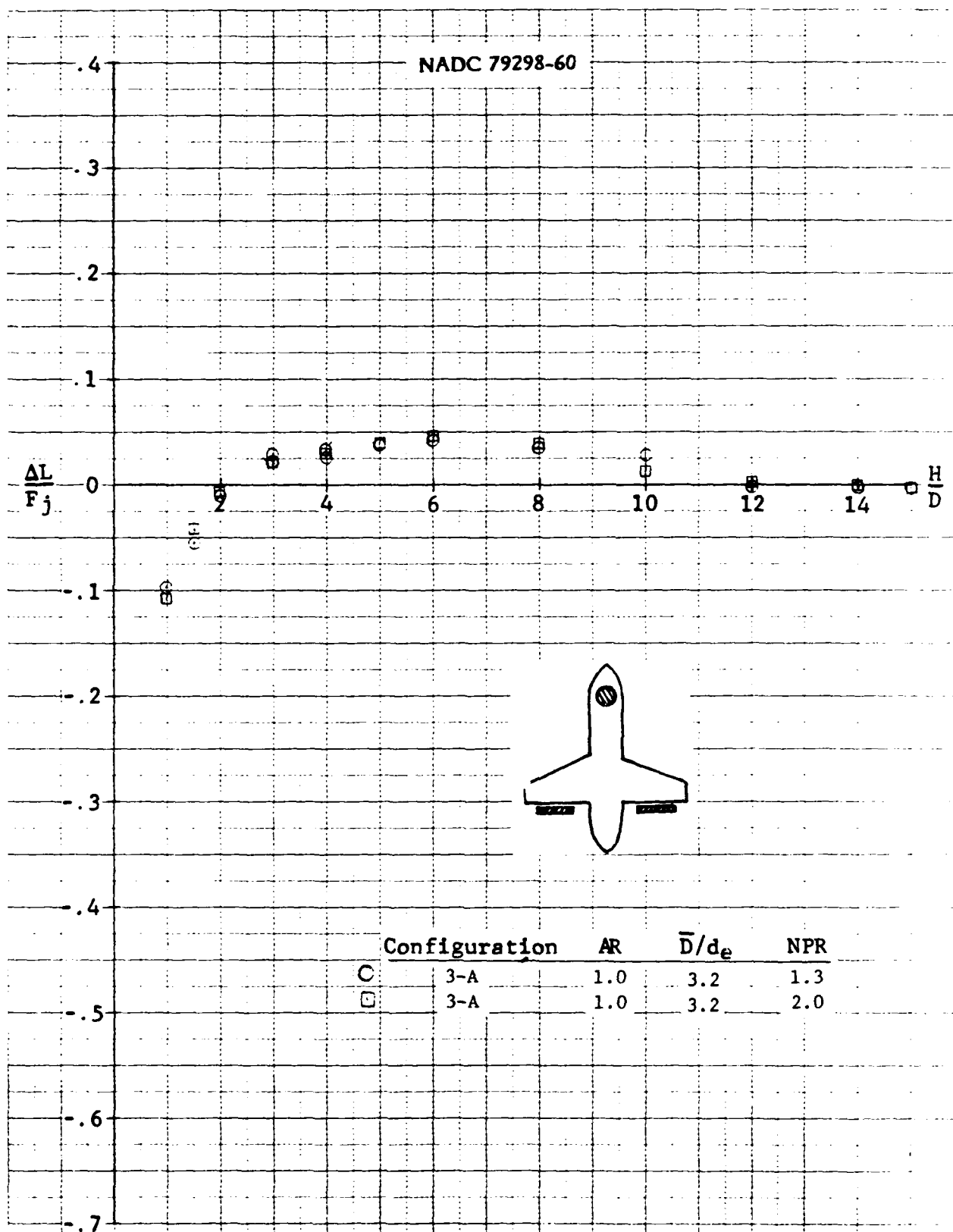
Figure A-22   Induced Lift vs Altitude

$$\frac{\Delta L}{F_j}$$

.4

.3

.2

.1

0

2   4   6   8   10   12   14 $\frac{H}{D}$

-.1

-.2

-.3

-.4

-.5

-.6

-.7

Contoured
Fuselage
$2r/W = 1.0$

Configuration	AR	$\overline{D}/d_e$	NPR
C 3-A Contoured	1.0	6.2	2.0
□ 3-A w/LID's	1.0	6.2	2.0
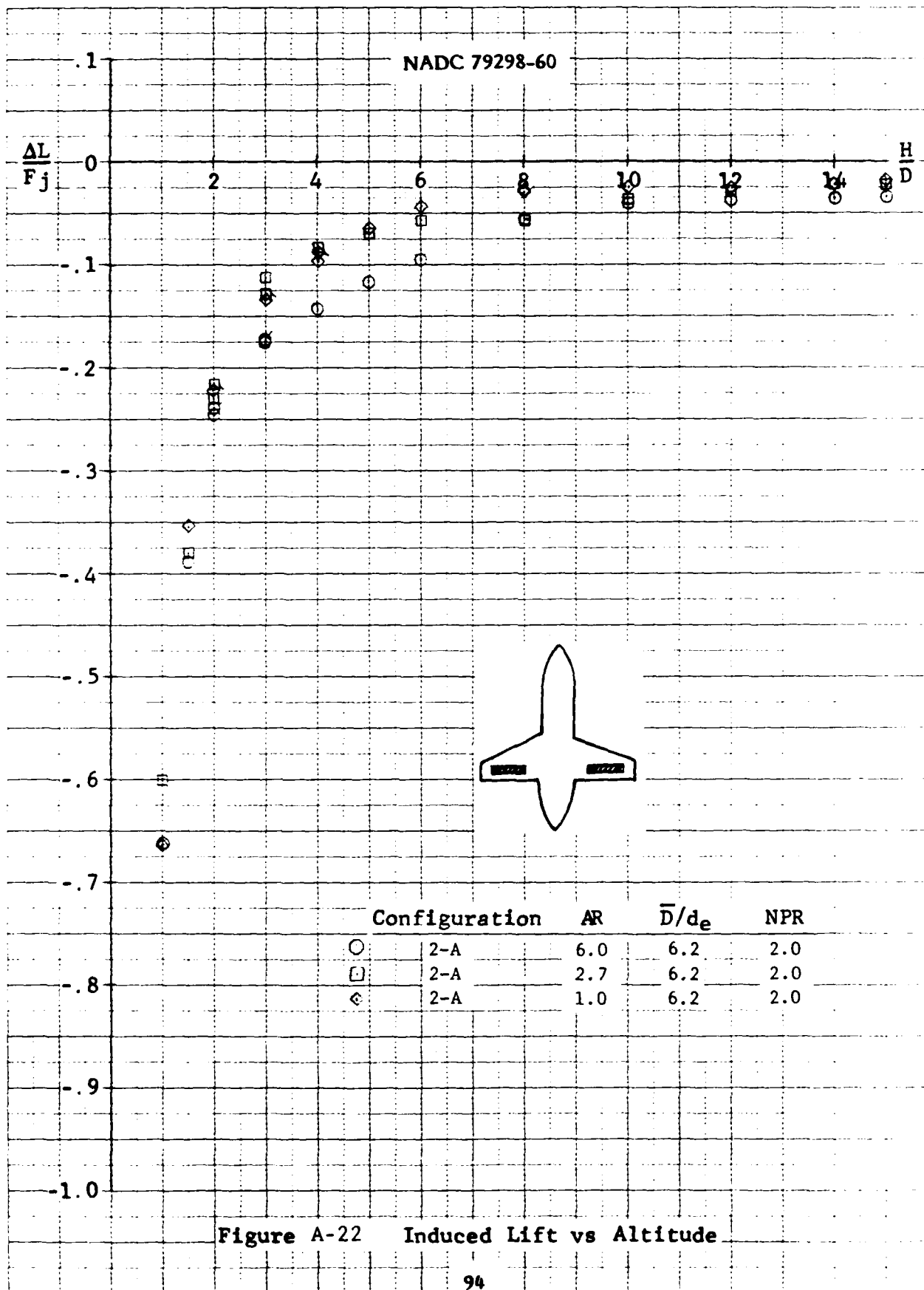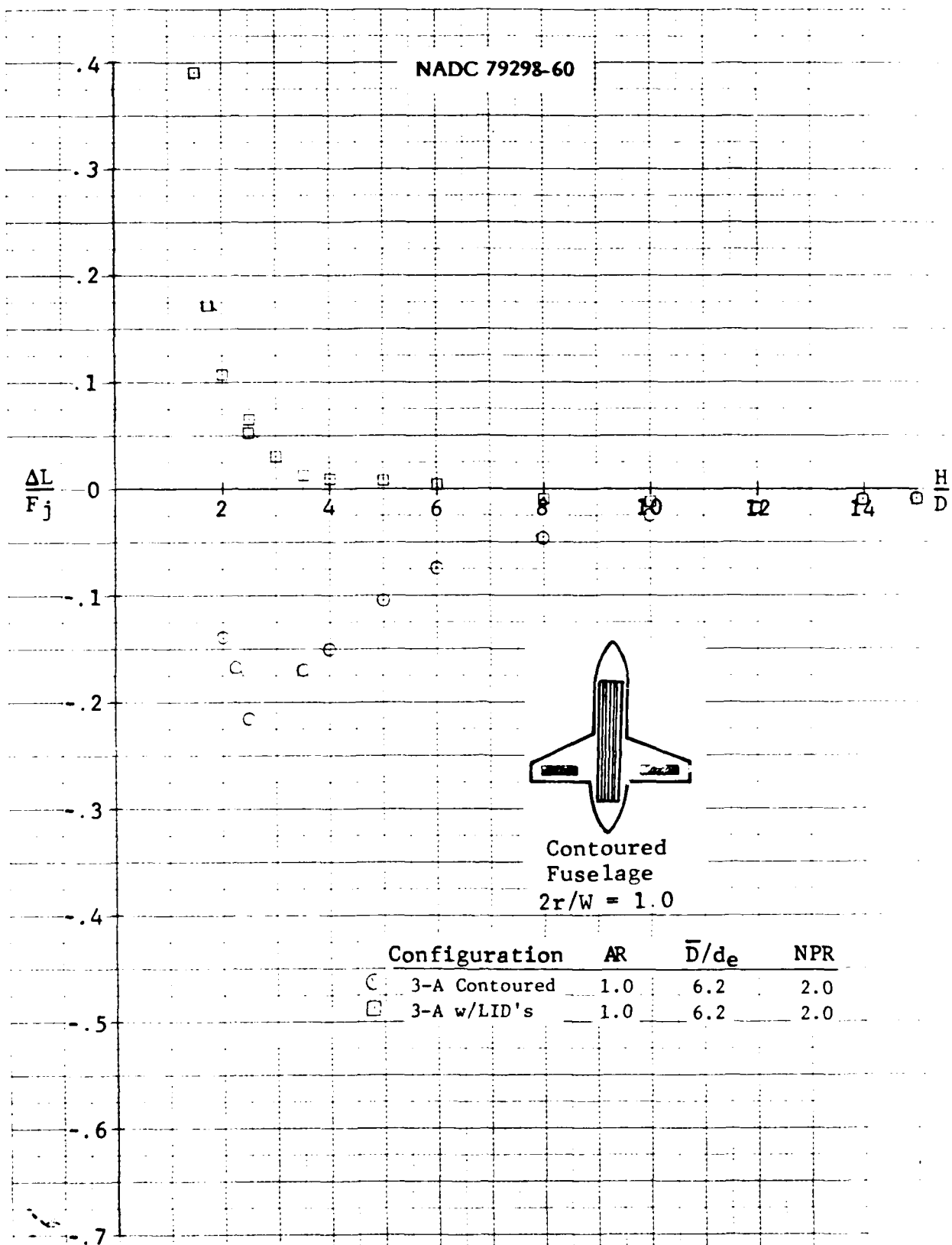
Figure A-23   Induced Lift vs Altitude

$\frac{\Delta L}{F_j}$

.4

.3

.2

.1

0

-.1

-.2

-.3

-.4

-.5

-.6

-.7

2   4   6   8   10   12   14 $\frac{H}{D}$

Contoured
Fuselage

Configuration	AR	$\overline{D}/d_e$	NPR
C 2-A Contoured	2.7	6.2	2.0
D 2-A Semi-Contoured	2.7	6.2	2.0
◇ 2-A w/LID's	2.7	6.2	2.0

Contoured Fuselage $2r/W = 1.0$
Semi-Contoured $2r/W = 0.5$

Figure A-24   Induced Lift vs Altitude

Figure A-25   Induced Lift vs Altitude
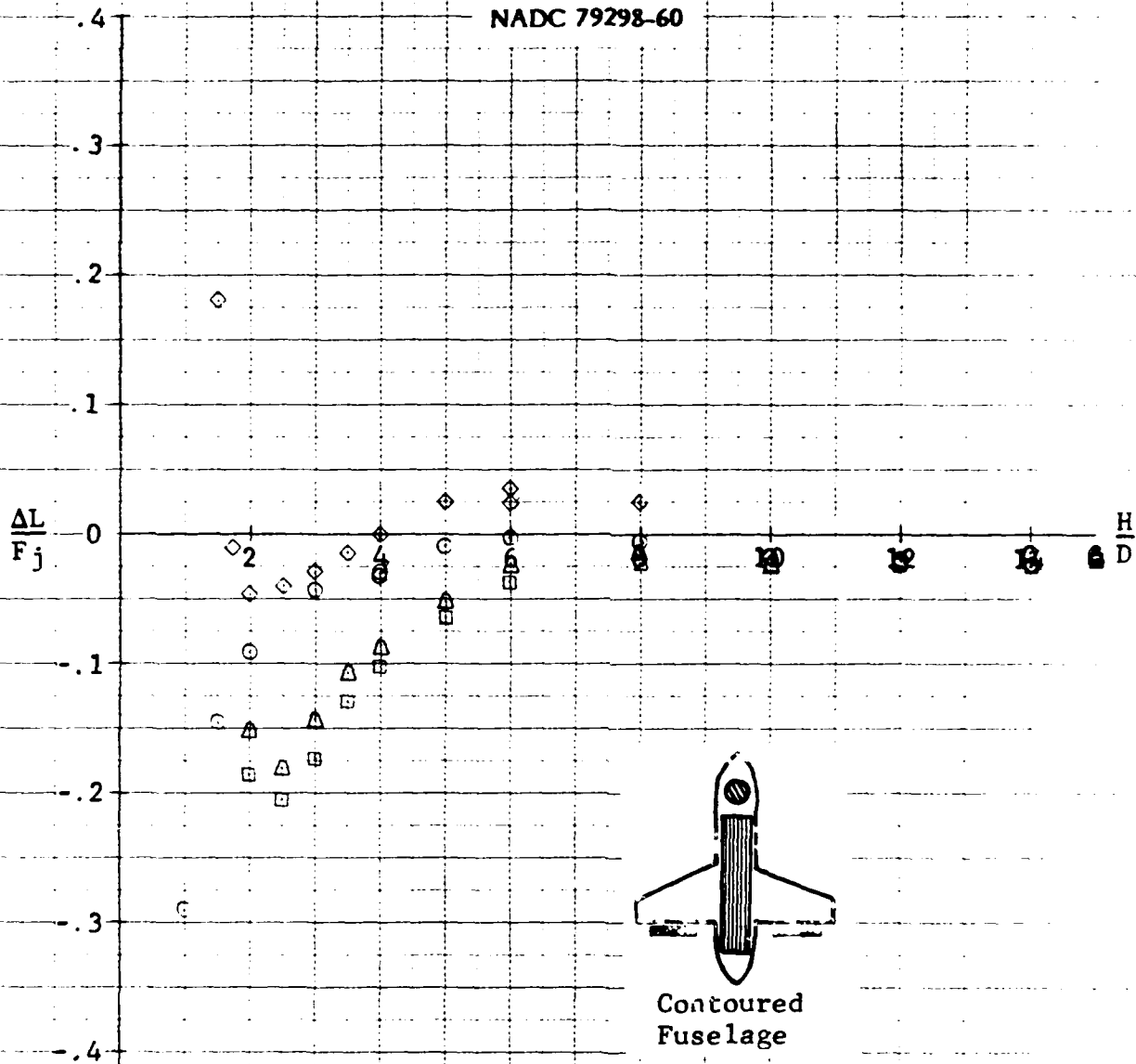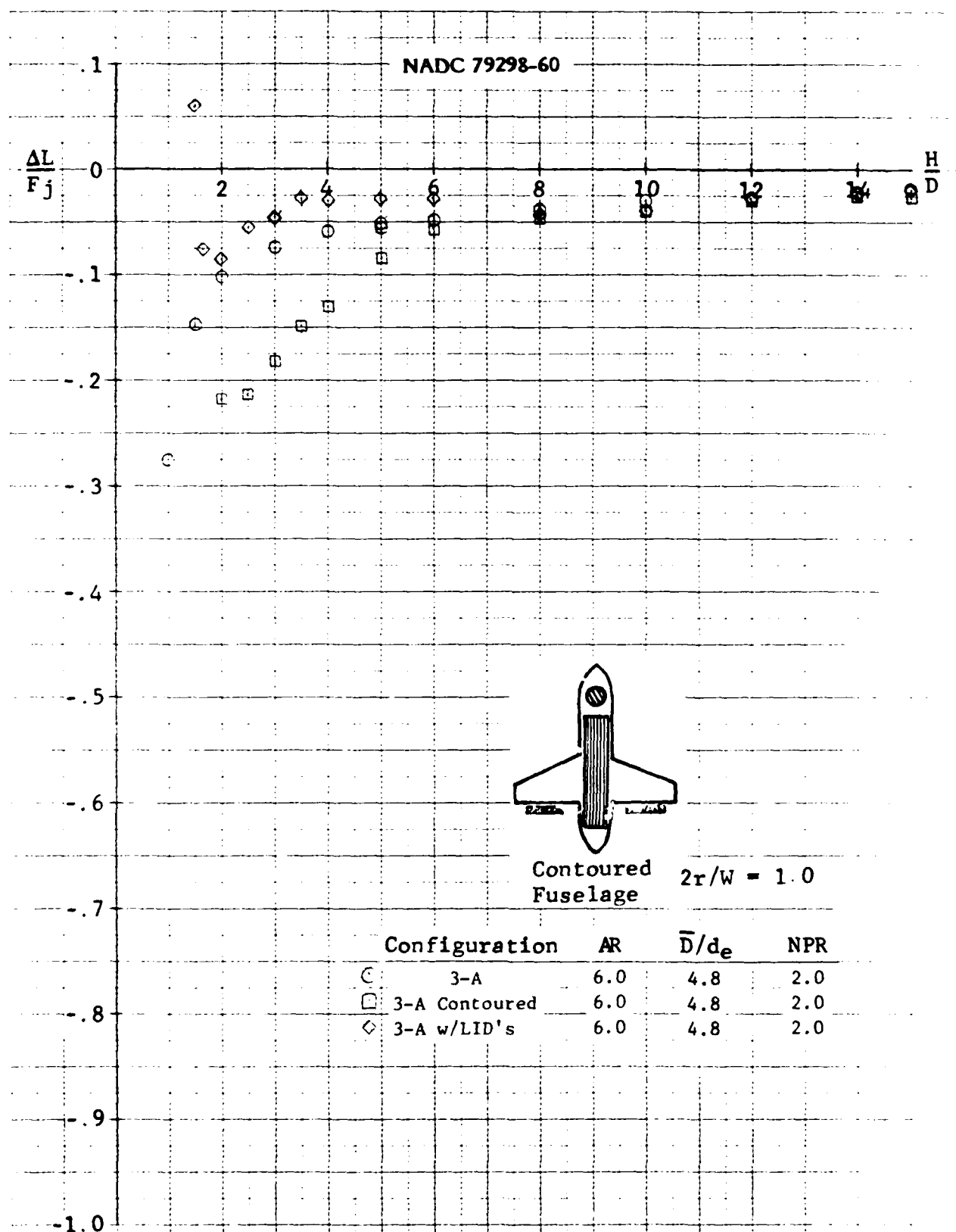
Figure A-26   Induced Lift vs Altitude

NADC 79298-60

Configuration	AR	$\overline{D}/d_e$	NPR
○ 2-A	2.7	8.8	2.0
□ 2-A	2.7	8.8	2.4
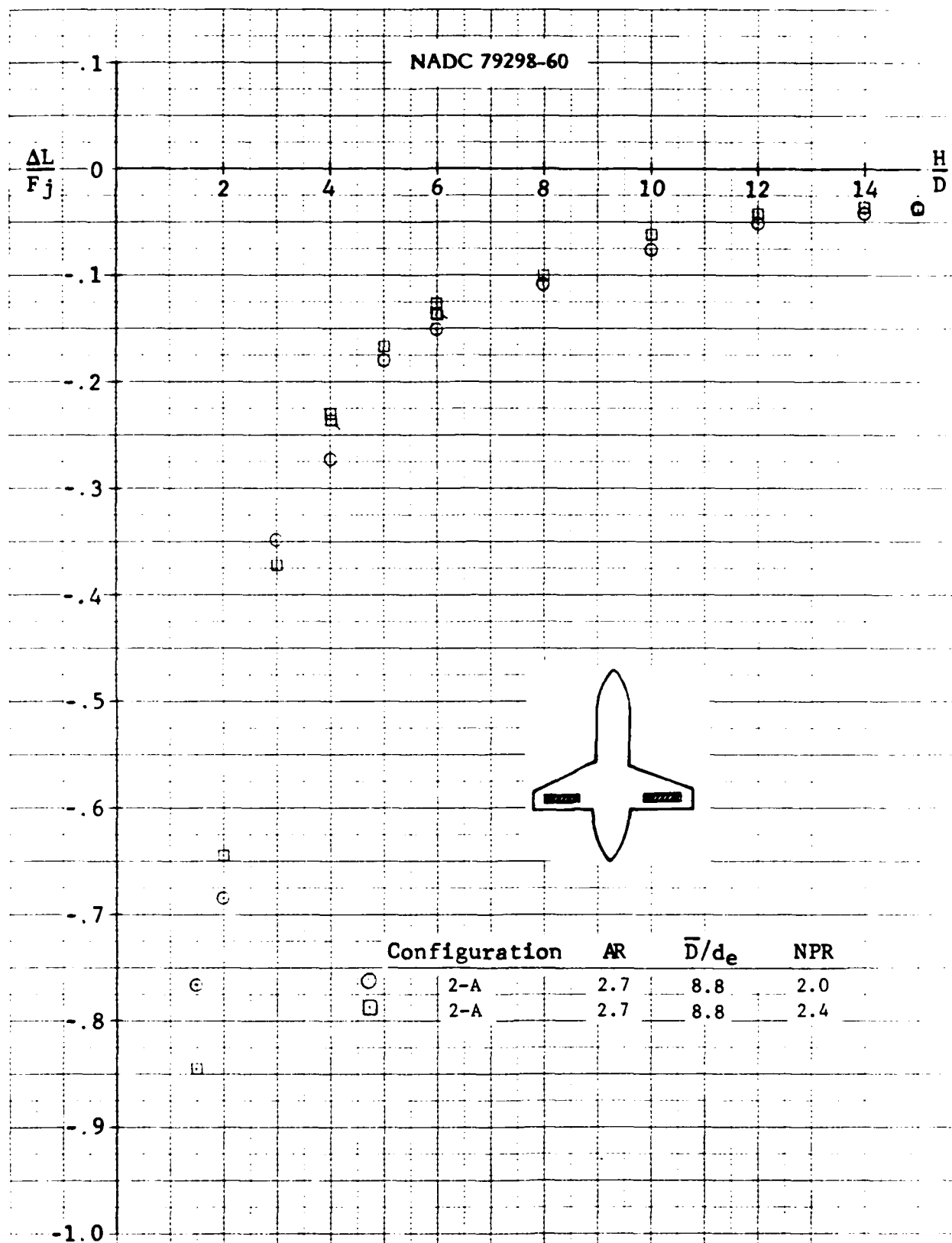
Figure A-27   Induced Lift vs Altitude

99

$\frac{\Delta L}{F_j}$

Graph axes: vertical axis $\frac{\Delta L}{F_j}$ from .1 to -1.0; horizontal axis $\frac{H}{D}$ with values 2, 4, 6, 8, 10, 12, 14.

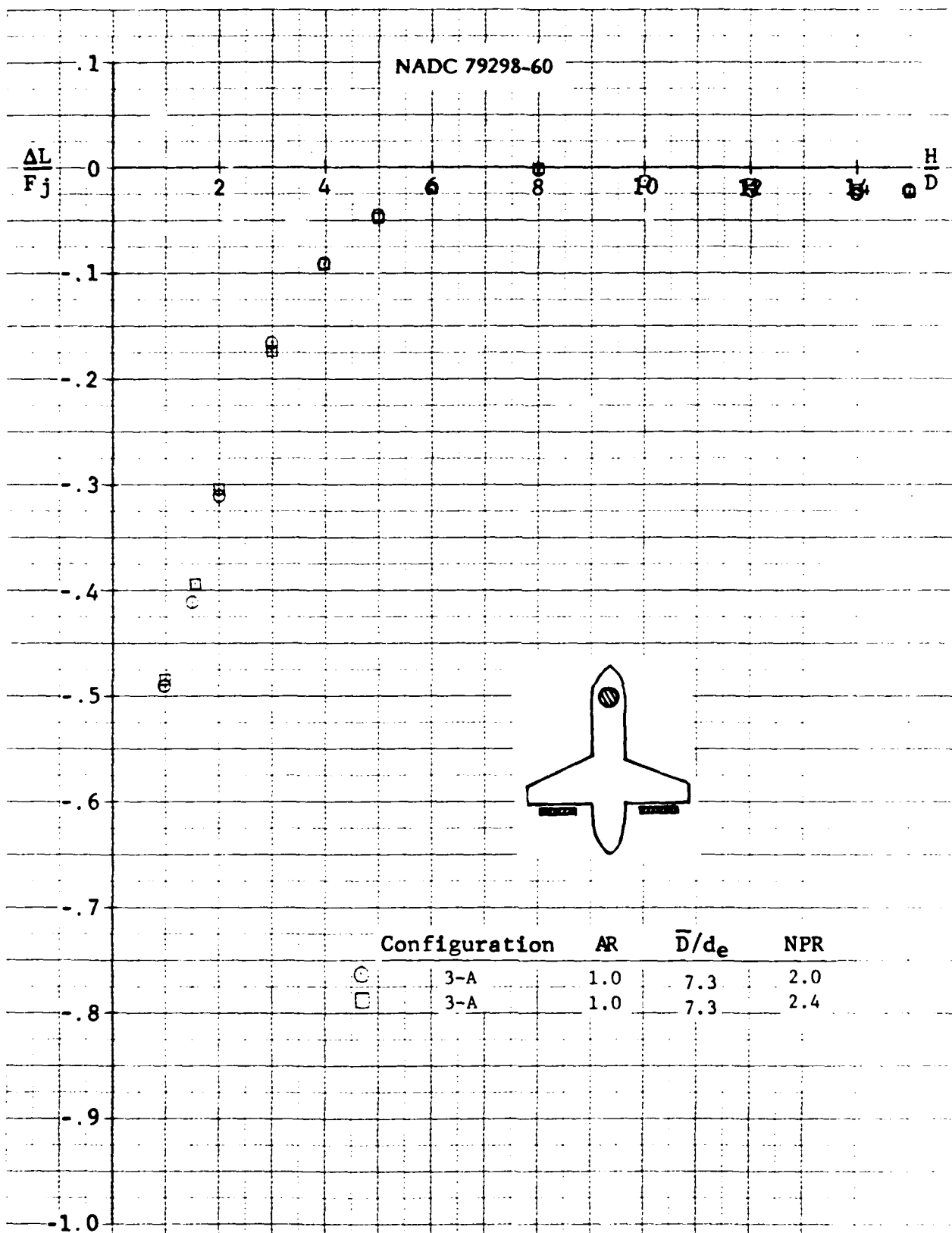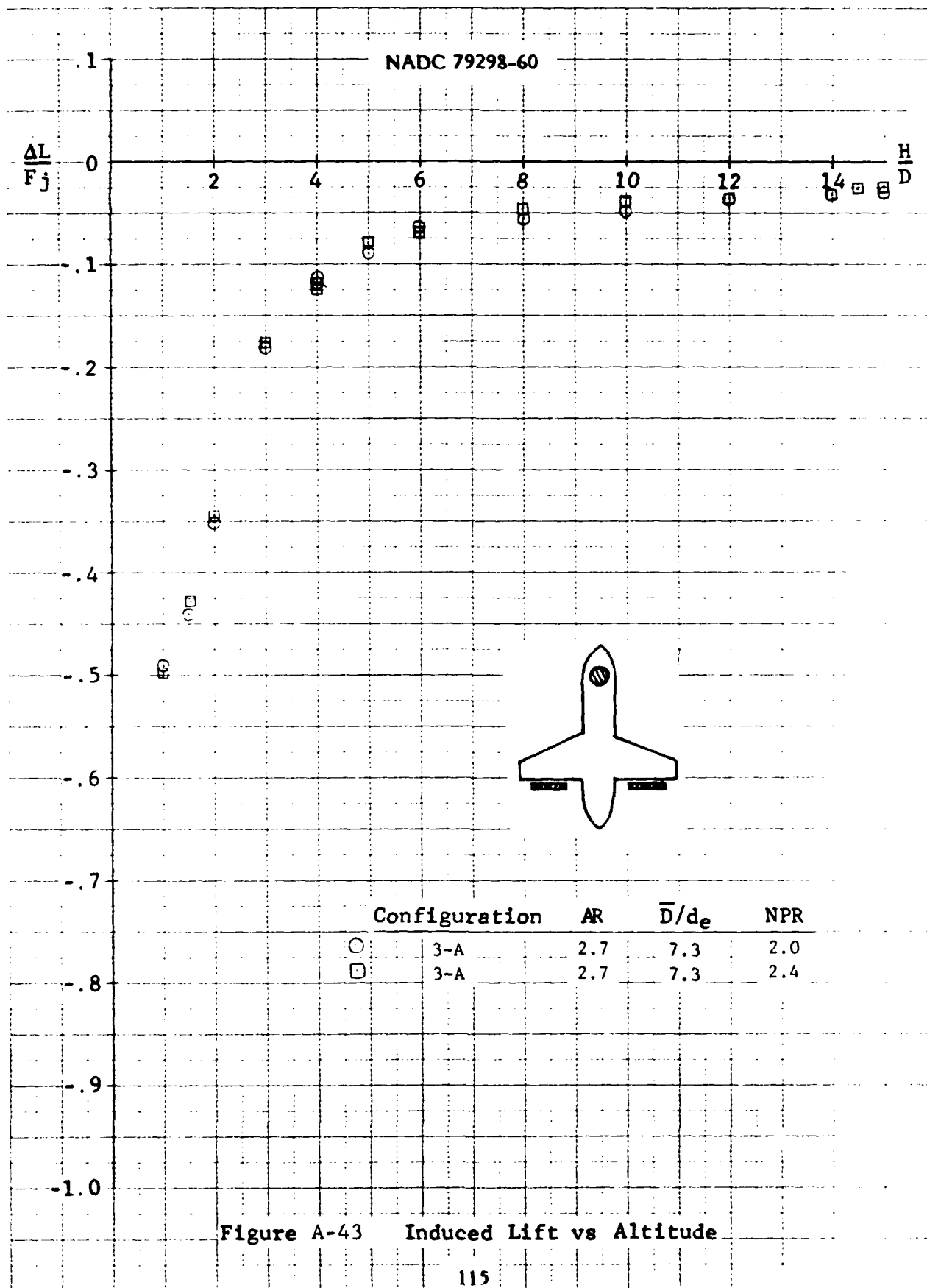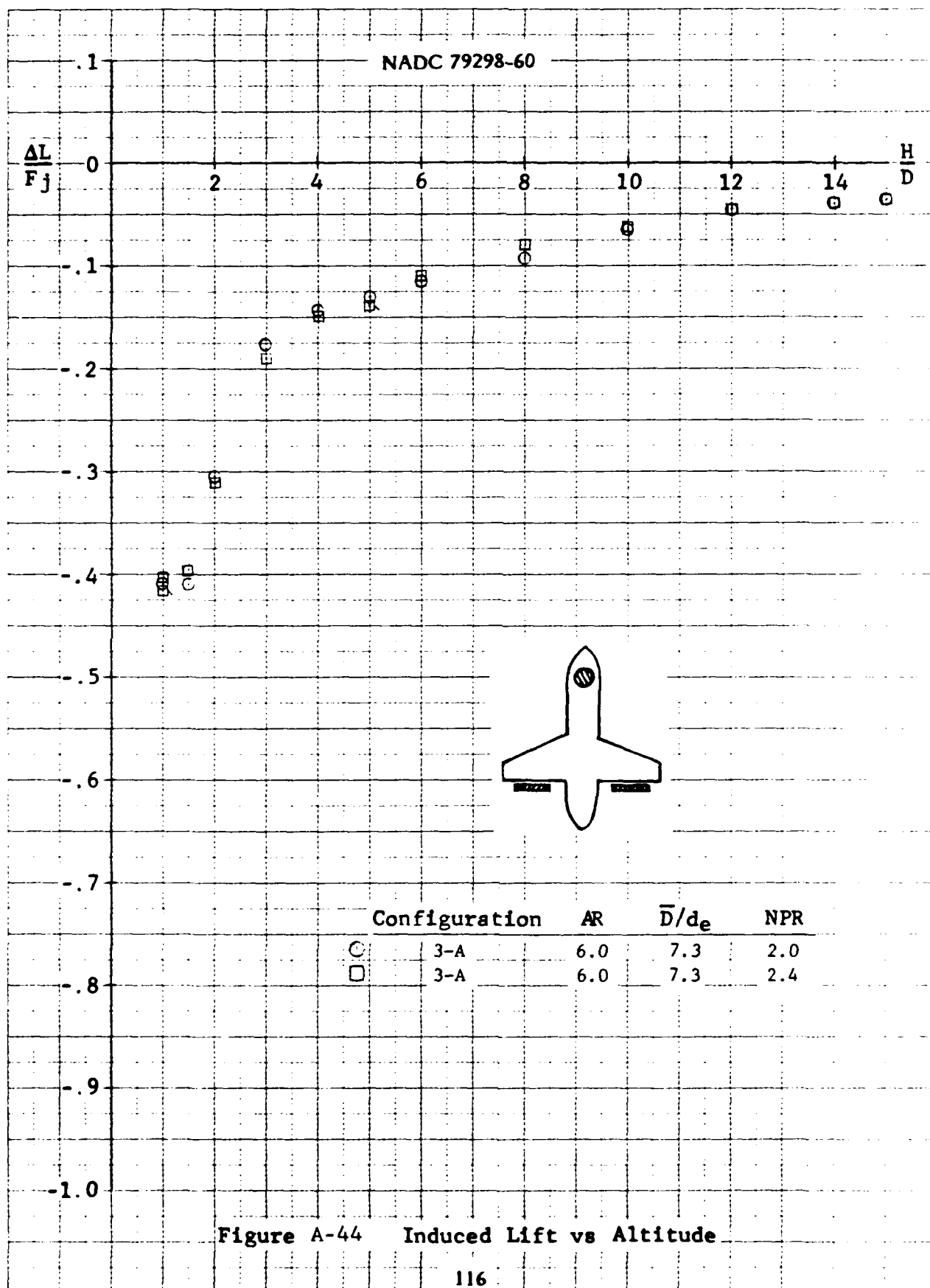| Configuration		AR	$\overline{D}/d_e$	NPR
⊙	2-A	6.0	8.8	2.0
▢	2-A	6.0	8.8	2.4

Figure A-28   Induced Lift vs Altitude

Figure A-29   Induced Lift vs Altitude

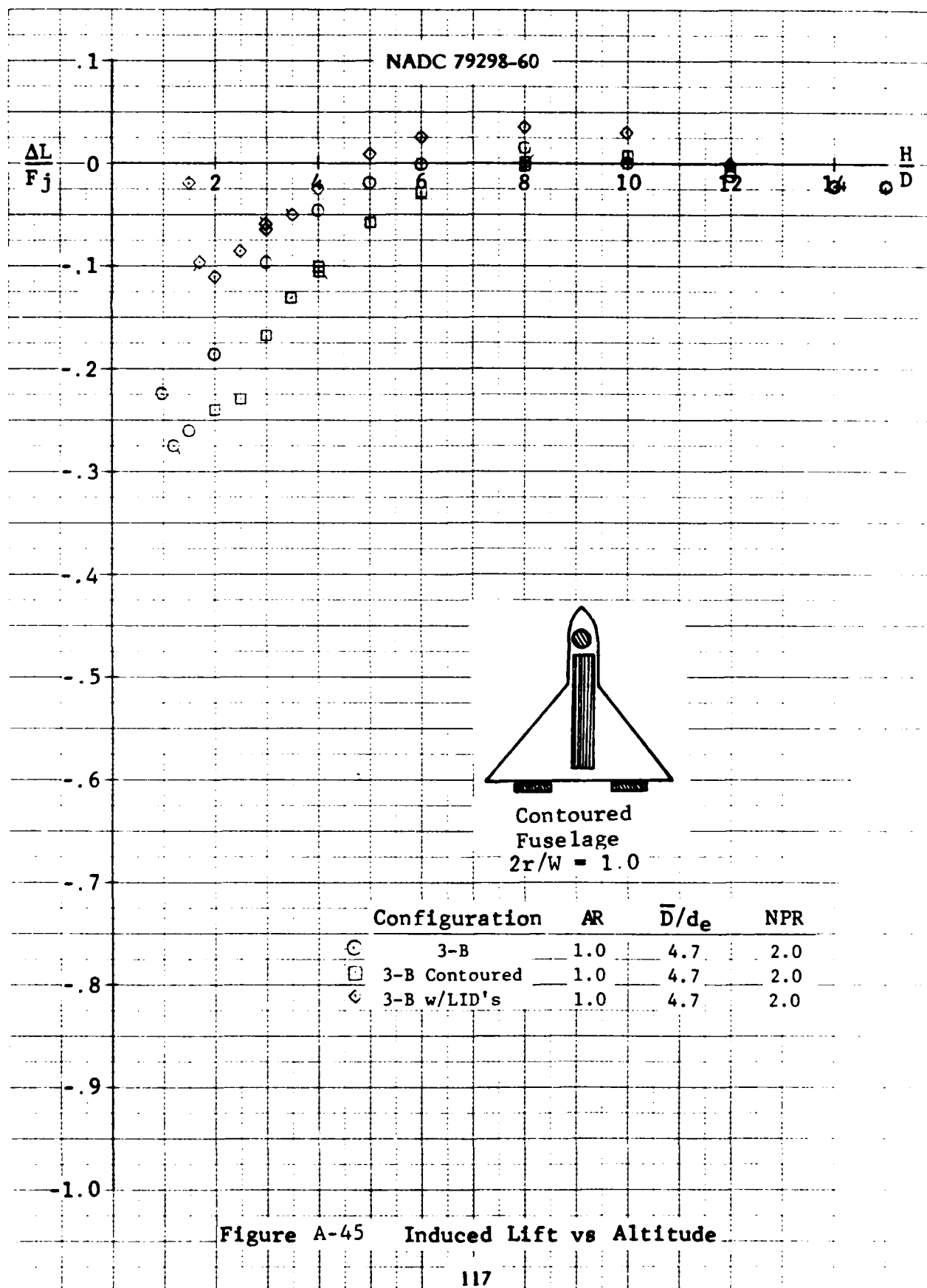Figure A-30   Induced Lift vs Altitude

$$\frac{\Delta L}{F_j}$$

Configuration	AR	$\overline{D}/d_e$	NPR
◐ 2-B	1.0	7.7	2.0
◻ 2-B	1.0	7.7	2.4

Figure A-31   Induced Lift vs Altitude

103

Figure A-32   Induced Lift vs Altitude

	Configuration	AR	$\overline{D}/d_e$	NPR
○	2-B	2.7	7.7	2.0
□	2-B	2.7	7.7	2.4

$\frac{\Delta L}{F_j}$

$\frac{H}{D}$

Configuration	AR	$\overline{D}/d_e$	NPR
⊙ 2-C	6.0	2.9	1.3
☐ 2-C	6.0	2.9	2.0

Figure A-33   Induced Lift vs Altitude

Figure A-34   Induced Lift vs Altitude
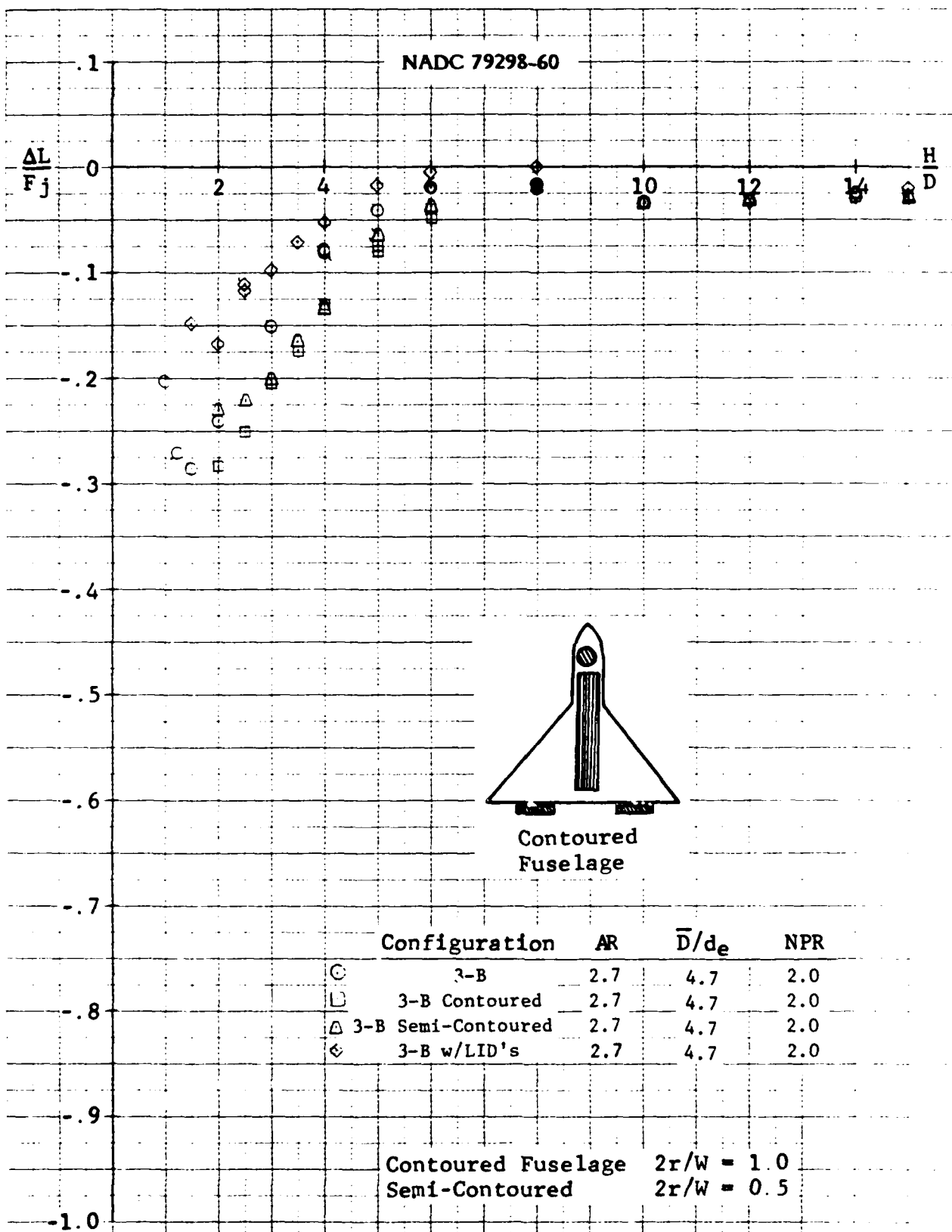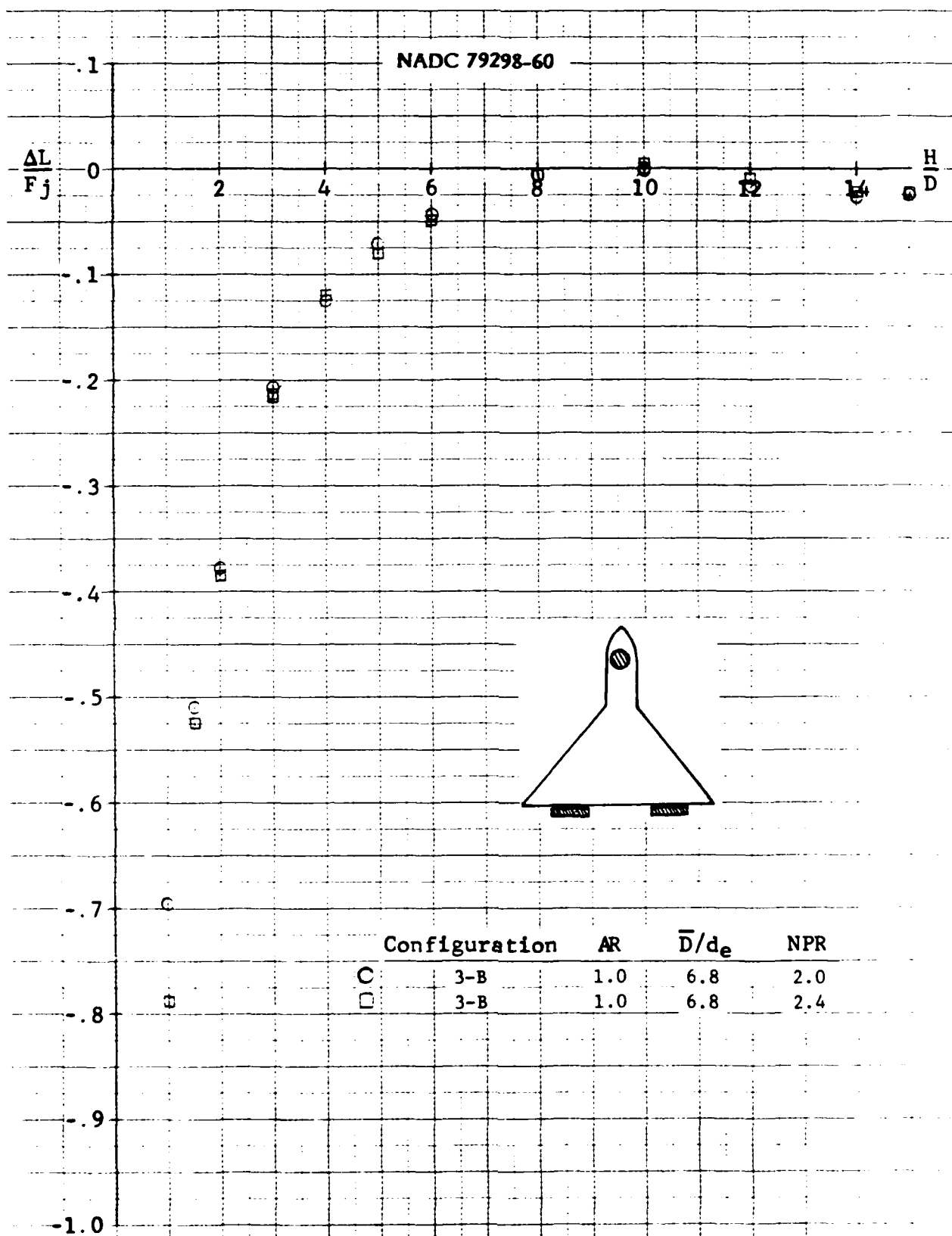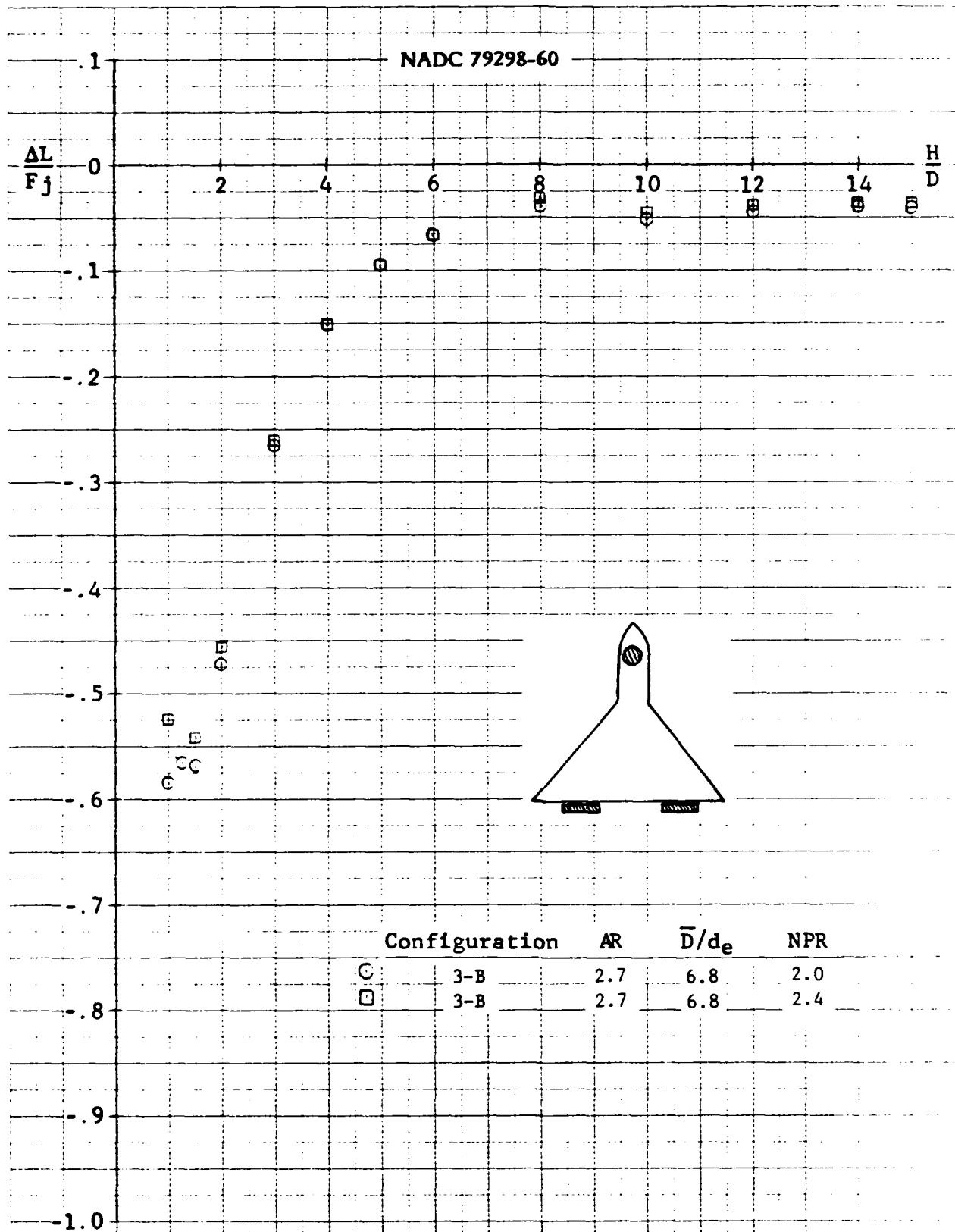
Figure A-35   Induced Lift vs Altitude

Figure A-36   Induced Lift vs Altitude

Configuration	AR	$\overline{D}/d_e$	NPR
C	3-A	1.0	3.2	1.3
□	3-A	1.0	3.2	2.0
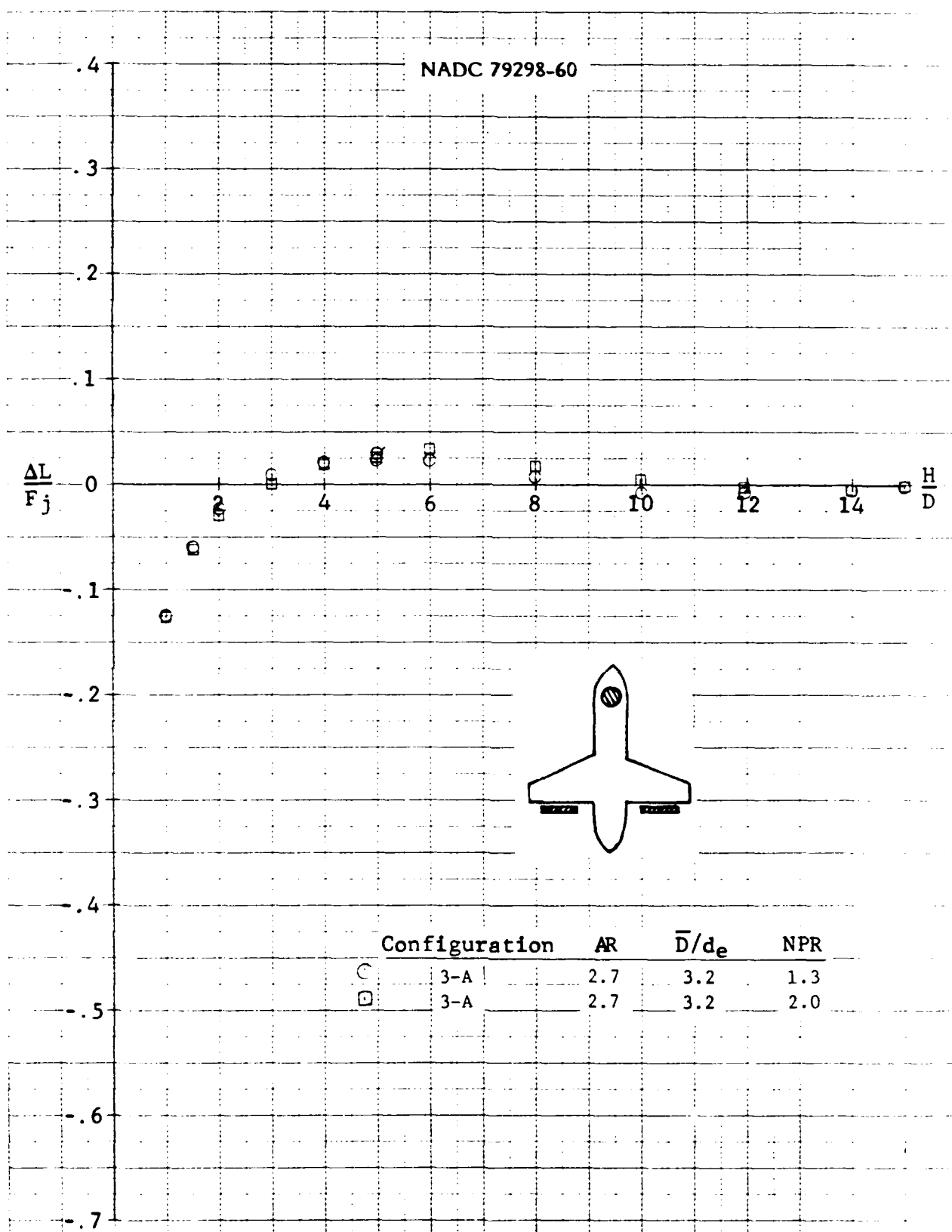
Figure A-37   Induced Lift vs Altitude
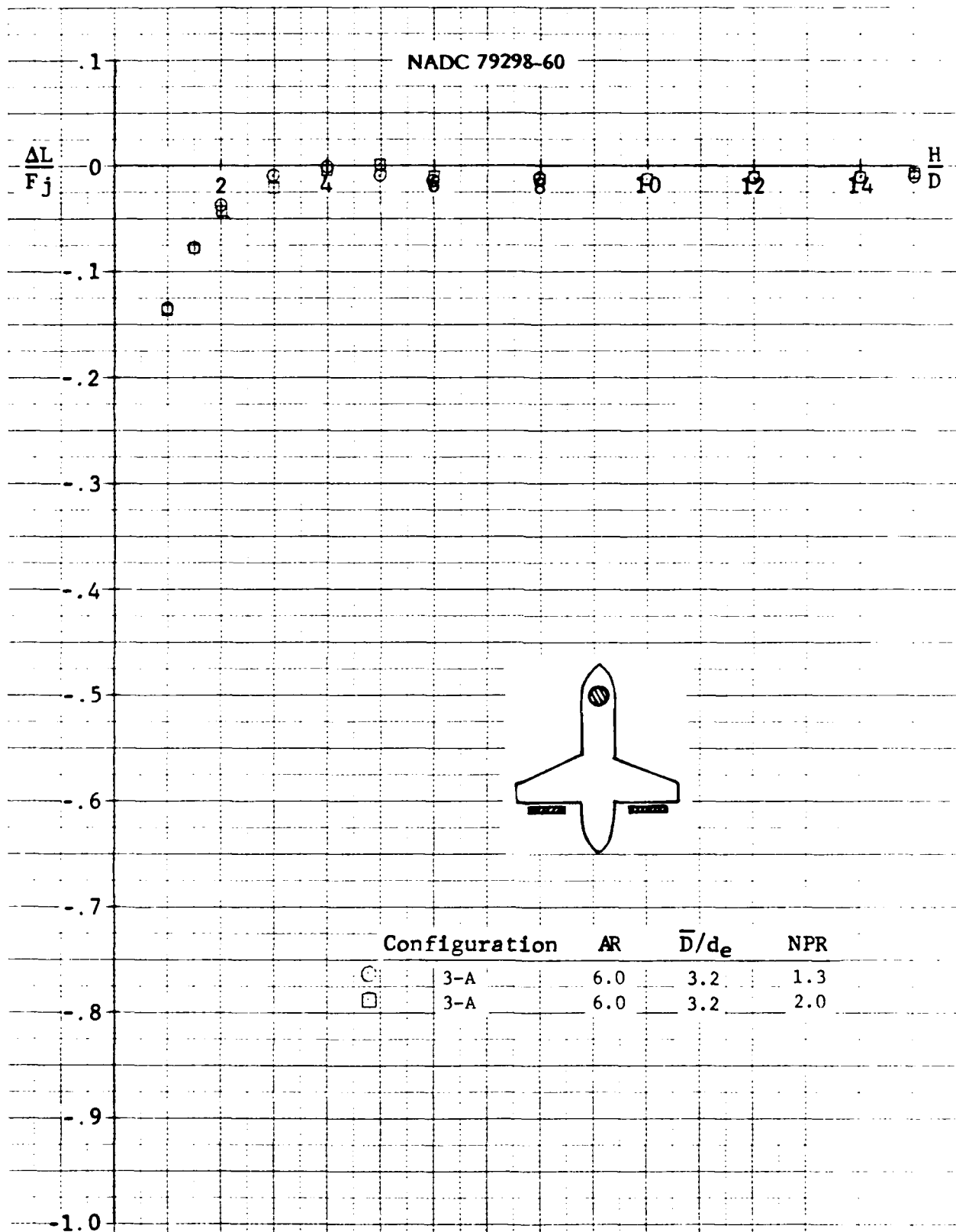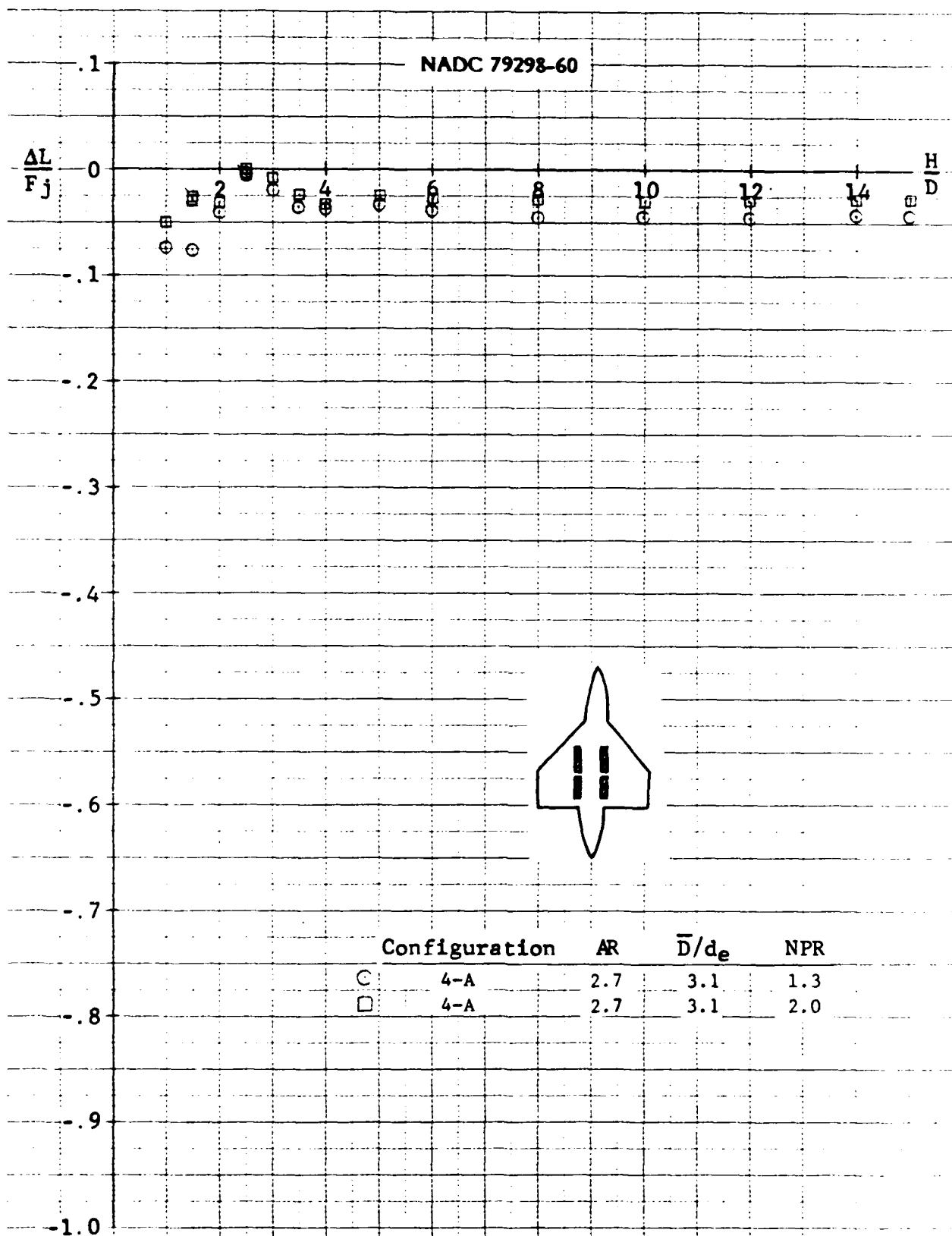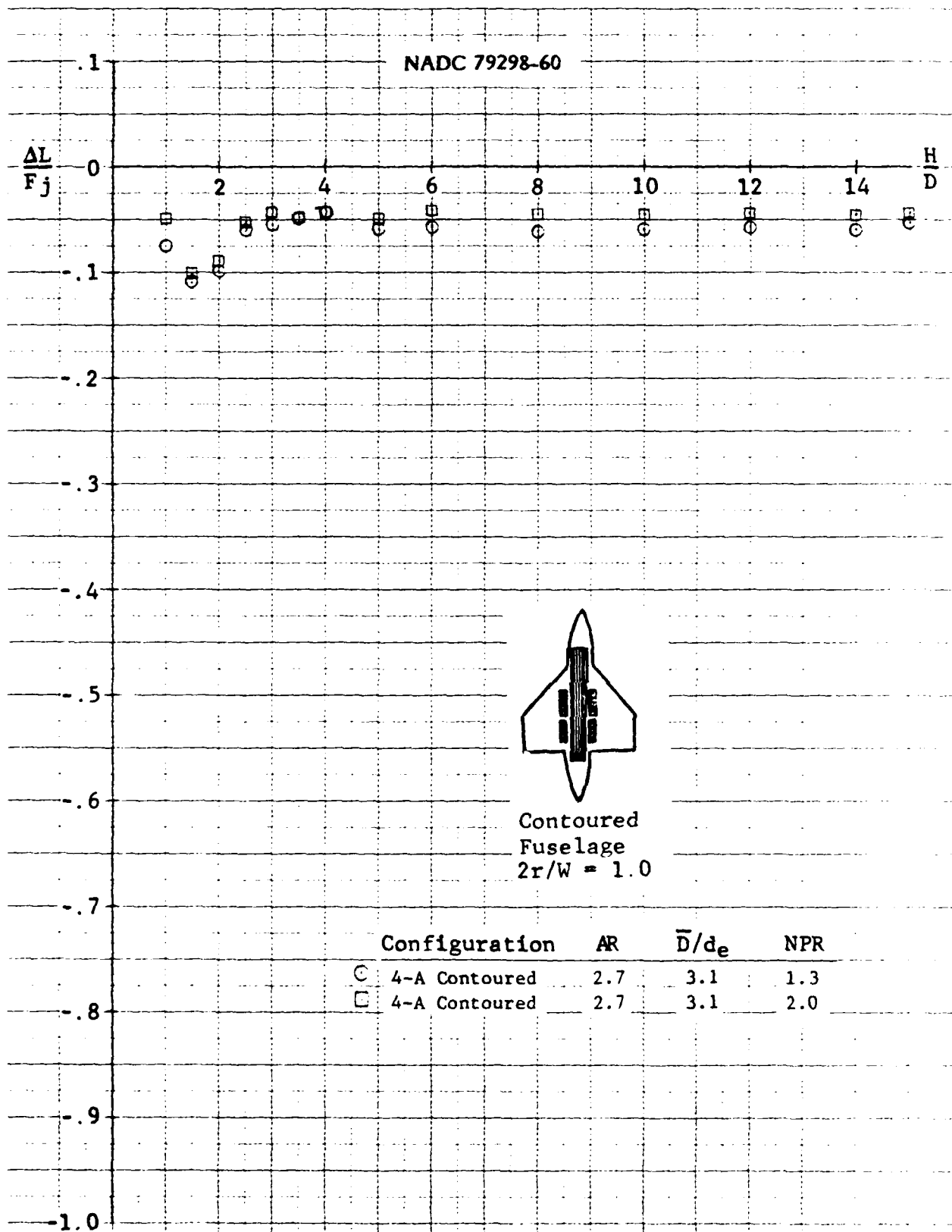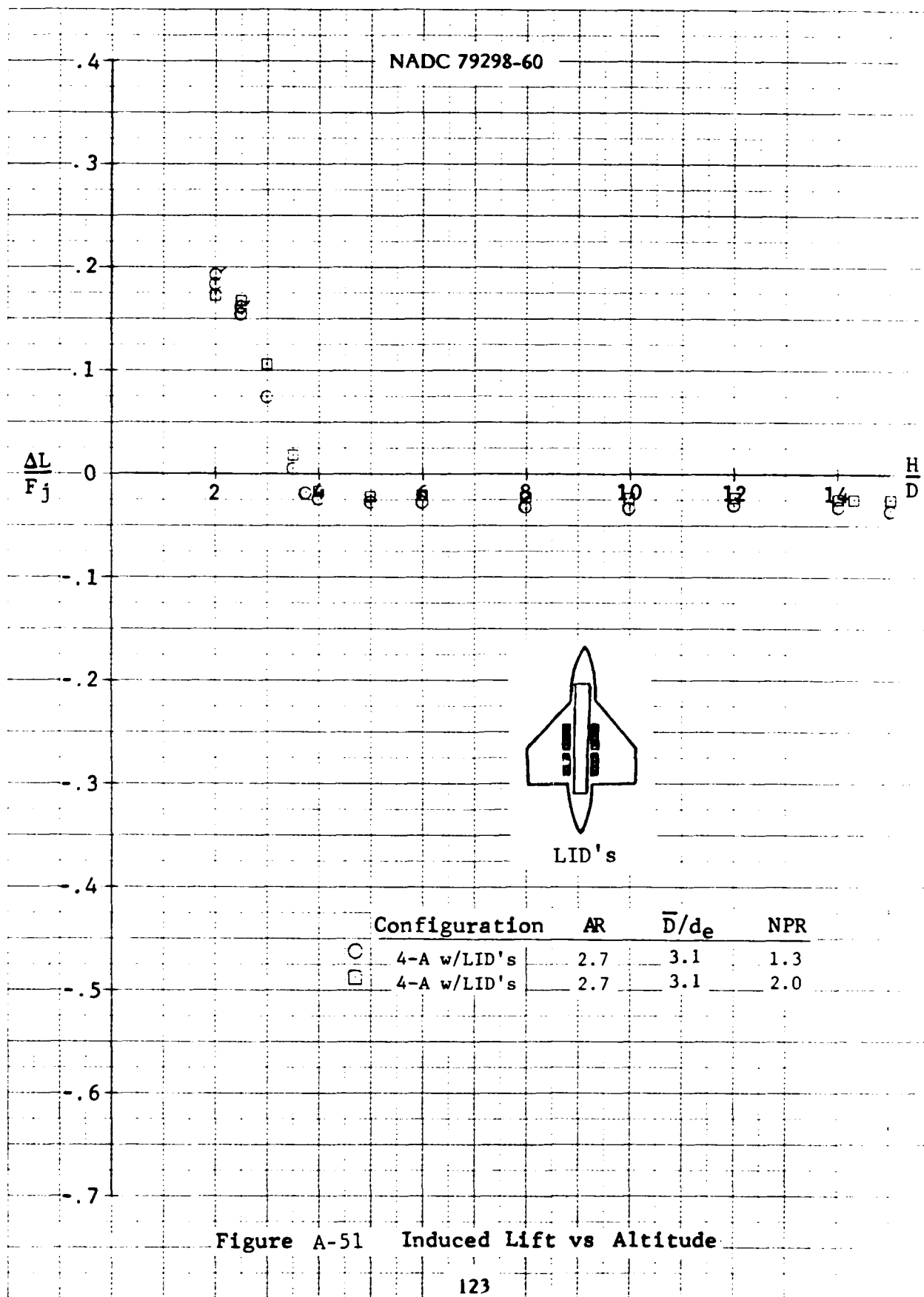
Figure A-38   Induced Lift vs Altitude
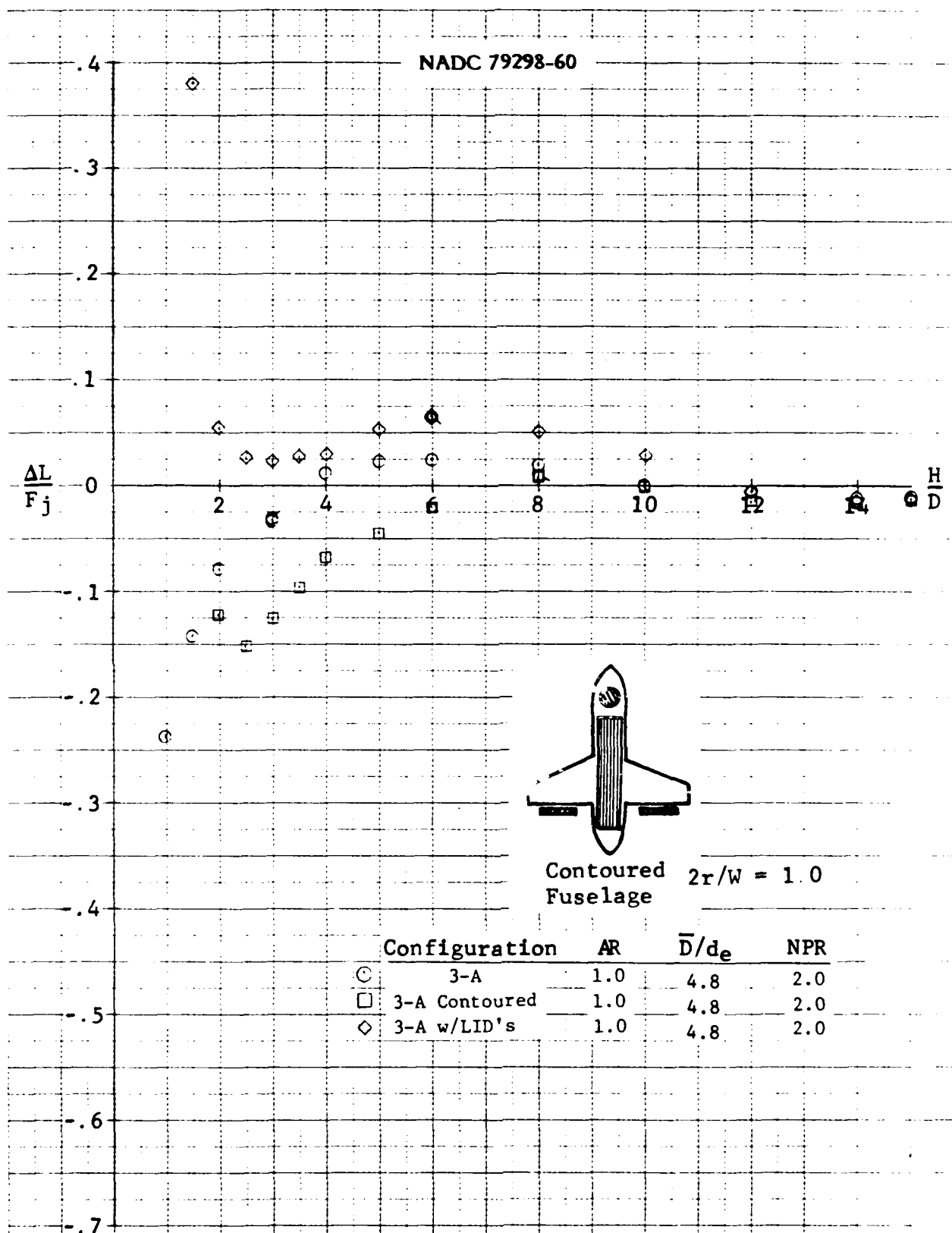
Figure A-39   Induced Lift vs Altitude
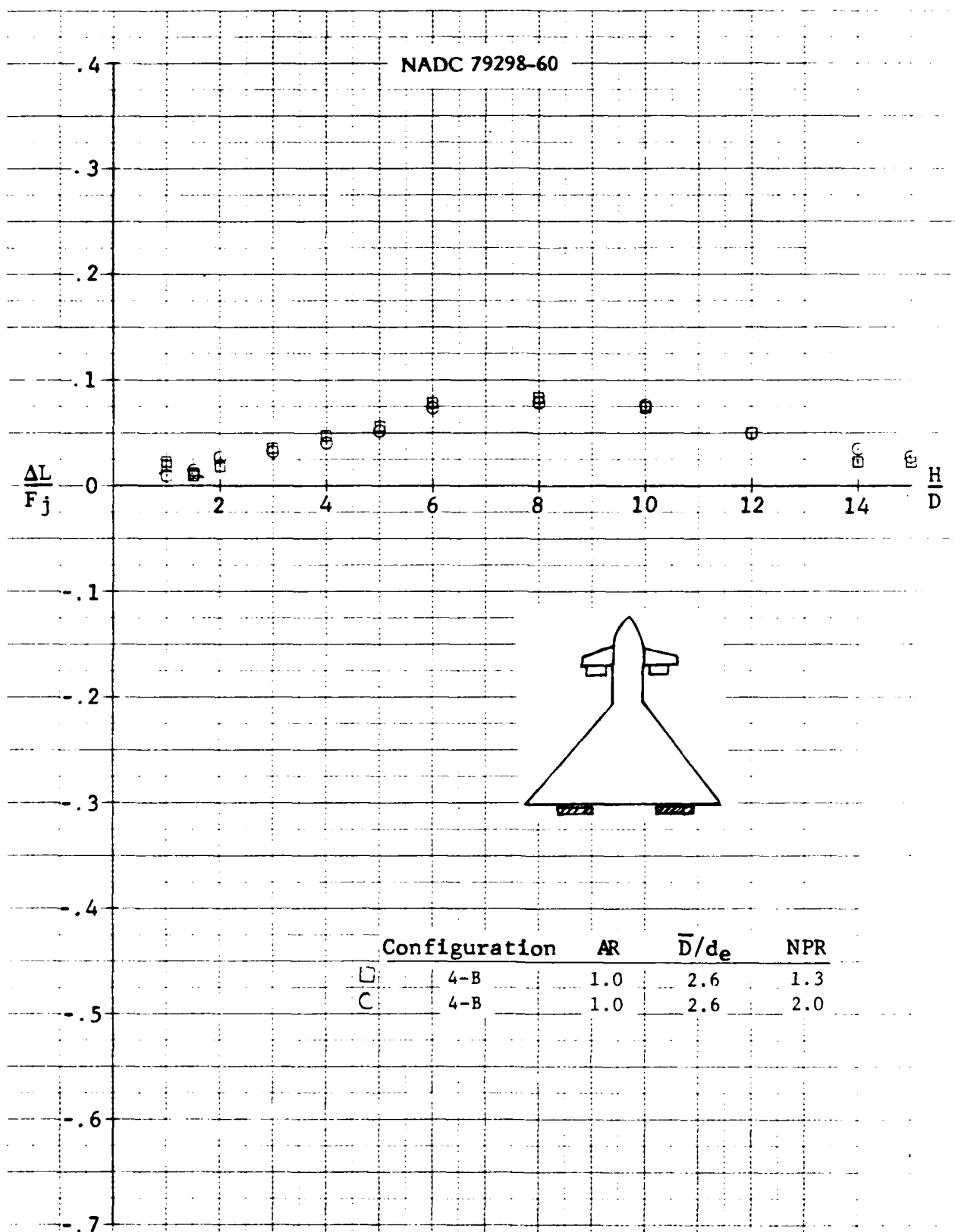
Figure A-40   Induced Lift vs Altitude

Figure A-41   Induced Lift vs Altitude

$\frac{\Delta L}{F_j}$

$\frac{H}{D}$

.1

0

-.1

-.2

-.3

-.4

-.5

-.6

-.7

-.8

-.9

-1.0

2   4   6   8   10   12   14

Configuration	AR	$\overline{D}/d_e$	NPR
C 3-A	1.0	7.3	2.0
□ 3-A	1.0	7.3	2.4

Figure A-42   Induced Lift vs Altitude

114

Configuration		AR	$\overline{D}/d_e$	NPR
○	3-A	2.7	7.3	2.0
□	3-A	2.7	7.3	2.4

Figure A-43   Induced Lift vs Altitude

115

$$\frac{\Delta L}{F_j}$$

Configuration	AR	$\overline{D}/d_e$	NPR
◯	3-A	6.0	7.3	2.0
☐	3-A	6.0	7.3	2.4

Figure A-44   Induced Lift vs Altitude

116

$\dfrac{\Delta L}{F_j}$

.1

0

-.1

-.2

-.3

-.4

-.5

-.6

-.7

-.8

-.9

-1.0

2   4   6   8   10   12   14 $\dfrac{H}{D}$

Contoured
Fuselage
$2r/W = 1.0$

Configuration	AR	$\overline{D}/d_e$	NPR
3-B	1.0	4.7	2.0
3-B Contoured	1.0	4.7	2.0
3-B w/LID's	1.0	4.7	2.0

Figure A-45   Induced Lift vs Altitude

$$\frac{\Delta L}{F_j}$$

.1

0

-.1

-.2

-.3

-.4

-.5

-.6

-.7

-.8

-.9

-1.0

$\frac{H}{D}$

2   4   10   12   14

Contoured
Fuselage

Configuration	AR	$\overline{D}/d_e$	NPR
3-B	2.7	4.7	2.0
3-B Contoured	2.7	4.7	2.0
3-B Semi-Contoured	2.7	4.7	2.0
3-B w/LID's	2.7	4.7	2.0

Contoured Fuselage   2r/W = 1.0
Semi-Contoured   2r/W = 0.5

Figure A-46   Induced Lift vs Altitude

118

Figure A-47   Induced Lift vs Altitude

$$\frac{\Delta L}{F_j}$$

Configuration	AR	$\overline{D}/d_e$	NPR
C 3-B	2.7	6.8	2.0
□ 3-B	2.7	6.8	2.4

Figure A-48   Induced Lift vs Altitude

120

Figure A-49   Induced Lift vs Altitude

$$\frac{\Delta L}{F_j}$$

$$\frac{H}{D}$$

Contoured
Fuselage
$2r/W = 1.0$

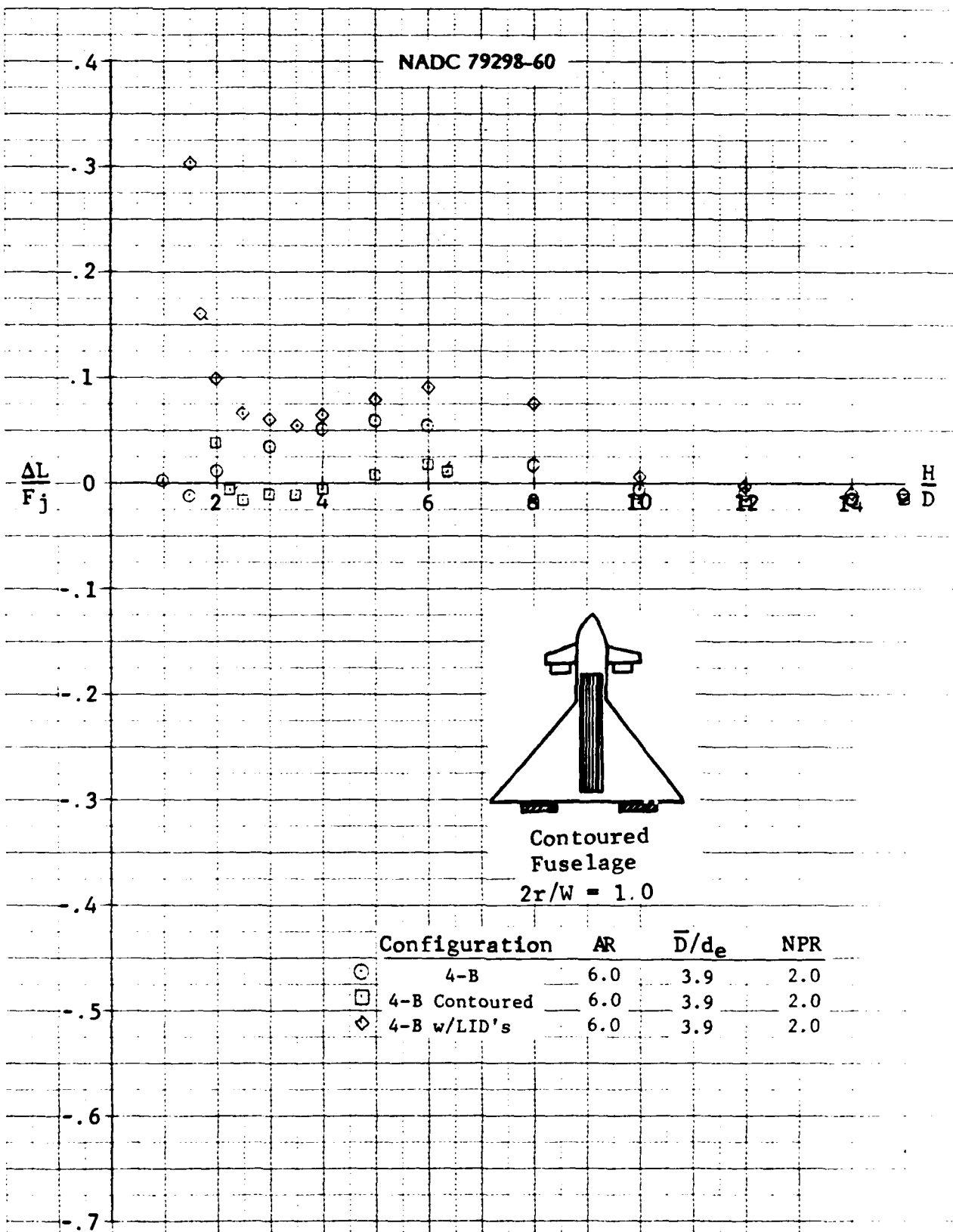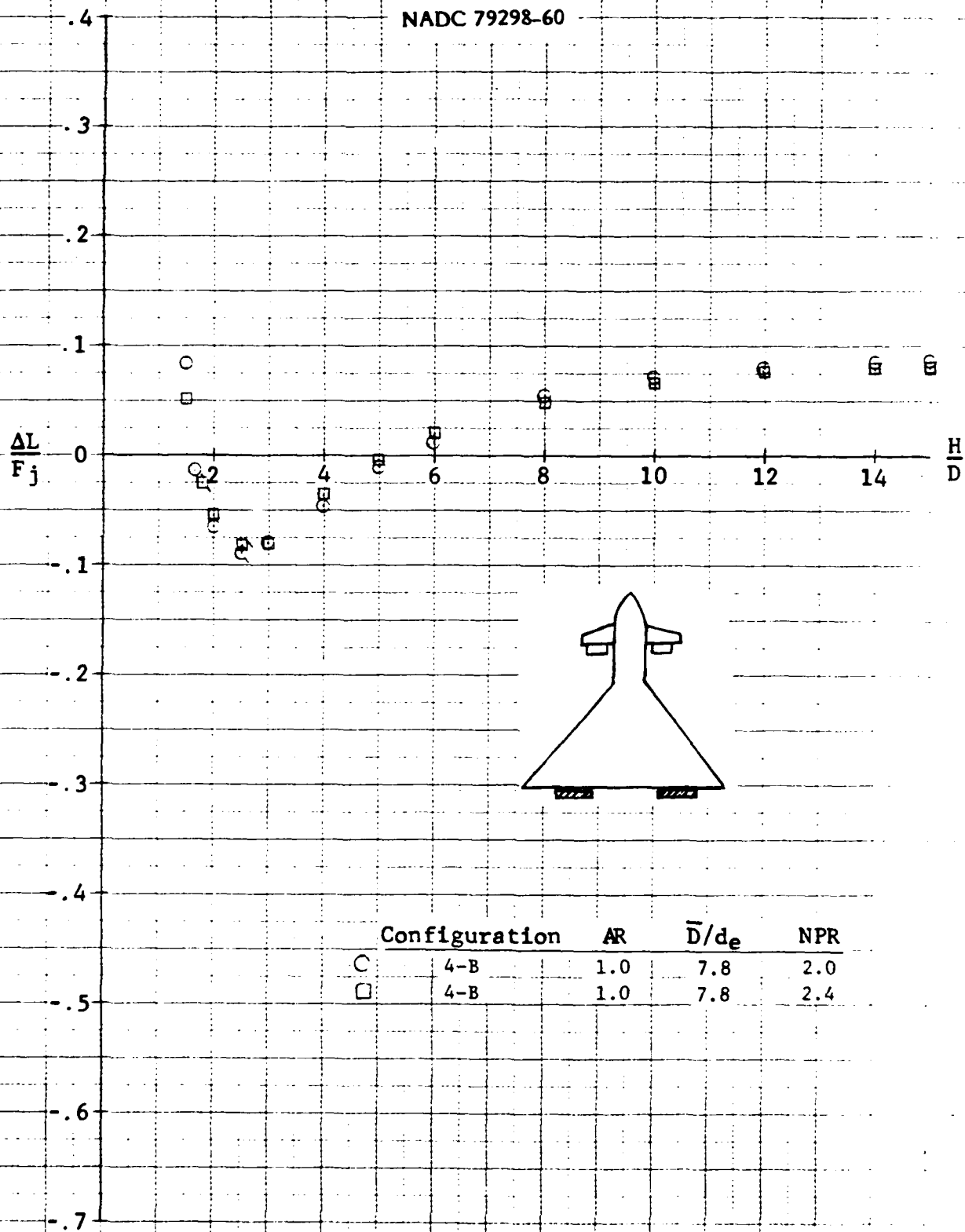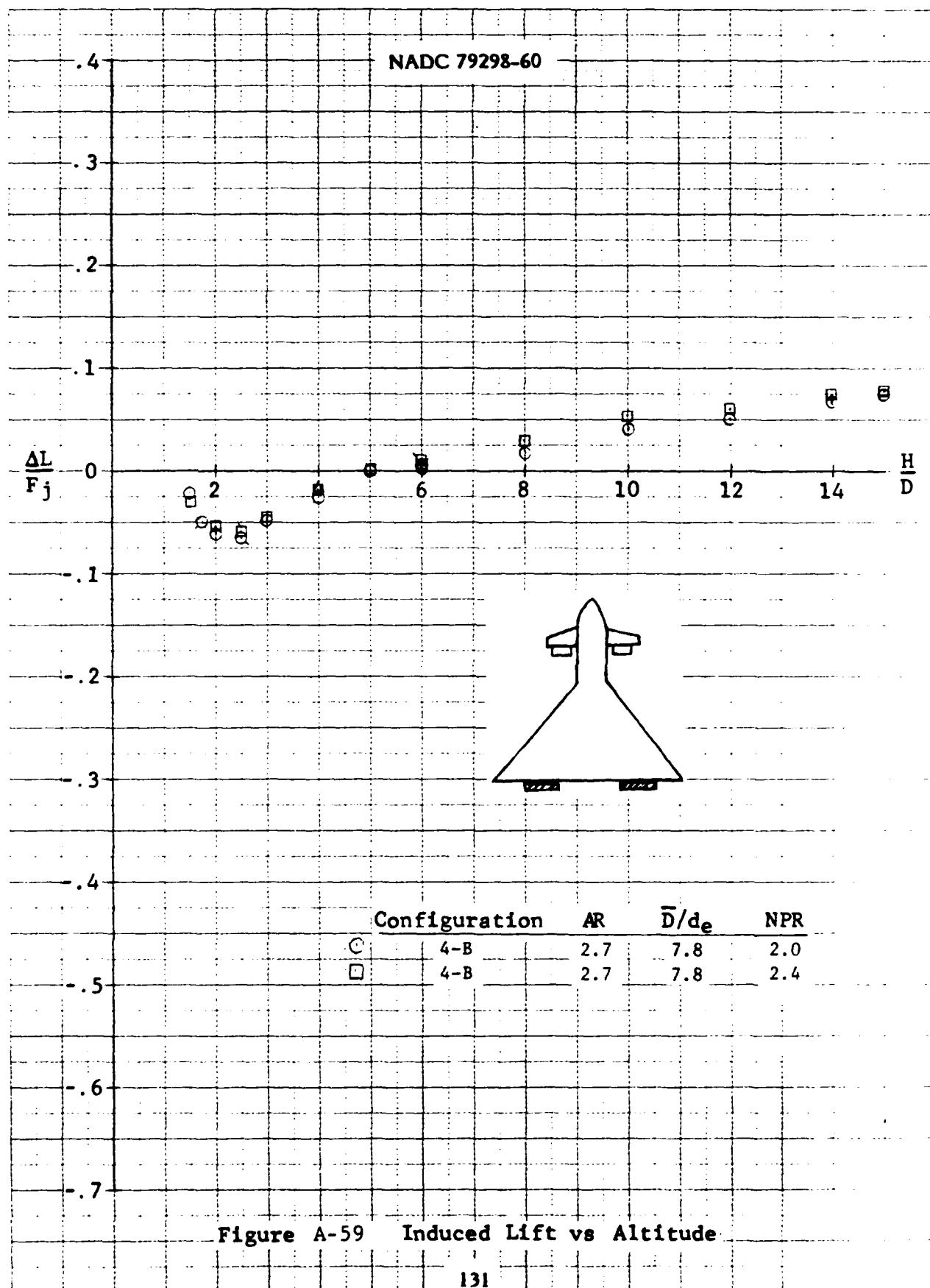| Configuration	AR	$\overline{D}/d_e$	NPR
⊙ 4-A Contoured	2.7	3.1	1.3
▢ 4-A Contoured	2.7	3.1	2.0

Figure A-50   Induced Lift vs Altitude

Figure A-51   Induced Lift vs Altitude

Figure A-52   Induced Lift vs Altitude

124
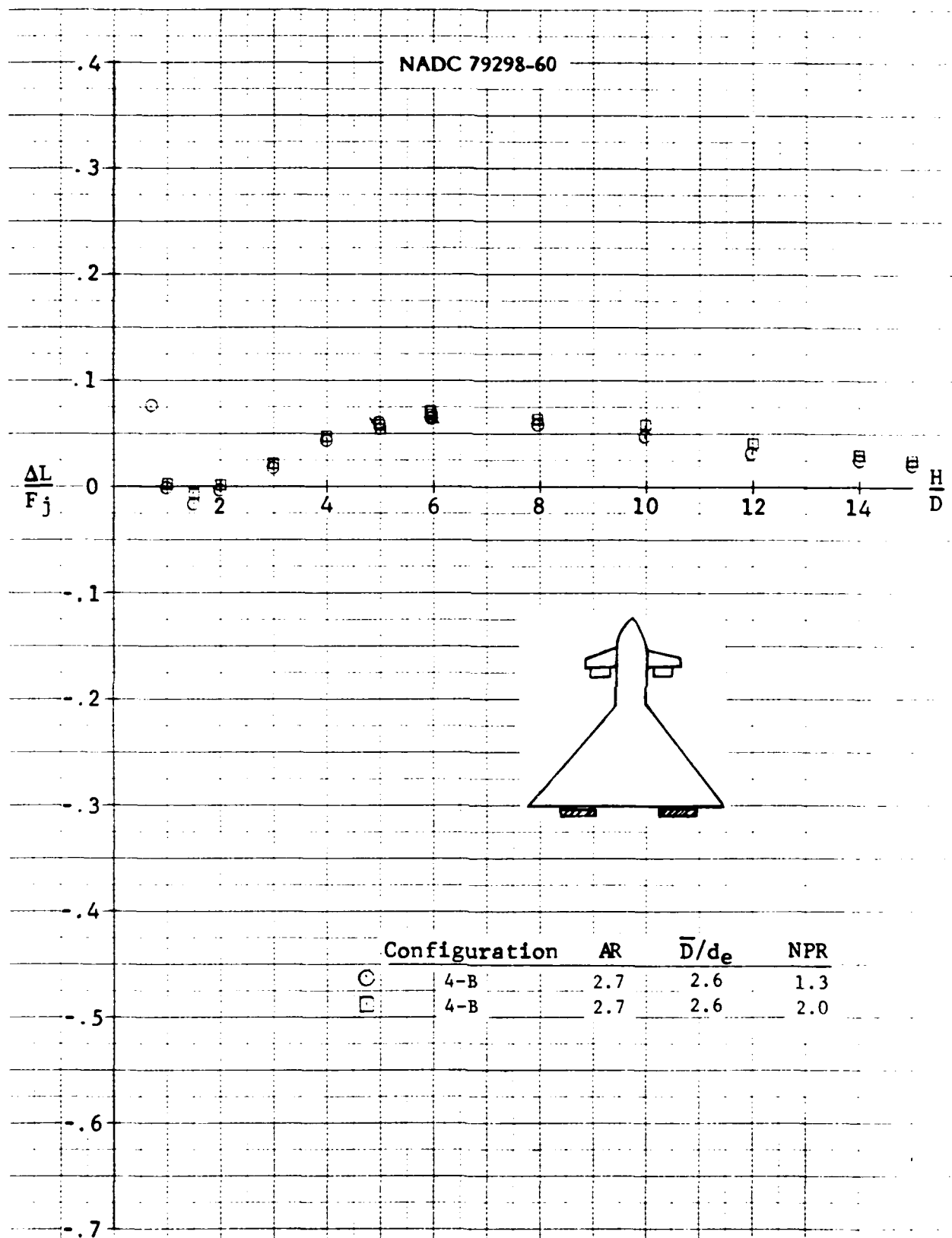
Figure A-53 Induced Lift vs Altitude

Configuration	AR	$\overline{D}/d_e$	NPR
C 4-B	6.0	2.6	1.3
□ 4-B	6.0	2.6	2.0
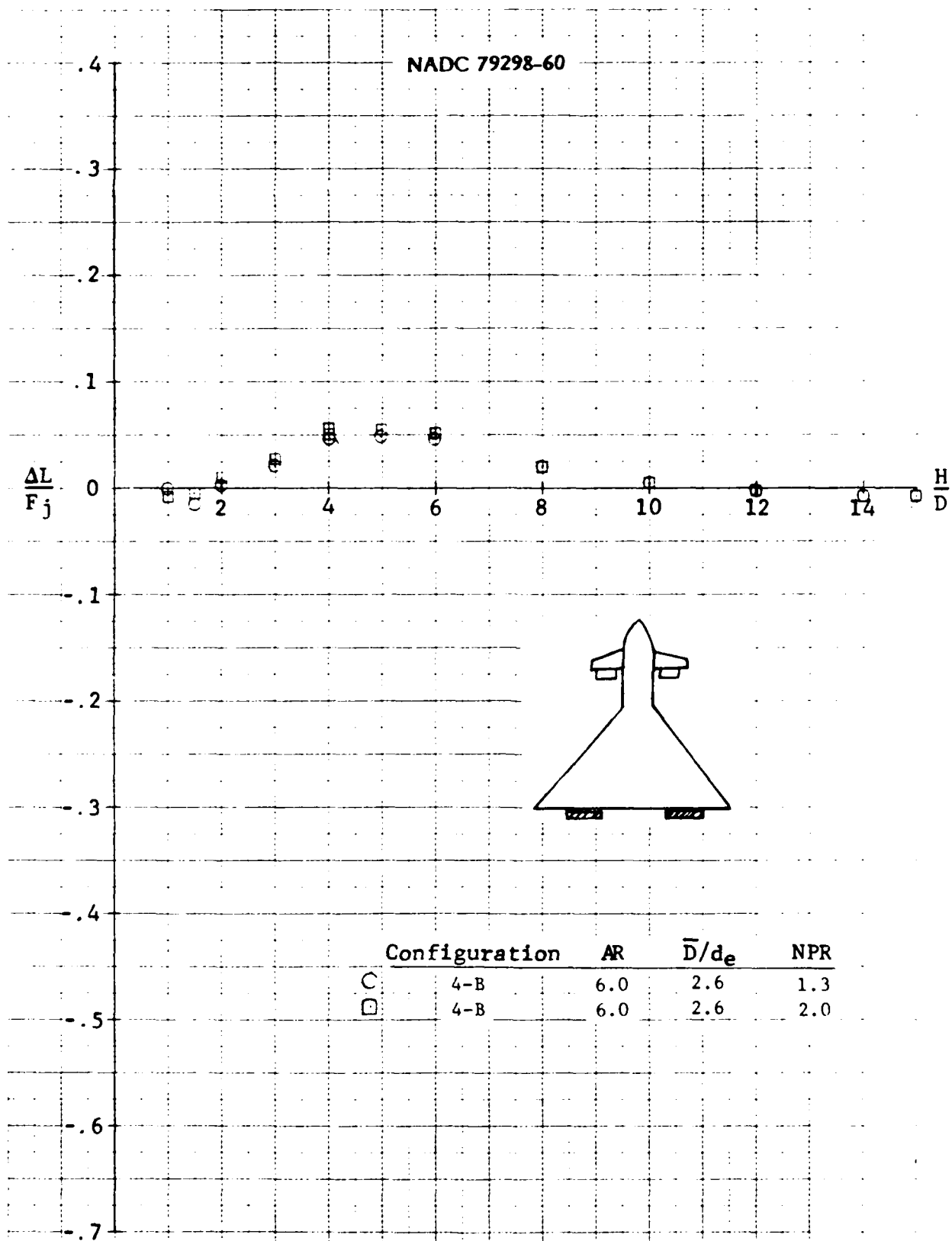
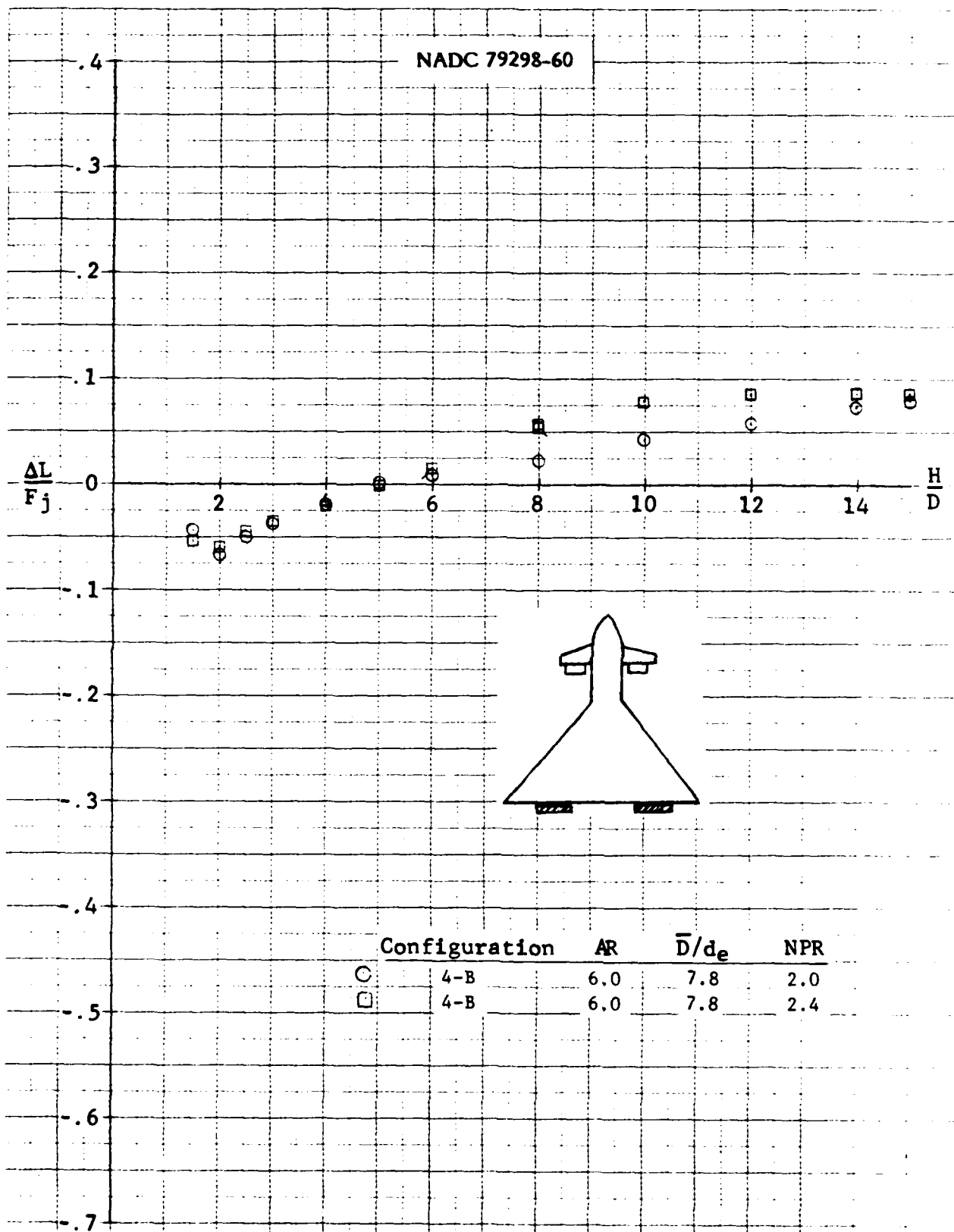Figure A-54   Induced Lift vs Altitude

126
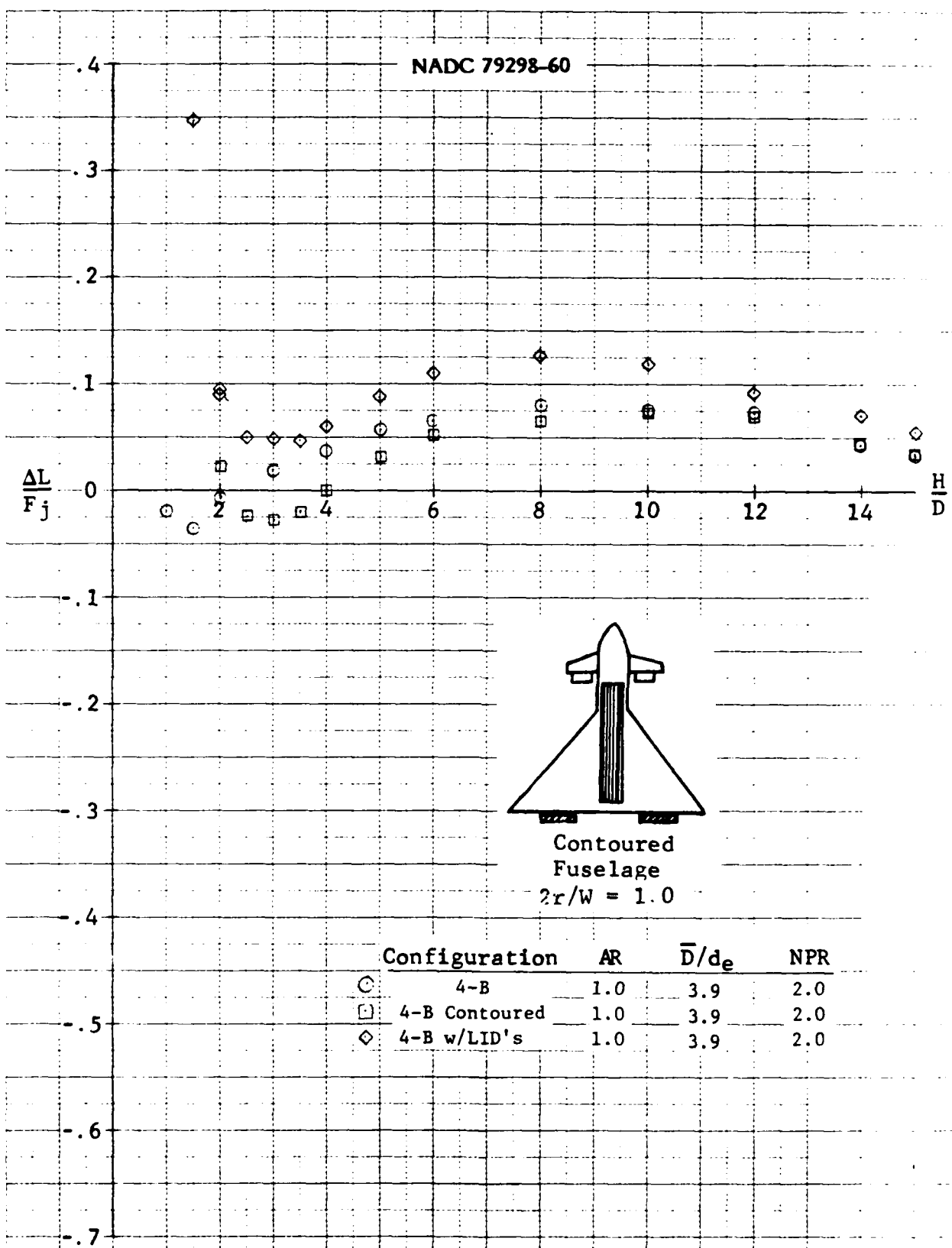
Figure A-55   Induced Lift vs Altitude
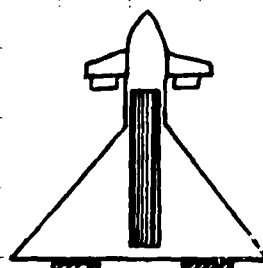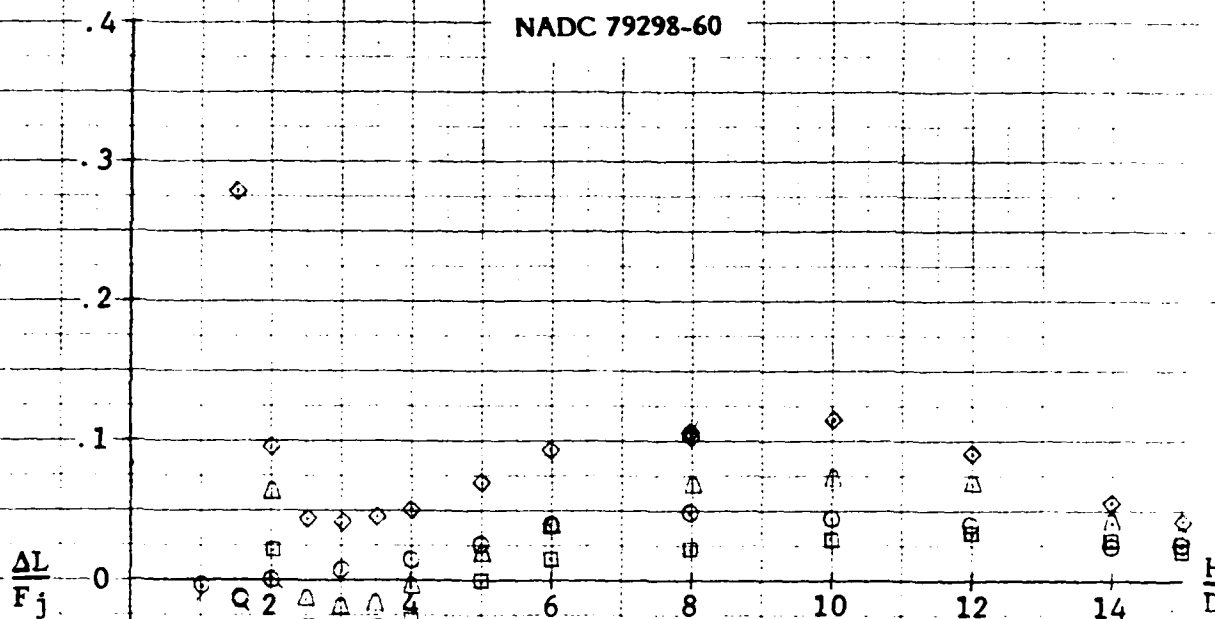
Figure A-56   Induced Lift vs Altitude

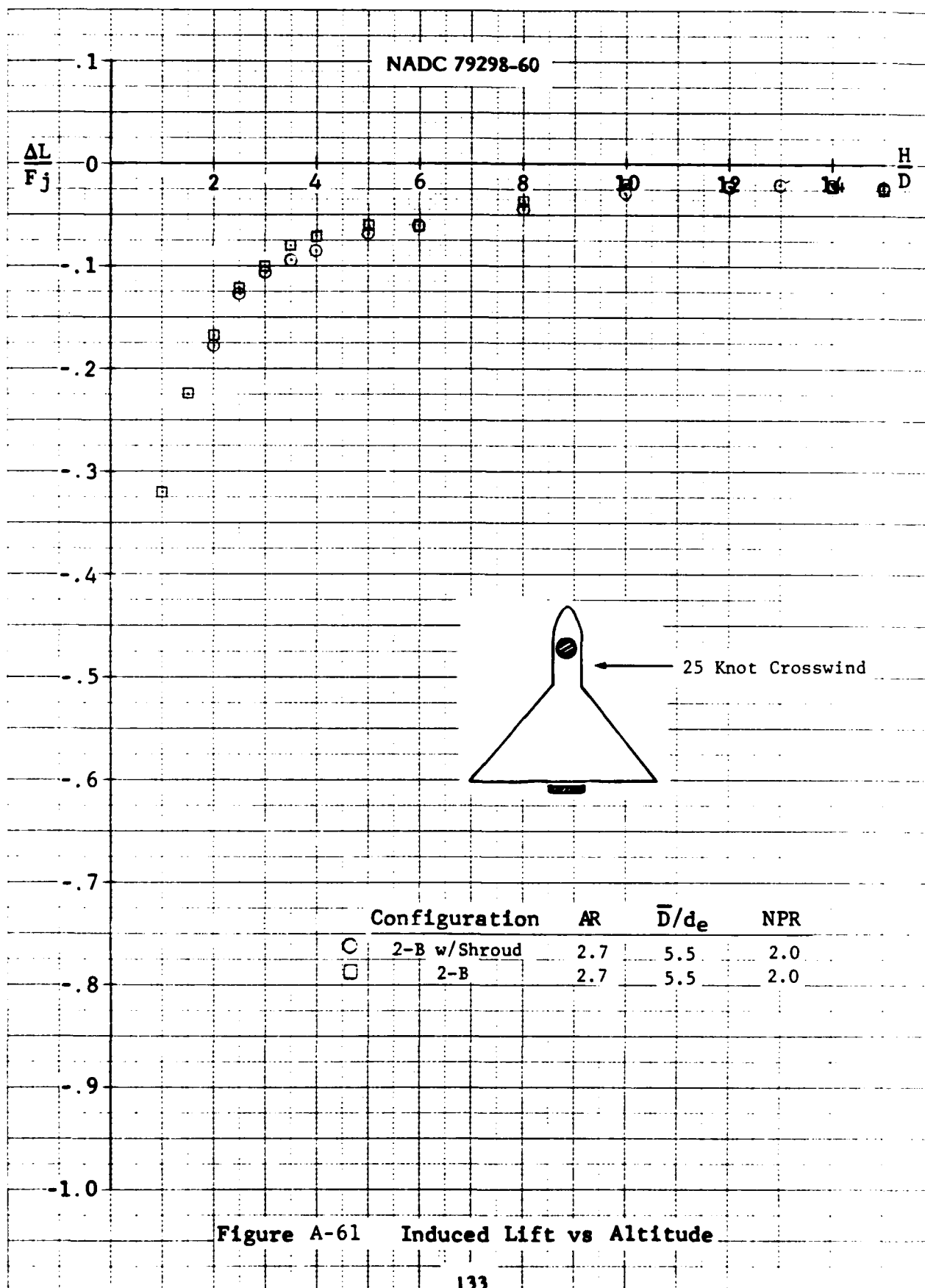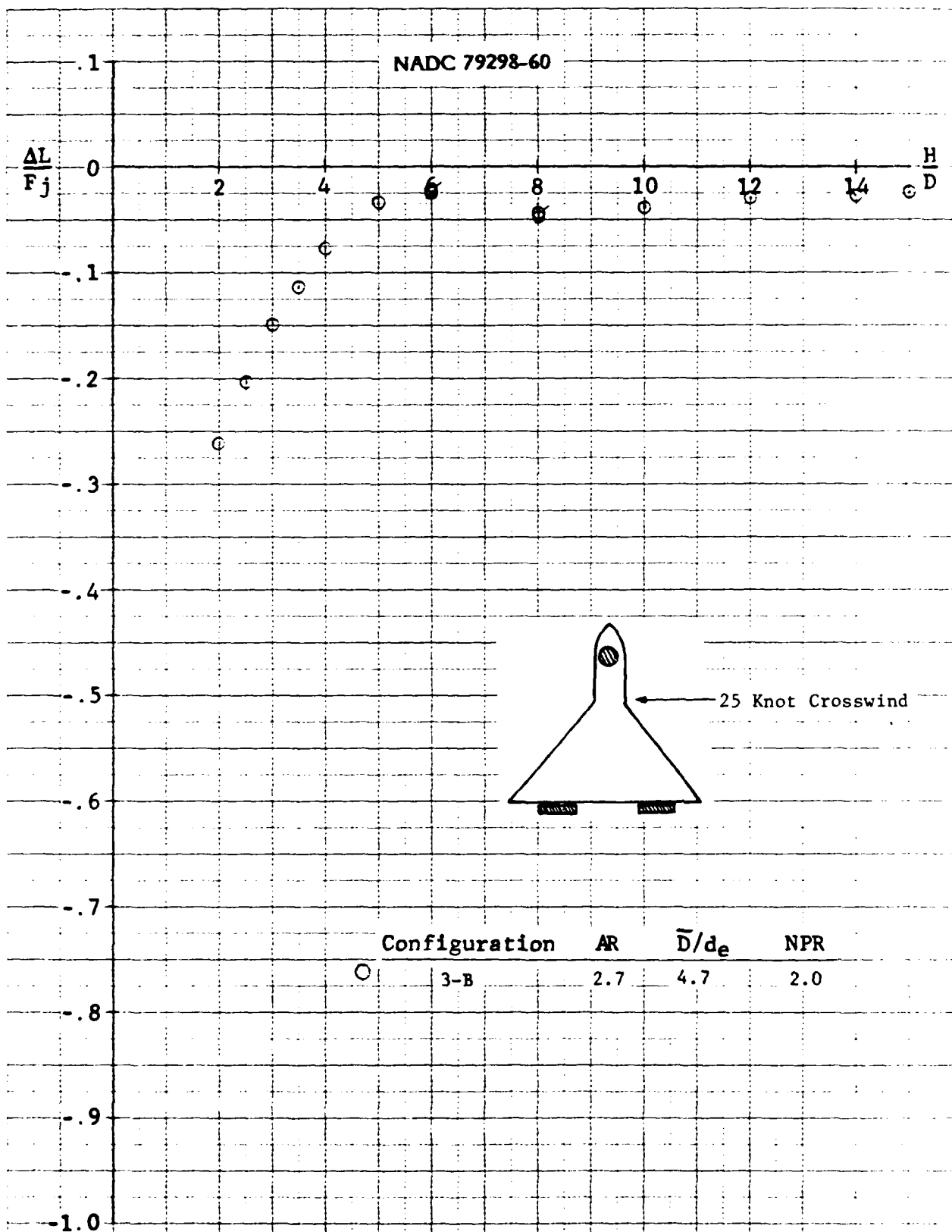Figure A-57   Induced Lift vs Altitude

Configuration	AR	$\overline{D}/d_e$	NPR
○ 4-B	1.0	7.8	2.0
□ 4-B	1.0	7.8	2.4

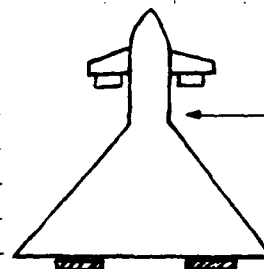Figure A-58   Induced Lift vs Altitude

Figure A-59   Induced Lift vs Altitude

Configuration	AR	$\overline{D}/d_e$	NPR
◯ 4-B	2.7	7.8	2.0
☐ 4-B	2.7	7.8	2.4

Figure A-60 Induced Lift vs Altitude

NADC 79298-60

Figure A-61   Induced Lift vs Altitude

133

25 Knot Crosswind

Configuration	AR	$\widetilde{D}/d_e$	NPR
3-B	2.7	4.7	2.0

Figure A-62   Induced Lift vs Altitude

$$\frac{\Delta L}{F_j}$$
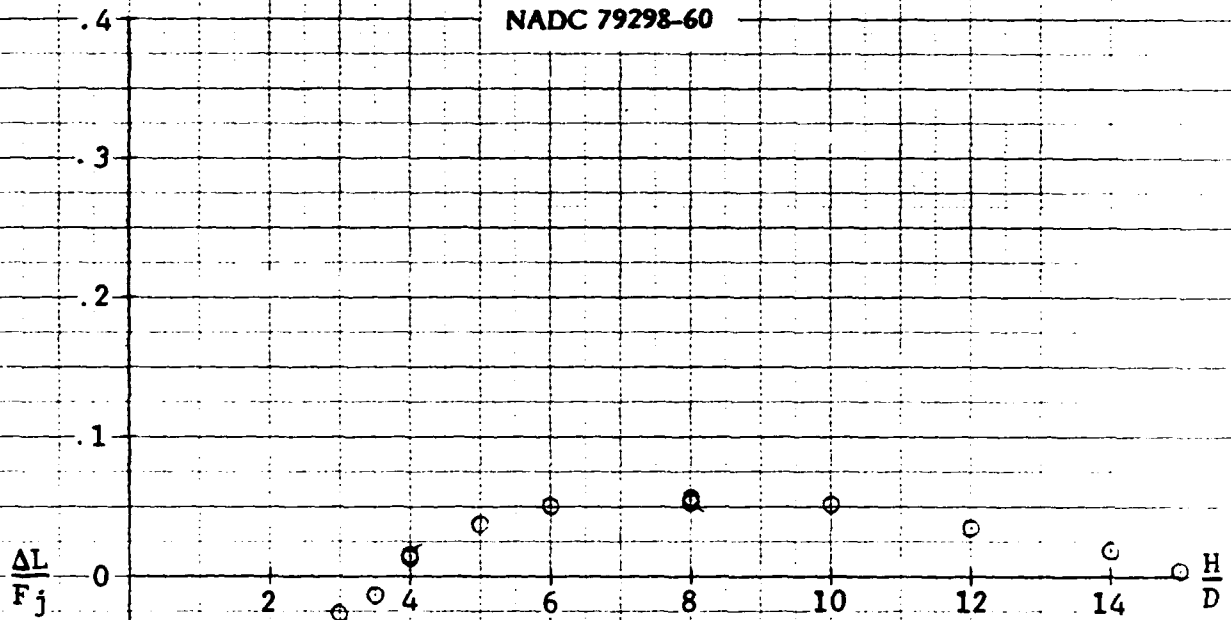
25 Knot Crosswind

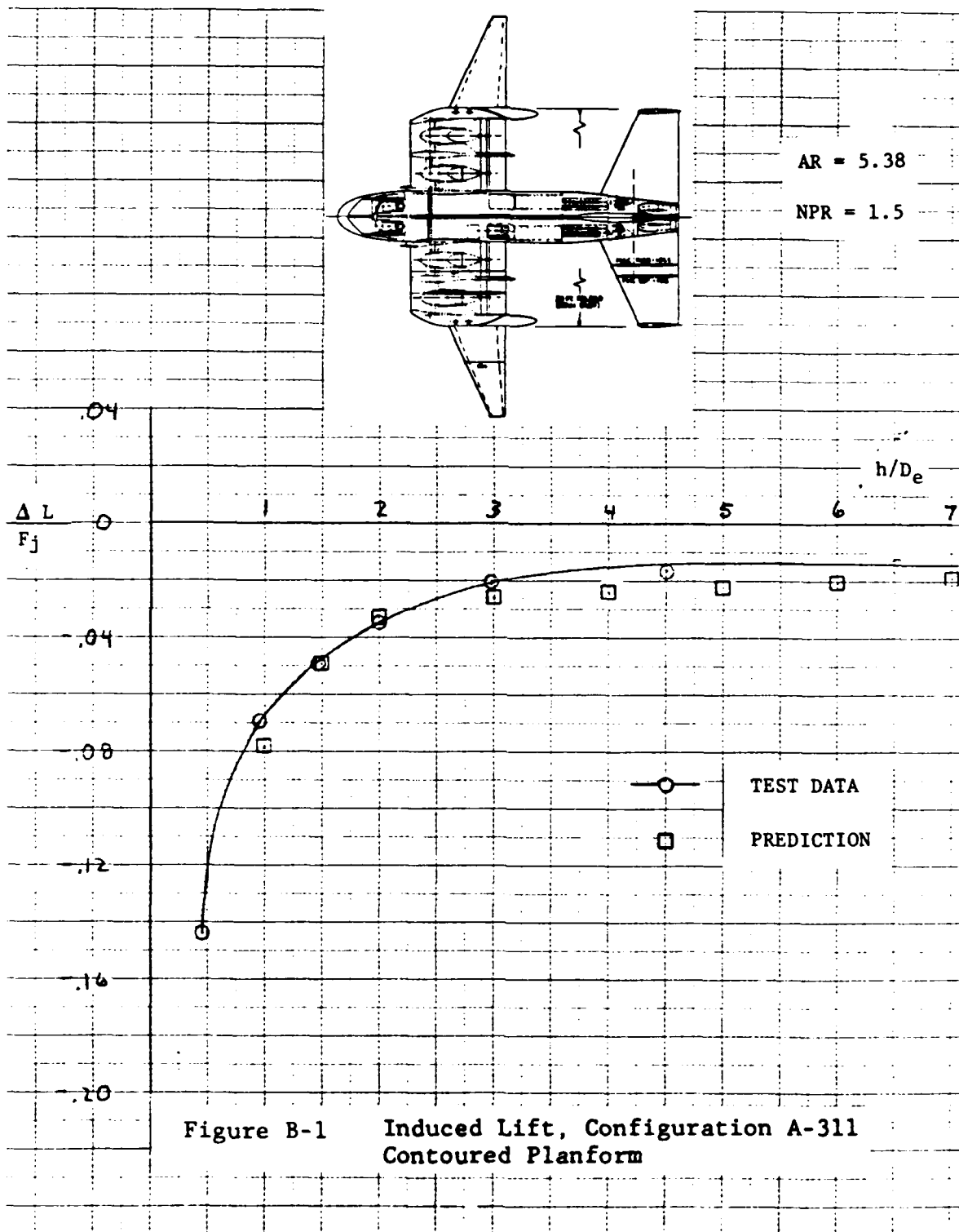| Configuration	AR	$\overline{D}/d_e$	NPR
4-B	2.7	3.9	2.0

Figure A-63   Induced Lift vs Altitude

APPENDIX B

CORRELATIONS

The methodology of Section 3 has been applied to several configuration taken from Refs. 17 through 19. The comparisons between the predictions and the test data are shown in Figures B-1 through B-5.

Figure B-1   Induced Lift, Configuration A-311
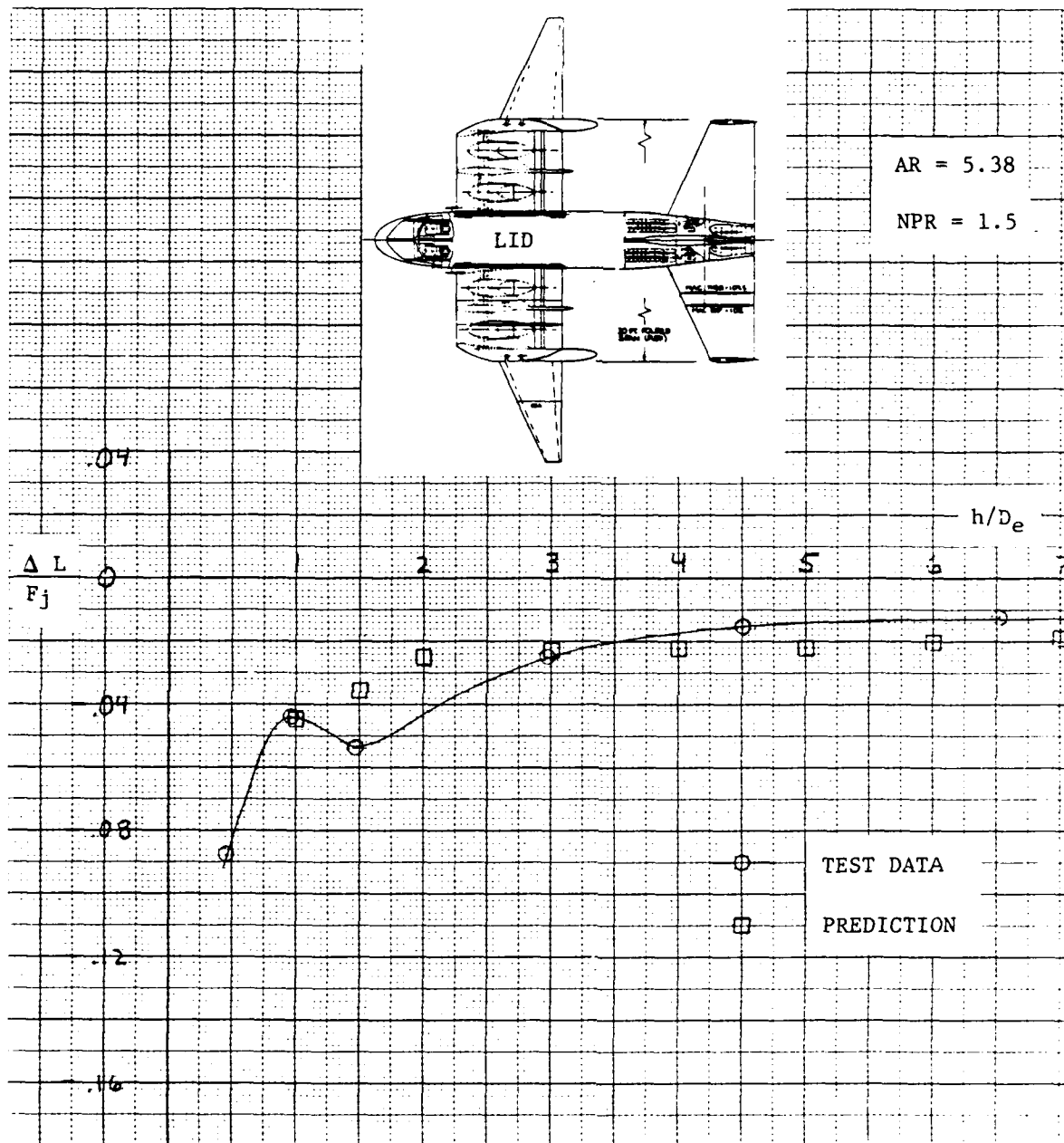Contoured Planform

Figure B-2   Induced Lift, Configuration A-311
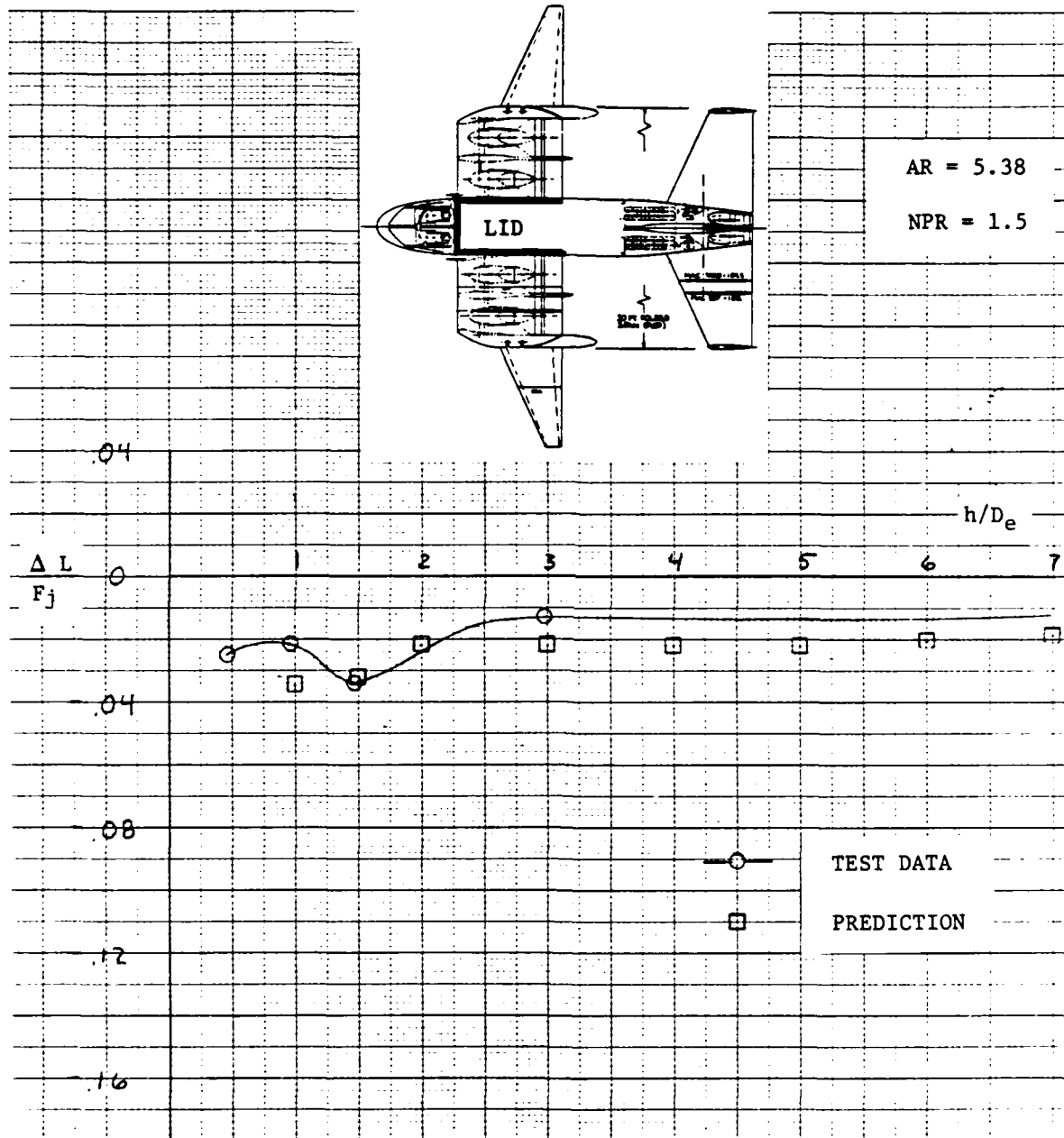Contoured Planform, 2-Sided LID

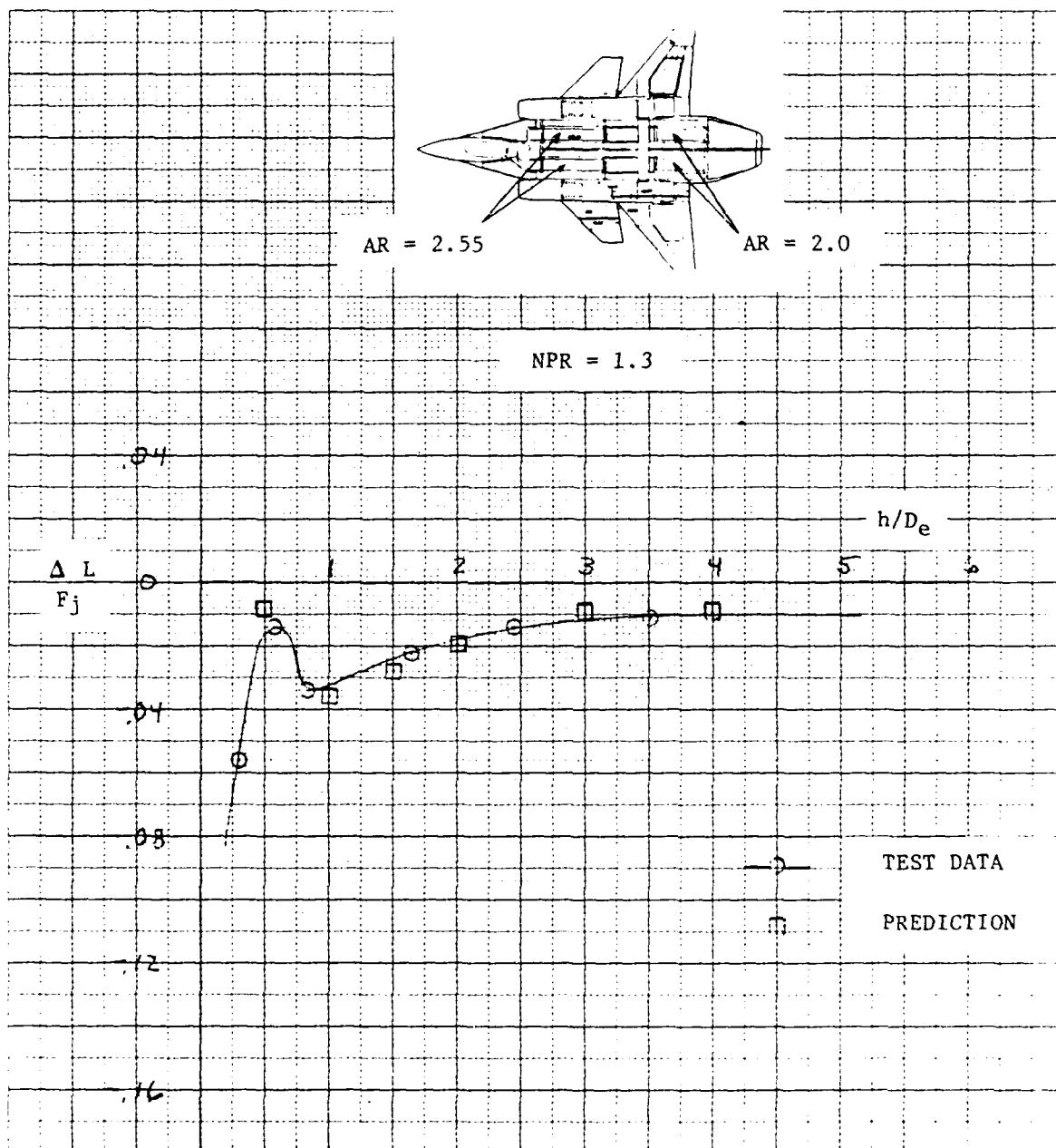Figure B-3 Induced Lift, Configuration A-311
Contoured Planform, 3-Sided LID

Figure B-4   Induced Lift, Configuration E-205
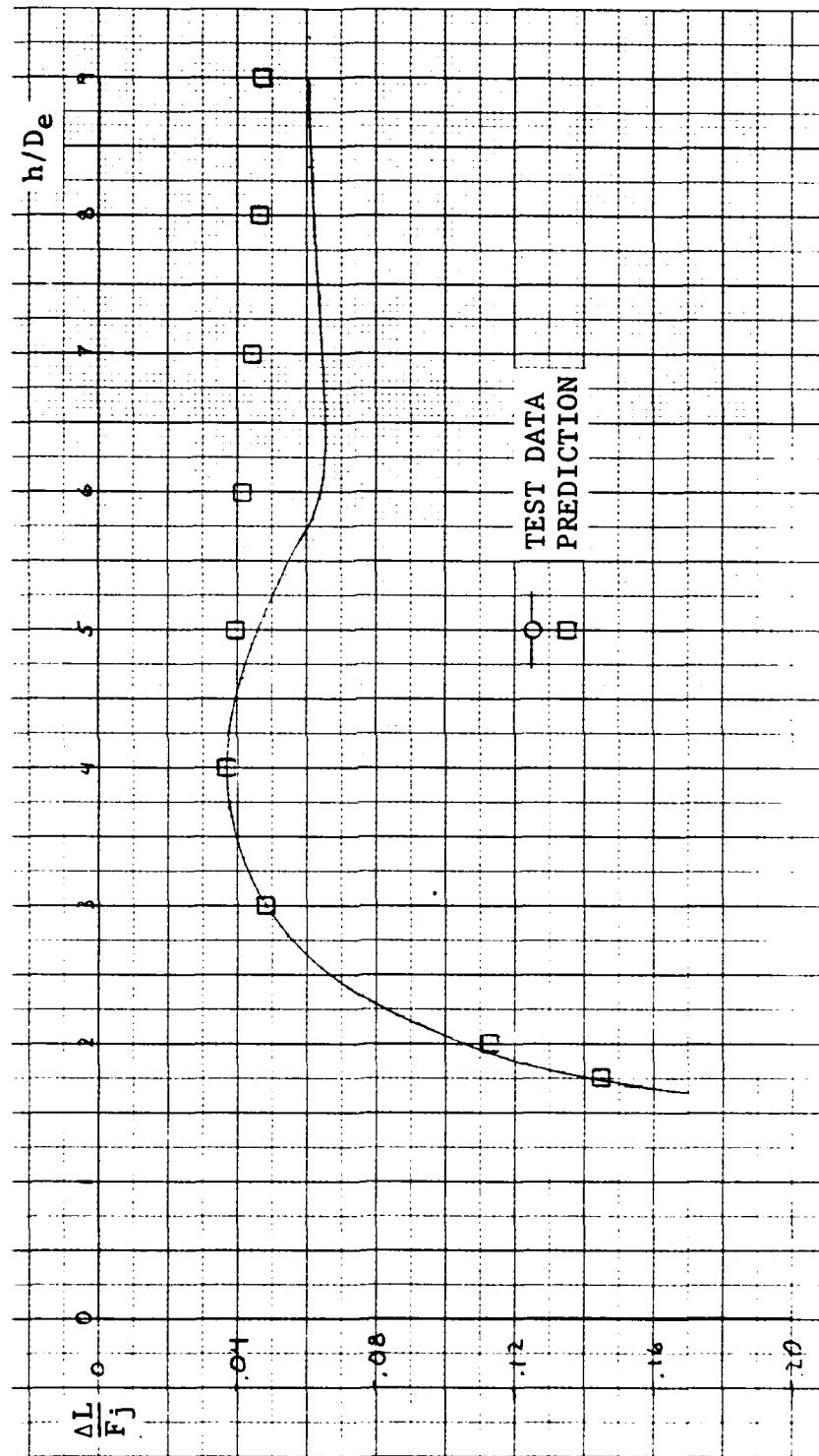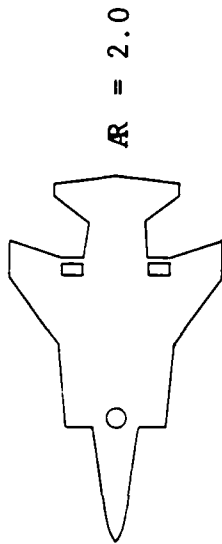Contoured Planform

Figure B-5 Induced Lift, Configuration 623
Contoured Planform

DISTRIBUTION LIST

Commander
Naval Weapons Center
China Lake, CA 93555

Commanding Officer
Naval Air Propulsion Center
Trenton, NJ 08628

Commander
Naval Air Test Center
Patuxent River, MD 20670

Commander
David Taylor Naval Ship Research
 & Development Center
Bethesda, MD 20034

Chief
Office of Naval Research
800 N. Quincy Street
Arlington, VA 22217

Institute of Defense Analysis
400 Army Navy Drive
Arlington, VA 22202
Attn: J. Attinello

Director
National Aeronautics & Space
 Administration
Ames Research Center
Moffett Field, CA 94035
Attn: D. Hickey

Director
National Aeronautics & Space
 Administration
Flight Research Center
Edwards Air Force Base, CA 93523

National Aeronautics & Space
 Administration
Langley Research Center
Hampton, VA 23365

Director
National Aeronautics & Space
 Administration
Lewis Research Center
21000 Brooke Park Road
Cleveland, OH 44135

Director
Air Force Flight Dynamics Laboratory
(ASD/ENFDH)
Wright-Patterson Air Force Base
Dayton, OH 45433

Commander
Air Force Aeronautical Systems
 Division
Wright-Patterson Air Force Base
Dayton, OH 45433

Superintendent
Naval Postgraduate School
Monterey, CA 93940

Commanding Officer
Army Aviation Systems Test Activity
Edwards Air Force Base, CA 93523

Commanding General
Army Aviation Ssytems Command
St. Louis, MO 63102

Commander
Naval Air Systems Command (AIR-954)
Department of the Navy
Washington, DC 20361
 7 copies: (2) for retention
           (2) for AIR-320D
           (1) for AIR-5301
           (1) for PMA-257
           (1) for AIR-03PA

DISTRIBUTION LIST (CONTINUED)

General Dynamics
Convair Division
P.O. Box 80986
San Diego, CA 92138

McDonnell-Douglas Corporation
P.O. Box 516
St. Louis, MD 63166

Lockheed-California Company
P.O. Box 551
Burbank, CA 91503

The Boeing Company
Seattle, WA 98101

LTV Aerospace Corporation
Dallas, TX 75221

Rockwell International
Columbus, OH 43216

General Dynamics
P.O. Box 748
FortWorth, TX 76101

Commander
Air Force Flight Test Center
Edwards Air Force Base, CA 93523

Administrator
Defense Documentation Center for
 Scientific & Technical Information
 (DDC)
Building #5, Cameron Station
Alexandria, VA 22314
(12 copies)

Office of Naval Research
800 N. Quincy Street
Arlington, VA 22214
Attn: Dr. R. Whitehead

Commander
Naval Air Development Center
Warminster, PA 18974
13 Copies: (3) for Code 813
            (10) for Code 6053
Attn: C. Henderson

McDonnell-Douglas Corporation
3855 Lakewood Boulevard
Long Beach, CA 90808

Pratt & Whitney Aircraft Division
Division of United Aircraft
 Corporation
East Hartford, CT 06108

Northrop Corporation
Hawthorne, CA 90250

Lockheed-Georgia Company
Marietta, GA 30061

Grumman Aerospace Corporation
Bethpage, Long Island, NY 11714

Rockwell International
Los Angeles, CA 90053

Fairchild-Republic Corporation
Farmingdale, Long Island, NY 11735

Royal Aeronautical Establishment
Bedford, England
Attn: A. Woodfield

Hughes Aircraft Company
Culver City, CA 90230

DISTRIBUTION LIST (CONTINUED)

A. L. Byrnes
Lockheed-California Company
Burbank, CA 91520

W. G. Hill, Jr.
Research Department, A-08-35
Grumman Aerospace Corporation
Bethpage, NY 11714

R. J. Kita
Grumman Aerospace Corporation
Bethpage, NY 11714

D. Koenig
Mail Stop 247-1
NASA Ames Research Center
Moffett Field, CA 94035

D. R. Kotansky
Section Chief, Aerodynamics
McDonnel Douglas Corporation
McDonnell Aircraft Company
P.O. Box 516
St. Louis, MO 63166

P. T. Wooler
Aerosciences Research
Department 3811, Zone 82
Northrop Corporation, Aircraft
 Group
3901 W. Broadway
Hawthorne, CA 90250

R. R. Jeffries
AFWAL/FIMM
Wright Patterson AFB, Ohio 45433

E. D. Spong
Branch Chief, Propulsion
Dept. 343, Bldg. 32/2
McDonnell Aircraft Company
P.O. Box 516
St. Louis, MO 63166

J. W. Paulson, Jr.
Mail Stop 286
NASA Langley Research Center
Hampton, VA 23665

S. Perkins
Nielsen Engineering & Research Inc.
510 Clyde Avenue
Mountain View, CA 94043

R. Perkins
AIR 320
Naval Air Systems Command
Washington, D. C. 20361

M. F. Platzer
Code 67Pl
Department of Aeronautics
Naval Postgraduate School
Monterey, CA 93940

D. B. Schoelerman
Vought Corporation
P.O. Box 5907
Dallas, TX 75222

J. H. Nichols, Jr.
Code 208A
David W. Taylor Naval Ship Research
 and Development Center
Bethesda, MD 20014